



Università degli Studi di Padova

Facoltà di Ingegneria

**Scuola di Dottorato in
Scienze dell'Ingegneria Civile e Ambientale**

Tesi di Dottorato

Advanced structural problematics in steel bridges

Dottorando:

Tetougueni Cyrille Denis

Supervisor:

Prof. Carlo Pellegrino

Ing. Paolo Zampieri

XXXII Ciclo - 2019



UNIVERSITÀ
DEGLI STUDI
DI PADOVA

Sede Amministrativa: Università degli Studi di Padova

Dipartimento di Costruzioni e Trasporti

SCUOLA DI DOTTORATO DI RICERCA IN:
SCIENZE DELL'INGEGNERIA CIVILE ED AMBIENTALE
CICLO XXXII

Advanced Structural problematics in steel bridges

Direttore della Scuola

Ch.mo Prof. Marco Marani

Supervisori

Ch.mo Prof. Carlo pellegrino

Dott. Ing. Paolo Zampieri

Dottorando

Ing. Tetougueni Cyrille Denis

ABSTRACT

The knowledge of the structural sensitivity of steel bridges, especially when its main structural elements are subjected to compressive forces, is one of the concerns of structural engineers. On the other hand, non-conventional actions or accidental actions require a certain robustness on the part of the structures in order to preserve their structural integrity, reduce the risk of severe consequences or even maintain their use. With a view to understanding the sensitivity of bridge structural elements to different categories of actions, this research work was conducted. In particular, aspects related to linear and non-linear elastic stability, structural capacity or performance of different bridges typologies were studied. With the help of a numerical tools designed for FEM modelling, studies, often parametric, have been carried out intensively. For example, in the case of girder bridges, the consideration of the interaction of the main in-plane loading applied to bridge girders of various dimensions was studied. After that, the structural capacity of steel arch bridges subjected to vertical loads of traffic or not made it possible to expose the consequence of sudden cable failure on the structural capacity of the bridge and to describe the post-buckling response of the bridge. Finally, a comparative study of structural performance between three stays configurations of cable-stayed bridges in the event that these bridges were subjected to extreme loads such as blast loading was made. All these studies have shown us that steel bridges are very sensitive to the type of actions applied to them. In more detail, the state of compressive stresses on a bridge girder or steel web's plate in the case of a combined in-plane loading effect can result in the reduction of the buckling elastic critical load by up to half. Also, in the case of suspension bridges, the arrangement of the stays elements plays an important role in the structure's ability to withstand extreme loads.

To the almighty God, to my family and my siblings, with gratitude

SOMMAIRE

La maîtrise de la sensibilité structurelle des ponts en acier surtout lorsque ces principaux éléments structurels sont soumis à des forces de compression fait partie d'une des prérogatives des ingénieurs structures. De l'autre côté, des actions non conventionnelles ou encore actions accidentelles demandent une certaine robustesse de la part des structures afin de préserver son intégrité structurelle, décroître le risque de conséquences aggravées ou encore de maintenir son usage. C'est dans l'optique de comprendre la sensibilité des éléments structurels de pont face aux différentes catégories d'actions que ce travail de recherche a été dirigé. En particulier, les aspects liés à la stabilité élastique linéaire et non linéaire, à la capacité structurelle ou encore à la performance de différentes typologies de pont ont été étudiés. A l'aide d'outil numérique conçu pour les modélisations FEM, des études souvent paramétriques ont pu être menées. Ainsi, dans le cas des ponts poutres, la prise en compte de l'interaction des principales forces dans plan s'appliquant sur les poutres de ponts de diverses dimensions a été étudiés. Après cela, la capacité structurelle des ponts bowstring fait en acier soumis à des charges verticales de trafics ou non a permis d'exposer la conséquence rupture soudaine d'un câble sur la capacité structurelle de pont. Finalement, une étude comparative de performance structurelle entre trois configurations de pont à haubans dans le cas où ces ponts étaient soumis à des charges extrêmes tel que l'explosion ou les charges d'impact. Toutes ses études nous ont révélé dans que les ponts en acier sont très sensibles du type d'actions qui leur sont appliquées. Plus en détail, l'état de contraintes de compression sur une plaque d'âme de poutre de pont en cas de effet combiné de charges internes au plan et peut entraîner la réduction de la charge critique élastique d'Euler jusqu'à une réduction de moitié. Aussi dans le cas des ponts à suspente, la disposition des éléments de suspente joue un rôle important dans la capacité de la structure à faire face à des actions extrêmes.

ACKNOWLEDGEMENTS

- The author gratefully acknowledges Prof. Carlo Pellegrino (University of Padova) for giving her the opportunity to work on this topic during the PhD studies. The authors will also be grateful toward Dr. Paolo Zampieri for his unconditional support during the development of this research activity. I will also thank Nicolò Simoncello for his help and his friendship.
- Secondly, I would like to have a sincere thought about a family I found in Italy. The Francophone African community of Padua, for their presence and for the warm welcome I have received since my arrival in Italy. I will not forget my friends from Padua, Therese, Ines, Francine, Beaudin, Idriss, the amazing team with whom I shared a very good time during this period of doctoral studies.
- A sincere thanks to the AIET family from Cameroon who have always supported me and with whom I share so many wonderful things.
- Lastly, special thanks go to my family, friends and colleagues for giving all their support, encouragement and patience during the last years.

TABLE OF CONTENTS

ABSTRACT.....	v
SOMMAIRE.....	vii
ACKNOWLEDGEMENTS.....	viii
TABLE OF CONTENTS	ix
LIST OF FIGURES	xiii
LIST OF TABLES	xviii
CHAPTER 1 INTRODUCTION.....	20
1.1 Introduction.....	20
1.2 Objectives of the study	22
1.3 Thesis organization	23
1.4 References.....	24
CHAPTER 2 LITERATURE REVIEW OF STEEL PLATE UNDER COMBINED IN-PLANE LOADING.....	26
2.1 Investigation of steel plate buckling before 1992.....	27
2.1.1 Unstiffened plate.....	28
2.1.1.1 Purposes and methodology of early researches	28
2.1.1.2 Results and comments.....	30
2.1.2 Unstiffened plate with hole	34
2.1.2.1 Purposes and methodology of the early research	34
2.1.2.2 Results and comments.....	35
2.1.3 Unstiffened plate with hole	35
2.1.3.1 Purposes and methodology of the early research	36
2.1.3.2 Results and comments.....	37
2.2 Investigation of steel plate buckling before 1992.....	39
2.2.1 Unstiffened girder	42
2.2.1.1 Purposes and methodology of the research	42
2.2.1.2 Purposes and methodology of the research	44
2.2.2 Unstiffened Plate with hole	48
2.2.3 Stiffened plate	51
2.3 Illustrative design example	56

2.3.1	Linear buckling analysis.....	57
2.3.2	Mesh validation	58
2.3.3	Interaction of combined loading.....	59
2.4	Conclusions	62
2.5	References	65
CHAPTER 3 Elastic Buckling of Steel Plate Subjected to Patch Loading Interacting with Bending and Shear		74
3.1	Abstract.....	74
3.2	Introduction	76
3.3	Theoretical background.....	77
3.4	Finite Element Method	80
3.5	Parametric studies	85
3.5.1	Research strategy	85
3.5.2	Investigation of a steel plate under M-F-V interaction	85
3.5.2.1	Influence of patch loading length and panel aspect ratio ..	85
3.5.2.2	Influence of patch loading magnitude and plate's slenderness	87
3.5.3	Failure mode of a steel plate under combined in-plane loadings	87
3.6	Elastic critical buckling of a steel plate under $M-F-V$ interaction	91
3.6.1	Investigation of a steel plate under $M-F-V$ interaction	91
3.6.2	Evaluation of the buckling load factor.....	92
3.6.2.1	Influence of patch loading length.....	93
3.6.2.2	Influence of patch loading magnitude.....	94
3.6.2.3	Influence of the plate's slenderness	94
3.6.2.4	Influence of the panel aspect ratio	94
3.6.3	Evaluation of the buckling load coefficient	97
3.7	Design example.....	98
3.8	Conclusions	101
3.9	References	102
CHAPTER 4 Post-buckling behaviour of Steel Network Arch bridges .		105
4.1	Abstract.....	105
4.2	Introduction	105
4.3	Description of the bridge in study.....	108

4.3.1	Structural layout.....	109
4.4	Finite Element Modeling	111
4.4.1	Theoretical background	111
4.4.2	Numerical modeling	113
4.4.3	Types of analysis	116
4.4.4	Validation of the FEM result.....	117
4.5	Linear buckling and geometric non-linear analyses.....	118
4.6	Structural behaviour of the arch under vertical loads at arch center	122
4.7	Structural behaviour of the arch under traffic loads.....	127
4.7.1	Structural performance of the arch under traffic load	127
4.7.1.1	Undamaged bridge.....	127
4.7.1.2	Damage Bridges.....	128
4.7.1.2.1	Cable loss scenario	128
4.8	Conclusion	133
4.9	References.....	134
CHAPTER 5 Structural performance of steel cable-stayed bridges under blast loading considering different stay patterns		138
5.1	Abstract.....	138
5.2	Introduction	138
5.3	FEM analysis.....	141
5.3.1	Description of the bridges	141
5.3.2	Blast loading modeling.....	142
5.3.3	FEM Modelling.....	143
5.3.4	Material characteristics	145
5.3.5	Load analysis.....	146
5.4	Numerical analysis and discussion	146
5.4.1	Stress analysis.....	146
5.5	Fragility analysis	151
5.5.1	Methodology	151
5.5.2	Material and geometry uncertainties of the bridges	152
5.5.3	Blast fragility analysis.....	153
5.5.4	Structural capacity.....	155
5.5.4.1	Limit states and Damage Index.....	156

5.5.5	Structural demand	157
5.5.6	Structural demand	159
5.5.6.1	Structural demand	160
5.6	Conclusion.....	163
5.7	References	164
CHAPTER 6	170
General Conclusions and Futures Researches	170
6.1	General conclusions	170
6.2	Future researches.....	171

LIST OF FIGURES

Fig. 1.1. Different example of instability problems: a) silos buckling; b) girder buckling; c) box profile buckling [1.3].....	
Fig. 1.2. Buckling description of structural element. a) Bifurcation of equilibrium; b)plate buckling and bifurcation at point A [1.7].....	
Fig. 2.1. Zetlin’s model in 1995 [2.11].....	
Fig. 2.2. Basler’s model in 1961 [2.14].....	
Fig. 2.3. Basic load cases of combined shear and patch loading [2.27].....	
Fig. 2.4. Failure mechanism assumed by Roberts [2.29].....	
Fig. 2.5. Buckling coefficient for unstiffened plates against shear [2.21].....[2.21]	
Fig. 2.6. a) M-V interaction diagram by Basler’s [2.14]; b) M-V interaction diagram by EN1993 – 1 – 5 [2.35]	
Fig. 2.7. Variation of buckling coefficient for plates longitudinally stiffened under shear [2.54].....	
Fig. 2.8. Histogram showing number of scientific papers used with respect to the published year.....	
Fig. 2.9. Configuration of steel plate girders in the research work.....	
Fig. 2.10. Research methodology.....	
Fig. 2.11. Overview of used of numerical software.....	
Fig 2.12. Different χ -functions to consider in instability problem of structural element [2.64].....	
Fig. 2.13: Proposed Patch loading and bending moment interaction from different authors [2.61].....	
Fig. 2.14. Comparison between numerical and analytical results [2.31].....	
Fig. 2.15. Boundary curves between failure zones for rectangular plate. (a): aspect ratio =1, (b): aspect ratio =2 [2.44].....	
Fig. 2.16. Buckling coefficient k for rectangular plates with circular hole [2.76].....	
Fig. 2.17. k vs d/b diagrams for RL holes with center in nodal points of the deformed configuration [2.71].....	

Fig. 2.18. Numerical model to study the effect of shear load of perforated plate [2.75]	
Fig. 2.19. Von Mises stresses in plate with $a/b = 2$ and circular plate with $\lambda=60$ and $\lambda=120$ [2.75].....	
Fig. 2.20. The increase in critical shear stress in function of number of stiffeners and aspect ratios [2.82].....	
Fig. 2.21. Geometry of the plate girder in the case study.....	
Fig. 3.1. Numerical model in the calibration phase.....	
Fig. 3.2. Plate subjected to combined patch loading, bending, and shear..	
Fig. 3.3. Plate under a pure shear.....	
Fig. 3.4. Variation of the critical buckling load factor for steel plate section subjected to combined patch loading, bending, and shear force: $F=100$ kN; $F_x=4F$; $V_y=F_x$	
Fig. 3.5. Influence of patch loading length in the critical buckling load multiplier.....	
Fig. 3.8. Influence of slenderness in the critical buckling load.....	
Fig. 3.9. Influence of slenderness in the critical buckling load.....	
Fig. 3.10. Critical buckling shape of plate under patch loading, bending and shear, varying slenderness.....	
Fig. 3.11. Critical buckling shape of plate under patch loading, bending, and shear for aspect ratio $a/b=3$	
Fig. 3.11. Critical buckling shape of plate under patch loading, bending, and shear for aspect ratio $a/b=3$	
Fig. 3.12. Comparison between FEM and design formula considering the patch loading length.....	
Fig. 3.13. 3D evolution of the critical buckling load multiplier ratio in term of patch loading magnitude.....	
Fig. 3.14. Geometric and loading characteristic of the section studied....	
Fig. 4.1. Hanger arrangement for existing tied-arch bridges.....	
Fig. 4.2. Global instability behaviour of free standing arch; a) Snap-through; b) In-plane buckling; c) Out-of-Plane buckling extracted from Spoorenberg et al. 2012 [4.11].....	

Fig. 4.3. Generic network arch bridge considered in the study.....

Fig. 4.4. a) transversal section of the bridge, b) longitudinal view of the arch.....

Fig. 4.5. Fiber beam element.....

Fig. 4.6. Radial hanger arrangement: (a) equal distribution on the arch; (b) equal distribution on the tie beam.....

Fig. 4.7. 3D FEM model of a network arch bridge.....

Fig. 4.8. Traffic load distribution on concrete deck.....

Fig. 4.9. Out of plane imposed imperfections for the investigated arches.....

Fig. 4.10. Deformed shape and yielding state of the arch model. Geometry taken from La Poutré et al. [4.18].....

Fig. 4.11. Calibration of numerical models (Figure elaborated from La Poutré et al. [4.23]).....

Fig. 4.12. Results from L.B.A; (a) Influence of angle hanger arrangement; (b) Influence of lateral bracing system.....

Fig. 4.13. Live load factor of the network arch from L.B.A and G.N.A analysis.....

Fig. 4.14. Influence of the lateral bracing stiffness in the live load factor..

Fig. 4.15. Influence of the lateral bracing stiffness in the live load factor; a) L.B.A; b) G.N.A.....

Fig. 4.16. Live load factor in function of the braced percentage of the arch in L.B.A.....

Fig. 4.17. Live load factor in function of the braced percentage of the arch in G.N.A; a) Variation in the live load factor; b) change in out-of-plane displacement of the arch.....

Fig. 4.18. Flowchart for the GMNIA procedure analysis in braced arches.....

Fig. 4.19. Global lateral behaviour of the unbraced network arch bridge under vertical loads; a) Stress variation in the section; b) Buckling behaviour of the arches.....

Fig. 4.20. Global lateral behaviour of the braced network arch bridge under vertical loads; a) Stress variation in the section; b) Buckling behaviour of the arches.....	
Fig. 4.21. Position of the three first hinges in the arch rib; a) First hinge close to the support; b) First hinges close to the arch midspan.....	
Fig. 4.22. Stress state in the arches, formation of plastic hinges: Unbraced arches.....	
Fig. 4.23. Stress state in the arches, formation of plastic hinges: Braced arches.....	
Fig. 4.24. Vertical live loads – lateral deflection curves for unbraced and braced arch bridge; (a) $L^{\text{Braced}}=50$ m; (b) $L^{\text{Braced}}=60$ m; (c) $L^{\text{Braced}}=70$ m; (d) $L^{\text{Braced}}=80$ m; (e) $L^{\text{Braced}}=90$ m.....	
Fig. 4.25. Out of plane behaviour of network arch bridges under traffic loads.....	
Fig. 4.26. Loading stages for analysis of global model: a) quasi-static analysis for permanent loads, b) time-history analysis for cable loss.....	
Fig. 4.27. Bridge configuration for cable loss scenario.....	
Fig. 4.28. Dynamic sensitivity of the bridge after cable loss scenarios.....	
Fig. 4.29. Structural capacity of the arch subjected to one cable loss scenario.....	
Fig. 4.30. Variation of the ultimate resistance of the arch considering various cable loss scenario for different braced length.....	
Fig. 5.1. Geometry and Section of structural elements of the cable-stayed bridge. a) Closed box section for pylon, transverse and base pylon b) Deck section.....	
Fig. 5.2. Blast pressure distribution over time.....	
Fig. 5.3. Geometrical characteristic of the bridges. a) Harp bridge; b) Fan bridge; c) Semi-Fan bridge; d) Longitudinal profile of the bridge; e) Transverse section of the pylon from the left to the right Harp, Fan and Semi-fan system.....	

Fig. 5.4. Structural response of the three cable configuration in the case of blast at $x= 6.2$ m. From the left to the right displacement, Strain and Stress of the bridge’s deck.....

Fig. 5.5. Structural response of the Harp pattern with blast at $x = 62.8$ m and $R = 1$ m. a) Displacement b) Strain c) Stress.....

Fig. 5.6. Structural response of the Harp pattern with blast at $x = 201.5$ m and $R = 1$ m. a) Displacement b) Strain c) Stress.....

Fig. 5.7. Blast loading analysis in cable-stayed bridge. a) $W = 500$ kg, b) $W = 500$ kg, c) $W = 500$ kg, d) $W = 500$ kg, e) $W = 1500$ kg.....

Fig. 5.8. Total fibre stress in MPa of the deck of Harp configuration for two different blast intensities at two different locations, a) $x = 6.2$ m and b) $x = 201.5$ m.....

Fig. 5.9. Geometrical characteristics of the bridges. From the left to the right: Inverted Y-shaped profile; H-shaped profile, A-shaped profile.....

Fig. 5.10. Flowchart for the capacity and demand assessment of cable-stayed bridges.....

Fig. 5.11. Bilinear force-displacement relationship of cable-stayed bridges a) Set of bilinear capacity curves of deck in Fan cable-stayed bridge; b) Set of the structural performance.....

Fig. 5.12. Force-displacement relationship of a damage index.....

Fig. 5.13. Distribution of blast parameters for blast demand.....

Fig. 5.14. Prediction of blast demand in cable-stayed bridges: a) Harp bridge model; b) Fan bridge model; c) Semi-fan bridge model.....

Fig. 5.15. Blast fragility for Fan cable-stayed bridge.....

Fig. 5.16. Blast fragility for Harp cable-stayed bridge.....

Fig. 5.17. Blast fragility for Semi-fan cable-stayed bridge.....

LIST OF TABLES

Table 1.1. Damage causes of various steel buildings [1.3]	
Table 2.1. Resume of early contribution involving the plate stability.....	
Table 2.2. Geometry and material properties used in the practical example.....	
Table 2.3. Geometry and material properties used in the practical example..	
Table 2.4. Buckling coefficient of plate under patch loading only.....	
Table 2.5. Buckling coefficient of plate under bending stress only.....	
Table 2.6. Buckling coefficient of plate under shear stress only.....	
Table 2.7. Buckling coefficient of plate under combined patch loading and bending.....	
Table 2.8. Buckling coefficient of plate under combined patch loading and shear.....	
Table 2.9. Buckling coefficient of plate under combined bending and shear..	
Table 2.10. Buckling coefficient of plate under combined bending, patch loading and shear.....	
Table 2.11. Appendix of proposed or updated formulas by authors.....	
Table 3.1. Characteristics of material and section tested for calibration.....	
Table 3.2. Geometry and mechanical characteristics of elastic restraint.....	
Table 3.3. Calibration of the elastic restraints ($F=100$ kN).....	
Table 3.4. Buckling coefficients of plate under patch loading only ($a/b=2$)....	
Table 3.5. Parameters taking into consideration in the FEM analysis.....	
Table 3.6. Parameters used to determine the critical buckling load factor...	
Table 3.7. Range of applicability of the design formula.....	
Table 3.8. Design coefficients used in case of patch loading length as parameter.....	
Table 3.9. Design coefficients used in case of patch loading magnitude as parameter.....	
Table 3.10. Design coefficients used in case of plate slenderness as parameter.....	

Table 3.11. Design coefficients used in case of panel aspect ratio as parameter.....	
Table 4.1. Cross-section of structural elements. (1) Tie beam, (2) Arch, (3) Secondary beam, (4) Arch transversal beam, (5) Cable, (6) Lateral bracing.....	
Table 4.2. Section dimensions of the structural elements considered in the analysis.....	
Table 4.3. Buckling shape of the first four mode for the Network arch bridge.....	
Table 5.1. Dimension of the structural element of the cable-stayed bridge....	
Table 5.2. Material characteristics of the structural members.....	
Table 5.3. Maximum vertical displacement of the deck under a blast loading at stand-off $R = 1\text{m}$	
Table 5.4. Uncertainties in geometrical and material characteristics of the bridge.....	
Table 5.5. Uncertainties in the section of structural component.....	
Table 5.6. statistic properties for structural parameters of cable-stayed bridges.....	
Table 5.7. Limit state for cable-stayed bridges under Blast loading [5.52]	

CHAPTER 1

INTRODUCTION

1.1 Introduction

Bridge failures have occurred since bridge construction began thousands of years ago. Much of the technical knowledge associated with bridge engineering today is based on past bridge failures. Over the past century, bridge engineers have learned a lot by studying historical bridge failures. Considering only steel structures, a study of the cause of damage and type of structures was made in [1.1]. The study is quite interesting since steel is widely used for various types of structures. 448 damage cases were reported. Approximately 98 % occurred in the period of 1955 to 1984 and 62% in less than 30 years after erection [1.2]. The damage cases can be assigned to the type of structures as follows [1.3]:

- Buildings (including industrial buildings and crane supporting structures) 45.1 %
- Railway bridges 16.1 %
- Cranes 15.0 %
- Road bridges 8.7 %
- Plant and big machinery used in surface mining 8.0 %
- Masts and towers 5.8 %
- Other steel structures 1.3%

As can be seen, bridges (combining railway and roadway) are among the structures most often damaged. Another way of looking at the study is to separate by the cause, which leads to each damage as it is presented in Table 1.1. From this table, it can be seen that the stability and static strength are often cited as the main cause of the collapse in bridges industry for recorded damages.

Table 1.1. Damage causes of various steel buildings [1.3]

Damage causes (multiple denomination possible)	Totality		Buildings		Bridges		conveyors	
	No	%	No	%	No	%	No	%
Static strength	1611	29.7	102	33.6	19	14.8	40	36.0
Stability (local and global)	87	16.0	62	20.4	11	8.6	14	12.6
Fatigue	92	16.9	8	2.6	49	38.3	35	31.5
Rigid body movement	44	8.1	25	8.2	2	1.6	17	15.3
Elastic deformation	15	2.8	14	4.6	1	0.8	0	0
Brittle fracture	15	2.8	9	3.0	5	3.9	1	0.9
Environment	101	18.6	59	19.4	41	32.0	1	0.9
Thermal loads	23	4.2	23	7.6	0	0	0	0
Others	5	0.9	2	0.7	0	0	3	2.7

Sum	543	100	304	100	128	100	111	100
-----	-----	-----	-----	-----	-----	-----	-----	-----

Indeed, the stability or instability problems might represent a major concern in the mechanical function of civil engineering structures. For these structures, the idea behind stability/instability is often confined to the elastic part of the phenomena. However, a structural engineer should also consider the inelastic state of the elements under buckling.

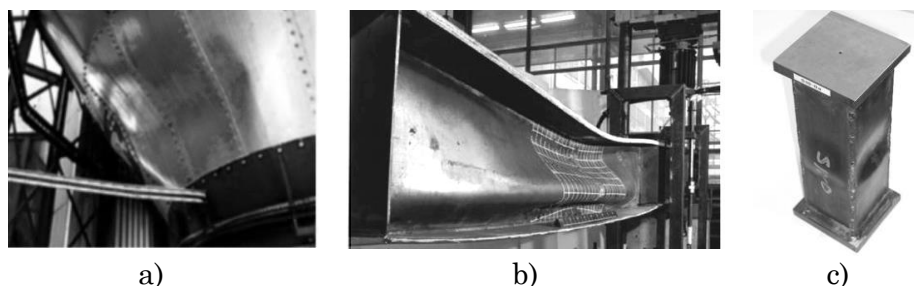


Fig. 1.1. Different example of instability problems: a) silos buckling; b) girder buckling; c) box profile buckling [1.3]

Buckling arisen in a structural element may involve the whole element through global buckling or locate only in particular region of the element known as local buckling (Fig. 1.1). Local buckling can lead to global buckling if adequate measures are not taken.

For a perfect understanding of the stability problem, the concept of an equilibrium state is raise. Under compressive load, steel structural member may become unstable and a new equilibrium is displayed. The bifurcation point or bifurcation load is an important concept in the stability theory. It represents the point which defines the stress state at which perfect structure becomes unstable. In the load-displacement curve describing the plate's behaviour under compressive stresses, a load level lower than the bifurcation point corresponds to a state where elastic buckling occurs [1.4] (Fig. 1.2a). In the specific case of thin plates, the in-plane loading might cause either local or global buckling leading to the reduction in the load-bearing capacity of the plate elements [1.5], [1.6]. At this level, the plate shows lateral deformations since the critical stress is reached and the deflection can be either positive or negative in regard to the plate's coordinate system Fig. 1.2b.

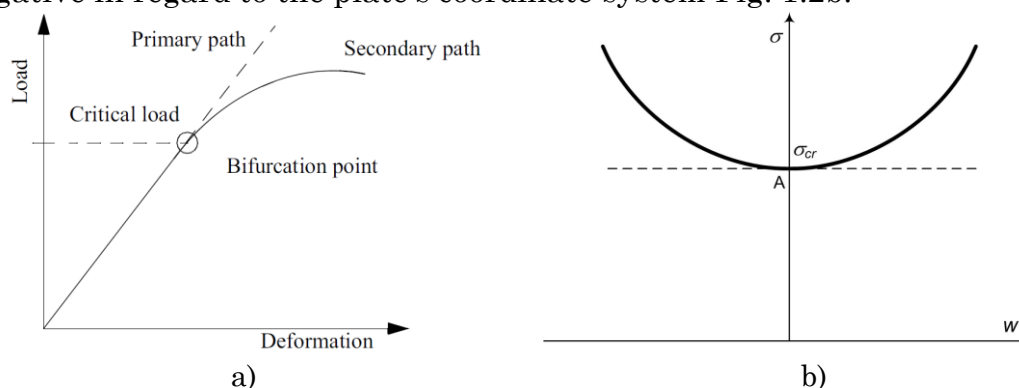


Fig. 1.2. Buckling description of structural element. a) Bifurcation of equilibrium; b) plate buckling and bifurcation at point A [1.7].

On the other hand, the above studies focused mainly on bridges subjected to conventional loads such as permanent and traffic while bridges during its service life might be sometimes subjected to malicious actions with a high impact on structural elements. Besides earthquake which is still considered as one of the frequent high impact loading actions in bridges industry, other actions such as collisions, blast loading, etc,... may present almost the same damage risk for existing bridges. Indeed, recent reports depicted an increase of structural failure due to extreme loading condition [1.8]–[1.11]. Many approaches such as elastic plate theory, Timoshenko beam theory or equivalent single degree of freedom system were used efficiently by previous authors to investigate the damage prediction of the structural element after a blast loading [1.12]. However, the bridge is a rigid structure which consists of several structural systems each one involved in the whole performance of the structure. The ability to withstand conventional or extreme actions is linked to the structural systems, to the material and to the structural sections [1.13]. This concept is also known as robustness is now possible to be evaluated for various typologies of structures or bridges, in particular, owing to the recent advancement of computational mechanics. Finally, since critical damages and collapses of bridges can affect its in service, the human lives, as well as the economy, can be disrupted, the robustness of bridges should be a critical concern for structural engineers.

1.2 Objectives of the study

Our research field was expanded to three main bridges typologies such as steel girder bridges, network arch bridges, and cable-stayed bridges. The research focuses mainly on the structural behaviour and/or performance of steel bridges subjected to conventional or extreme loading conditions.

Steel girders bridges probably represent one of the most steel bridge typologies in service around the world. These bridges consist of concrete or steel deck supported by steel girders. During the launching process of the bridge, unstiffened girders made of thin plates may undergo buckling problems [1.6]. On the other hand, the possible combined effect of in-plane loading around the piers may accelerate the buckling phenomenon. In this stage, intensive parametric analyses are performed to give a new insight into the buckling response of the steel plate in the case of interaction of in-plane loading.

Secondly, the network arch bridges were investigated. This typology of steel bridges is still competitive for small to medium span since in recent years numerous projects were concluded or recently started. However, a problem that remains constant is related to the out-of-plane instability of the steel arch structure that this type of structure may encounter. Thus, as part of our research, through intensive non-linear analysis, a detailed description of the out-of-plane behaviour of the structure under traffic loads was presented. The

consequences of sudden cable losses in the post-critical buckling of the bridges were also assessed.

Finally, the structural consequences induced by accidental actions applied on cable-stayed bridges are also investigated. In particular, the structural performance of cable-stayed bridges subjected to blast loadings was the main interest. In this study, three types of cable-stayed bridges were evaluated, namely Fan, Semi-fan and Harp bridges. The objective of the study was first to evaluate the stresses, strains, and displacement on the deck and other structural elements and then to evaluate the likelihood of failure of the structural elements observed following such an event. This study also raises the concept of robustness and progressive collapse of a structure that is a Phenomenon of the global collapse of a structure observed following a failure of one or more structural elements adjacent to the structure.

1.3 Thesis organization

To reach the objectives defined above the thesis has been structured in the following outline and will consist of 5 chapters besides the conclusion.

- **Chapter 1.** A general introduction is presented to set the context, and define the objectives, outlines, results and observations made following each case study.
- **Chapter 2.** presents, as with all scientific work, the recent progress on the problem of instability of steel plates. Thus, research on the stability of steel plates between two periods marked on the one hand by the use of analytical methods and on the other by the spread of numerical resources that have made it possible to give an overview of this issue.
- **Chapter 3.** In this chapter, FEM model investigations are conducted to study the instability of steel plates subjected to an interaction between in-plane loading. At the end of the various analyses carried out, the results made it possible to derive analytical equations to determine the influence of the load combinations.
- **Chapter 4.** Presents the study of lateral resistance or post-critical behaviour of network arch bridges subjected to vertical actions. Among other things, the consideration of the sudden breakage of a cable and the lateral sensitivity observed following such event on the lateral capacity of the bridge were highlighted.
- **Chapter 5.** Investigates the structural performance of cable-stayed bridges subjected to extreme actions. In this particular case, three patterns of stays were considered to be exposed to the blast loading

action and their structural response was presented to determine the most robust. Finally, the study of the likelihood of rupture of the different typologies through the blast fragility curve is presented to conclude our work.

- **Chapter 6.** The chapter summarizes the outcomes from the various intensive numerical investigations made in the research. Some important results are reported in this section and the thesis ends with the outgoing research or future developments.

1.4 References

- [1.1] Y. Aoki, “Analysis of the Performance of Cable-Stayed Bridges under Extreme Events,” no. April, 2014.
- [1.2] C. Loss and P. G. Parke, “STRUCTURAL RESPONSE OF CABLE-STAYED BRIDGES TO OLUREMI OLAMIGOKE . BEng , MSc A Thesis submitted in partial fulfilment for The Degree of Doctor of Philosophy Civil and Environmental Engineering Faculty of Engineering and Physical Sciences University of Surrey Supervised by :,” 2017.
- [1.3] J. Gozzi, “DOCTORAL THESIS Patch Loading Resistance of Plated Girders -Ultimate and serviceability limit state-,” 2007.
- [1.4] Z. Qinghua, B. U. Yizhi, and L. I. Qiao, “Review on Fatigue Problems of Orthotropic Steel Bridge Deck China Journal of Highway and Transport Review on Fatigue Problems of Orthotropic Steel Bridge Deck,” no. November, 2017.
- [1.5] B. Kövesdi, J. Alcaine, L. Dunai, E. Mirambell, B. Braun, and U. Kuhlmann, “Interaction behaviour of steel I-girders; Part II: Longitudinally stiffened girders,” J. Constr. Steel Res., vol. 103, pp. 344–353, 2014.
- [1.6] B. Kövesdi, “Patch loading resistance of slender plate girders with longitudinal stiffeners,” J. Constr. Steel Res., vol. 140, pp. 237–246, 2018.

- [1.7] M. Clarin, “Plate Buckling Resistance - Patch Loading of Longitudinally Stiffened Webs and Local Buckling,” 2007.
- [1.8] S. P. Stefanidou and A. J. Kappos, Bridge-specific fragility analysis: when is it really necessary?, vol. 17, no. 4. Springer Netherlands, 2019.
- [1.9] A. Kumar and V. Matsagar, “Blast Fragility and Sensitivity Analyses of Steel Moment Frames with Plan Irregularities,” *Int. J. Steel Struct.*, vol. 18, no. 5, pp. 1684–1698, 2018.
- [1.10] S. Stefanidou and A. Kappos, “Optimum Selection of Retrofit Measures for R/C Bridges Using Fragility Curves,” no. July, pp. 894–911, 2017.
- [1.11] Y. Pang, X. Wu, G. Shen, and W. Yuan, “Seismic Fragility Analysis of Cable-Stayed Bridges Considering Different Sources of Uncertainties,” *J. Bridg. Eng.*, vol. 19, no. 4, p. 04013015, 2013.
- [1.12] H. Hao and E. K. C. Tang, “Numerical simulation of a cable-stayed bridge response to blast loads, Part II: Damage prediction and FRP strengthening,” *Eng. Struct.*, vol. 32, no. 10, pp. 3193–3205, 2010.
- [1.13] E. K. C. Tang and H. Hao, “Numerical simulation of a cable-stayed bridge response to blast loads, Part I: Model development and response calculations,” *Eng. Struct.*, vol. 32, no. 10, pp. 3180–3192, 2010.
- [1.14] . S. V., “Blast Resistant Design of Structure,” *Int. J. Res. Eng. Technol.*, vol. 04, no. 25, pp. 64–69, 2016.

CHAPTER 2

LITERATURE REVIEW OF STEEL PLATE UNDER COMBINED IN-PLANE LOADING

The use of incremental launching process as an erection methodology of bridges has undergone big diffusion from the second half of the twentieth century to the present day. This is a result of the several advantages this method can provide in terms of optimizing time-consuming and auxiliary support elements involved. On the other hand, the incremental launching method becomes inevitable when the bridge is to be built in a challenging site like deep valleys, deep-water crossings or environmentally protected species, etc... Due to several advantages in terms of durability, speed of design and construction, cost-effectiveness and sustainability, steel material is commonly used in the bridge industry. The incremental launching process implies that bridge superstructure is firstly assembled on one side of the obstacle before being crossed and pulled longitudinally into its final position. Steel material stands out as a must-have material for this construction process due to its relatively low weight.

Due to the bearing's reaction that can be raised near the bridge piers and under the effect of self-weight of the launching nose equipment as well as the distance between two consecutive bridge supports, steel girders which are mostly built-in with thin plate elements are often subjected to various actions during the erection of the bridge. These actions are exerted on girder elements as concentrated loads, bending and shear forces or as the combined effect of loadings. The slender plates are then prone to buckle under those various forces. Depending on the slenderness ratio of the steel plate, it is a common practice to provide on girders, transversal and/or longitudinal stiffeners to limit the risk of local or global buckling of the structural element. Thus, to avoid unacceptable damage whether during the erection or in the bridge's service, it becomes important not to study only the failure of the structural element by reaching the admissible stress but also to focus on the elastic buckling of the slender plate. The different results will bring new insights into the problem and will allow the use of steel material efficiently.

The existence of stiffeners in steel plate may provide several advantages. From a stability point of view, stiffeners increase the buckling capacity of the plate. In particular, if they are well designed, they will change the buckling mode from global to the local subpanel. A stiffener is a plate or section attached to a plate to resist buckling or to strengthen the plate [2.1]. It is connected to a plate through continuous welding and can be either longitudinal or transversal. In bridge engineering, the choice of using steel girder with either thick unstiffened web plate or stiffened thin plate is governed by the allowed

financial resources. The engineers should be able to make a comparison between the costs of the welding process of stiffeners on thin-plate and the price of a thicker steel section [2.2]. Several scientists studied in recent decades the influence of stiffeners, the optimal geometry and position in the critical, post-critical buckling [2.3], [2.4], [2.5]. Others focused their investigations on the improvement of ultimate strength provided by the presence of one or many stiffeners [2.6], [2.7].

According to several authors, thin steel plates are used in many engineering fields. In marine engineering, ship structures are made of steel plate. In bridge engineering, the use of a steel plate is common for girders. Finally, for offshore as well as aerospace structures, steel plates are also used. From one reason to another, the presence of holes is often indispensable. In particular, for what regards bridge engineering, openings are provided for maintenance and inspection utilities or for the architectural purpose [2.8]. The presence of holes can extremely change the structural behaviour of steel plate through redistribution of normal and shear stresses leading to a considerable reduction of ultimate strength and critical buckling of steel plate. For this reason, significant researches have been carried out in order to better understand the modification in the failure mechanism of steel plate due to holes' presence.

This chapter aims to present a general review of current developments about ultimate resistance and critical buckling of steel plate girders considering plate without stiffeners, plates with longitudinal and/or transversal stiffeners and plates with a hole. It will be possible from this paper to have great insight on the behaviour of steel plate under loading condition, the importance of using stiffeners and the influence of hole position, shape and dimension in the steel plate response. To attain this goal more than 90 scientific papers published in international journals have been viewed in details. The methodology of searching and selection of articles was made on the basis of keywords as interaction, bridge launching, plate buckling, failure mechanism, perforated plate...

Firstly, an introduction is addressed where historical studies on different topics (loading configurations) are presented, then as the second part and third part, first results and recent developments within this field are presented and finally before conclusion, an illustrative practical example to prove the applicability of developed formulas found in the literature is done. In addition, two important periods as advised by Hajdin and Markovic [2.9] have been considered. The second part of the document will be focused on the results of the pioneers' investigation done before 1992 while the third part will present conclusions and solutions found recently after 1992.

2.1 Investigation of steel plate buckling before 1992

This period is characterized by researches done unfrequently due to the lack of resources. In particular, investigations were based on intensive experimental

campaign and theoretical investigation. Most of the results found in this period have been used for the development of design codes.

2.1.1 Unstiffened plate

In bridge engineering, patch loadings are defined as concentrated loads generated by piers reaction during bridge launching. In fact, during the construction process of many steel and/or composite bridges using the incremental launching method, steel girders are pulled from one end to another and they will pass through flange over intermediate bridge piers. In general, these loads are considered applied over a portion of area or length of a structural element.

2.1.1.1 Purposes and methodology of early researches

The problem related to plate stability started to become a research topic very long time ago. In fact, Girkmann [2.10] is considered as the first researcher to study this phenomenon although some authors attribute it to Timoshenko. In 1936, Girkmann [10] worked on a rectangular plate with simply supported edge condition; he investigated the critical buckling coefficient of the plate under edge loading and the results were valid only for aspect ratio. After, Zetlin [2.11], Khan et al. [2.12] and Chin et al. [2.13] have done some theoretical studies aiming to determine numerically the linear buckling load of a simply supported plate. Several other authors continued the investigation around the same period; Zetlin [2.11] in 1955, Basler [2.14] in 1961, Rocky and Bagchi [2.15] in 1970, Khan et al. [2.12] in 1972 for the most relevant. All of them were looking for the critical buckling coefficient under partial edge loading within most cases similar constraint condition and using different methods. Zetlin [2.11], Khan et al. [2.12] used the energy method based on the principle of conservation of energy while Rocky and Bagchi [2.15] used the finite element method. Fig. 2.1 shows the plate configuration used by Zetlin with simply supported edges condition. Basler [2.14] considered two boundary conditions: a simply supported condition and the clamped condition. For the clamped condition, it is worth notating that only the edge under load was clamped and the other three edges without load were simply supported. An example of the Basler's [2.14] model used in the campaign is presented in Fig. 2.2.

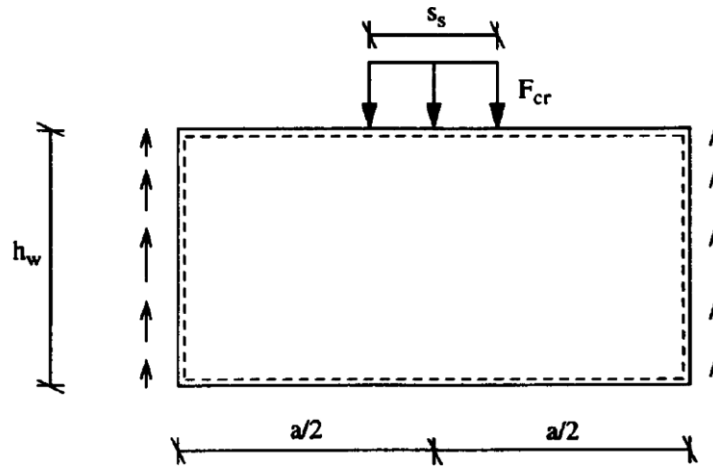


Fig. 2.1. Zetlin's model in 1995 [2.11]

The investigation of elastic buckling load does not allow determining the full capacity in steel plate. Rockey and Bagchi [2.15] did early researches on the ultimate strength of plate girders. They included in their investigation the interaction between flange and web. Bergfelt [2.16], Dubas and Tchamper [2.17] performed numerous experiments and developed solutions for the ultimate load; it was related to the critical buckling load based on Karman approach.

More recently with respect to other authors, Al-Bermani and Kitipornchai [2.13] in 1992 focused their work on the validation of innovative method of analysis through numerical techniques. The aim was to compare their results with those from previous experimental and analytical investigations.

Elgaaly and Nunan [2.18] in 1989 were the firsts to perform experimental and numerical analysis on steel girder under patch loading applied eccentrically. The tests performed were done at Maine University. After, several scientists continued to work on the topic; Elgaaly and Salkar [2.19], Lučić and Drdacky [2.20] from the Czech Academy of Sciences also did some investigations in the topic.

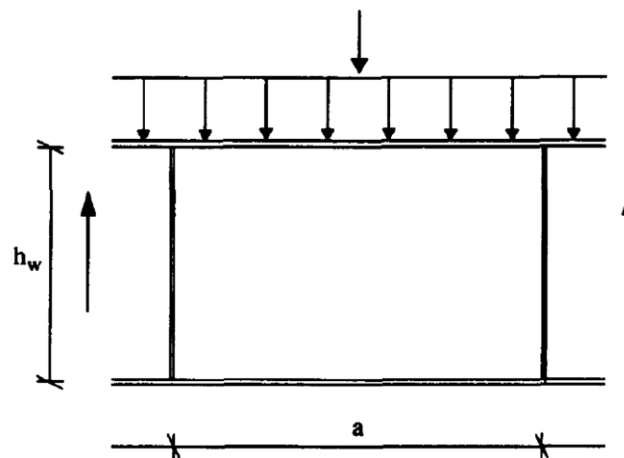


Fig. 2.2. Basler's model in 1961 [2.14]

Shear loading individually has not been studied in-depth in this period like others loading configuration; the most significant works on this topic were done on steel plates with two different boundary conditions: simply supported and clamped plate. Numerical analysis to investigate the shear-loading effect on simply supported plates has been carried by Stein and Neff in 1947 [2.21]. Concerning experimental works, D'Apice et al. [2.22] performed several tests on unstiffened as well as longitudinal stiffened girders focusing on the collapse mode of girder under shear forces while Delesques [2.23] in 1974 presented a new model to find critical shear stresses. Höglund [2.24] used the rotated stress field theory to define the resistance against shear of steel plates susceptible to buckle.

Concerning bending loading, D'Apice et al. [2.22] in 1966 have conducted an experimental survey on the resistance of slender plate while Dubas and Tschamber [2.17] focused experimentally on buckling issues of unstiffened as well as longitudinally stiffened slender girders.

Many researchers [2.16], [2.25], [2.26] have been involved in the investigations of the interaction between of loading configurations (M-V, M-F, and V-F), their investigations were focused mainly on resistance or ultimate strength of plate girders respect to the elastic buckling. Some of them initiated researches during their PhD thesis [2.25].

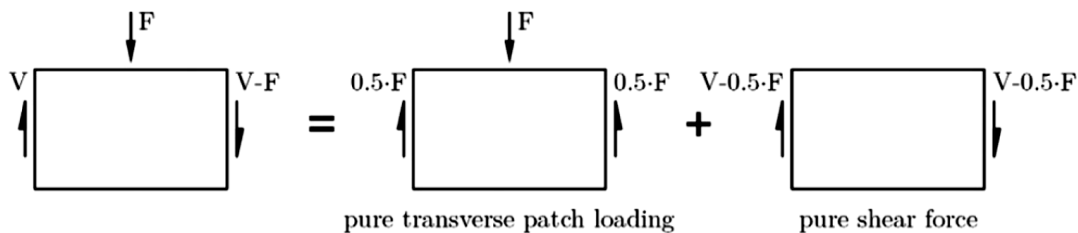


Fig. 2.3. Basic load cases of combined shear and patch loading [2.27]

Being the most common case in bridge engineering, several researchers in the past proved that the combined effect of bending and transverse force is an important issue of the bearing capacity of the plate. Bergfelt [2.16] started the first research on this topic in 1971; several tests have been performed to determine the combined effect of both patch loading and bending applied simultaneously. From Bergelt [2.16] to Ungermann [2.25], different equations describing the M-F interaction have been proposed.

The combined effect of both shear and patch loading on steel plate has also been investigated. In most studies, the analysis of combined shear and patch loading is subdivided into two different cases (“pure patch loading” and “pure shear force”) as shown in Fig. 2.3.

2.1.1.2 Results and comments

From the early researches, different expressions of the critical buckling coefficients were found. The buckling coefficients presented by Basler [2.14] in 1961 were not a function of the edge loading length but only on the plate aspect

ratio as shown by [Eq.(2.1)] and [Eq.(2.2)] for cases of simply supported edge and clamped edge condition respectively.

$$k_F = 2.0 + \frac{4}{(a/h_w)^2} \quad (2.1)$$

$$k_F = 5.5 + \frac{4}{(a/h_w)^2} \quad (2.2)$$

The critical buckling coefficient defined by Al-Bermami and Kitipornchai [2.13] in 1992 was more accurate with respect to those proposed by Basler. They presented a new expression of k_F as function of a/h_w , s_s/h_w , and s_s/a for a plate with simply supported edge [Eq.(2.3)]. The results presented showed a good correlation with those of previous authors.

$$k_{F,ss} = 2.1 + 1.2 \left(\frac{h_w}{a}\right)^2 + \left(\frac{s_s}{h_w}\right)^2 \left[0.4 + 2.0 \left(\frac{h_w}{a}\right)^2\right] \text{ for } \frac{s_s}{h_w} \leq 1.0 \quad (2.3)$$

The evaluation of elastic buckling load can be done using the [Eq.(2.4)]. In fact, knowing the elastic critical buckling load is very important in a physical point of view during the design phase, because as the plate configuration is changing, it is actually the critical step that will eventually lead to complete failure. This formula is effective for different single loading configuration of bending stress, patch loading, and shear force. The critical buckling coefficient changes its value in term of loading and boundary condition. A great job on the theory of structural analysis of plates has been done by Timoshenko [2.28].

$$F_{cr} = k \frac{\pi^2 E}{12(1-\nu^2)} \frac{t^3}{h} \quad (2.4)$$

Roberts and Rockey [2.29] presented a failure mechanism observed on steel I-profile under edge loading as shown in Fig. 2.4. The model was characterised by the formation of four plastic hinges in the flange and three yield lines in the web near the loaded flange. Roberts and Markovic [2.30] continued investigation in order to develop new models for the ultimate load-carrying capacity.

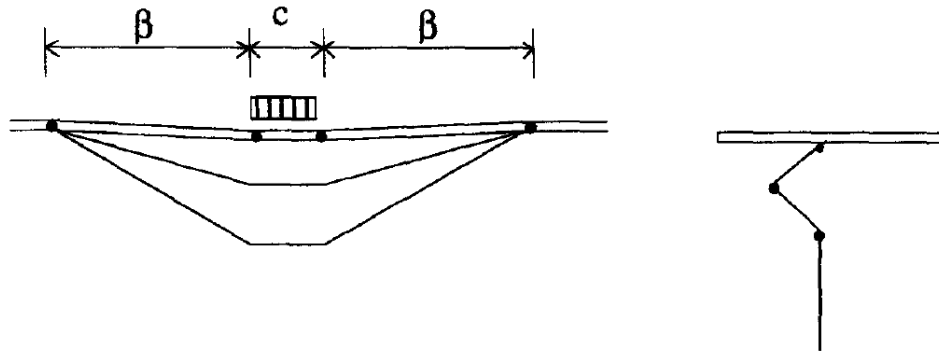


Fig. 2.4. Failure mechanism assumed by Roberts [2.29]

Bergfelt [2.16], Dubas and Tchamper [2.17] performed numerous experiments and developed equations to obtain the ultimate load of steel plate

under compressive forces; it was related to the critical buckling load based on Karman approach.

$$P_{ult} = \sqrt{P_{cr} \times P_y} \quad (2.5)$$

According to Roberts [2.29], the ultimate resistance P_u of slender plate girder against patch loading is given by the minimum between two resistances: the first one P_{ub} is resistance due to the fold development at a position near the loaded flange and the second one P_{uy} resistance due to web yielding whose expressions are the following:

$$P_{ub} = \frac{1.1t_w^2}{F} (E\sigma_{yw})^{0.5} \left\{ \frac{t_f}{t_w} \right\}^{0.25} \left\{ 1 + \frac{c_e t_w}{d_w t_f} \right\} \left[1 + \frac{3c}{d} \left(\frac{t_w}{t_f} \right)^{3/2} \right] \quad (2.6)$$

$$P_{uy} = (16M_{pf}\sigma_{yw}t_w)^{0.5} + \sigma_{yw}t_w c_e \quad (2.7)$$

The final solution obtained by Roberts with some simplifications and adapted to match experimental results was adopted in the British Standard [2.8] and became part of the 1992 version of the Eurocode 3 [2.1].

$$P_u = 0.5t_w^2 \left(E\sigma_w \frac{t_f}{t_w} \right)^{1/2} \left[1 + \frac{3c}{d} \left(\frac{t_w}{t_f} \right)^{3/2} \right] \quad (2.8)$$

Data obtained from the analysis of tests performed by Elgaaly and Nunan [2.18] in 1989, Elgaaly and Salkar [2.19], Lučić and Drdacky [2.20] showed that the ultimate resistance of plate girder was reduced from the moment that the eccentricity was increased. A reduction coefficient “R” has been defined to show the influence of eccentricity in the reduction ultimate resistance of plate. Detailed information can be found in [2.31].

Höglund [2.24] derived from the tension field theory an equation [Eq.(2.9)] to describe the ultimate shear resistance of both stocky and slender steel plate. It was innovative works since the two methods already present in EC3-1-1 have been replaced after by his results. Johansson [2.32] and Höglund [2.24] gave more details about the shear investigation. From the analysis performed by Stein and Neff [2.21] in 1947, it was possible to draw the variation of buckling coefficient of unstiffened plated under shear force in terms of panel aspect ratio.

$$\frac{\tau_u}{f_v} = \frac{\sqrt[4]{4}}{\lambda_w} \sqrt{\sqrt{1 - \frac{1}{4\lambda_w^4} - \frac{1}{2\sqrt{3}\lambda_w^2}}} \quad (2.9)$$

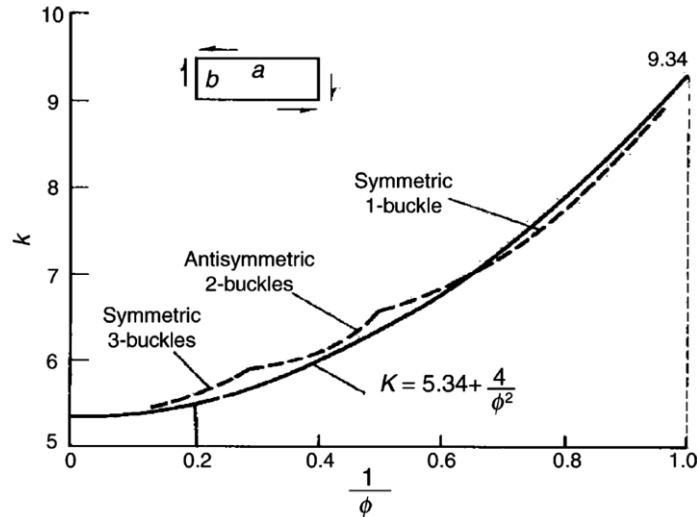


Fig. 2.5. Buckling coefficient for unstiffened plates against shear [2.21][2.21]

Cooper [2.34] in 1964 worked on both steel class 3 and class 4 section and at the end, an empirical equation has been proposed to determine the ultimate resistance of plate girder under bending stress as shown in [Eq.(2.10)].

$$M_u = M_y \left\{ 1 - 0.0005 \frac{A_w}{A_f} \left(\frac{d_w}{t_w} - 5.7 \sqrt{\frac{E}{\sigma_{yf}}} \right) \right\} \quad (2.10)$$

In regards to plate girder under combined in-plane loading, the shear force is generally carried by the web only when the uniform yielding of the web governs the ultimate resistance of girder against shear and this should be only possible when the full bending capacity of the flange is not reached. The combined effect of shear and bending is then possible in the web when flanges are not able anymore to sustain bending stress. Basler [2.14] proposed the first formulation of the M-V interaction. After, several investigations have been performed to draw the actual current EN1993-1-5 [2.35]. Fig. 2.6 shows the M-V interaction proposal from Basler and EN 1991-3-5 [2.35].

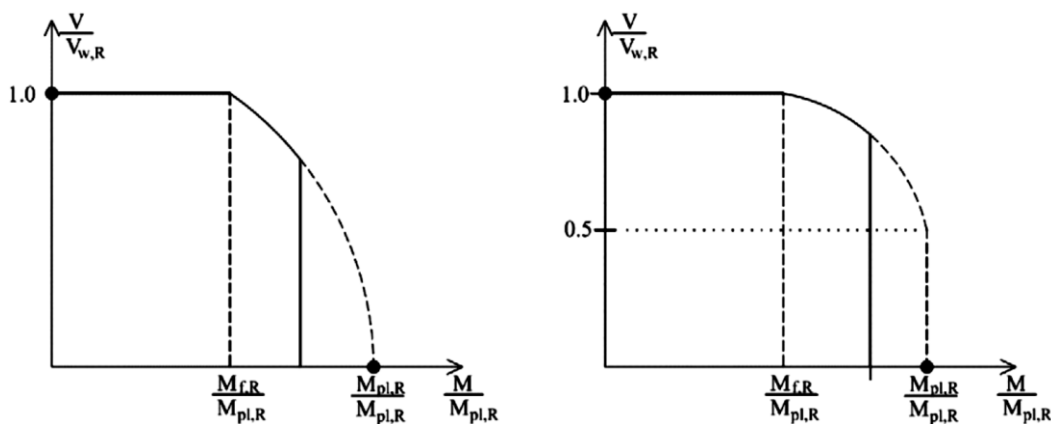


Fig. 2.6. a) M-V interaction diagram by Basler's [2.14]; b) M-V interaction diagram by EN1993 – 1 – 5 [2.35]

From Bergelt [2.16] to Ungermann [2.25], different equations describing the M-F interaction have been proposed. Eq.(2.11) and Eq.(2.12) are respectively interaction equations derived by Bergelt and Ungerman in 1971 and 1990.

$$\left(\frac{F}{F_R}\right)^8 + \left(\frac{M}{M_R}\right)^2 \leq 1.0 \quad (2.11)$$

$$\left(\frac{F}{F_R}\right) + \left(\frac{M}{M_R}\right) \leq 1.4 \quad (2.12)$$

The combined effect given by shear and patch loading on steel plate has also been investigated. In most studies, the analysis of combined shear and patch loading is subdivided into two different cases (“pure patch loading” and “pure shear force”) as shown in Fig. 3. Elgaaly [2.18] proposed first results from experimental tests on this topic and Oxfort et al. [2.36] in 1981 performed experimental research activity on three specimens. The result from experiments showed that the effect of high shear force did not influence considerably the ultimate resistance of steel plate against patch loading. Zoetemeier [2.37] performed special experiments on I-girders, and he found the following interaction equation.

$$\left(\frac{V - 0.5 F}{V_R}\right)^{2.0} + \left(\frac{F}{F_R}\right)^{2.0} \leq 1.0 \quad (2.13)$$

Further information about the investigation in the combined M-V, M-F and V-F is provided in [2.38], [2.27]. Regarding the combined M-V-F, there is no past information in the literature on the topic. In the last two decades, some researches started to study the structural behaviour of plate girders under the combined effect of these loads.

2.1.2 Unstiffened plate with hole

In civil engineering and particularly in bridge engineering, built structures usually need technical inspection either to change coating surface or to strengthen or repair some defaults. For these reasons, holes can be unavoidable on structural elements. Sometimes aesthetic reasons are also considered as other justification why holes with variable geometries are presents in structural elements. When using steel girders in bridge construction, changes in structural behaviour due to the redistribution of plane stresses as a consequence of the presence of the holes will always occur. For this reason, the effect of holes in terms of geometry, diameter, and position have been researching topics of some scientists is' the last two decades.

2.1.2.1 Purposes and methodology of the early research

Finite element method, which used numerical techniques to solve problems and Conjugate Load/Displacement (CLDM) Method have been widely used for the structural analysis of holes effect on a steel plate. In 1967, Rockey et al. [2.39] analysed the effect of circular holes on square shear panel; several authors like Shanmugam et al. [2.40] in 1982, Azizian et al. [2.41] in 1983 and

Sabir et al. in 1983 also worked on this topic. All of these authors used FEM to study the stability of a perforated square panel under compression.

Redwood et al. [2.42] carried out other significant studies in 1978; they tested slender webs with holes while between 1987 and 1990. Brown et al. [2.43] used CLDM to determine the critical load of plates with rectangular holes located at the center under different loading conditions.

Shakerley and Brown [2.44] also used CDLM and they focused their research on the study of hole position in the instability analysis of square plate under axial or shear loads. Ravinger and Laščekov [2.44] focused their research on experimental verification of girders with circular holes. In 1984, Narayanan and Chow [2.45] analysed perforated plates in order to find their ultimate resistance when subjected to uniaxial compression while one year later Narayanan and Darwish [2.45] gave an insight to the effect of eccentric holes on the strength of slender web plates. Roberts and Azizian [2.41] have developed further works on plates with holes. From 1981 to 1984, Narayanan et al. [2.45] performed several experimental tests on perforated thin web plate of girders bridges with various geometries. The aim was to study the ultimate capacity of perforated plates under shear in one hand and in another hand under axial force.

2.1.2.2 Results and comments

From various investigations made by Rockey et al. [2.46], Shanmugam et al. [2.40] and finally Azizian et al. [2.41], they found that the increase in hole diameter up to a critical value leads to an increase of critical stress while the ultimate strength will decrease. A few years after, Brown et al. [2.43] found that the critical shear stress was more influenced by the increase in hole size in comparison to the critical axial and flexural stress which showed a slight change due to the moderate increase in hole diameter

According to Shakerley and Brown [2.44], a square hole with small size should be avoided to be positioned at the center of the plate under axial or shear loading while the effect is less important for the large square hole. Furthermore, in the case of a rectangular hole, it should be arranged on plates in an optimal way such that his major direction is perpendicular to the axis of loading.

The results of researches done from 1981 to 1984 by Narayanan et al. [2.45] led to the proposition of a design chart useful to find the ultimate capacity of perforated plates under shear or axial force. In the meantime, Shanmugam and Evans [2.40] used FEM analysis to find the ultimate load strength of plate under axial compression with the presence of circular or square hole located in the center of the plate. The results showed that both size's hole and plate slenderness ratio affect significantly the ultimate resistance. Further information in this topic is found in the following literature [2.39].

2.1.3 Unstiffened plate with hole

There are two principal ways commonly used to increase steel plate carrying capacity: either the plate slenderness is decreased by increasing the plate thickness or the bending stiffness of plate is increased by placing some

stiffeners in an appropriate location and designed properly. For these reasons, the behaviour of stiffened plates under different loading configuration have been widely studied experimentally as well as numerically. This subpart reviews first investigations on stiffened plates.

2.1.3.1 Purposes and methodology of the early research

The tremendous collapses of bridges occurred in the 1960s have led to a systematic investigation of instability on slender steel plate since it had been detected in most cases as the principal cause of many collapses. Among investigations, the shear strength of unstiffened web plate, as well as steel plate with transversal stiffeners, were studied [2.47]. Scientists like Komatsu, Porter et al. [2.46], Cooke et al., Evans and Charlier and Maquoi [2.48] performed experimental tests on steel plates with longitudinal stiffeners and from the results, mechanical models were proposed considering two extreme situations. The first one called “Cardiff model” and the second one “models of Ostapenko or Cooper”. In the first situation, the study was focused on only critical shear load on a steel plate with longitudinal stiffeners while in a second model, longitudinal stiffener was designed to create sufficient rigid support leading to local buckling instead of a global one.

In regards of the shear buckling, Stein and Fralich [2.21] in 1948 have analysed long plates transversally stiffened with simply supports as boundary conditions. Basler and Thürlimann [2.14] carried out analyses and experimental studies regarding the post-buckling strength of plate girders. Cook and Rocky [2.49] studied the critical shear buckling of infinitely long plates for both the simple support and clamped boundary conditions using transverse stiffeners made by closed section instead of open section stiffeners. Rockey and Cook [2.49] continued their earlier work and were able to obtain a useful design relationship between the critical shear buckling stress and the ratio of the torsional to flexural rigidity of the stiffener as shown in Fig. 2.7. The case of transverse stiffened plate infinitely long and clamped at edges was considered. Loughlan and Hussain [2.50] have done good literature on first works and conclusions developed on the subject in 2014.

In most cases, interaction equations for design verification of steel plate girder either unstiffened or with longitudinal stiffener are related. Schueller and Ostapenko [2.51] performed in 1970, experimental tests on I-girders with longitudinal stiffener under a combined effect of shear and bending stress. The aim was to study the local instability behaviour of the stiffened panel. In 1987, Evans [2.52] did further experimental tests on girders stiffened in the compression zone aiming to investigate the global buckling of stiffened. In regards of bending and patch loading, or shear load and patch loading interaction behaviour on steel girders, several experimental investigations have been performed in the past for unstiffened plate girders but there is not information when considering stiffened girders. The same situation is observed when bending stress, shear and patch loading are applied at the same time on the steel plate.

2.1.3.2 Results and comments

Longitudinal stiffener, when placed in judicious positions, could influence the behaviour of steel plate for what regards the mode of buckling and stress level. Rockey [2.15] found that the position of the longitudinal stiffener to obtain an optimal structural response for steel plate under pure bending stress was one-fifth of the height of the plate girders from the edge in compression. This position is not optimal when the ultimate shear strength of plate girder is analysed. Theoretical and experimental studies from T. Galambos [2.53] have led to the conclusion that longitudinal stiffeners should be placed at the middle of the steel plate to get maximum shear resistance of plate. Dubas [2.54] in 1948 and Rockey and Leggett [2.55] in 1962, worked on buckling of a longitudinally stiffened plate under bending stress; the first considered the case of simply supported edge panel while the latter worked on fixed edge condition. From their researches, it was decided that the optimum position of the longitudinal stiffener is 0.20 times the height of the web for simply supported plates and 0.22 times the height of the web for a clamped plate. Further information regarding first investigations of the influence of longitudinal stiffeners on plate girders can be found in [2.54], [2.55].

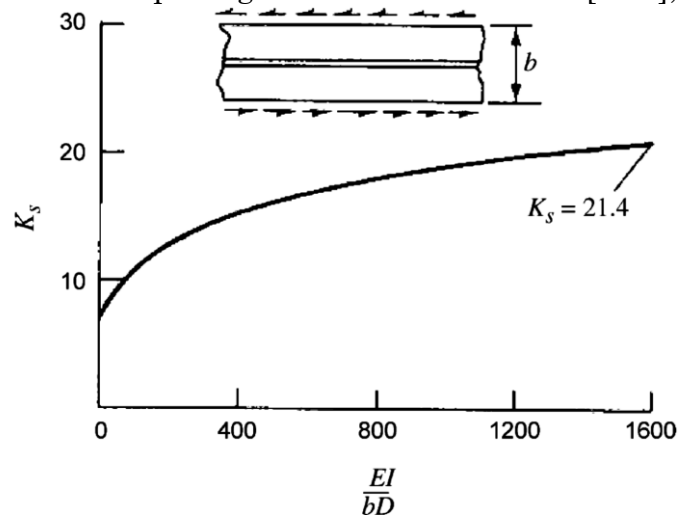


Fig. 2.7. Variation of buckling coefficient for plates longitudinally stiffened under shear [2.54]

Several authors from Rockey et al. [2.46] to Dubas and Tschamper [2.17] investigated the mechanism of failure for slender plates; they showed that single longitudinal stiffener does not provide a sufficient rigidity to work as support against out of plane deflection of the plate. In addition, Rockey et al. [2.46] showed that the optimum position obtained for bending can also be used for the **patch loading** case while Kutmanova and Skaloud [2.56] have shown that one-tenth of girder depth is the optimum position to get a large increase of the patch loading capacity. His mode of failure is similar to the case of unstiffened plate: presence plastic hinges in the flange and yield lines in the web. Markovic and Hajdin [2.9] did a systematic review of existing information on the ultimate load of unstiffened as well as longitudinally stiffened girders. Based on an analysis of the available database, a proposal for taking into account the influence of longitudinal stiffeners was given by the definition of a correction factor. It represents a correction factor dependent on the relative

position as shown in [Eq.(2.14)] that should be applied in order to find the ultimate load of the plate.

$$f(s) = 1.28 - 0.7 s/d \quad (2.14)$$

Table 2.1. Resume of early contribution involving the plate stability

No	Author(s)	Ref.	Year	Type of Loading	Methodology	Studies involved	Remarks
1	Girkmann	[2.10]	1936	Compressive force	Experimental tests	Elastic stability	Restricted range of validity of the results $\alpha \leq 1.1$
2	Zetlin	[3.9]	1955	Partial Edge loading	Theoretical studies	Linear buckling	They used the principle of the conservation of energy
3	Khan et al.	[3.13]	1972	Localized Edge loading	Theoretical studies	Linear buckling	They used the principle of the conservation of energy
4	Chin et al.	[2.13]	1992	Edge loading	Numerical studies	Elastic stability	The critical buckling coefficient found can be used for $\frac{s_s}{h_w} \leq 1.0$
5	Basler	[2.14]	1961	Partial Edge loading	Theoretical studies	Linear buckling	The buckling coefficient derived were not function of edge loading length
6	Rockey and Bagchi	[3.12]	1970	Partial edge loading	FEM	Linear buckling	
7	Bergfelt	[2.16]	1979	Patch loading	Experimental tests	Ultimate strength	The ultimate strength proposed was based on Karman approach
8	Dubas and Tschamper	[2.17]	1990	Patch loading and bending	FEM	Linear buckling	
9	Roberts and Rockey	[2.29]	1979	Patch loading	Experimental tests	Failure mechanism	The mechanism proposed is characterized by the formation of plastic hinges in the flange and yield line in the web
10	Roberts and Markovic	[2.30]	1983	Edge loading	Experimental tests	Ultimate resistance	The ultimate resistance of the girders is the minimum between the flanges and the web resistance.
11	Elgaaly and Nunan	[Elgaaly and Nunan, 1989]	1989	Eccentric patch loading	Experimental tests and Numerical	Ultimate resistance	A strength reduced coefficient have been found to consider the eccentricity of patch loading
12	Stein and Neff	[2.21]	1947	Shear force	Numerical analysis	Linear buckling	A set of buckling coefficients have been found in terms of plate aspect ratio
13	D'Apice et al.	[2.22]	1966	Shear force	Experimental tests	Ultimate strength	Both unstiffened and longitudinally stiffened plates have been investigated
14	Delesques	[2.23]	1974	Shear force	Experimental tests	Linear buckling	
15	Zoetemeier	[2.37]	1980	Combined patch loading and shear force	Experimental tests	Ultimate resistance	Design equation has been derived function of the applied patch loading and shear force.
16	Azizian and Roberts	[2.41]	1983	Concentrated loading	FEM	Linear buckling	The study involved the behaviour of perforated steel plate under concentrated force.

17	Brown et al.	[2.43]	1987	In-plane loads	CLDM	Linear buckling	The buckling shear load decreases drastically with the increase of the holes' size.
18	Narayanan and Chow	[2.45]	1984	Compressive force	Experimental tests	Ultimate capacity	They suggested an approximate design method to analytically determine the ultimate capacity of plates.
19	Charlier and Maquoi	[2.48]	1987	Shear force	Experimental tests	Ultimate capacity	They proposed a model to describe the high post-critical shear resistance of stiffened panels.
20	Cook and Rocky	[2.49]	1962	Shear force	Experimental tests	Linear buckling	They proposed shear critical buckling coefficient in terms of flexural rigidity
21	Rockey	[3.12]	1961	Pure Bending	Theoretical studies	Linear buckling	He considered the influence of both torsional and flexural stiffness of the stiffener.
22	Basler and Thurlimann	[2.14]	1961	Compressive force	Experimental tests	Linear buckling	Longitudinal stiffener doesn't influence the lateral and torsional buckling modes.
23	Rockey and Leggett	[2.55]	1962	Bending	Experimental test	Linear buckling	
24	Dubas	[2.54]	1948	Bending	Experimental test	Linear buckling	

In regards to collected information, it is clearly observed that early investigations have been done through experimental or theoretical studies with the aim to study the behaviour of steel plate under a single loading situation in most cases. Other analysis showed that two constraint's conditions have been considered by different authors namely simple supported edge or clamped edge. Table 2.1 shows the resume of some interesting works done on the topic before 1992.

2.2 Investigation of steel plate buckling before 1992

In the second period, several investigations on the plate stability were done whether to confirm the approach used by early researchers whose results have been published in design codes or to go in deep in the analysis considering other loading cases or combined loading cases involving the plate stability. Fig. 2.8 shows in the function of the published year the number of papers revised for this part.

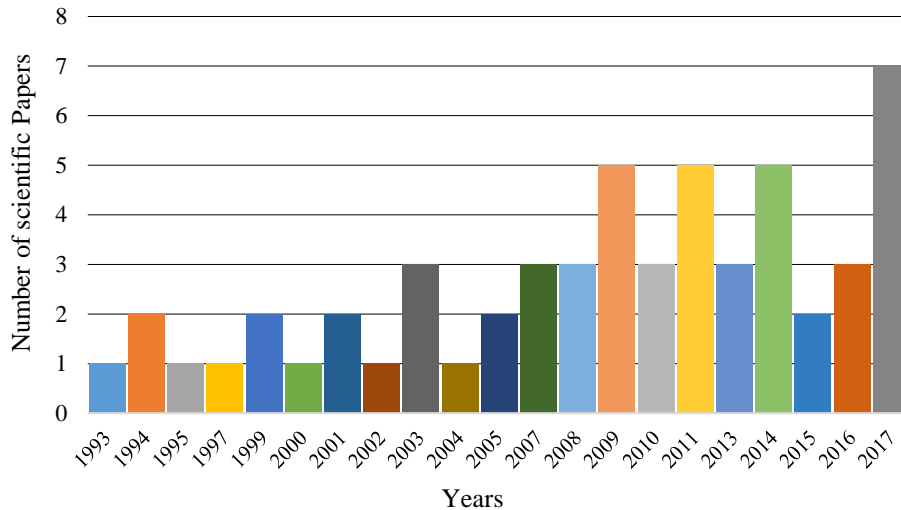


Fig. 2.8. Histogram showing number of scientific papers used with respect to the published year

Due to a great influence that stiffeners can provide in the buckling strength or in the response behaviour of steel plate under loads, a great interest has been observed in the investigation of stiffened steel plate girders these recent years. Longitudinal and transversal stiffeners are often used to control the web thickness governed by the amplitude of patch loading and finally allow the efficient management of construction costs. Fig. 2.9 presents the configuration of plate girders in studies from the various scientific papers in recent years.

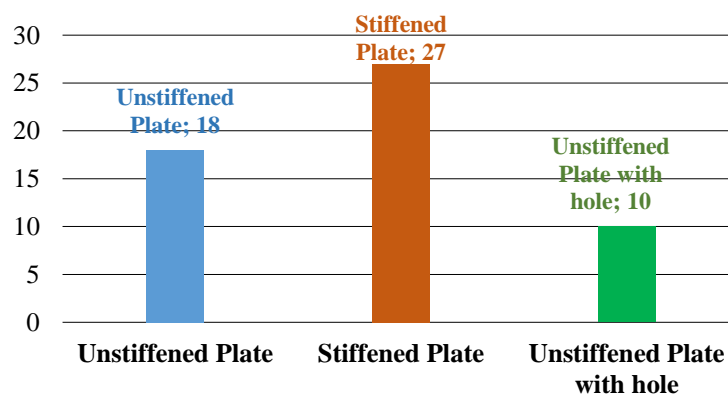


Fig. 2.9. Configuration of steel plate girders in the research work

It should be noted that many of the results obtained from recent researches come from numerical analysis, either linear or non-linear. Just a few of them were obtained by experimental tests or to theoretical development; even where experimental tests were performed, the authors in most of the cases combine them with numerical studies. Fig. 2.10 presents in term of percentage the methodology used by different researchers in their investigation.

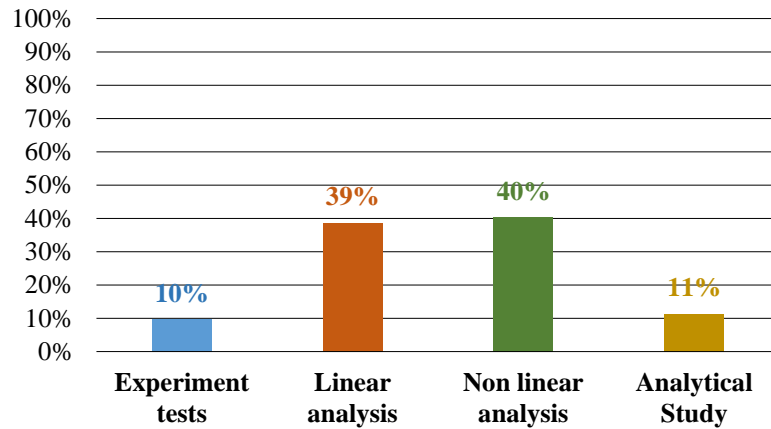


Fig. 2.10. Research methodology

The extent of numerical analysis has allowed a great development this recent year in the investigations of plate behaviour under different in-plane loading. Due to the difficulty from an economical or technical point of view, many authors in their research used numerical analysis respect to the experimental test. The development of computational mechanics has given to numerical software a great possibility to develop also complex models, which could not be possible by experimental tests. Several numerical software is being used nowadays. Fig. 2.11 presents an overview of numerical software used by some authors in their researches. This part presents part of investigations and analysed performed from 1992.

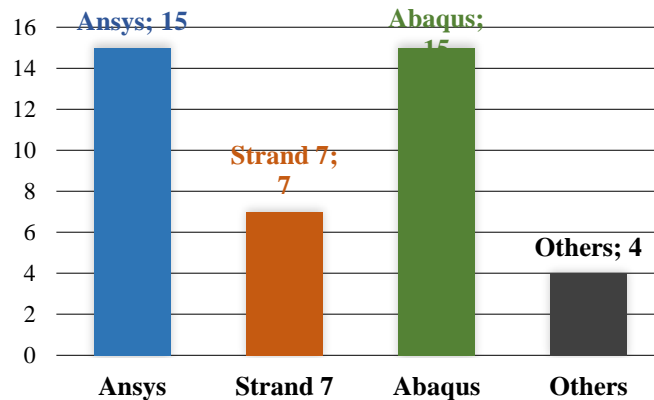


Fig. 2.11. Overview of used of numerical software

The finite element analysis from different software presents more or less the same step starting by definition of the numerical model, mesh validation and application of further analysis. Elements with shell elements, four nodes or eight nodes and 6 degrees of freedom have been used by authors. When doing analysis with Ansys and Abaqus, the flange element has been modelled while authors using Strand 7 did not consider the flange part of the girder. As well as only half of the plate in the study was considered due to symmetry of the geometry when Ansys and Abaqus were used while the whole plate was considered in analysis with Strand.

2.2.1 Unstiffened girder

Many experimental and numerical analyses have been performed after 1979, the year in which Roberts and Rockey [2.29] described the mechanism of failure of girder plate under patch loading. It will be necessary to wait until 1994 to see emerge a new method to evaluate the ultimate capacity of steel girder under patch loading derived by Lagerqvist [2.57].

Regarding the stability of slender plate girder, several authors have oriented their research on the topic in order to give better insight concerning the critical buckling load. Various authors from 1955 to 1970 have studied the instability of thin plates [2.58]. The plate was subjected to in-plane loads and from analytical analysis, elastic critical loads were determined. Several simplifications of the problem were used in the analysis since it required the resolution of complex equations associated with the distribution of pre-buckling stress. Analytical, finite-difference and finite element methods have widely been used in the past to solve complex equations deriving from instability problem; but due to the development of numerical technics and the simplicity with which they can be used, finite element analysis is much more nowadays used to solve such problems.

2.2.1.1 Purposes and methodology of the research

Shahabian and Roberts [2.58] in 1999 did an excellent work investigating the buckling of steel plate subjected to combined in-plane loads and possible interaction between them.

In 1994, Duchene and Maquoi [2.61] derived formulas to calculate elastic buckling coefficient of a plate under patch loads. Rectangular plates with different panel aspect ratio have been considered: $0.5 \leq \alpha \leq 1.8$, $1.8 \leq \alpha \leq 4$ and $\alpha \geq 4$. Reng and Tong [2.60] in 2005 used ANSYS to carry out investigation to simulate the real loading and restraint situations of I-section web girders under patch loading and wheel loading while Maiorana et al. [2.62] in 2008 developed an expression for critical buckling coefficient which takes in consideration both the panel aspect ratio and the patch loading length.

As well as great improvements in the expression of buckling coefficient have been found in the literature in case of elastic stability of steel plate subjected to individual effect of bending stress, shear or patch loading, there is still lack of information on the prediction of buckling coefficient in case of combined loading. Very few authors achieved to give insights on the problem. Shahabian and Roberts [2.58] studied the instability problem related to rectangular steel plate girders under combined effects of in-plane patch loading, compression, bending stress and shear stress. Maiorana et al. [2.62] in 2008 developed a numerical model with Strand 7 [2.63] to study the combined effect of patch loading and bending on web girders.

Being the most common case in bridge launching, problems related to patch loading have been widely studied. For this reason, up to now, there exists a huge amount of information describing the behaviour of the plate under patch loading in literature [2.38]. Two concepts have been developed to describe the failure mechanism of plate girders under patch loading. The old one characterizes the failure of the plate by the formation of four plastic hinges in the flange and three yield lines in the webs while in the recent one the strength curve or χ -functions have been integrated into the mechanism.

In the goal to investigate the behaviour of steel plate under combined loading, many authors firstly focused on the literature overview of previous researches on M-V; M-F and F-V. Concerning the M-F interaction, several scientists continued to focus their attention on M-F interaction after the first investigation in the field done by Bergfelt [2.16] while Lagerqvist [2.65] resumed existing interaction equations. Johansson and Lagerqvist [2.57], made an experimental investigation including tests and they proposed a formula [Eq.(2.28)] to describe the M-F interaction. Granath et al. [66] in 2000 performed numerical computation in order to analyse the serviceability limit state of the plate when bending is associated with travelling patch load.

Latest investigation on M-F interaction on plate girders has been the focus of Braun and Kuhlmann [2.27]. The work was subdivided into three parts: database creation, evaluation of previous interaction equations and development of new interaction equations as shown in [Eq.(2.29)]. Vigh [2.27] performed further numerical investigations in 2012. the author analysed the interaction between the flange to web connection in case of I-sections.

Several works to characterize individual resistances of plate girder under shear or under patch loading have been done but just a few have devoted attention in the interaction between the two. Zoetemeijer [2.37] studied three decades ago how does the strength capacity of rolled section subjected to concentrated loading is influenced when adding shear stress; further experimental investigation has been performed by Roberts et al. [2.67]. They performed experimental tests on several I-girders under combined shear and axial forces. Intensive works have been done in 2006 by Kuhlmann and Braun to study the combined effect of shear stress and patch load [2.6]. Two main structural information were looking for the structural behaviour of girders I-profiles and the carrying load capacity. The first has been studied through experimental tests while the second has been defined through extensive numerical analysis.

Jáger et al. [2.70] in 2017 performed an intensive numerical analysis to investigate the behaviour of slender webs of I-profile girders without stiffeners and subjected to the combined effect of bending and shear. The aim was to study the range of applicability of current EN 1993-1-5 [2.35] M-V interaction resistance model.

A typical situation of interaction between various solicitations namely patch loading, bending and shear may happen during the bridge launching. To allow efficient use of material during the process, the ultimate strength of plate girder should be investigated under these three forms of loading. The patch loading resistance may decrease if the steel plate is simultaneously subjected to combined bending moment and shear stress. Estimation of the reduction percentage is a tricky issue since the experimental test and numerical analysis already performed were not sufficient. Roberts and Shahabian [2.67], proposed a formula describing the ultimate strength of slender web panels subjected to a combination of those three types of loading. The proposed interaction formula has been validated by test results. More recently, a formulation was presented [Eq.(2.33)] by Braun and Kuhlmann [2.27] for the interaction behaviour of patch loading, bending and shear stress. For that, they took into consideration the existing equations for the combined patch loading and shear (F-V) and bending and shear (M-V). Graciano and Ayestarán [2.38] used finite element analysis to investigate the nonlinear behaviour of webs under combined concentrated loading, bending and shear.

2.2.1.2 Purposes and methodology of the research

From Shahabian and Roberts's research [2.58], the results for instability of plate under a combined effect of in-plane load showed a very good agreement with the results from Timoshenko and Gere [2.28]. This satisfactory results contrasted with the case of plate girder under patch loading since the pre-buckling stresses used firstly did not satisfy compatibility equations.

Graciano and Lagerqvist [2.59] proposed a new equation as derived in [Eq.(2.15)] to compute the critical buckling coefficient of steel I-girders subjected to patch load.

$$k_{cr} = 5.82 + 2.1 \left(\frac{h_w}{a} \right)^2 + 0.46 \sqrt{\beta} \quad (2.15)$$

In this formula, the rotational restraints provided by flanges on web plate have been taken into account considering the β coefficient. It represents the ratio between the torsional stiffness of the flange to the bending stiffness of the web; the expression is defined by [Eq.(2.16)].

$$\beta = \frac{b_f t_f^3}{h_w t_w^3} \quad (2.16)$$

After extensive numerical analysis, Reng and Tong [2.60] in 2005 defined new formulae to determine the critical instability coefficients of web girders. Good agreement in the results with respect to existing results was found. The equations defining the critical buckling coefficient of a plate subjected to patch loading with simply support and clamped boundary condition have been proposed and are showed in [Eq.(2.17)] and [Eq.(2.18)] respectively.

$$k_{crs} = 2.05 + \frac{1.2}{(a/h_w)^2} + s_s^2 \left[0.5 + \frac{2.0}{(a/h_w)^2} \right] \quad (2.17)$$

$$k_{crf} = (1 + 0.65s_s^2) \left[6.3 - 0.05 \left(\frac{a}{h_w} \right)^2 + \frac{0.6}{(a/h_w)^2} \right] \quad (2.18)$$

The results found by Maiorana et al. [2.62] in 2008 showed a good agreement with respect to the results of Shahabian and Roberts [2.58] in terms of patch loading. The critical buckling coefficient developed by Maiorana et al. [2.62] is expressed as follow:

$$k = 3.2048 \frac{c_1}{c_2} \quad (2.19)$$

The coefficients c_1 and c_2 depend respectively on the panel aspect ratio and the patch loading length and are determined with these formulas.

$$c_1 = -0.0446 \left(\frac{h}{a} \right)^6 + 0.4067 \left(\frac{h}{a} \right)^5 - 1.3512 \left(\frac{h}{a} \right)^4 + 1.8338 \left(\frac{h}{a} \right)^3 - 0.3869 \left(\frac{h}{a} \right)^2 - 0.2617 \left(\frac{h}{a} \right) + 0.8035 \quad (2.20)$$

$$c_2 = 1.9774 \left(\frac{l_0}{a} \right)^6 - 6.0815 \left(\frac{l_0}{a} \right)^5 + 7.1163 \left(\frac{l_0}{a} \right)^4 - 3.5774 \left(\frac{l_0}{a} \right)^3 + 0.2617 \left(\frac{l_0}{a} \right)^2 - 0.1669 \left(\frac{l_0}{a} \right) + 1 \quad (2.21)$$

Shahabian and Roberts [2.58] proposed an interaction formula [Eq.2.22]-[Eq.2.25] in terms of buckling coefficient to take into account combined loading. Panel aspect ratio from 1/2 to 3 while patch loading length equal to 1/10, 1/4, and 4/10 have been considered in the analysis.

$$\left(\frac{k_{bp}}{k_b} \right)^{\alpha_1} + \left(\frac{k_{pb}}{k_p} \right)^{\alpha_1} = 1 \quad (2.22)$$

$$\left(\frac{k_{sp}}{k_s} \right)^{\alpha_2} + \left(\frac{k_{ps}}{k_p} \right)^{\alpha_2} = 1 \quad (2.23)$$

$$\left(\frac{k_{sb}}{k_s} \right)^{\alpha_3} + \left(\frac{k_{bs}}{k_b} \right)^{\alpha_3} = 1 \quad (2.24)$$

$$xy(x^{\alpha_1} + y^{\alpha_1}) + xz(x^{\alpha_2} + z^{\alpha_2}) + yz(y^{\alpha_3} + z^{\alpha_3}) = xy + xz + yz - \eta xyz \quad (2.25)$$

Bending stress at a certain level on steel webs when applied at the same time with patch loading can greatly reduce the critical buckling load if patch loading was applied only. It is one of the conclusions from the analysis performed by Maiorana et al. [2.62]. In addition, coefficient c_3 has been found to take into account the effect of bending stress in the final value of the critical buckling load of steel plate under patch loading and bending.

$$F_{cr,y} = \left[3.2048 \frac{\pi^2 E}{12(1-\nu^2)} \right] \frac{t^3 c_1}{h c_2 c_3} \quad (2.26)$$

The new model to design a steel plate under patch loading has been presented by Lagerqvist and is function particularly of three parameters [2.38].

- The plastic resistance F_y
- The slender parameter $\lambda = \sqrt{F_y/F_{cr}}$
- The resistance function $\chi(\lambda)$

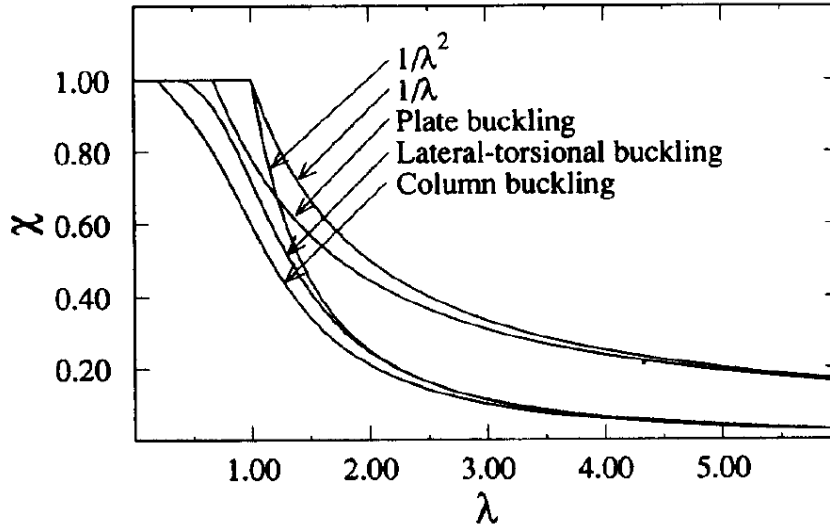


Fig 2.12. Different χ -functions to consider in instability problem of structural element [2.64]

From the investigation done by Johansson and Lagerqvist [2.57], different problems of buckling are described by quite different χ -functions. Fig. 2.12 shows the relationships between the χ -functions and slenderness. Graciano [2.64] makes a systematic review on the previously developed patch loading resistance models and the recent improvements. From this work, new expressions of patch loading resistance are drawn.

Johansson and Lagerqvist [2.57] defined the expression to obtain the resistance of unstiffened girder plate under patch loading as shown in [Eq.(2.27)]. All the parameters involved in the expression of F_{RD} are found in [2.65]:

$$F_{RD} = F_y \chi_F(\bar{\lambda}_F) / \gamma_{M1} \quad (2.27)$$

The results from the different analysis [2.57], [2.65] and [2.66] involving combined effect between bending and patch loading showed that small bending moment led to the raise of patch loading capacity in the slender girder. In addition, the authors presented a comparison between interactions from bending and patch loading as shown in Fig. 2.13 with resistance capacities from Eurocode expressions and the ones proposed by Lagerqvist and Johansson [2.65].

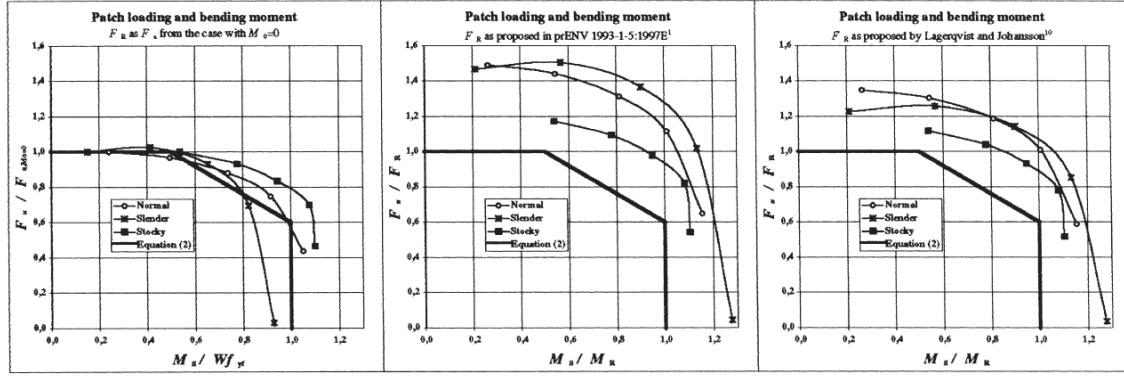


Fig. 2.13: Proposed Patch loading and bending moment interaction from different authors [2.61].

$$\left(\frac{F}{F_R}\right) + 0.8\left(\frac{M}{M_R}\right) = 1.4 \quad (2.28)$$

$$\left(\frac{F}{F_R}\right) + \left(\frac{M}{M_{pl,R}}\right)^{3.6} \leq 1.0 \quad (2.29)$$

Satisfactory results have been found from the analysis of steel plate under combined shear and patch loading performed by Roberts et al. [2.67] and the interaction equation is expressed through the [Eq.(2.30)].

$$\left(\frac{V - 0.5 F}{V_R}\right)^{2.0} + \left(\frac{F}{F_R}\right)^{3.6} \leq 1.0 \quad (2.30)$$

From numerical simulations, Braun during his PhD thesis in 2010 showed that the interaction equations proposed by Roberts et al. [2.67] may be used for a particular limit of $s_s/h_w \leq 0.25$. Within this range of validity, the use of this formula becomes limited in so far as in bridge industry situation where $0.2 \leq s_s/h_w \leq 0.6$ might happen [2.6].

Considering the interaction between bending and shear, Kuhlmann and Braun developed the interaction curve based on a large study of parameter range. The equations [Eq.(2.31)] and [Eq.(2.32)] take into consideration the bending and shear plastic resistance. Lee et al. [2.6] revised the proposal of the AASHTO [2.68] and AISC [2.69] specification for M-V interaction behaviour and proposed a modified version. Crisan and Dubina [2.6] performed further investigation and a new expression for the interaction equation has been derived.

$$\left(\frac{V - 0.5 F}{V_R}\right) + \left(\frac{M}{M_{pl,R}}\right)^{3.6} \leq 1.0 \quad (2.31)$$

$$\frac{M}{M_{pl,R}} + \left(1 - \frac{M_{f,R}}{M_{pl,R}}\right) \left(\frac{2V}{V_{pl,R}} - 1\right) \leq 1.0 \quad (2.32)$$

Jager et al. [2.70] in 2017 proposed a refined equation describing the M-V interaction, changing index κ from 1.0 to an increased value, which ensures a better fit for the numerical simulations. Statistical evaluation of the numerical results showed good agreement with analytical results.

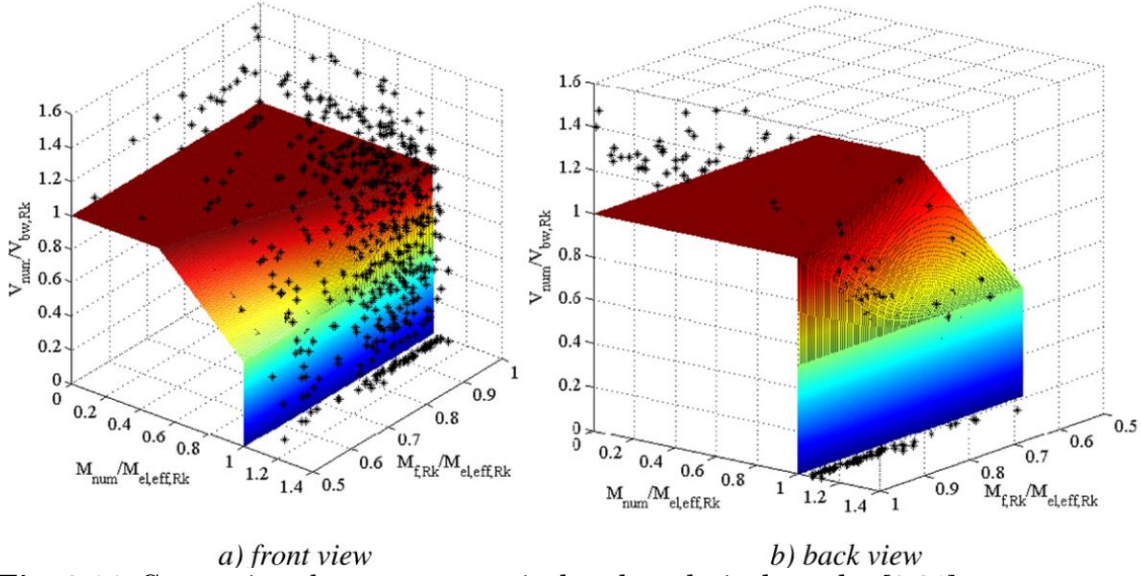


Fig. 2.14. Comparison between numerical and analytical results [2.31]

Braun and Kuhlmann [2.27] presented a formulation [Eq.(2.33)] to describe the interaction behaviour of patch loading, bending and shear stress while Graciano and Ayestarán [2.38] showed that the reduction of the patch loading resistance is most influenced by bending stress.

$$\left(\frac{P}{P_R}\right) + \left(\frac{M}{M_{pl,R}}\right)^{3.0} + \left(\frac{F}{F_R}\right)^{1.6} \leq 1.0 \quad (2.33)$$

2.2.2 Unstiffened Plate with hole

The presence of holes in plate girders may sometimes be unavoidable. A change in structural behaviour of the plate under compressive forces and bending starts to occur. A perfect understanding of the structural response of the plate becomes an issue. Several authors have concentrated their investigations on this problem; recently, extensive numerical and experimental analysis has been done to bring insights and new conclusions on the structural behaviour of the plate. Some of them have focused their investigation on linear buckling under uniaxial compression [2.71] - [2.78]. Maiorana et al., [2.71] performed linear analysis using Strand7 [2.63] of steel plates under symmetrical localized load, with circular and rectangular holes; they considered simply supported rectangular plates subjected to uniaxial compressive loads of length s_s . The results showed that a steel plate under localized symmetrical loads behave differently when a uniform compressive load is applied. Many authors found that the difference is significant [2.71]-[2.77]. Extensive numerical analysis has been performed by El-Sawy and Nazmi [2.76] in 2001 to study the effect of plate aspect ratio, the hole location and size on the instability coefficient of rectangular plates with holes under uniaxial compression; they found that using girder plate with rectangular RS hole gives optimal solution that using plate with circular RL hole. Furthermore, they found an interval $x_{edge}/b = [0.25 - 0.5]$ for the use of a circular hole for different panel aspect ratio; it defines properly a critical zone. They recommended avoiding the hole of a certain diameter in order to have a

good critical buckling resistance from the plate. Fig. 2.16 shows the variation of the buckling coefficient in the function of hole size and hole position; further information can be found in the work done by El-Samy and Nazmi [2.76]. Komur and Sonmez [2.78] found that when analyzing perforated plate, the critical buckling load is sensitive to where the load is located; furthermore, they found that the buckling coefficient values dramatically decrease when the loads are applied near the center of the steel plate. El-Sawy et al. [2.76] found that for a thick plate, the increase of the hole's size led to a decrease of the critical stress; the plate goes to elasto-plastic buckling before the failure. In addition, the critical loads will depend on the yielding strength of the steel as they increase as well as high steel grade is used. Furthermore, the failure due to buckling of steel plates with concentric holes remains elastic if the hole's size is small so long as slenderness ratio of the plate is larger than typical value for different grade of plate steel independently to the aspect ratio as shown in the Fig. 2.15. Attention has been paid on the orientation of rectangular holes by some authors; the buckling load will be greatly affected due to the orientation of the hole with respect to the loading [2.40].

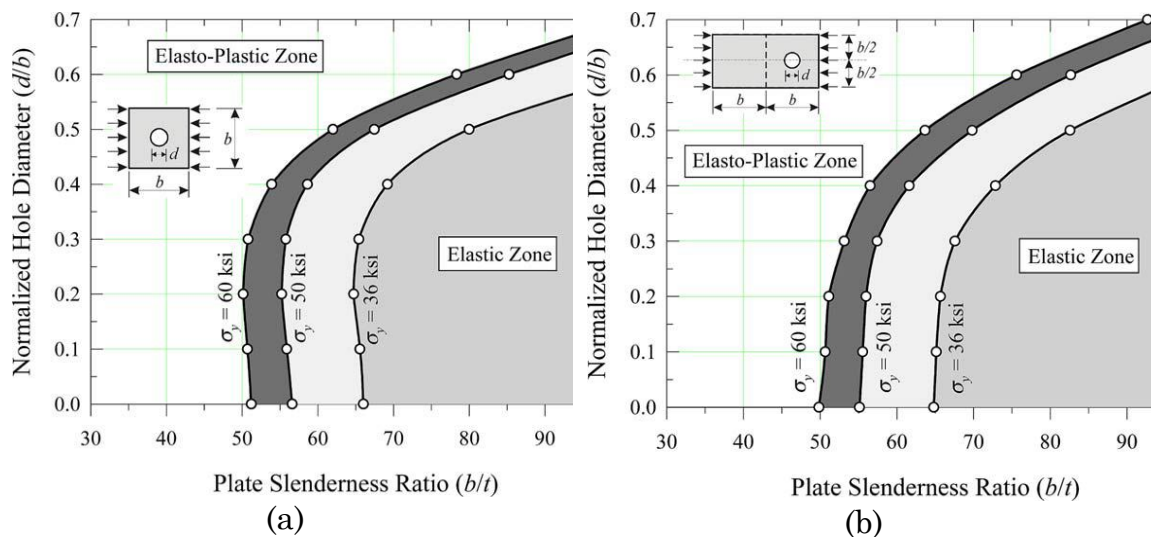


Fig. 2.15. Boundary curves between failure zones for rectangular plate. (a): aspect ratio =1, (b): aspect ratio =2 [2.44]

El-Sawy et al. [2.42] found that the buckling load does not vary with the aspect ratio of the plate when the center of the hole belongs to the deformed configuration. The buckling coefficient increases of approximately four times in a case where the length of the compressive force decreases as seen in Fig. 2.17. Circular and rectangular holes have been investigated to find the best position in steel plates when subjected to combined bending moment and axial force have been performed [2.76], [2.44]. Sharkerley and Brown [2.44] defined mechanisms to explain the behaviour of steel plates with perforations of various sections. The buckling coefficient of the perforated plate using RS holes gives higher value with respect to the case when RL holes are used [2.76]; the result was in good agreement to what El-Sawy and Nazmi [2.76]. Sharkeley and Brown [2.44] found that the orientation of the holes on the plate has a

major effect on the critical buckling load. Furthermore, they found that the perforation major dimension should not be perpendicular to the load axis.

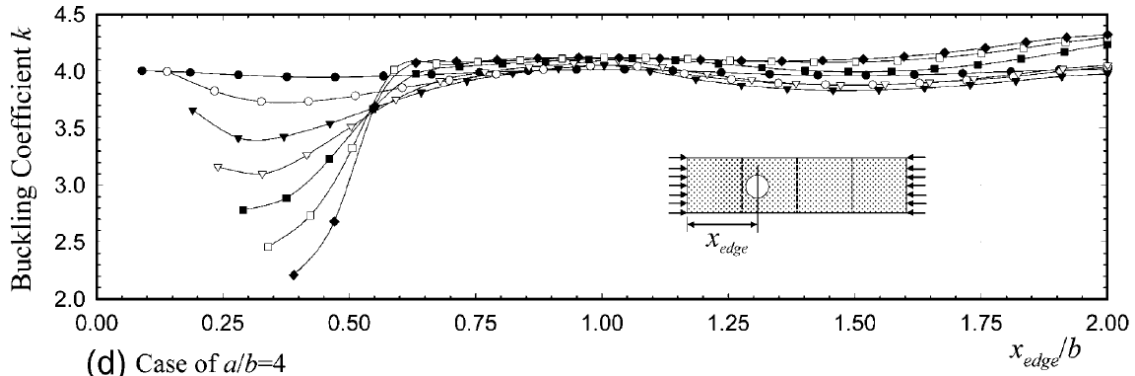


Fig. 2.16. Buckling coefficient k for rectangular plates with circular hole [2.76]

RL and RS holes should be avoided near panel edges, the plastic field is reduced when the stress ratio increases, the increase of the hole size causes the reduction of plastic strength and rectangular perforated plates showed pronounced plastic behaviour than square plates [2.44], [2.76].

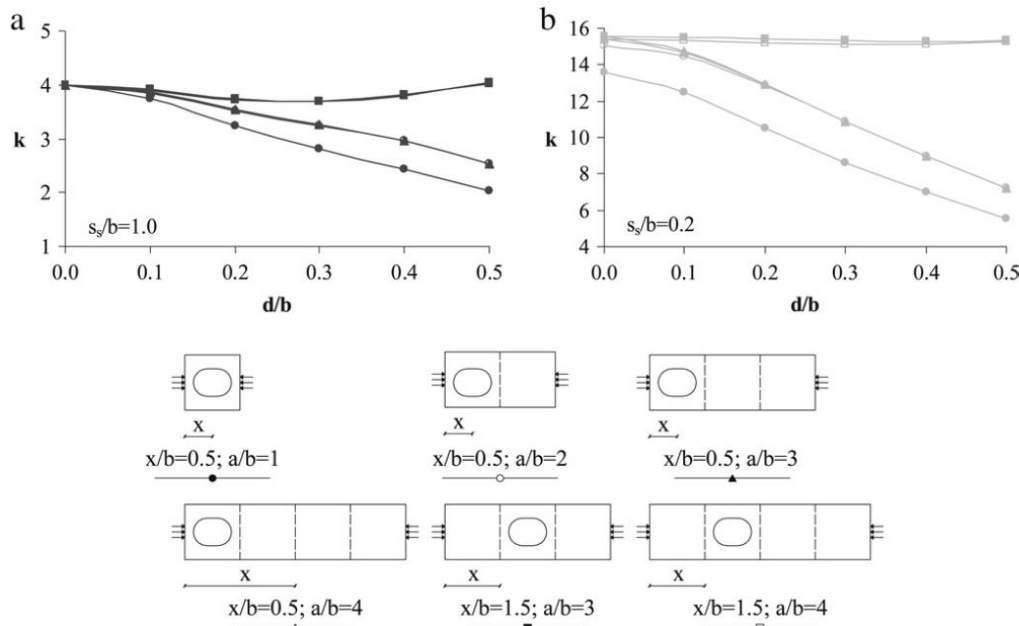


Fig. 2.17. k vs d/b diagrams for RL holes with center in nodal points of the deformed configuration [2.71]

Regarding the behaviour of perforated plates subjected to shear load, Pellegrino et al. [2.75] analysed by numerical models, the dimension, the hole orientation and the position in regards to the main axes to study the non-linear behaviour and linear buckling of steel plates with one perforation. In order to get a numerical model near to the real case, constraints to out of plane have been applied at each edge and on the four corners of the plate were used elastic restraints with negligible rigidity modelled as beam elements in the x - and y -direction. Fig. 2.18 shows the numerical scheme with constraint condition considered in [2.75].

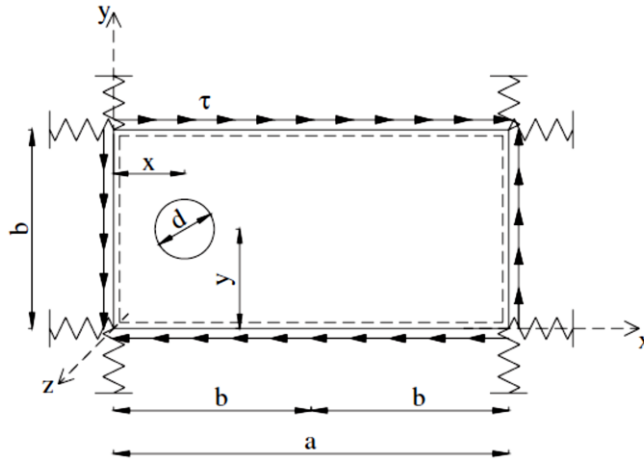


Fig. 2.18. Numerical model to study the effect of shear load of perforated plate [2.75]

For thick panel [2.75], the sliding of the two parts of the plate are caused by the plasticization of the region closed to the hole as revealed the non-linear analysis of perforated plate while the collapse due to buckling will occur with two shear bands for slender panel and deformed shape different from each other as shown in Fig. 2.19.

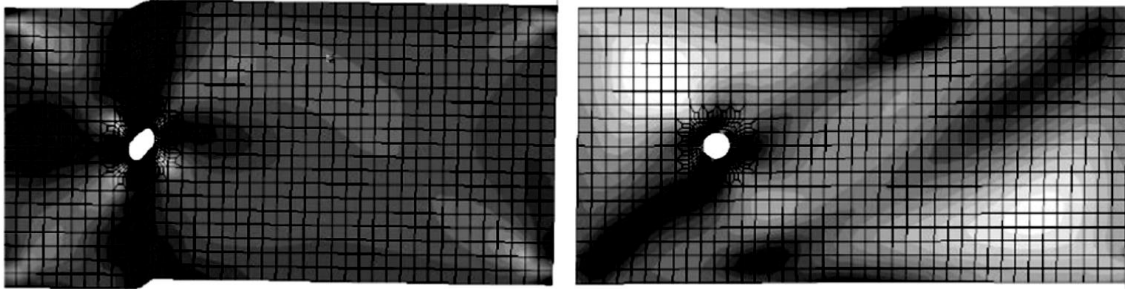


Fig. 2.19. Von Mises stresses in plate with $a/b = 2$ and circular plate with $\lambda=60$ and $\lambda=120$ [2.75]

Studies on nonlinear behaviour of perforated plates under localized symmetrical loads have shown that high-grade steel may undergo instability and the possibility to develop from the plate, mechanisms of post-critical buckling will then be reduced. The justification for this is that the increase in steel grade may lead to critical slenderness reduction. Extensive finite element analysis using Abaqus aimed to study the behaviour on post-buckling of a perforated plate and his ultimate load capacity under axial compression has been performed by Shanmugam et al. [2.40]; a formula has been established to determine the ultimate load-carrying capacity [Eq.(2.35)]. Furthermore, slenderness ratio and hole's size, as well as the external condition of the edge, are considered as affecting the ultimate load of the perforated plate.

$$\frac{P_u}{P_s} = -0.97 \frac{b}{d} + 0.98 \quad (2.34)$$

2.2.3 Stiffened plate

Incremental launching is the most used technique nowadays in bridge construction due to several reasons. One of the big challenges of this process is observed when the bridge overpasses rivers or valleys, and cross-section of thin plate girders will automatically pass through temporary supports or bridge

piers already built. Thus, the use of heavy construction equipment will create a concentrated force as reaction forces of those piers acting on both unstiffened and longitudinally stiffened thin sections. Either an increase of web thickness or use of vertical and longitudinal stiffness is adopted by engineers to come out of this problem. Chacón et al. [2.79] - [2.81] studied the influence of transverse stiffener of steel girders subjected to patch loading. The results obtained from experimental and numerical investigations were compared and showed good agreement. Great differences were observed in the structural response of girders with largely spaced stiffeners and arranged transversally with respect to the case with closely spaced ones; two different modes of failure are presented [2.80], [2.81]. The first mode is linked to web folding without the contribution of the flange rotational capacities for panel with largely spaced transverse stiffeners while the second mode is linked to the hinge mechanism involving the web, loaded flange and transverse stiffeners [2.80]. Furthermore, a post-peak capacity was developed in order to find the ultimate load capacity of the girder [2.80]. The proposed formula is shown in [Eq.(2.36)]. This formula is particularly attractive for cases of hybrid girders defined as plate girders with different steel grades in web and flanges; in this particular case, flanges are made with steel plate having higher strength than the web.

$$\frac{\chi_F f_{yw} l_y t_w}{\gamma_{M1}} + \frac{b_f t_f^2 f_{yf}}{(a - s_s)} [2 - (\chi_{f0} + \chi_{fi})] \quad (2.35)$$

Alinia [2.82] - [2.84] performed an extensive numerical analysis using ANSYS to investigate the structural effect of stiffeners and to bring insights on the optimization of the design procedure. During the analysis, the effect of number and type of stiffeners have been taken into account. The critical shear stress will increase by stiffening rectangular plate; in addition, intermediate stiffeners should be placed such that the number of steel panels is always higher than the value of the aspect ratio of the plate.

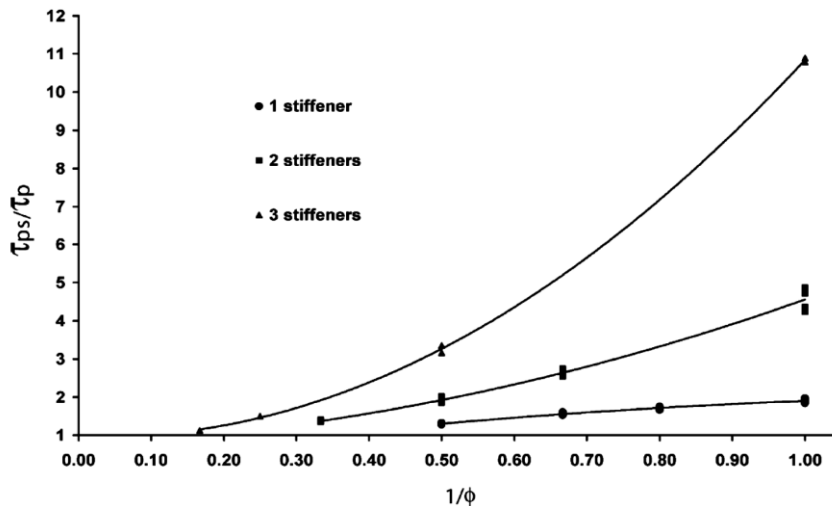


Fig. 2.20. The increase in critical shear stress in function of number of stiffeners and aspect ratios [2.82]

To predict how critical shear load increases is a great challenge since it is related to the type and the number of stiffeners as well as to the plate aspect

ratio [2.82]. Fig. 2.20 shows how the critical shear load varies with respect to the stiffeners number and the aspect ratio. Loughlan and Hussain [2.50] also studied the instability and the post-buckling failure capacities of thin plates subjected to in-plane shear. They found that the in-plane shear displacement loading at the stiffened panel with simply supported edge allows a lower bound estimate of the post-buckled elastoplastic in-plane shear response of the panels.

Regarding investigations on longitudinal stiffened girders, several authors have focused their research on this topic to bring new developments about stiffened plate stability and critical post-buckling and ultimate capacity of the stiffened plate under different loading conditions. Some authors [2.3], [2.4], [2.85] studied the optimum size of longitudinal stiffeners and his possible ideal location under bending loading conditions. Longitudinal stiffeners are properly designed when they are sufficiently rigid leading to a change in the critical state of the plate by the creation of a nodal line. In this situation, global buckling of the plate will turn into buckling of created sub-panels [2.86]. Many researchers [2.3]-[2.4] found that the optimum position of a single stiffener for steel plate under pure bending is one-fifth of the whole plate depth as recommended by most design codes. The stiffeners flexural rigidity and the panel aspect ratio may strongly change this result [2.3]. Alinia and Shirazi [2.2] in 2009 found that the stiffener is arranged in an optimal way if it divides the panel into two subpanels; then the critical stresses obtained for the whole stiffened plates are exactly the same observed in a subpanel. Maiorana et al. [2.4], investigated the effect of different typologies of stiffeners on stiffened plates under axial force and shear loading or in-plane bending. Optimum position location of longitudinal stiffener moves from 0.2 to 0.5 time the height of panel for loading changing from pure bending to uniform compression. In addition, they found that open section stiffeners would not present good performance with respect to the closed one; in fact, the flexural rigidity of open section being smaller compared to the closed section, the open section stiffeners are less prone to divide the whole panel in two subpanels. Furthermore, for what regards the shear stress investigation, they reached the same conclusion as previous investigations; one-half of the panel height being the ideal position of the longitudinal stiffener when steel panel is subjected to shear force. Ajeesh and Sreekumar [2.87] found the same results for the optimal position of longitudinal stiffened under shear; further information can be found in [2.4]. Graciano and Lagerqvist [2.59] in 2003 found that longitudinal stiffener lead to a significant increase in critical buckling stress when investigating plate girder under patch loading. The expressions of critical buckling coefficients are given by the following expressions [Eq. (2.37) – [Eq. (2.38)].

$$k_F = 5.82 + 2.1 \left(\frac{h_w}{a} \right)^2 + 0.46 \sqrt[4]{\beta} + k_{sl} \quad (2.361)$$

$$k_{sl} = \left(5.44 \frac{b_1}{a} - 0.21 \right) \sqrt{\gamma_s} \quad (2.37)$$

Cevik [2.85] in 2007 proposed a new expression for patch loading stress on stiffened webs. He used genetic programming to study an important existing database of previous experimental tests. The advantage of using this new

approach comes to the fact that it allows for solving a very complex equation, which may take a long time with the analytical method. Hajdin and Markovic [2.9], defined the failure mechanism to describe the ultimate loads of longitudinally stiffened I-girders undergoing patch loading. The result was based on Robert's [2.29] previous work on plate girder without longitudinal stiffener.

Different stiffeners' geometry has been studied by some authors; for the case of the trapezoidal stiffener, the bending stiffness and his optimal position have been studied by Pavlovčič et al. [2.47]. They investigated through numerical and experimental analysis the influence of one trapezoidal stiffener on buckling plate behaviour and its shear resistance [2.47], [2.88]. The study revealed that imperfection variation until the allowable tolerances in the fabrication process did not influence the shear capacity of the plate [2.88]. Further information concerning the study of the influence of the imperfections on the actual behaviour of plate girders can be found in [2.88]-[2.91]. Graciano et al. [2.92] in 2011 also studied the imperfections on the post-buckling behaviour of steel plate longitudinally stiffened subjected to patch loading. Consideration of initial deformed shape of the girders due to imperfection was investigated. Chica et al. [2.90] gave some indications on how to take into account the imperfections of steel plates during the design of plated element subjected to in-plane forces. Recommendations from Eurocode 3 Parts 1-5 [2.35], Annex C in general shows good results; in addition, they found that pure shear stress is less sensitive to initial geometric imperfections with respect to the patch loading in case of plated beams [2.90]. When studying the behaviour of post-critical buckling of steel element, the first mode of buckling should be considered as initial imperfections of plate girder [2.89], [2.90]. Amani et al. [2.91] in 2013 defined tools to evaluate post-buckling capacities and instability of imperfect steel plate; they used empirical equation. [Eq.(2.37)] shows expressions of critical buckling stress for respectively mild carbon steel plates, stainless steel plates, and aluminium plates. For slender plate, the buckling load is affected by the amplitude imperfection and it will decrease by increasing the amplitude while the ultimate capacities and post-buckling reserves will not change significantly. In contrast, the stocky plates will be highly affected by initial imperfection.

$$\sigma_{cr} = [0.22 - 0.45(w_0/t)^{0.5}]\sigma_y \quad (2.38)$$

$$\sigma_{cr} = [0.23 - 0.39(w_0/t)^{0.5}]\sigma_y \quad (2.39)$$

$$\sigma_{cr} = [0.33 - 0.37(w_0/t)^{0.5}]\sigma_y \quad (2.40)$$

Pavlovčič et al. [2.88], studied the arrangement of longitudinal stiffeners and his influence on panels shear resistance. They found that open T-stiffeners provided less efficiency with respect to the trapezoidal one. In addition, an overestimation of the flange contribution in the analysis of shear resistance of steel panel has been observed.

Graciano et al. [2.93]-[2.97] intensively investigated stiffened plate girder under different loading conditions in the last decade. The elastic

buckling of longitudinally stiffened plate girder under patch load has been investigated herein using the finite element method combined with factorial design analysis [2.93]. They found that the most influential parameters on the buckling coefficient are the relative the stiffener position, the flexural rigidity of the stiffener and the patch loading length [2.94]. Graciano and Edlund [2.95] studied stiffened girder webs subjected to patch loading to investigate the ultimate load behaviour. The optimum position was found at a distance less than 40 times the thickness of the web. In addition, they found that relative stiffener's flexural rigidity in steel plate produces less impact in the analysis of ultimate strength due to loss of his stiffness while it plays a major role in increasing the critical elastic buckling load of steel girders under patch loading [2.95]. Stiffeners as trapezoidal or V-shaped which presents high torsional stiffness allow a substantial increase in efficiency since the small dimension of those stiffeners will produce the same effects of using large open stiffeners. Inversely, relative flexural rigidity may be reduced avoiding the formation of a nodal line [2.96], [2.92]. By using closed stiffeners advantages appear on torsional rigidity but special attention should be made on their flexural rigidity. Graciano [2.97] developed a correction factor found in [Eq. (2.42)] by regression analysis. The aim was to investigate how the ultimate resistance of steel girders under patch loading is increased by using longitudinal stiffeners [2.5]. The use of the formula is limited to a certain value of the relative position of the stiffener. The recent investigation of Loaiza et al. [2.5], showed that the ultimate load of stiffened girders will not be only influenced by the presence of multiple stiffeners but also by the size and bearing length. They studied the contribution of load-bearing length on the ultimate strength of stiffened girder webs.

$$f_s = 0.556 - 0.277 \ln \left[\frac{b_1}{h_w} \left(\frac{f_{yf}/f_{yw}}{t_f/t_w} \right) \right] \quad (2.41)$$

Graciano [2.64] has done a systematic review of recent works on stiffened and unstiffened plate girder under patch loading. Then, the expressions of plastic yield resistance, critical buckling load and resistance function of the stiffened plate under patch loading have to be found. Starting from the previous investigation the plastic resistance was developed and confirmed by Gozzi while Davaine and Clarin [2.64] proposed expression to compute the critical buckling load. Further information can be found in [2.64].

Stiffened plate girders subjected to combined high bending moment and shear load has been discussed by Sinur, Sinur, and Beg [2.98]. Stiffeners were positioned in the compressed part of the web; residual stresses, as well as initial geometric imperfection, have been taken into consideration. For girders stiffened longitudinally, they found that M-V interaction diagram provided by EN 1993-1-5 does not give good correlation with the results from the numerical analysis [2.27]. Braun made a comprehensive study on bending and patch loading interaction behaviour of both stiffened and unstiffened I-girders profile in 2010. In regards of the interaction behaviour under shear and patch loading, Kuhlmann et al. [2.27] conducted an extensive investigation on this subject. The equation developed as seen in [Eq.(2.43)] takes into account the interaction curve and a large number of parameter range; in addition, it covers a wider

application range. Kovesdi et al. [2.27], developed model to investigate the combined effect of bending, shear and patch loading on the load-carrying capacity of longitudinally stiffened I-girders; an interaction equation was found and a close conclusion has been highlighted. It was found that the use of the plastic bending resistance in the equation as assumed by Braun is adequate.

$$\left(\frac{M}{M_{pl,R}}\right)^{3.6} + \left(\frac{V - 0.5 F}{V_R}\right)^{1.6} + \left(\frac{F}{F_R}\right) \leq 1.0 \quad (2.42)$$

2.3 Illustrative design example

A case study, design example has been done to cover some of the recently developed formulae for the computation of buckling coefficient of unstiffened plate girder under different in-plane loading conditions. This part is to provide a practical example from the investigations performed by Shahabian and Roberts [2.58] and thus to give insight through an example on the computation of the buckling coefficient in the case of different in-plane loads interaction. Fig. 2.21 shows the geometry of the girder plate used in the case study. Material properties and dimensions used for the girder in the practical example are given in Table 2. In the example, we consider the steel section subjected to patch loading combined with bending and shear force. Details about the intensity of different actions are presented in Table 3 while the expressions from FEM analysis to evaluate the elastic critical stress is given [Eq.(2.47)].

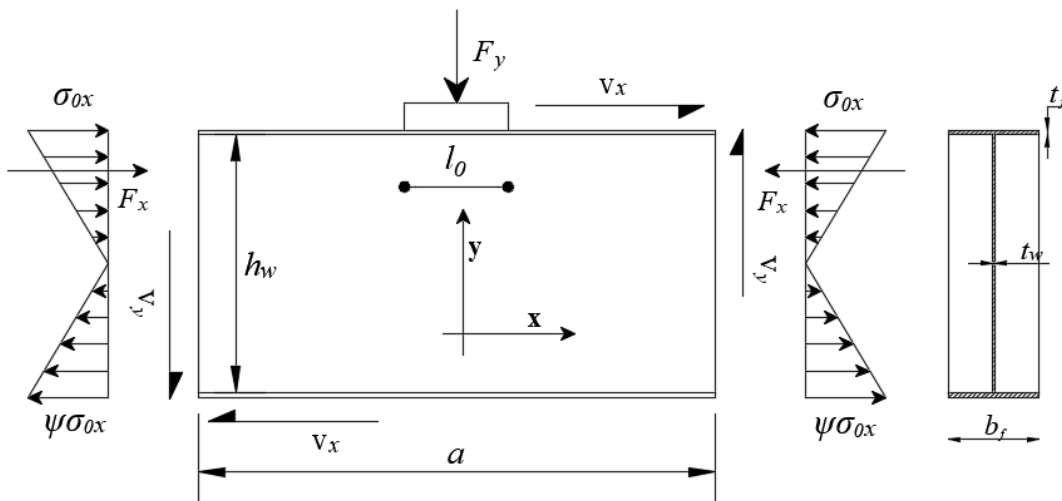


Fig. 2.21. Geometry of the plate girder in the case study

Table 2.2. Geometry and material properties used in the practical example

a	h_w	$\beta =$	b_f	t_w	t_f	l_0	E	ν	$\sigma_{0,el}$
[mm]	[mm]	a/h_w	[mm]	[mm]	[mm]	[mm]	[MPa]		[MPa]

2000	1000	2	500	10	10	400	206000	0.3	18.62
------	------	---	-----	----	----	-----	--------	-----	-------

Table 2.3. Geometry and material properties used in the practical example

F_y [kN]	ψ	F_x [kN]	V_x [kN]	V_y [kN]
100	-1	200	400	200

2.3.1 Linear buckling analysis

From a numerical point of view, the theory presents the global stiffness matrix k as a sum of a two-stiffness matrix; the first one, constant being the stiffness of small deformation k_E and the second one variable with stress level k_s , which takes into account the effect of stress σ on the plate. Maiorana et al. [2.62] briefly developed the theory for solving buckling problem using matrix; some steps are presented below as follow:

$$k(\sigma_0) = k_E + k_s(\sigma_0) \tag{2.43}$$

$$dF = [k_E + k_s(\lambda \times \sigma_0)]du \tag{2.44}$$

$$[k_E + k_s(\lambda \times \sigma_0)]du = 0 \tag{2.45}$$

[Eq.(2.44) to Eq.(2.46)] present the preceding steps before the expression of critical buckling stress. At buckling, it is observed that the displacement continue to increase while the applied force remained constant. For this reasons, it is imposed that the stiffness matrix has the determinant equal to zero.

The problem deriving the critical buckling loads are classified as Eigen value problem where load multiplier is obtained by solving the determinant equal to zero. The lowest eigenvalue λ_1 will be considered as the critical load multiplier. [Eq.(2.47)] showed the expression of critical buckling stress in terms of the critical load multiplier and the initial applied stress.

$$\sigma_{cr} = \lambda_1 \times \sigma_0 \tag{2.46}$$

For this analysis, the major challenge was to calibrate the numerical model as well as to find the boundary condition to apply at different edges since the combined effect of various in-plane loading has also been analysed. Previous results have shown boundary condition applied for plate girder under bending or patch loading separately and under shear force. The out of plane deflection has been prevented in the z-axis. The deformation in the x- and y-directions has been controlled by applying beam elements at each corner of steel plate with specific rigidity such that the internal stresses distribution and plate stability are not influenced.

2.3.2 Mesh validation

Firstly, preliminary analysis for cases of plate girder under singular patch loading, bending or shear are performed. The buckling coefficient is obtained by the [Eq.2.48].

$$k_{cr} = \frac{\lambda_{cr} \times \sigma_0}{\sigma_{0,el}} \quad (2.47)$$

The numerical analysis has been done through Strand7 [2.63]. The mesh is done with (Quad4) plate elements of typical size equal to $b/20$ and each node has six degrees of freedom.

Previous investigations of Maiorana et al., in 2008 give information concerning boundary conditions for girder panel under combined bending moment and patch loading [2.62], [2.4] and for girder subjected to shear [2.75]. In the case of combined patch loading, bending moment and shear force, no information is found from literature when investigating the elastic stability of steel plate.

The validation of the numerical model is presented; in this part, a simple steel plate is analysed firstly under patch loading, bending and shear force take singularly and we compared the results given by the numerical model are compared with the one found in the literature. Different values of critical buckling coefficients have been computed considering three loading conditions as mentioned above. These values are presented in Table 2.4, Table 2.5 and Table 2.6 where a comparison shows a good correlation between FEM results and results from other authors.

Table 2.4. Buckling coefficient of plate under patch loading only

a/b	l_0/h_w	$k_{p,FEM}$	Modified k_p parabolic shear [2.67]	k_p [2.62]	k_p [2.64]	k_p [2.60]
2	4/10	2.54	2.56	2.45	6.73	5.21

Table 2.5. Buckling coefficient of plate under bending stress only

a/b	Stress ratio ψ	k_b FEM	k_b [2.67]
2	-1	23.86	23.98

Table 2.6. Buckling coefficient of plate under shear stress only

a/b	$k_{s,FEM}$	k_s [2.67]	k_s [2.2]
2	6.53	6.58	6.34

The results from the numerical study show good agreement with the value found in the literature since the maximum deviation is computed and equal to 4%. In regards to the patch loading case, it is observed a large deviation between results from numerical analysis and some authors. This large deviation is obtained for plate girder where the influence of the flange rotational stiffness is taken into account.

2.3.3 Interaction of combined loading

After the validation of the mesh, interaction between patch loading and bending in the first case, patch loading and shear in the second case, bending and shear in the third case and finally bending, patch loading and shear is analysed according to the work done by Roberts and Shahabian [2.58] and the results are found below.

Table 2.7. Buckling coefficient of plate under combined patch loading and bending

a/b	l_0/h_w	$\frac{k_{bp}}{k_b}$	$\frac{k_{pb}}{k_p}$	$\frac{k_{bp}}{k_b}$ FEM	$\frac{k_{pb}}{k_p}$ FEM
		0.40	0.80		
2	4/10	0.60	0.66	0.59	0.70
		0.80	0.44		
$\left(\frac{k_{bp}}{k_b}\right)^{\alpha_1} + \left(\frac{k_{pb}}{k_p}\right)^{\alpha_1}$				1.04	

$$\alpha_2 = 2.10 - 0.77\beta + 0.37\beta^2 - 0.05\beta^3 \quad (2.48)$$

Table 2.8. Buckling coefficient of plate under combined patch loading and shear

a/b	l_0/h_w	$\frac{k_{sp}}{k_s}$	$\frac{k_{ps}}{k_p}$	$\frac{k_{sp}}{k_s}$ FEM	$\frac{k_{ps}}{k_p}$ FEM
		0.40	0.89		
2	4/10	0.60	0.73	0.58	0.74
		0.80	0.45		
$\left(\frac{k_{ps}}{k_p}\right)^{\alpha_2} + \left(\frac{k_{sp}}{k_s}\right)^{\alpha_2}$				1.02	

$$\alpha_2 = 2.10 - 0.77\beta + 0.37\beta^2 - 0.05\beta^3 \quad (2.49)$$

Table 2.9. Buckling coefficient of plate under combined bending and shear

a/b	Stress ratio ψ	$\frac{k_{sb}}{k_s}$	$\frac{k_{bs}}{k_b}$	$\frac{k_{sb}}{k_s}$ FEM	$\frac{k_{bs}}{k_b}$ FEM
		0.40	0.92		
2	-1	0.60	0.81	0.67	0.74
		0.80	0.60		
$\left(\frac{k_{bs}}{k_b}\right)^{\alpha_3} + \left(\frac{k_{sb}}{k_s}\right)^{\alpha_3}$				1.00	

$$\alpha_3 = 1.56 + 0.34\beta - 0.14\beta^2 + 0.04\beta^3 \quad (2.50)$$

Table 2.10. Buckling coefficient of plate under combined bending, patch loading and shear

a/b	l_0/h_w	$\frac{k_{spb}}{k_s}$	$\frac{k_{bps}}{k_b}$	$\frac{k_{pbs}}{k_p}$	$\frac{k_{spb}}{k_s}$ FEM	$\frac{k_{bps}}{k_b}$ FEM	$\frac{k_{pbs}}{k_p}$ FEM
		0.40	0.20	0.80			
2	4/10	0.40	0.40	0.70	0.47	0.51	0.60
		0.40	0.60	0.55			
		0.40	0.80	0.30			
$xy(x^{\alpha_1} + y^{\alpha_1}) + xz(x^{\alpha_2} + z^{\alpha_2}) + yz(y^{\alpha_3} + z^{\alpha_3})$						0.583	
$xy + xz + yz - \eta xyz$						0.585	

$$x = \frac{k_{pbs}}{k_p} \quad (2.51)$$

$$y = \frac{k_{bps}}{k_b} \quad (2.52)$$

$$z = \frac{k_{spb}}{k_s} \quad (2.53)$$

$$\eta = 1.78 + 2.05\beta - 1.82\beta^2 + 0.39\beta^3 \quad (2.54)$$

From this example, it is observed that the initial buckling coefficient under a single loading condition will be affected if other different types of loading are applied to the plate. In Table 2.7, the results from the numerical analysis showed that under combined patch loading and bending, the decrease of critical buckling is more influenced by the patch loading. It can be understanding since the bending stress used provided some tension fields to the section while the patch load creates compressive stress on the plate girder. Initial buckling load of the plate under bending is reduced of 41% when patch loading is added while adding bending will cause a decrease of 30% of critical buckling load under patch loading.

From Table 2.8, the same conclusion can be drawn since the initial buckling load of a plate under shear is reduced of 42% when patch loading is added while adding shear will cause a decrease of 26% of critical buckling load under patch loading.

From Table 2.9, we observe a slight difference in the case where the patch loading is not applied. The initial critical shear load of the plate is reduced by 33% when bending stress is added at the same time while the initial critical bending will decrease by 25%.

From Table 2.10, the interaction between patch loading, bending and shear is analysed; shear and bending moment provides to the plate some tension fields to the web panel leading to less decrease of critical buckling of

web plate under patch loading only. The initial critical shear load of the plate is reduced of 53% when bending stress and patch loading are; it is reduced of 49 % when shear force and patch loading are added and finally, the initial critical patch loading will decrease of 40% when shear force and bending moment are added. Finally, Table 2.11 presents some outcomes recently found from previous investigations.

2.4 Conclusions

In this chapter, a review of recent investigation, analysis and experimental tests of plate girders under different loading configurations has been reported. Great attention has been devoted to web panel status (stiffened plate, unstiffened plate and unstiffened plate with the presence of hole). At first, an overview of first works and investigations in a period before 1992 have been presented, after latest advances concerning laboratory investigations, numerical analysis from 1992 to the present days have been reviewed. From this intensive work, it has been possible to draw the following conclusions.

In regards to the unstiffened plate, some authors questioned the failure mechanism of girders proposed by Roberts and proposed a new failure mechanism. A new methodology to find the patch loading resistance based on the resistance curve approaches have been developed and is now used by the current norm. Extensive analytical investigations allowed deriving expressions of critical buckling load and ultimate resistance for plates under combined in-plane loading. The results show that the combined loads change the structural response of the plate leading to rapid failure with respect to the case of single loading condition. New correction factors have been found or the existing has been updated to consider the influence of longitudinal stiffener on a plate girder while determining the critical buckling coefficient and the ultimate resistance of stiffened plate.

Longitudinal stiffeners when used increase the buckling capacity and the ultimate resistance of plate girders; the optimum location found for longitudinal stiffener will depend on the load condition. It correspond to one fifth of the compressed edge in the case of compressive load and the central position where pure bending is applied on plates. In addition, stiffener with closed-section due to its torsional stiffness presents a good structural response than the one with the open one.

The interaction between the three loads commonly presents during the bridge launching have been widely studied. Bending stress and shear force when applied simultaneously on plate girders being already subjected to patch loading can drastically reduce the resistance of steel plate girder. The numerical results showed that between shear load and bending stress, the latter is considered as the main action influencing the patch loading resistance dropping.

Non-linear analysis of steel plate with hole have shown that the sliding of the two distinct parts limited by hole in the plate is the consequence of plasticization of the zone near the hole,. Both RS and RL holes should be avoid near the panel edges whatever loading condition since their presence decrease considerably the buckling coefficient of steel plate.

Due to recent developments of FEM, the last few decades have been dedicated to extensive research on plate girders behaviour and today it seems to be understood but some works still remain important to focus on deeply as

the behaviour of stiffened girders plate under a combined bending stress, patch load, and shear force.

Table 2.11. Appendix of proposed or updated formulas by authors

N°	Authors	Ref. no.	Year	Developed formulas	Range of validity
1.	Johansson and Lagerqvist	[2.57]	1995	$\alpha = 1 + \left(\frac{l_c}{s_s}\right)^{1/8} + \left(\frac{2b_f b_f^3}{h_w t_w^3}\right)^{1/8}$ $k_{F,f} = 2.1\alpha + 1.2 \left(\frac{h_w}{a}\right)^2 + \left(\frac{s_s}{h_w}\right)^2 \left[0.4 + 2.0 \left(\frac{h_w}{a}\right)^2\right]$	The coefficient of instability takes into account the contribution of flange; the expression should be used for steel plate with height of the web less than $100t_w$
2.	Lagerqvist and Johansson	[2.65]	1996	$\chi^{(y)} = 0.06 + 0.47/\lambda \leq 1$ $F_{R,d} = F_y \chi^{(y)} / \gamma_{M1}$	The design procedure is limited for unstiffened plate
3.	Jäger et al.	[2.70]	2017	$\kappa = \left(\frac{M_{f,R}}{M_{el,eff,R}}\right)^{15} + 1$ $\frac{M}{M_{el,eff,R}} + \left(1 - \frac{M_{f,R}}{M_{el,eff,R}}\right) \left(\frac{2V}{V_{bw,R}} - 1\right)^\kappa \leq 1.0$	The interaction formula takes into account the flange contribution in case of girders for $\frac{A_f}{A_w} \leq 1.9$
4.	Kövesdi et al.	[2.27]	2014	$\left(\frac{M}{M_{pl,R}}\right)^{3.6} + \left(\frac{V - 0.5F}{V_R}\right)^{1.6} + \left(\frac{F}{F_R}\right)$ $\left(\frac{M}{M_{pl,R}}\right)^3 + \left(\frac{V - 0.5F}{V_R}\right)^{1.6} + \left(\frac{F}{F_R}\right)$	The interaction formula is valid for unstiffened plate with non-participation of flange in patch loading resistance and shear buckling The interaction formula is valid for unstiffened plate with participation of flange in patch loading resistance and shear buckling
5.	Maiorana et al.	[2.62]	2008	$c_1 = -0.0813 \left(\frac{h}{a}\right)^3 + 0.512 \left(\frac{h}{a}\right)^2 - 0.0398 \left(\frac{h}{a}\right) + 0.6167$ $c_2 = 0.3466 \left(\frac{l_0}{a}\right)^3 - 0.7462 \left(\frac{l_0}{a}\right)^2 - 0.0699 \left(\frac{l_0}{a}\right) + 0.999$ $F_{cr,y} = \left[3.2048 \frac{\pi^2 E}{12(1-\nu^2)}\right] \frac{t^3 c_1}{h c_2 c_3}$	The critical buckling load formula is valid for unstiffened plate girder. For this reason it is valid for the aspect ratio $1 \leq \alpha \leq 3$
6.	Ren and Tong	[2.60]	2005	$k_{crs} = 2.05 + 1.2 \left(\frac{h_w}{a}\right)^2 + \left(\frac{s_s}{h_w}\right)^2 \left[0.5 + 2.0 \left(\frac{h_w}{a}\right)^2\right]$ $k_{crf} = (1 + 0.65s_s^2) \left[6.3 - 0.05 \left(\frac{a}{h_w}\right)^2 + \frac{0.6}{(a/h_w)^2}\right]$ $k_{cr} = \frac{k_{crs} + k_{crf} \lambda \beta}{1 + \lambda \beta}$	The buckling coefficient of unstiffened plate with participation of flange is obtained by linear combination between the buckling coefficient of simple supported plate and the one of clamped plate. A large range of validity is considered during the analysis for patch loading length.
7.	Alinia	[2.82]	2005	$\frac{\tau_{ps}}{\tau_p} = -0.9331 \left(\frac{1}{\phi^2}\right) + 2.5912 \left(\frac{1}{\phi}\right) + 0.2433$ $\frac{\tau_{ps}}{\tau_p} = 2.9473 \left(\frac{1}{\phi^2}\right) + 0.8459 \left(\frac{1}{\phi}\right) + 0.7662$ $\frac{\tau_{ps}}{\tau_p} = 10.552 \left(\frac{1}{\phi^2}\right) - 0.6914 \left(\frac{1}{\phi}\right) + 0.9767$	The formulas present the influence of vertical stiffened in terms of number and typologies. A large range of aspect ratio is considered in the different formulas.
8.	Chacón et al.	[2.81]	2017	$\Delta F_f = \frac{b_f t_f^2 f_{yf}}{(a - S_s)} [2 - (\chi_{f0} + \chi_{fi})]$	The ultimate load carrying capacity of

				$F_{Rk,proposed} = \chi f_{yw} a t_w + \Delta F_f$	plate under concentrated force is expressed for the case of unstiffened plate.
9.	Graciano and Laerqvist	[2.59]	2003	$k_{sl} = \left(5.44 \frac{b_1}{a} - 0.21 \right) \sqrt{\gamma_s}$ $k_{\bar{n}} = 5.82 + 2.1 \left(\frac{h_w}{a} \right)^2 + 0.46 \sqrt{\beta} + k_{sl}$	The buckling coefficient of steel plate with presence of stiffener is expressed. The range of validity is $0.05 \leq b_1/a \leq 0.3$ and
10.	Graciano and Mendes	[2.93]	2014	$k_{sl} = -1.87 + 36.94(b_1/h_w) - 62.86(b_1/h_w)^2 - 8.09(s_s/a) + 16.38(s_s/a)^2 - 0.0036\gamma_s + 0.44(t_f/t_w) + 30.95(b_1/h_w)(s_s/a) + 0.031(b_1/h_w)\gamma_s + 0.0035(s_s/a)\gamma_s$	The contribution of longitudinal stiffener is given. The application of this expression is limited since it has been found for the aspect ratio a/h_w
11.	Graciano and Edlund	[2.95]	2003	$P_{u1} = 8f_{yw}t_w^2 \sqrt{\frac{E t_f}{8a f_{yf}}} + \frac{2(c_e - \eta)M_w}{a \cos \theta} \text{ if } b_1/t_w \leq 40$ $P_{u1} = 4t_w^2 \sqrt{\frac{E f_{yw} t_f}{b_1}} + \frac{24 E I_f (c_e - \eta) M_w}{b_1 M_f^2} \text{ if } b_1/t_w > 40$	The expression of the ultimate strength for plate girder considering only one stiffener is given with two stiffeners configurations.
12.	Graciano	[2.97]	2003	$f_s = 0.556 - 0.277 \ln \left[\frac{b_1}{h_w} \left(\frac{f_{yf}}{f_{yw}} \right) \right]$ $F_{Ro} = f_{yw} t_w l_y \chi^{(\lambda)}$ $F_{R1} = F_{Ro} \times f_s$	The correction factor to take into consideration the longitudinal stiffness in the resistance of stiffened plate is expressed. The formula presents an used restriction . It can be used only for girder webs with stiffener position $b_1 \leq 0.3 h_w$

2.5 References

- [2.1] 1993-1-1, Eurocode 3 (EC3): Design of Steel Structures. Part 1.1 General Rules and Rules for Buildings. ENV, 1992.
- [2.2] M. Alinia and R. Shirazi, "On the design of stiffeners in steel plate shear walls," *Journal of Constructional Steel Research*, no. 65, pp. 2069-2077, 2009.
- [2.3] M. M. Alinia and S. H. Moosavi, "Stability of longitudinally stiffened web plates under interactive shear and bending forces," *Thin-Walled Structures*, no. 47, pp. 53-60, 2009.
- [2.4] E. Maiorana, C. Pellegrino and C. Modena, "Influence of longitudinal stiffeners on elastic stability of girder webs," *Journal of Constructional Steel Research*, no. 67, pp. 51-64, 2011.
- [2.5] N. Loaiza, C. Graciano , R. Chacon and E. Casanova, "Influence of bearing length on the patch loading resistance of multiple longitudinally stiffened webs," in *EUROSTEEL*, Copenhagen, 2017.
- [2.6] B. Kovesdi, J. Alcaine, L. Dunai, E. Mirambell, B. Braun and U. Kuhlmann, "Interaction behaviour of steel I-girders; part II: Longitudinally stiffened girders," *Journal of Constructional Steel Research*, no. 103, pp. 344-353, 2014.
- [2.7] C. Graciano and B. Edlund, "Nonlinear FE analysis of longitudinally stiffened girder webs under patch loading," *Journal of Constructional Steel Research*, no. 58, pp. 1231-1245, 2002.
- [2.8] C. Pellegrino, E. Maiorana and C. Modena, "Linear and non-linear behaviour of steel plates with circular and rectangular holes under shear loading," *Thin-Walled Structures*, no. 47, pp. 607-616, 2009.
- [2.9] N. Hajdin and N. Markovic, "Failure mechanism for longitudinally stiffened I girders subjected to patch loading," *Architectural Applied Mechanics*, no. Elsevier, pp. 1377-1391, 2012.
- [2.10] K. Girkmann, "Die Stabilitat der Stegbleche vollwanger Trager bei Berucksichtigung ortlicher Lastangriffe," in *IABSE 3rd Congress*, Berlin, 1936.

- [2.11] L. Zetlin, "Elastic instability of flat plates subjected to partial edge loads," ASCE, vol. 1, no. 795, p. 81, 1955.
- [2.12] M. Khan and K. Johns, "Buckling of plates subjected to localized edge loadings," *The Structural Engineer*, vol. 50, no. 6, pp. 225-32, 1972.
- [2.13] C. Chin, F. Al-Bermani and S. Kitipornchai, "Finite element method of buckling analysis of plate structures," *Journal of Structural Engineering*, vol. 119, no. 4, pp. 1048-68, 1993.
- [2.14] K. Basler, "New Provisions for plate girder design," National Engineering Conference, Proc. AISC, pp. 607-11, 1961.
- [2.15] K. Rockey and D. Bagchi, "Buckling in plate girder webs under partial edge loadings," *Int. J. Mech. Sci.*, no. 12, pp. 61-76, 1970.
- [2.16] Bergfelt, "Patch loading on a slender web-influence of horizontal and vertical web stiffeners on the load carrying capacity," Chalmers University of Technology, Dept of Structural Engineering, Div. of Steel and Timber Structures,, no. Publ. S79:1, 1979.
- [2.17] P. Dubas and H. Tschamper, "Stabilité des âmes soumises à une charge concentrée et à une flexion globale," *Construction Métallique*, vol. 27, no. 2, pp. 25-39, 1990.
- [2.18] M. Elgaaly and W. Nunan, "Behaviour of Rolled Section Web Under Eccentric Compressive Edge Loads," *Proc. ASCE J. Struct. Eng*, vol. Vol. 115, no. No. 7, pp. 1561-1578, 1989.
- [2.19] M. Elgaaly and R. Salkar, "Behaviour of webs under eccentric compressive edge loads. In: Contact loading and local effects in thin-walled plated and shell structures," in IUTAM 1990 symposium. Berlin, 1990.
- [2.20] M. Drdacky, "On two particular problems of plate girders webs under partial edge loads," in Internal publication (prepared for Tihomy Colloquium): ITAM, Prague, 1990.
- [2.21] M. Stein and Neff, NACA Technical note No 1222, 1947.
- [2.22] M. D'Apice, D. Fielding and P. Cooper, "Static Tests on Longitudinally Stiffened Plate Girders," *Weld. Res. Counc. Bull.*, no. N0. 117, 1966.

- [2.23] R. Delesques, "Résistance des âmes de poutres sans raidisseurs intermédiaires.," *Construction Métallique*, no. 2, pp. 5-19, 1974.
- [2.24] T. Hoglund, "Design of thin plate I-girders in shear and bending with special reference to web buckling." Division of Building Statics and Structural Engineering, Royal Institute of Technology, Stockholm, 1981.
- [2.25] D. Ungernmann , "Bemessungsverfahren für Vollwand- und Kastenträger unter besonderer Berücksichtigung des Stegverhaltens," *Stahlbau*, RWTH Aachen, no. Heft 17, 1990.
- [2.26] M. Elgaaly, "Failure of thin-walled members under patch loading and shear," *Proceedings of the 3rd International Specialty Conference on Cold Formed Structures*, pp. 357-81, 1975.
- [2.27] B. Kovesdi, J. Alcaine, L. Dunai, E. Mirambell, B. Braun and U. Kuhlmann, "Interaction behaviour of steel I-girders Part I: Longitudinally unstiffened girders," *Journal of Constructional Steel Research*, no. 103, pp. 327-343, 2014.
- [2.28] S. Timoshenko and J. Gere, *Theory of Elastic Stability*, 2nd ed., New Jersey: McGraw-Hill, 1986.
- [2.29] T. Roberts and K. Rockey, "A mechanism solution for predicting the collapse loads of slender plate girders when subjected to in-plane patch loading," *Proc Inst Civ Eng*, vol. 67, no. 2, pp. 155-75, 1979.
- [2.30] T. Roberts and N. Markovic, "Stocky plate girders subjected to edge loading," *Proc Inst Civ Eng*, vol. 75, no. 2, pp. 539-50, 1983.
- [2.31] L. Gil-Martin, B. Scepanovic, E. Hernandez-Montes, M. Aschheim and D. Lucic, "Eccentrically patch-loaded steel I-girders: The influence of patch load length on the ultimate strength," *Journal of Constructional Steel Research*, no. 66, pp. 716-722, 2010.
- [2.32] B. Johansson, R. Maquoi and G. Sedlacek, "New design rules for plated structures in Eurocode 3," no. 57, pp. 279-311, 2001.
- [2.33] T. Hoglund, "Shear Buckling Resistance of Steel and Aluminium Plate Girders," *Thin-Walled Structures*, vol. 29, pp. 13-30, 1998.

- [2.34] P. Cooper, B. Lew and B. Yen, "Welded constructional alloy steel plate girder," *J. Struct. Div. ASCE*, vol. 90, no. 1, pp. 1-36, 1964.
- [2.35] EN 1993-1-5:2006: EUROCODE3-Design of steel structures Part 1-5: Plated structural elements, 2006.
- [2.36] J. Oxfort and H. Gauger, "Beultraglast von Vollwandtragern unter Einzellasten,," *Stahlbau*, vol. 58, no. 11, pp. 331-9, 1989.
- [2.37] P. Zoetemeijer, "The influence of normal-, bending- and shear stresses on the ultimate compression force exerted laterally to European rolled sections," Delft, 1980.
- [2.38] C. Graciano and A. Ayestaran, "Steel plate girder webs under combined patch loading, bending and shear," *Journal of Constructional Steel Research*, no. 80, pp. 202-212, 2012.
- [2.39] D. Porter, K. Rockey and H. Evans, "The collapse behaviour of plate girders loaded in shear," *The Struct Eng*, vol. 53, no. 8, pp. 313-25, 1975.
- [2.40] N. Shanmugam and V. Thevendran, "Design formula for axially compressed perforated plates," *Thin-Walled Structures*, no. 34, pp. 1-20, 1999.
- [2.41] Z. Azizian and T. Roberts, "Buckling and elasto-plastic collapse of perforated plates," in *Proceedings of the international conference on instability and plastic collapse of steel structures.*, Granada, 1983.
- [2.42] El-Sawy, A. Nazmi and M. Martini, "Elasto-plastic buckling of perforated plates under uniaxial compression," *Thin-Walled Structures*, no. 42, pp. 1083-1101, 2004.
- [2.43] C. Brown, A. Yettram and M. Burnett, "Stability of plates with rectangular holes,," *Journal of Structural Engineering, ASCE*, vol. 113, no. 5, pp. 1111-6, 1987.
- [2.44] T. Shakerley and C. Brown, "Elastic buckling of plates with eccentrically positioned rectangular perforations," *International Journal of Mechanical Science*, vol. 38, no. 8-9, pp. 825-838, 1996.
- [2.45] R. Narayanan and F. Chow, "Ultimate capacity of uniaxially compressed perforated plates," *Thin-Walled Structures*, no. 2, pp. 241-64, 1984.

- [2.46] D. Porter, K. Rockey and H. Evans, "The collapse behaviour of plate girders loaded in shear," *The Struct Eng*, vol. 53, no. 8, pp. 313-25, 1975.
- [2.47] L. Pavlovic, A. Detzel, U. Kuhlmann and D. Beg, "Shear resistance of longitudinally stiffened panels—Part 1: Tests and numerical analysis of imperfections," *Journal Of Constructional Steel Research*, no. 63, pp. 337-350, 2006.
- [2.48] R. Charlier and R. Maquoi, "Ultimate shear strength of plate girders fitted with closed shape longitudinal stiffeners," *Proc. in the int. colloquium on stability of plate and shell structures*, pp. 59-64, 1987.
- [2.49] Cook and K. Rocky, *Aeronaut Quart*, vol. 13, no. 1, p. 41, 1962.
- [2.50] Loughlan and N. Hussain, "The in-plane shear failure of transversely stiffened thin plates," *Thin-Walled Structures*, no. 81, pp. 225-235, 2014.
- [2.51] W. Schueller and A. Ostapenko, "Tests on transversally stiffened and on longitudinally stiffened unsymmetrical plate girders," *Welding research council*, 1970 156.
- [2.52] B. Kovesdi, J. Alcaine, L. Dunai, E. Mirambell, B. Braun and U. Kuhlmann, "Interaction behaviour of steel I-girders; part II: Longitudinally stiffened girders," *Journal of Constructional Steel Research*, no. 103, pp. 344-353, 2014.
- [2.53] T. V. Galambos, "Guide to stability design criteria for metal structures," 5th ed., p. 911, 1998.
- [2.54] C. Dubas, "A contribution to the study of buckling stiffened plates," *Int Assoc Bridge Struct Eng Prelim* 1948, 1948.
- [2.55] Rockey and D. Leggett, "The buckling of a plate girder web under pure bending when reinforced by a single longitudinal stiffener," *Proc Inst Civ Eng*, no. 21, 1962.
- [2.56] Kutmanova and M. Skaloud, "Ultimate limit state of slender steel webs subjected to (i) constant and (ii) repeated partial edge loading.," *J Construct Steel Research*, Vols. 147-62, no. 21, 1992.

- [2.57] B. Johansson and O. Lagerqvist, "Resistance of plate edges to concentrated forces," *Journal of Constructional Steel Research*, no. 32, pp. 69-105, 1995.
- [2.58] R. Shahabian and T. Roberts, "Buckling of slender web plates subjected to combinations of in-plane loading," *Journal of Constructional Steel Research*, no. 51, pp. 99-121, 1999.
- [2.59] C. Graciano and O. Lagerqvist, "Critical buckling of longitudinally stiffened webs subjected to compressive edge loads," *Journal of Constructional Steel Research*, no. 59, pp. 1119-1146, 2003.
- [2.60] T. Ren and G. Tong, "Elastic buckling of web plates in I-girders under patch and wheel loading," *Engineering Structures*, pp. 1528-1536, 2005.
- [2.61] Y. Duchene and R. Maquoi, "Contribution par voie numérique à l'étude de la résistance des âmes aux charges transversales," *Construct Métall*, no. 2, pp. 43-56, 1994.
- [2.62] E. Maiorana, C. Pellegrino and C. Modena, "Linear buckling analysis of unstiffened plates subjected to both patch load and bending moment," *Engineering Structures*, no. 30, pp. 3731-3738, 2008.
- [2.63] Competing G+D, *Strand7 user's manual*, 2005.
- [2.64] C. Graciano, "Patch loading resistance of longitudinally stiffened girders - A systematic review," *Thin-Walled Structures*, no. 95, pp. 1-6, 2015.
- [2.65] O. Lagerqvist and B. Johansson, "Resistance of I-girders to concentrated loads," *Journal of Constructional Steel research*, vol. 39, no. 2, pp. 87-119, 1996.
- [2.66] P. Granath, A. Thorsson and B. Edlund, "I-shaped steel girders subjected to bending moment and travelling patch loading," *Journal of Constructional Steel Research*, no. 54, pp. 409-421, 2000.
- [2.67] T. M. Roberts and F. Shahabian, "Ultimate resistance of slender web panels to combined bending shear and patch loading," *Journal of Constructional Steel Research*, vol. 57, pp. 779-790, 2001.

- [2.68] AASHTO, "LRFD, Bridge Design Specifications," American Association of State Highway and Transportation Officials, 2004.
- [2.69] AISC, "Specification for structural Steel Buildings," Steel Construction Manual, 2005.
- [2.70] B. Jager, B. Kovesdi and L. Dunai, "I-girders with unstiffened slender webs subjected by bending and shear interaction," *Journal of Constructional Steel Research*, no. 131, pp. 176-188, 2017.
- [2.71] E. Maiorana, C. Pellegrino and C. Modena, "Linear buckling analysis of perforated plates subjected localised symmetrical load," *Engineering Structures*, no. 30, pp. 3151-3158, 2008.
- [2.72] E. Maiorana, C. Pellegrino and C. Modena, "Elastic stability of plates with circular and rectangular holes subjected to axial compression and bending moment," *Thin-Walled Structures*, no. 47, pp. 241-255, 2009.
- [2.73] E. Maiorana, C. Pellegrino and C. Modena, "Elasto-plastic behaviour of perforated steel plates subjected to compression and bending," *Steel and Composite Structures*, vol. 11, no. 2, pp. 131-147, 2011.
- [2.74] E. Maiorana, C. Pellegrino and C. Modena, "Non-linear analysis of perforated steel plates subjected to localised symmetrical load," *Journal of Constructional Steel Research*, no. 65, pp. 959-964, 2009.
- [2.75] C. Pellegrino, E. Maiorana and C. Modena, "Linear and non-linear behaviour of steel plates with circular and rectangular holes under shear loading," *Thin-Walled Structures*, no. 47, pp. 607-616, 2009.
- [2.76] El-Sawy and A. Nazmi, "Effect of aspect ratio on the elastic buckling of uniaxial loaded plates with eccentric holes," *Thin-Walled Structures*, no. 39, pp. 983-998, 2001.
- [2.77] K. Paik, "Ultimate strength of perforated steel plates under edge shear loading," *Thin-Walled Structures*, no. 45, pp. 301-306, 2007.
- [2.78] Komur and M. Sonmez, "Elastic buckling behaviour of rectangular plates with holes subjected to partial edge loading," *Journal of Constructional Steel Research*, no. 112, pp. 54-60, 2015.

- [2.79] R. Chacon, E. Mirambell and E. Real, "Transversally stiffened plate girders subjected to patch loading. Part 1. Preliminary study," *Journal of Constructional Steel Research*, no. 80, pp. 483-491, 2013.
- [2.80] R. Chacon, E. Mirambell and E. Real, "Transversally stiffened plate girders subjected to patch loading Part 2. Additional numerical study and design proposal," *Journal of Constructional Steel Research*, no. 80, pp. 492-504, 2013.
- [2.81] R. Chacon, J. Herrera and L. Fargier-Gabaldon, "Improved design of transversally stiffened steel plate girders subjected to patch loading," *Engineering Structures*, no. 150, pp. 774-785, 2017.
- [2.82] M. Alinia, "A study into optimization of stiffeners in plates subjected to shear loading," *Thin-Walled Structures*, no. 43, pp. 845-860, 2005.
- [2.83] Alinia, S. Hosseinzadeh and H. Habashi, "Numerical modelling for buckling analysis of cracked shear panels," *Thin-Walled Structure*, vol. 45, no. 12, pp. 1058-67, 2007.
- [2.84] Alinia, S. Hosseinzadeh and H. Habashi, "Buckling and post buckling strength of shear panels degraded by near border cracks," *J Construct Steel Research*, 2008.
- [2.85] Cevik, "A new formulation for longitudinally stiffened webs subjected to patch loading," *Journal of Constructional Steel Research*, no. 63, pp. 1328-1340, 2007.
- [2.86] Galea, Y., & Martin, p. (2010). Longitudinally stiffened plates in Eurocode 3: Calculation of the global critical buckling stress. *Journal of Constructional Steel Research*(66), 1345-1353. doi:doi:10.1016/j.jcsr.2010.05.001
- [2.87] S. Ajeesh and S. Sreekumar, "Shear Behaviour of Stiffened Plate Girders," in *Proceeding of International Structural and Civil Engineering*, India, 2011.
- [2.88] L. Pavlovic, D. Beg and U. Kuhlmann, "Shear resistance of longitudinally stiffened panels—Part 2: Numerical parametric study," *Journal of Constructional Steel Research*, no. 63, pp. 351-364, 2007.

- [2.89] E. Maiorana , C. Pellegrino and C. Modena, "Imperfections in steel girder webs with and without perforations under patch loading," *Journal of Constructional Steel Research*, no. 65, pp. 1121-1129, 2008.
- [2.90] J. Chica, J. San José, F. Millanes and J. Manso, "Recommendations on imperfections in the design of plated structural elements of bridges," *Journal of Constructional Steel Research*, no. 86, pp. 183-194, 2013.
- [2.91] Amani, M. Alinia and M. Fadakar, "Imperfection sensitivity of slender/stocky metal plates," *Thin-Walled Structures*, no. 73, pp. 207-215, 2013
- [2.92] C. Graciano, E. Casanova and J. Martinez, "Imperfection sensitivity of plate girder webs subjected to patch loading," *Journal of Constructional Steel Research*, no. 67, pp. 1128-1133, 2011.
- [2.93] C. Graciano and J. Mendes, "Elastic buckling of longitudinally stiffened patch loaded plate girders using factorial design," *Journal of Constructional Steel Research*, no. 100, pp. 229-236, 2014.
- [2.94] C. Graciano and B. Edlund, "Nonlinear FE analysis of longitudinally stiffened girder webs under patch loading," *Journal of Constructional Steel Research*, no. 58, pp. 1231-1245, 2002.
- [2.95] C. Graciano and B. Edlund, "Failure mechanism of slender girder webs with a longitudinal stiffener under patch loading," *Journal of Constructional Steel Research*, no. 59, pp. 27-45, 2003.
- [2.96] C. Graciano and B. Johansson, "Resistance of longitudinally stiffened I-girders subjected to concentrated loads," *Journal of Constructional Steel Research*, no. 59, pp. 561-586, 2003.
- [2.97] C. Graciano, "Ultimate resistance of longitudinally stiffened webs subjected to patch loading," *Thin-Walled Structures*, no. 41, pp. 529-541, 2003.
- [2.98] F. Sinur and D. Beg, "Moment–shear interaction of stiffened plate girders—Tests and numerical model verification," *Journal of Constructional Steel Research*, no. 85, pp. 116-129, 2013.

CHAPTER 3

Elastic Buckling of Steel Plate Subjected to Patch Loading Interacting with Bending and Shear

3.1 Abstract

In bridge erection, a steel girder undergoing in-plane loading is commonly subjected to the interaction of several forces. Many previous studies have highlighted the effects of single in-plane loads on plate buckling but only a few works concentrated on the combined effects. For this reason, the stability of steel plates subjected to the combined action of patch loading, bending moment, and shear stress was studied through parametric analysis in this work. In particular, the effect of patch loading length combined with bending and shear stress was investigated. Other parameters like patch loading magnitude, panel aspect ratio, and plate slenderness have also been considered to characterize the plate stability. Through an intensive finite element method (FEM) analysis, new design equations have been defined to describe the influence of plate and load parameters on critical buckling loads of plates subjected to combined loads, with regard to plates subjected to patch loading. A comparison with the FEM results offers good accuracy, with a maximum deviation equal to 5%. To validate the analytical equations, a practical example is given.

A	Coefficient ratio between the patch loading and equivalent compressive force from bending stress
B	Coefficient ratio between transversal shear force and the equivalent compressive force from bending stress
F	Patch loading
$F_{0,el}$	Eulerian critical force
F_x	Equivalent compressive force from bending stress
F_y	Equivalent compression corresponding to the patch loading
$F_{cr,F}$	Critical patch loading force for plate under patch loading

$F_{cr,M+V+F}^F$	Critical patch loading force for plate under patch loading interacting with bending and shear
M	Bending moment
$M + F + V$	Combined bending, patch loading and shear
V	Shear
V_x	Equivalent shear force in horizontal direction
V_y	Equivalent shear force in vertical direction
a	Length of the steel plate (length between successive vertical stiffener)
b	Height of the steel plate (height of the steel web)
b_f	Width of the steel flange
k_F	Critical buckling coefficient of plate subjected to patch loading
l_0	Patch loading length
t	Thickness of the steel plate (thickness of the steel web)
t_f	Thickness of the steel flange
α	Panel aspect ratio
β	Parameter describing the stress variation
λ	Plate Slenderness
λ_{cr}	Critical buckling load factor
$\lambda_{cr,F}$	Critical buckling load factor for plate under patch loading
$\lambda_{cr,M+V+F}$	Critical buckling load factor for plate under patch loading interacting with bending and shear
ν	Poisson coefficient
σ_0	Maximum normal stress
τ_{xy}	Shear stress in the y direction
τ_{yx}	Shear stress in the x direction
ψ	Stress ratio

3.2 Introduction

Different technologies are used for bridge erection around the world, among which, the incremental launching method appears to be preferred according to the statistics presented by many researchers [3.1]-[3.4]. Although it is not considered the most economical technique, the incremental launching method has become unavoidable in bridge construction over a wide range of challenging sites that feature limited or restricted access such as valleys, deep water crossings, steep slope conditions, and protected species beneath the bridge. During the launching process, slender girders may overpass on bearings where a concentrated force from the support reaction may arise. In addition, as the beam is pulled from one support to another and considering the self-weight of both of the girder and equipment as well as other construction loads, a large bending moment and shear force can also arise. If special attention is not taken with the steel girders, the instability of the slender web will occur leading to the loss of the section in the construction phase.

The current EN1993-1-5 standard [3.5] provides verification methods for a steel plate subjected to patch loading, bending and shear. In addition, for a steel plate subjected to the following in-plane loads, such as bending–patch loading (M-F), bending–shear buckling (M-V), and shear buckling–patch loading (V-F) interactions, the associated interaction equations are found within the EN1993-1-5 standard [3.5] for design in such situations. In the meantime, the lack of a straightforward M-V-F interaction equation in the design standard has forced many researchers to address this issue. In 2010, during his PhD thesis, Braun [3.6] developed 3D interaction curves to design a steel plate under combined in-plane loadings. The 3D domain was built from the database of the numerical results of both M-F and V-F interactions. Later, Graciano and Ayestarán [3.7] and Kövesdi et al. [3.1] provided more general and accurate 3D interaction curves obtained from merging the individual M-F, V-F, and M-F interaction curves. The two studies combined offer a wide range of applicability since each research work was based on the analysis of different geometrical parameter ranges [3.1]. Tong et al. [3.8] proposed 3D non-dimensional interactive surfaces to describe the stability of a steel plate subjected to combined patch loading, bending, and shear force. The interaction equation derived covers a wide range of variability in the steel girder geometry.

From parts of the previous studies, it appears that both the stability and ultimate capacity of a steel plate under different loading conditions have been intensively investigated but till now, only a few studies have directed their research toward a steel plate subjected to combined M-F-V loading. In addition, all the existing studies' outcomes solved the problem through the 3D interaction domain while most of the time, designers and practitioners are

looking for straightforward analytical expressions that are useful in the predesign stage before moving ahead into the design phase.

In the present research, intensive numerical analyses were performed to derive a unique equation to determine the critical buckling load multiplier of a steel plate under combined M-V-F loading. In addition, a large portion of the authors' previous work [3.9] developed an innovative equation to determine the critical patch loading for a steel plate under combined in-plane loading. A detailed description of the research aim is found in the next section at the end of the literature review. The study was completed systematically following the research strategy listed below. In particular, the following points will be discussed.

1. Literature overview of work on steel plate behavior under combined in-plane loading, both singular and combined.

2. Development of numerical models based on Quad 4 shell elements taking into account different aspects related to the steel plate's geometry and loading conditions and validation of the numerical model based on previous experimental, analytical, and finite element method (FEM) analysis results.

3. Parametric numerical analysis to study the structural behavior of a steel plate subjected to combined in-plane loadings such as buckling shape and critical buckling load factor; different geometrical and loading parameters will be considered.

4. Development of a design equation to determine the critical buckling load multiplier based on FEM results and validation of the proposed equations through a comparison of the analytical equation proposed and the FEM results.

5. Application of the proposed formula in a design example to show the applicability of the formula in a real world situation.

The research results showed that additional bending and shear loadings may considerably reduce the critical patch loading resistance up to 50%. On the other hand, high accuracy was obtained comparing both FEM and analytical results with a discrepancy lower than 5%. Finally, through a practical example, the current research results showed their reliability in application to a real world design.

3.3 Theoretical background

The instability of a steel plate subjected to various loading conditions has been widely studied either experimentally or numerically. The topic became a definitive research interest after the collapse of some bridges due to the loss of stability in the 1950s with the presentation of the first results on a

related topic. For the most part, the results were based on experimental campaigns and theoretical investigations. Several researchers such as Zetlin [3.10], Basler [3.11], Rockey and Bagchi [3.12], and Khan and Walker [3.13] derived the critical buckling coefficient of both clamped and simply supported steel plates subjected to partial edge loading. Recently, there have been substantial research works that have been carried out with the aim of either studying new aspects or providing further details and explanations of the pioneering research.

Graciano and Lagerqvist [3.14] studied the stability of a steel plate under compressive loads. They considered the rotational restraint of the flange in the definition of the critical buckling coefficient of a simply supported plate. Ren and Tong [3.15] focused their research on the restraining conditions of the plate girder web. They proposed a buckling coefficient in terms of patch loading for both simply supported and clamped rectangular plates (Eq. [3.1] and Eq. [3.2]).

$$k_{\text{crs}} = 2.05 + 12/(a/h_w)^2 + s_s^2 \left[0.5 + 2.0/(a/h_w)^2 \right], \quad (3.1)$$

$$k_{\text{crf}} = (1 + 0.65s_s^2) \left[6.3 - 0.5 + 2.0/(a/h_w)^2 \right], \quad (3.2)$$

Other expressions to determine the critical buckling coefficient were proposed [3.9], [3.16]. Porter and Rockey [3.17] studied the critical condition of plate girders. Through extensive numerical analysis, Alinia [3.18] investigated the critical buckling of a stiffened plate under shear while Maiorana et al. [3.19] studied the optimal position of a longitudinal stiffener for plates subjected to bending. Graciano and Mendes [3.20] used a factorial design to study the influence of geometrical parameters on the critical buckling coefficient of a stiffened steel girder subjected to patch loading. The proposed method is useful to predict output variables from input data through a mathematical model. They found that the relative position of the stiffener, its flexural rigidity, and the patch loading length are the most influential parameters for plate buckling.

In regards to studies on steel plate stability under combined in-plane loading, an analytical formula was proposed to estimate the critical buckling coefficient of a steel plate under patch loading and bending moment [3.9]. The influence of the longitudinal stiffener on the interaction curves describing the plate stability subjected to bending–shear interaction has also been studied [3.21]. Within the same scope, Quang-Viet et al. [3.22] carefully studied the optimum position of a multi-stiffened plate under combined bending and shear forces through the gradient-based interior point optimization algorithm. The results showed that the presence of two stiffeners on a steel plate would increase the critical buckling coefficient up to 180% and may lead to the optimization of the plate thickness to approximately 62%.

Shahabian and Roberts [3.23] investigated the buckling of rectangular plates subjected to a combination of in-plane patch loading, compression, bending, and shear stress. They proposed different equations according to a case study that had a wide range of validity (Eq. (3.3) – Eq. (3.5)).

$$\left(\frac{k_{bp}}{k_b}\right)^{\alpha_1} + \left(\frac{k_{pb}}{k_p}\right)^{\alpha_1} = 1, \quad (3.3)$$

$$\left(\frac{k_{sp}}{k_s}\right)^{\alpha_2} + \left(\frac{k_{ps}}{k_p}\right)^{\alpha_2} = 1, \quad (3.4)$$

$$\left(\frac{k_{sb}}{k_s}\right)^{\alpha_3} + \left(\frac{k_{bs}}{k_b}\right)^{\alpha_3} = 1, \quad (3.5)$$

Recently, through extensive FEM analysis, 3D non-dimensional interactive surfaces have been proposed to describe the stability of a steel plate subjected to combined patch loading, bending, and shear force [3.7]. In the study, it is also provided a single equation to define the 3D interaction curve (Eq. (3.6)). Further information regarding the parameters involved in this equation is found within the paper.

$$\chi \left(\frac{\sigma_b}{\sigma_{bcr0}}\right)^{\beta} + \left(\frac{\tau}{\tau_{bcr0}}\right)^2 + \left(\frac{\sigma_c}{\sigma_{cr0}}\right)^{\beta_{ct}} = 1, \quad (3.6)$$

Other significant studies on the ultimate resistance of a steel plate under various in-plane loadings have been done. The latest research on plated structures under M-F interaction behavior can be found in [3.4]. Jager et al. [24] performed an intensive numerical analysis to investigate the M-V interaction behavior of longitudinally unstiffened I-girders with a slender web. They proposed a refined M-V interaction equation changing the index k from 1.0 to a higher value that better fits the numerical simulations (Eq. (3.6)).

$$\frac{M}{M_{el,eff,R}} + \left(1 - \frac{M_{f,R}}{M_{el,eff,R}}\right) + \left(\frac{2V}{V_{bw,R}} - 1\right)^2 \leq 1, \quad (3.7)$$

The investigation of the ultimate load behavior of longitudinally stiffened girder webs under patch loading can be found in [3.25]. The authors discovered that the influence of stiffener's relative flexural rigidity is less important for ultimate strength analysis due to loss of the stiffener's rigidity but it plays an important role in increasing the critical elastic buckling load of a plate girder under patch loading. Braun [3.6] developed a 3D interaction formula to describe the interaction behavior of a steel plate subjected to combined patch loading, bending, and shear stress (Eq. (3.8)).

$$\left(\frac{P}{P_R}\right) + \left(\frac{M}{M_R}\right)^{3.6} + \left(\frac{V}{V_R}\right)^{1.6} \leq 1, \quad (3.8)$$

Graciano and Ayestarán [3.7] investigated the nonlinear behavior of unstiffened girder webs subjected to combined concentrated loading, bending, and shear stress using the finite element method. They showed that the bending action is the most influential factor to cause a reduction in patch loading resistance. Finally, Kövesdi et al. [3.1] updated the interaction equation derived by Braun [3.6] through statistical analysis. Different plate geometries were considered in the investigation and the results showed that the flange greatly influences the design equation:

$$\left(\frac{M}{M_{pl,R}}\right)^{3.0} + \left(\frac{V - 0.5 \cdot F}{V_R}\right)^{1.6} + \left(\frac{F}{F_R}\right) \leq 1, \quad (3.9)$$

Maiorana et al. [3.8] derived an innovative calculation for the critical buckling coefficient of a steel plate under M-F combined load. The investigation omitted the presence of shear buckling. In the present study, new analyses have been performed to take into account the influence of both bending and shear stress in the critical patch loading force. Therefore, the principal aim of the present investigation is to extend the authors' previous work [3.8] and the following points will be addressed in detail:

1. Description of the influence of geometrical and load parameters on the critical buckling load multiplier by performing a parametric analysis.
2. Derivation of a new analytical equation through linear FEM analysis to obtain the critical buckling load factor $\lambda_{cr,M+V+F}$ of a steel plate under combined M-V-F load.
3. Derivation of the critical patch loading buckling coefficient $k_{Fcr,F+M+V}$ to estimate the critical patch loading of a steel plate subjected to combined M-V-F loads.
4. Presentation of a practical design case with a specific geometry currently used in the bridge industry to show the applicability of the derived equation.

3.4 Finite Element Method

The elastic stability of a rectangular steel plate subjected to combined patch loading, bending, and shear stress is studied through finite element analysis using Strand 7 [3.26]. Shell elements with four nodes, Quad 4, and six degrees of freedom are used in the analysis. The material is considered linear elastic since linear buckling is to be performed.

Constraint in the z-direction has been applied along the four sides of the plate to avoid out-of-plane displacement. At each corner node, elastic restraint with a specific stiffness is applied to allow the corner nodes to move

in the x- and y-directions. In order to keep the direction of the load fixed in the deformed shape of the plate, it is directly applied to each node as a system of conservative forces.

In order to validate the numerical results, two calibrations were carried out. In the calibration process, a steel plate with the characteristics presented in Table 3-1 and displayed in Fig. 1a is considered. At the first stage, it was necessary to define an appropriate beam element with a specific elastic restraint (Table 3-2) giving FEM results close to the results from the literature. The steel plate under combined patch loading and bending stress was analyzed and the numerical results were compared to Maiorana et al. [3.9] and they showed a good agreement with a maximum difference equal to 2.9% as presented in Table 3-3.

Table 3.1. Characteristics of material and section tested for calibration

E (N/mm ²)	ν	a (mm)	t (mm)	b (mm)
206 000	0.3	2000	10	1000

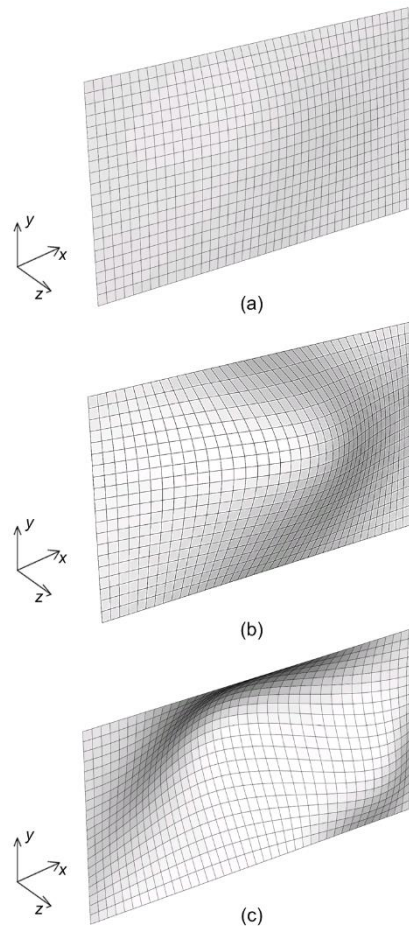


Fig. 3.1. Numerical model in the calibration phase

(a) Flat steel plate; (b) Buckling shape of steel plate under patch loading; (c) Buckling plate of steel plate under combined patch loading and bending moment

Table 3.2. Geometry and mechanical characteristics of elastic restraint

Diameter (mm)	L (mm)	E (MPa)	EA/L (N/mm)
3	300	206 000	4853.76

A' is the section, L is the length of the elastic restraint, and EA/L is the axial stiffness of the elastic restraint.

The second calibration concerns the accuracy of the mesh. A steel plate with the same characteristics presented in Table 3.1 subjected to patch loading was studied and the numerical results are compared with the results of previous studies. A good correlation is found in accordance with previous results as presented in Table 3.4. In Figs. 3.1b and 3.1c, the first buckling mode of the steel plate under patch loading and combined patch loading and bending moment are presented, respectively, whereas in Fig. 3.2, the typical loading scheme and boundary conditions of the model investigated in the next parts of the study are presented.

Table 3.3. Calibration of the elastic restraints ($F=100$ kN)

ψ	Method	λ_{cr}		
		$\sigma_0=10$ MPa	$\sigma_0=50$ MPa	$\sigma_0=100$ MPa
-1	Maiorana et al., 2008	4.23	3.53	2.79
	FEM	4.23	3.54	2.81
	Δ	0.0%	0.3%	0.7%
-0.5	Maiorana et al., 2008	3.99	2.83	2.01
	FEM	3.98	2.83	2.02
	Δ	0.3%	0.0%	0.5%
0	Maiorana et al., 2008	3.76	2.27	1.36
	FEM	3.75	2.27	1.40
	Δ	0.3%	0.0%	2.9%
1	Maiorana et al., 2008	3.34	1.41	0.71
	FEM	3.33	1.45	0.73
	Δ	0.3%	2.8%	3%

Table 3.4. Buckling coefficients of plate under patch loading only ($a/b=2$)

l/a	$k_{F,FEM}$	k_F			
		Alinia, [3.18]	Shahabian and Roberts, [3.23]	Graciano and Lagerqvist, [3.14]	Ren and Tong, [3.15]
0.0	3.31	3.25	–	3.23	3.22
0.1	3.39	3.30	3.27	3.26	–

0.2	3.51	3.45	–	3.34	3.36
0.3	3.68	3.60	–	3.49	3.51
0.4	3.90	3.70	3.68	3.67	3.71
0.5	4.17	3.95	3.90	3.92	3.97

$k_{F,FEM}$ is the critical buckling coefficient from FEM analyses of a steel plate under patch loading; k_F is the critical buckling coefficient of a steel plate under patch loading found in the literature, σ_0 is the maximum normal stress, and l_0 is the patch loading length

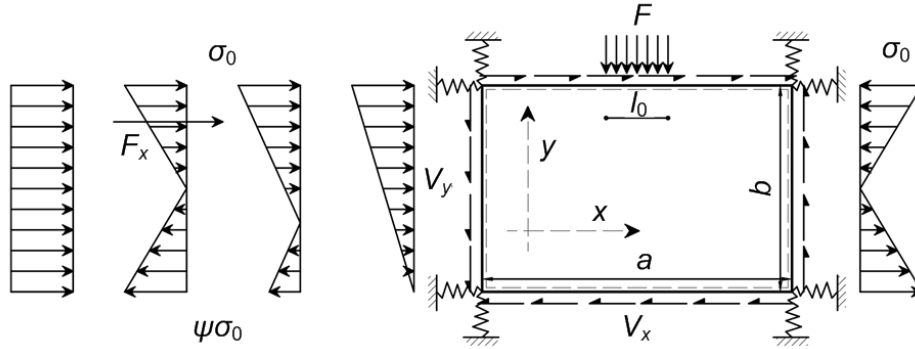


Fig. 3.2. Plate subjected to combined patch loading, bending, and shear

In regards to the loading configuration, the bending stresses with different stress ratios ($\psi=-1$, $\psi=-0.5$, $\psi=0$, and $\psi=1$) are applied in the x -direction where the magnitudes are chosen according to current observations of a real project as highlighted by Maiorana et al. [3.9]. However, only the compressive part of the bending stress will be considered since it is relevant in the buckling analysis. In Eq.(3.10) and Eq.(3.12), the existing relationship between patch loading, bending moment, and shear force is presented.

$$F_x=A \cdot F \tag{3.10}$$

$$V_y=B \cdot F_x=B \cdot A \cdot F, \tag{3.11}$$

$$V_x = \frac{a}{b} \cdot V_y = \frac{a}{b} \cdot B \cdot A \cdot F, \tag{3.12}$$

where the coefficients A and B represent the loading parameters which describe the relationship between different in-plane loadings and are defined in Table 3.5. V_x and V_y are the equivalent shear force in the horizontal and vertical directions, respectively. F_x represents the integral of the compressive part of the bending stress and can be obtained:

$$F_x = \begin{cases} \sigma_0 \frac{b \cdot t}{4}, & \psi = -1, \\ \sigma_0 \frac{2b \cdot t}{3}, & \psi = -0.5, \\ \sigma_0 \frac{b \cdot t}{2}, & \psi = 0, \\ \sigma_0 \cdot b \cdot t, & \psi = 1, \end{cases}$$

Where σ_0 is the maximum normal stress, b is the height of the steel plate, and t is the plate's thickness.

In theory, there is no mathematical relationship between patch loading F and the resulting compressive force F_x obtained from the bending moment. The loading parameters have been chosen with the aim to match as close as possible to real cases whereas a and b are related to the geometrical characteristics of the steel plate.

$$V_x = \int \tau_{xy} \, dA', \tag{3.13}$$

$$V_y = \int \tau_{yx} \, dA', \tag{3.14}$$

Where τ_{xy} and τ_{yx} represent the shear stress in the y and x directions, respectively as shown in Fig. 3.3.

Since $\tau_{xy}=\tau_{yx}$, τ_{xy} is supposed to be constant along edge b and τ_{yx} is supposed to be constant along side a , Eq. (3.13) and Eq. (3.14) will become, respectively, Eq. (3.15) and Eq. (3.16).

$$V_x = \int \tau_{xy} \, dA', \tag{3.15}$$

$$V_y = \int \tau_{yx} \, dA', \tag{3.16}$$

Table 3.5. Parameters taking into consideration in the FEM analysis

A	B	ψ	F (kN)	a/b	b/t	l_0/a
2.0	1/5	-1.0	100	1.0	50	0.0
2.5	2/5	-0.5	200	1.5	100	0.1
3.0	3/5	0.0	300	2.0	150	0.2
3.5	4/5	1.0	400	2.5	200	0.3
4.0	5/5		500	3.0	250	0.4
						0.5

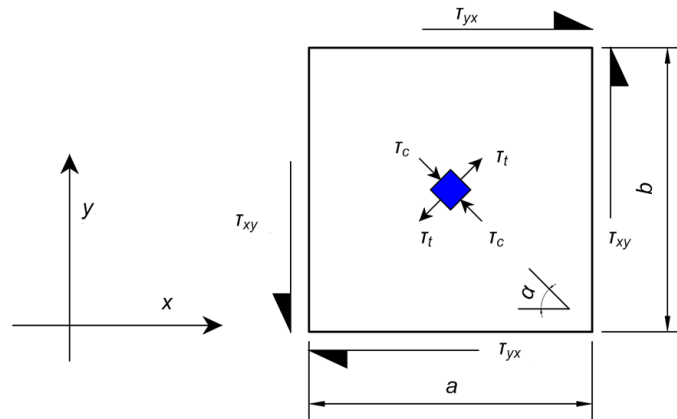


Fig. 3.3. Plate under a pure shear

Where τ_c and τ_t are respectively the internal diagonal compression and tension stresses involved in the shear mechanism.

3.5 Parametric studies

Several parameters may influence the stability of a steel plate under in-plane combined loading conditions. The patch loading length, the patch loading magnitude, the panel aspect ratio, and the plate's slenderness defined as the plate's height-to-thickness ratio are the most important since many researchers [3.9], [3.18] and [3.27] have focused their research on either one or a couple of them. In this section, the influence of each parameter will be studied through the following strategy.

3.5.1 Research strategy

The plate's geometry corresponds to one of the most important parameters in the parametric analysis of the buckling of steel plates. The geometry is chosen based on current situations. A steel plate with the following geometry was considered: $a=1000$ mm, $b=1000$ mm, and $t=10$ mm. Then, to consider different situations, the geometrical parameters such as the panel aspect ratio a/b and the plate's slenderness b/t are varied. The geometrical parameters considered starting from the initial plate's geometry are the following: $a/b=1, 1.5, 2, 2.5, 3$, $b/t=50, 100, 150, 200, 250$.

At the first step, the steel plate subjected to patch loading was studied carefully. For each geometrical configuration, different patch loading magnitudes of different lengths were applied. Then shear force and bending stress through their equivalent compressive force were added to the model to consider the interaction of the three in-plane loadings. For the added shear and bending forces, patch loading F was incremented from 100 kN to 500 kN and the l_0/a parameter from 0.0 to 0.5.

3.5.2 Investigation of a steel plate under M-F-V interaction

A steel plate subjected to in-plane loading interactions may behave differently according to the loading which is applied: bending, shear or patch loading. Considering the interaction of the stresses generated by each force, the worst case for the steel plate is always observed when the bending stress acting on it has a stress ratio $\psi=0$ because this condition adds more compressive stress in the plate. However, the plate will be less prone to instability for $\psi=-1$ as seen in Fig. 3.4.

3.5.2.1 Influence of patch loading length and panel aspect ratio

Several analyses showed that the critical buckling load of a plate subjected to combined in-plane loadings will increase and the patch loading length will increase as well (Fig. 3.4a). The same conclusion cannot be drawn

for the variation of the panel aspect ratio. In fact, Fig. 3.4b shows that the critical buckling load multiplier goes slightly down by increasing the panel aspect ratio for the case of $\psi=-1$ while it will slightly increase and decrease alternately for other stress ratios. The critical buckling load will depend on the number of half-waves induced by the deformation of the plate and consequently on the length of the half-wave.

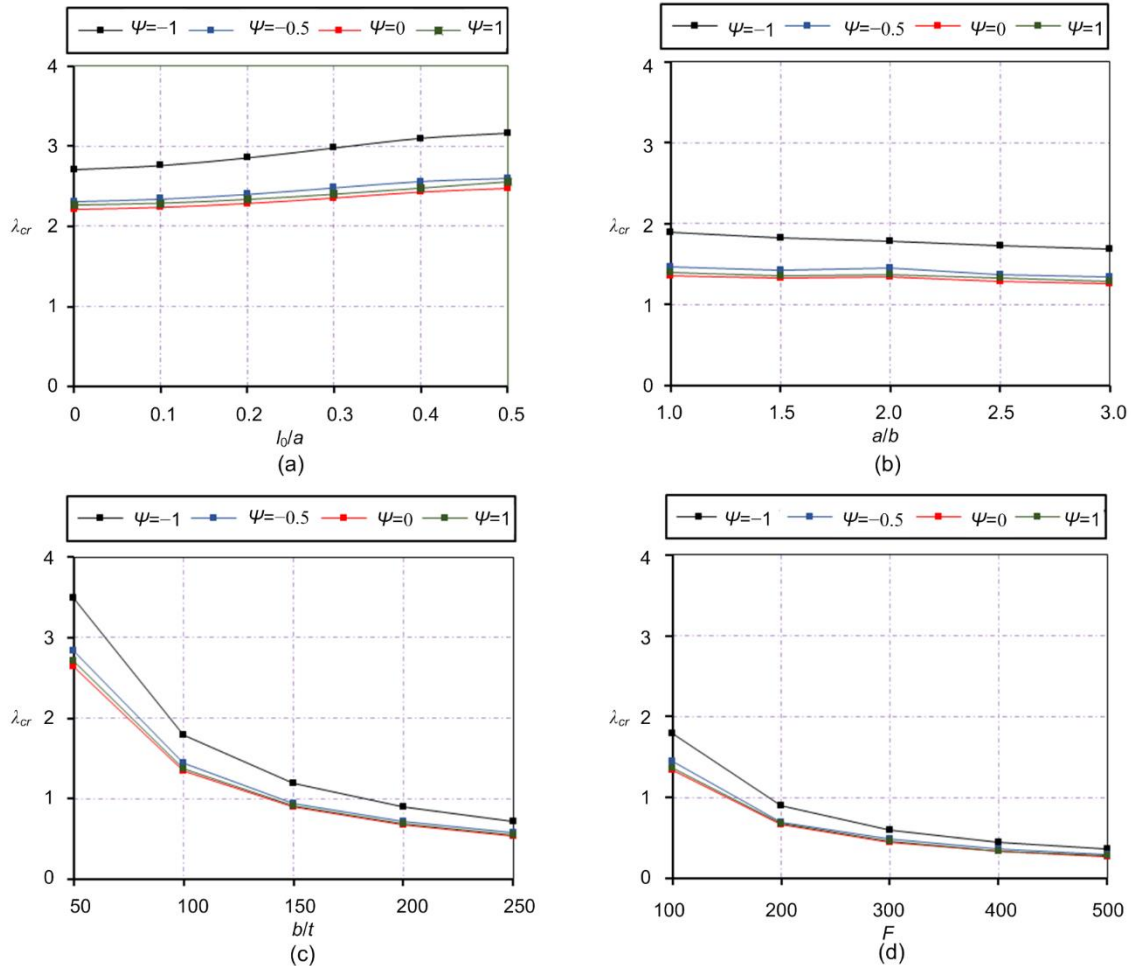


Fig. 3.4. Variation of the critical buckling load factor for steel plate section subjected to combined patch loading, bending, and shear force: $F=100$ kN; $F_x=4F$; $V_y=F_x$
 (a) Influence of patch loading length; (b) Influence of the panel aspect ratio; (c) Influence of the slenderness; (d) Influence of the patch loading magnitude.

Besides the mechanical characteristics of the material and the parameters of the structural elements able to modify the stress state, the intensity of the patch loading, bending, and shear force is clearly important in the plate stability. In fact, patch loading applied in a small beam portion will increase the instability process of the beam. In addition, in the situation where the section is also subjected to both bending and shear forces, the instability will happen at an early stage. For different lengths of patch loading, the instability is more sensitive to the bending variation with respect to the shear's variation. Fig. 3.5 shows that considering a maximum value of bending

stress interacting with different levels of shear force, the critical buckling load decreases at a slow rate.

When the bending stress is increasing gradually, the plate goes to instability faster as a steeper slope describes the variation of the critical buckling stress. In addition, it can be seen in Fig. 6 that the variation of bending or shear forces generates a greater impact on the critical buckling load multiplier with respect to the variation of the panel aspect ratio. This conclusion is validated by observing the slight variation of the load multiplier as a function of the panel aspect ratio in Fig. 3.4b.

3.5.2.2 Influence of patch loading magnitude and plate's slenderness

With respect to the impact of slenderness and patch loading magnitude (Fig. 3-4c and Fig. 3-4d), the conclusion for the steel plate subjected to combined loading is similar to the case of the plate under a single load type. Slender plates will have higher exposure to buckling than compact steel plates. Meanwhile, a steel I-profile bridge girder will undergo instability faster if the reaction at the support pillar is high.

It is worth noting that the critical buckling stress of the plate subjected to combined loading when the patch loading magnitude rises is interconnected while the level of bending and shear stresses defined by A and B , respectively, remains the same. The patch loading, in this case, governs the buckling mode and the plate behaves exactly as if it were subjected to only patch loading. Contrary to what has been observed in Fig. 3.5 and Fig. 3.6, the patch loading magnitude and the slenderness of the steel plate greatly influence the critical buckling load (Fig. 3.7 and Fig. 3.8). In particular, the slenderness of the steel plates is considered the critical parameter (Fig. 3.8) leading to the plate's instability because it is the unique parameter that strongly influences the critical buckling load multiplier. It is worth noting that as the patch loading magnitude is increased, the increase of shear stress will change the critical load from a slight reduction to a quasi-constant value (Fig. 3.7).

3.5.3 Failure mode of a steel plate under combined in-plane loadings

Steel plates under loads may present different buckling shapes depending on the type of loads and the geometrical parameters. When dealing with plates under combined loads, the buckling shape of the plate can be described in general in four ways as shown in Fig. 3.9.

If the shear force is significantly low with respect to both bending and patch loading and in the meantime, the patch loading is dominant in relation to bending, the buckling shape of the plate will be similar to the case of the plate under patch loading (Fig. 3.9a). The plate will display a deformation following the direction of patch loading. From the moment that the bending stress is increasing up to the point that it is dominant in relation to patch loading, the

deformation shape will then follow the direction of bending with the number of half-wave functions to the plate's geometry and constraint condition as shown in Fig. 3.9b and Fig. 3.10b.

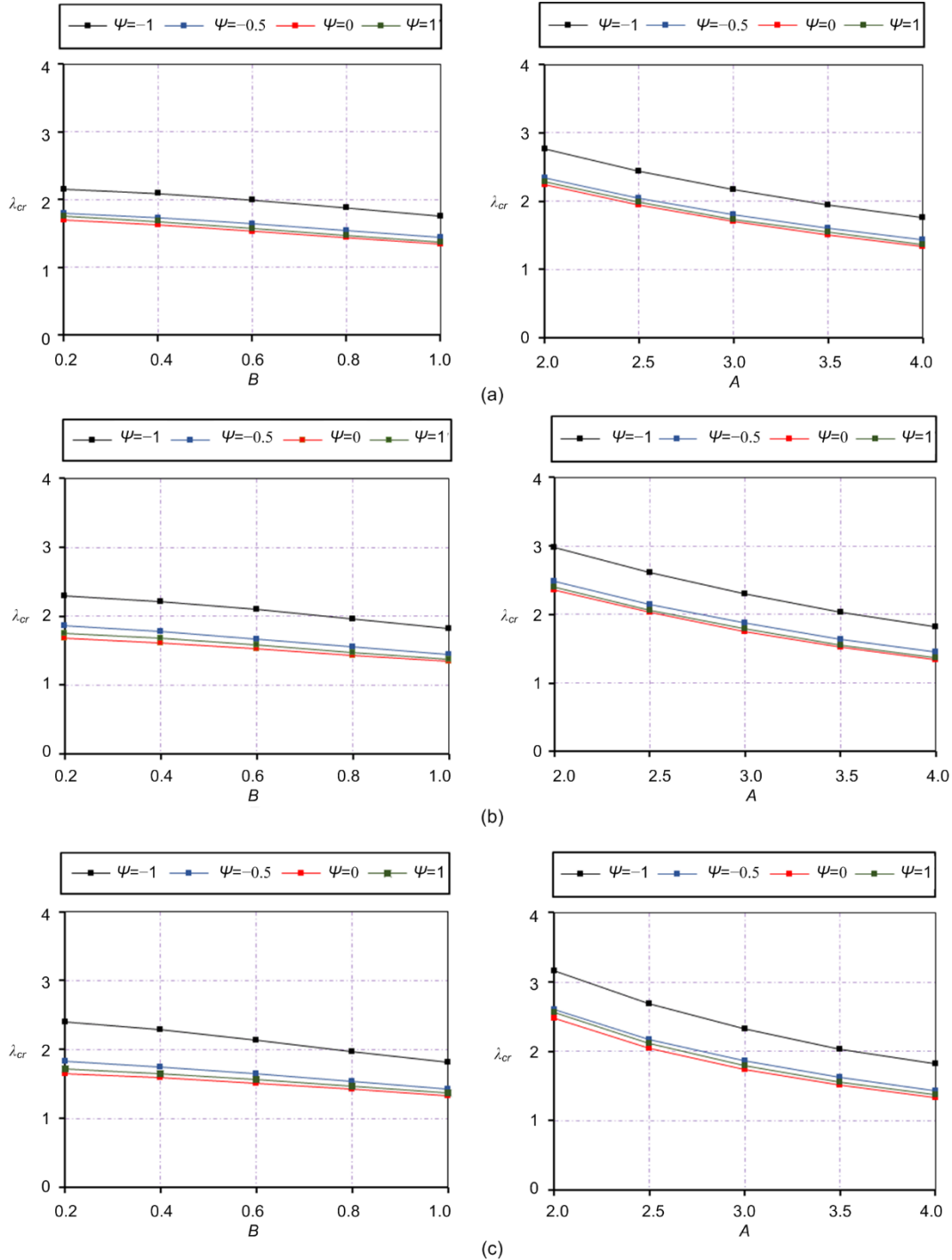


Fig. 3.5. Influence of patch loading length in the critical buckling load multiplier
 (a) $l/a=0.1$; (b) $l/a=0.3$; (c) $l/a=0.5$

Finally, if the shear is increased in the same mode as the bending moment, the situations in Fig. 3.9b, Fig. 3.9c, Fig. 3.10a, and Fig. 3.11 will be

observed. A tension field inclined at a certain angle with respect to the horizontal will be gradually developed following the diagonal of the plate in the case of one half-wave as shown in Fig. 3-9c or the diagonal of each tension field created in the case of multiple wavelengths will be as shown in Fig. 3.10a and Fig. 3.11.

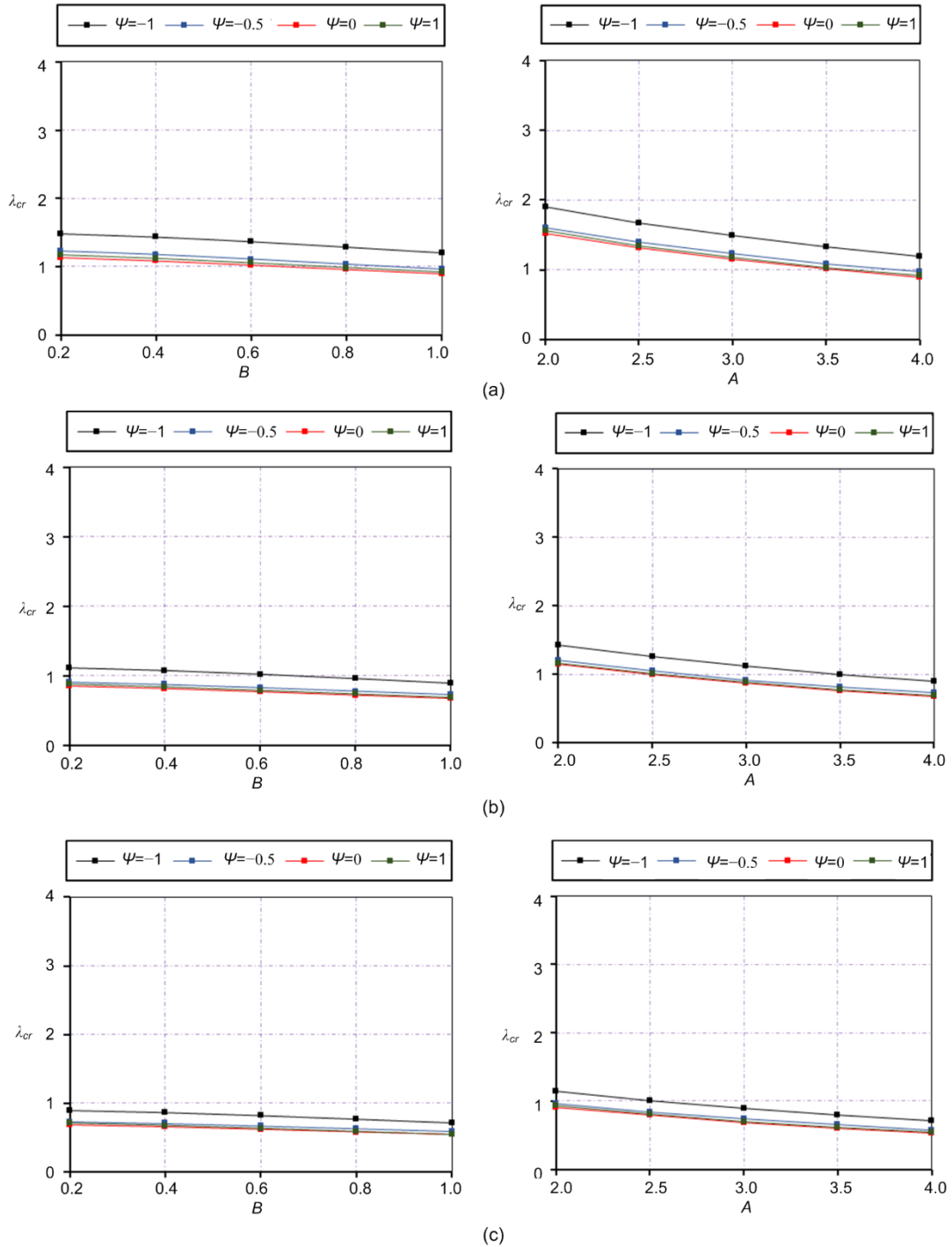


Fig. 3.8. Influence of slenderness in the critical buckling load
(a) $b/t=150$; (b) $b/t=200$; (c) $b/t=250$

It is interesting to add that the patch loading length can in some cases influence the buckling shape. Fig. 9c and Fig. 9d present two plates' deflections observed for the same state of loading. When the patch loading is very small, it will lead to one wave-deformed shape and then the situation will progressively change as well as the patch loading length increases.

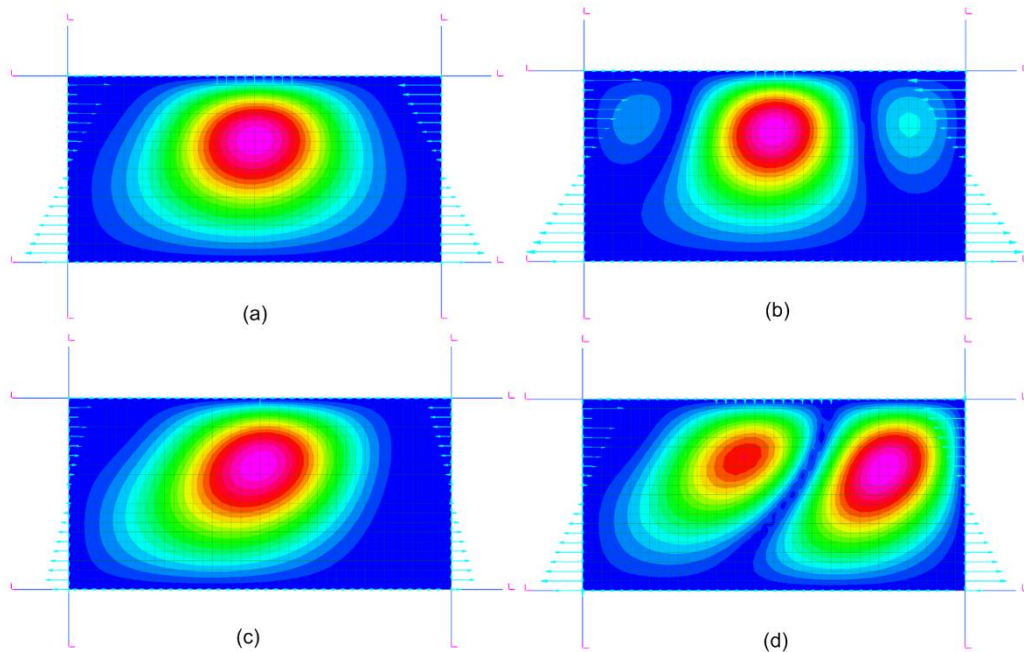


Fig. 3.9. Influence of slenderness in the critical buckling load

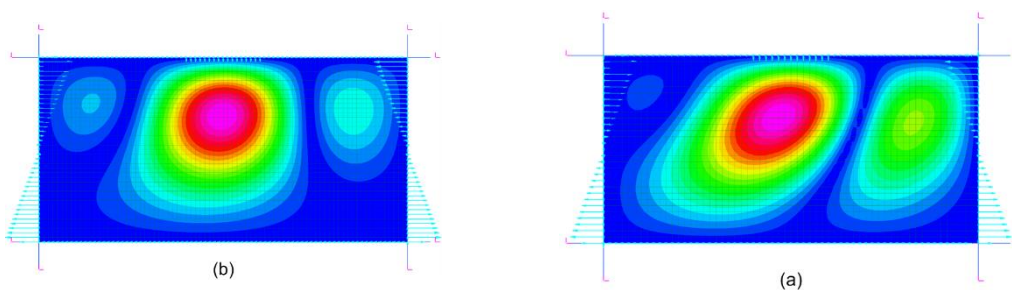


Fig. 3.10. Critical buckling shape of plate under patch loading, bending and shear, varying slenderness

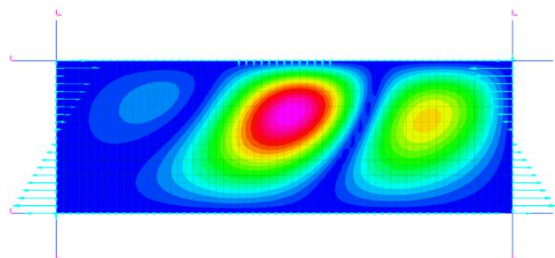


Fig. 3.11. Critical buckling shape of plate under patch loading, bending, and shear for aspect ratio $a/b=3$

3.6 Elastic critical buckling of a steel plate under M - F - V interaction

The elastic critical buckling of a steel plate subjected to patch loading F can be obtained by theory as described in [3.28] or using FEM analysis. When the theory is used, it is necessary to know the critical buckling coefficient, which is found in the literature since several researchers have worked on the topic ([3.28], [3.16], [3.9]) while from the numerical analysis, the critical buckling load factor is expected. Eq. (3.17) defines the relationship between the approaches. Therefore, it is possible to find the buckling load multiplier for a steel plate under patch loading throughout Eq. (3-18) knowing the geometrical characteristics of the steel plate, the patch loading, and the critical buckling coefficient.

$$F_{cr,F} = k_F \cdot \frac{\pi^2 Et^3}{12(1-\nu^2)b} = \lambda_{cr,F} \cdot F \quad (3.17)$$

$$\lambda_{cr,F} = k_F \cdot \frac{\pi^2 Et^3}{12(1-\nu^2)b} / F \quad (3.18)$$

where $\lambda_{cr,F}$ is the critical buckling load multiplier of the steel plate subjected to patch loading; k_F is the critical buckling coefficient of the steel plate subjected to patch loading; $F_{cr,F}$ is the critical patch loading force of the steel plate.

3.6.1 Investigation of a steel plate under M - F - V interaction

In this section, the equations in terms of parameters from Table 3.5 that describe the influence of bending and shear forces in the critical buckling load are proposed. In the previous section, it was possible to observe that these parameters influenced in some way the critical buckling load factors of steel plate subjected to the interaction of in-plane loading. On the other hand, the critical buckling load factors do not evolve linearly with the geometrical and loading parameters investigated in the previous section. For this reason, each parameter will be studied separately. To reach our goal the following strategy is adopted.

A steel plate with the following geometry $a=2000$ mm, $b=1000$ mm, $t=10$ mm is considered. In the first step, the patch loading with different configurations of load length is applied to the steel plate whereas the shear force and bending moment are varied through the A and B coefficients. Table 3.6 shows the different fixed and varying parameters considered in the first step. For each combination of variables presented in Table 6, the buckling load factors are computed, hence over 500 numerical models were investigated in this step. The results from the analysis lead to discovery of a unique function

in terms of load parameters A and B and patch loading length l_0/a , which accurately describes the reduction of critical buckling loads.

In the next steps, the other parameters such as patch loading magnitude, panel aspect ratio, and the plate's slenderness will be investigated one at a time. However, it is worth noting that the following plate geometries, $a=2000$ mm, $b=1000$ mm, $t=10$ mm, and the patch loading length $l_0/a=0.2$, are the benchmark for the analysis. In the variation of panel aspect ratio, only the length of the plate is changed whereas when the slenderness is varied, both the length and the height of the plate are involved to keep the panel aspect ratio fixed to 2. The shear force and bending moment are varied through the A and B coefficients similarly to the previous analysis. Thus, over 400 numerical models were investigated for each parameter involved and the influence of shear force and bending moment in the reduction of the buckling loads factor can be derived. The design equation will be proposed with the aim to match it as close as possible to the different values from the FEM analysis. Therefore, the comparison of values from the design formula and FEM calculations was done to assess in some way the uncertainty of the design parameters. In order to limit the deviation as much as possible, a maximum error of $\pm 5\%$ was fixed between the different values compared.

Table 3.6. Parameters used to determine the critical buckling load factor

a/b	b/t	F (kN)	A	B	l_0/a
2	100	100	2.0	1/5	0.0
			2.5	2/5	0.1
			3.0	3/5	0.2
			3.5	4/5	0.3
			4.0	5/5	0.4
					0.5

3.6.2 Evaluation of the buckling load factor

By reworking the data set obtained from numerical analysis, a critical buckling load factor, which takes into account the interaction of patch loading with both shear and bending forces, has been defined. The relationship derived and expressed in Eq. (3.19) and Eq. (3.20) in terms of A and B parameters allows us to determine how the additional forces lower the critical buckling load. The P_{ij} coefficients are determined through a regression fitting analysis and are influenced by the parameters investigated. For this reason,

these coefficients have been defined accordingly to the involved parameter. It is worth noting that the equations are applicable to within a specific range of the plate's geometry and the loading cases that have been considered in the analysis and this range is presented in Table 3.7. On the other hand, users should first identify the geometrical and loading characteristics of the problem. Then, with the design parameters, they will be able to determine which equations should be used.

$$\frac{\lambda_{cr,F}}{\lambda_{cr,M+F+V}} = f(A, B), \tag{3.19}$$

$$\frac{\lambda_{cr,F}}{\lambda_{cr,M+F+V}} = P_{20} \cdot A^2 + P_{02} \cdot B^2 + P_{11} \cdot A \cdot B + P_{10} \cdot A + P_{01} \cdot B + P_{00}, \tag{3.20}$$

where P_{ij} are polynomial coefficients depending on the geometrical and loading characteristics (patch loading length, patch loading magnitude, panel aspect ratio, and plate slenderness λ).

3.6.2.1 Influence of patch loading length

Through Matlab [3.29] tools, a 3D chart describing the variation of the critical buckling load multiplier of the steel plate involved in the first step is drawn. We recall that in this case, only shear forces, bending moment, and patch loading length are varied. Then using the regression fitting curve analysis, the P_{ij} coefficients are obtained as a function of the patch loading length (Table 3.8).

Over 500 numerical results have been assessed and compared to the design formula. The comparison between FEM analysis and analytical equations showed a good agreement in this case. Checks were done separately for each bending stress ratio. All the values compared are located inside the limits imposed as shown in Fig. 3.12.

Table 3.7. Range of applicability of the design formula

F_x (kN)	V_y (kN)	l/a	λ	a
[2F, 4F]	[0.2F _x , F _x]	[0, 0.5]	100	2
[2F, 4F]	[0.2F _x , F _x]	0.2	100	2
[2F, 4F]	[0.2F _x , F _x]	0.2	[50, 250]	2
[2F, 4F]	[0.2F _x , F _x]	0.2	100	[1, 3]

Table 3.8. Design coefficients used in case of patch loading length as parameter

Parameter	$\psi=-1,$	$\psi=-0.5,$	$\psi=0,$	$\psi=1,$
P_{00}	$-0.391\left(\frac{l_0}{a}\right)+1.145$	$-0.593\left(\frac{l_0}{a}\right)+1.362$	$-1.018\left(\frac{l_0}{a}\right)+1.485$	$-0.603\left(\frac{l_0}{a}\right)+1.405$
P_{10}	$0.196\left(\frac{l_0}{a}\right)+0.107$	$0.380\left(\frac{l_0}{a}\right)+0.112$	$0.703\left(\frac{l_0}{a}\right)+0.050$	$0.438\left(\frac{l_0}{a}\right)+0.067$
P_{01}	$-0.329\left(\frac{l_0}{a}\right)-0.453$	$0.001\left(\frac{l_0}{a}\right)-0.673$	$0.158\left(\frac{l_0}{a}\right)-0.721$	$0.035\left(\frac{l_0}{a}\right)-0.705$
P_{11}	$0.179\left(\frac{l_0}{a}\right)+0.163$	$0.160\left(\frac{l_0}{a}\right)+0.244$	$0.013\left(\frac{l_0}{a}\right)+0.289$	$0.022\left(\frac{l_0}{a}\right)+0.300$
P_{20}	$0.022\left(\frac{l_0}{a}\right)+0.023$	$0.033\left(\frac{l_0}{a}\right)+0.029$	$0.014\left(\frac{l_0}{a}\right)+0.043$	$0.049\left(\frac{l_0}{a}\right)+0.037$
P_{02}	$0.431\left(\frac{l_0}{a}\right)+0.260$	$0.197\left(\frac{l_0}{a}\right)+0.332$	$0.266\left(\frac{l_0}{a}\right)+0.320$	$0.304\left(\frac{l_0}{a}\right)+0.317$

3.6.2.2 Influence of patch loading magnitude

The patch loading magnitude is another parameter involved in the analysis as defined in the research strategy. By reworking the numerical results obtained from analysis, the 3D charts from Matlab [3.29] showed that the patch loading magnitude considered in Table 3.5 does not influence Eq. (3.20) since the ratio gives the same value for each patch loading magnitude (Fig. 3.13). For this reason, the coefficients P_{ij} are easily found and are constants. Table 3.9 presents different values for P_{ij} coefficients found after a regression fitting of the 3D charts.

3.6.2.3 Influence of the plate's slenderness

Similar to the case of patch loading magnitude, the same observation has been made by analyzing the numerical results through a 3D chart. In fact, even if the variation of plate slenderness influences the critical loading in the case of combined in-plane loading, the ratio described in Eq. (3.19) remains constant. For this reason, the coefficients P_{ij} are easily found and are not a function of the slenderness. Table 3.10 presents different values for P_{ij} coefficients found after a regression fitting of the 3D charts.

3.6.2.4 Influence of the panel aspect ratio

Panel aspect ratio is the plate's parameter that did not present a specific conclusion. Indeed, the elaboration of P_{ij} coefficients in the case of varying the panel aspect ratio encountered some difficulties since the convergence was difficult to reach. For this reason, P_{ij} coefficients are defined in this case as a polynomial equation of grade 3 as presented in Table 3.11.

The comparison of numerical results and analytical equations showed good agreement with the maximum deviation equal to 5% when the patch loading length, the patch loading magnitude, and the plate's slenderness were considered separately. On the other hand, when the panel aspect ratio was involved the results presented large deviation especially when there were long plates. Nevertheless, the results are acceptable with the maximum observed deviation up to 10%. Table 3.12 briefly summarizes a comparison between FEM and analytical results of the critical buckling load factor for steel plate under combined in-plane loading with different plates and load characteristics.

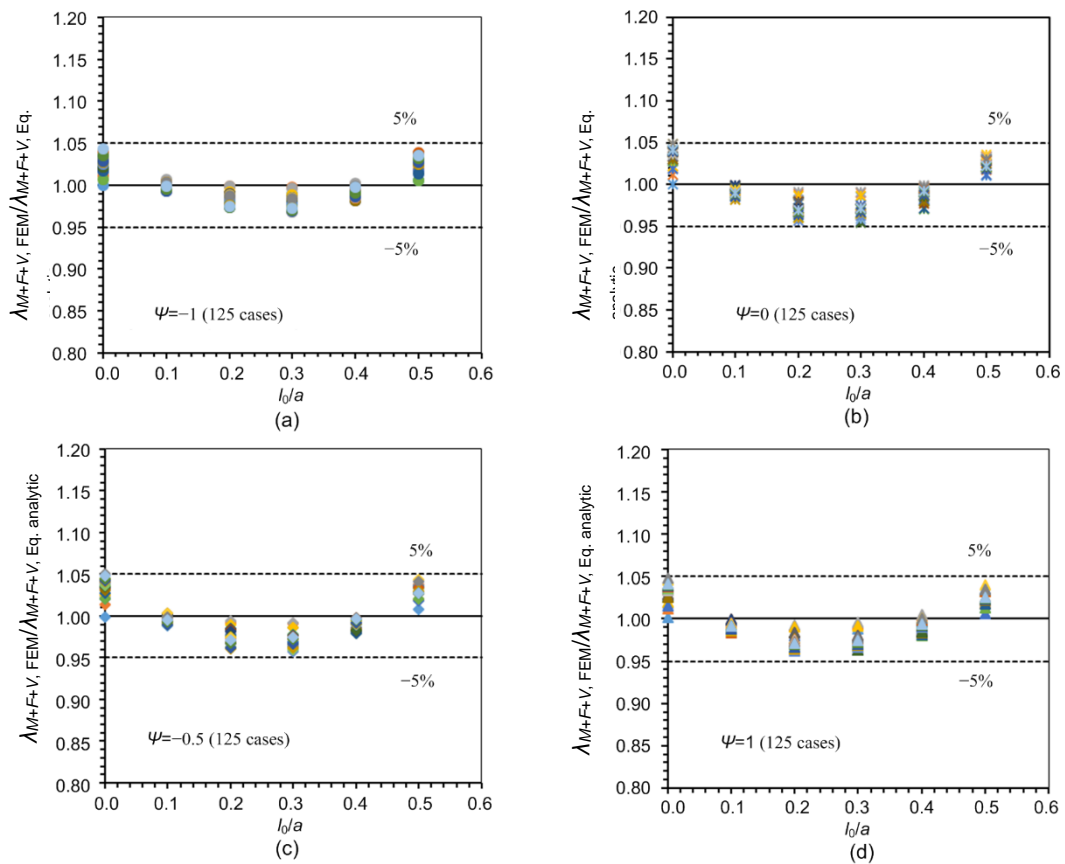


Fig. 3.12. Comparison between FEM and design formula considering the patch loading length

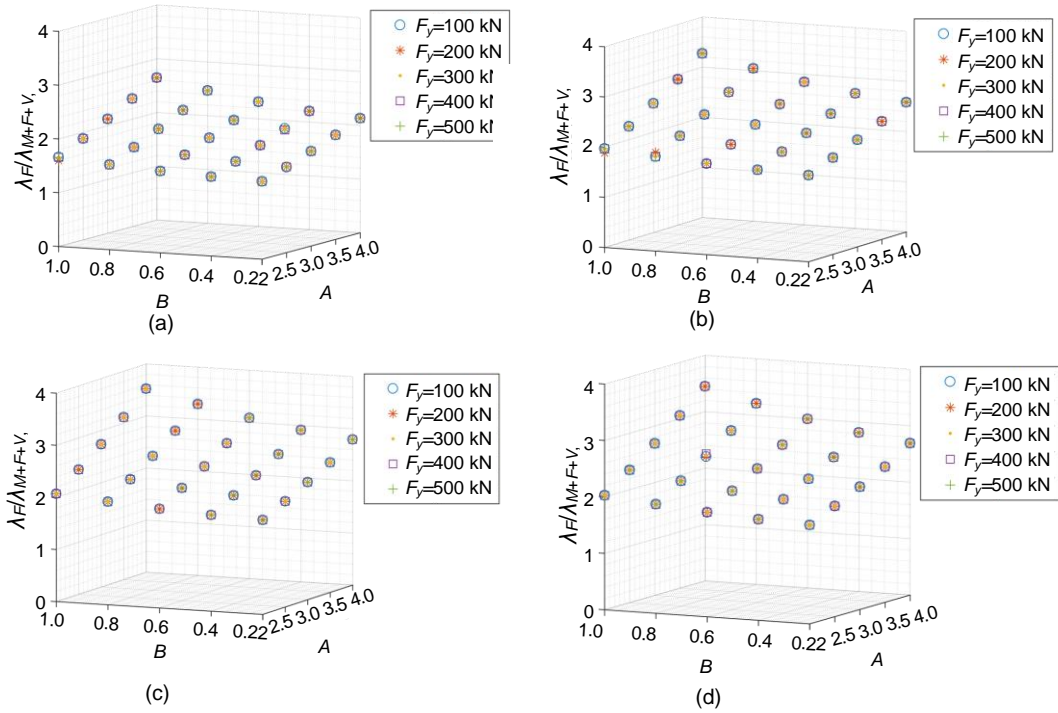


Fig. 3.13. 3D evolution of the critical buckling load multiplier ratio in term of patch loading magnitude
 (a) $\psi = -1$; (b) $\psi = -0.5$; (c) $\psi = 0$; (d) $\psi = 1$

Table 3.9. Design coefficients used in case of patch loading magnitude as parameter

ψ	P_{00}	P_{10}	P_{01}	P_{11}	P_{20}	P_{02}
-1	1.086	0.139	-0.515	0.196	0.026	0.318
-0.5	1.306	0.159	-0.703	0.275	0.034	0.371
0	1.451	0.081	-0.728	0.304	0.056	0.362
1	1.385	0.090	-0.706	0.311	0.050	0.358

Table 3.10. Design coefficients used in case of plate slenderness as parameter

ψ	P_{00}	P_{10}	P_{01}	P_{11}	P_{20}	P_{02}
-1	1.088	0.137	-0.507	0.191	0.026	0.325
-0.5	1.296	0.163	-0.698	0.277	0.033	0.369
0	1.450	0.083	-0.737	0.307	0.055	0.362
1	1.384	0.090	-0.713	0.311	0.050	0.364

Table 3.11. Design coefficients used in case of panel aspect ratio as parameter

ψ	P_{00}	P_{01}	P_{10}	P_{11}	P_{20}	P_{02}
-1	$0.239a^3-1.476a^2$ $+2.744a-0.376$	$-0.233a^3+1.426a^2$ $-2.777a+1.129$	$-0.243a^3+1.672a^2$ $-3.646a+2.669$	$0.071a^3-0.444a^2$ $+0.894a-0.361$	$0.008a^3-0.066a^2$ $+0.159a-0.098$	$0.077a^3-0.475a^2$ $+0.978a-0.328$
-0.5	$0.153a^3-1.146a^2$ $+2.555a-0.525$	$-0.060a^3+0.499a^2$ $-1.319a+0.425$	$-0.158a^3+1.292a^2$ $-3.294a+2.900$	$0.022a^3-0.175a^2$ $+0.478a-0.155$	$-0.006a^3+0.015a^2$ $+0.025a-0.036$	$0.006a^3-0.082a^2$ $+0.323a+0.011$
0	$0.098a^3-0.917a^2$ $+2.382a-0.608$	$-0.045a^3+0.419a^2$ $-1.197a+0.398$	$-0.083a^3+0.918a^2$ $-2.799a+2.806$	$-0.007a^3-0.018a^2$ $+0.235a-0.057$	$-0.016a^3+0.067a^2$ $-0.058a-0.009$	$0.026a^3-0.177a^2$ $+0.442a-0.013$
1	$0.089a^3-0.884a^2$ $+2.407a-0.752$	$-0.048a^3+0.447a^2$ $-1.275a+0.474$	$-0.053a^3+0.717a^2$ $-2.395a+2.549$	$-0.016a^3+0.032a^2$ $+0.141a+0.003$	$-0.016a^3+0.073a^2$ $-0.073a+0.018$	$0.039a^3-0.265a^2$ $+0.629a-0.137$

3.6.3 Evaluation of the buckling load coefficient

From the previous section, analytical formulas describing the variation of the critical buckling load multiplier for steel plate were developed. These formulas have been derived through parametric analysis considering four relevant parameters influencing the plate buckling. One of the major issues presented by these formulas is the limited range of applicability because, in a real design situation, the four parameters should be associated together and secondly, many engineers prefer to deal directly with critical buckling coefficient to design the buckling resistance of steel plate. For this reason, a single formula to determine the critical plate-buckling load has been proposed. Starting from the previous results of Maiorana et al. [3.9], where the critical buckling load of steel plate subjected to patch loading was presented and the formula was updated to take into consideration the effect of bending stress and shear force.

According to the previous research [3.9], the critical buckling load of steel plate under patch loading with various lengths is obtained using Eq. (3.21) where the coefficients c_1 and c_2 defined by Eq. (3.22) and Eq. (3.23) are related to the plate geometry and the patch loading length. Finally, it is worth noting that the critical buckling load of steel plate under patch loading can be obtained knowing either the critical buckling coefficient $k_{cr,F}$ or the critical load multiplier λ_{cr} . Both factors are quite different and use a different approach to determine the critical buckling load of a single plate. The main difference is due to the fact that the first factor uses the geometric characteristics of steel plate to find the critical load while the second factor needs the magnitude of the applied patch loading:

$$F_{cr,F} = \left[3.2048 \cdot \frac{\pi^2 E}{12(1-\nu^2)} \right] \frac{t^3}{b} \cdot \frac{c_1}{c_2}, \quad (3.21)$$

where b is the height of the steel plate, c_1 and c_2 are coefficients of reduction of the critical buckling load for steel plate subjected to combined patch loading and bending moment, respectively.

The analysis showed that when dealing with combined in-plane loading, the influence of the patch loading magnitude and the plate's slenderness change proportionally with the patch loading and the plate geometry, respectively. On the other hand, the panel aspect ratio does not have much influence on the result since we observed a slight variation of the critical buckling load multiplier (as displayed in Fig. 3.4). For this reason, the new analytical equation describing the change of critical patch loading is strictly dependent on the patch loading length.

$$c_1 = -0.0446\left(\frac{b}{a}\right)^6 + 0.4067\left(\frac{b}{a}\right)^5 - 1.3512\left(\frac{b}{a}\right)^4 + 1.8338\left(\frac{b}{a}\right)^3 - 0.3869\left(\frac{b}{a}\right)^2 - 0.2617\left(\frac{b}{a}\right) + 0.8035 \quad (3.22)$$

$$\frac{\lambda_{cr,F}}{\lambda_{cr,M+F+V}} = P_{20} \cdot A^2 + P_{02} \cdot B^2 + P_{11} \cdot A \cdot B + P_{10} \cdot A + P_{01} \cdot B + P_{00} \quad (3.23)$$

The new expressions of critical buckling patch loading and critical buckling patch loading coefficient of steel plate subjected to bending, shear and patch loading acting simultaneously are presented in Eq. (3.24) and Eq. (3.25). The coefficient c_4 can be calculated as a function of the patch loading length, the relationship between different solicitations provided by A and B coefficients and will be different according to different stress ratios. Table 3.13 summarizes the expressions of c_4 for the corresponding stress ratio.

$$F_{cr,F+M+V}^F = \left[3.2048 \cdot \frac{\pi^2 E}{12(1-\nu^2)} \right] \frac{t^3}{b} \cdot \frac{c_1}{c_2} \cdot \frac{1}{c_4}, \quad (3.24)$$

$$k_{cr,F+M+V}^F = 3.2048 \cdot \frac{c_1}{c_2} \cdot \frac{1}{c_4}, \quad (3.23)$$

where c_4 is the coefficient of reduction of the critical buckling load which takes into account the shear force.

3.7 Design example

In this section, an application is presented to prove the validity of the analytical equations; the aim of this example is firstly to show how the formula can be used in a practical case and on the other hand to compare the analytical result with the FEM result as proof of acceptance.

Considering a case of a twin girder composite bridge in the launching phase, each girder is made by a structural steel double T-section without longitudinal stiffener but with vertical stiffeners equally spaced to each other. Young's modulus of the material is $E=206\,000$ MPa and Poisson's ratio $\nu=0.3$. Fig. 3.14 shows a typical section of the girder under study subjected to combined bearing reaction, bending moment, and shear stress. The

information provided shows that the plate representing the web girder is under pure bending where the top bending stress is 171.4 MPa and also subjected to shear stress, the value of which is 17.1 MPa. Through a short calculation, it is possible to summarize different stress parameters useful for the design of the plate. Table 3.14 gives information about stress parameters whereas Table 3.15 gives the geometry of the steel plate.

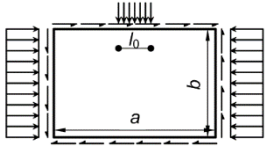
In this example, only the plate element corresponding to the web girder has been modeled in Strand 7. The accurate mesh was done with Quad 4 plate elements of typical size equal to $b/75$ and each node was set to have six degrees of freedom. The first step of the design is to find the critical buckling load for the plate under patch loading $F=300$ kN.

From the numerical analysis, the critical buckling load multiplier was found to be equal to $\lambda_{cr,F}=3.048$ giving the critical buckling load equal to $F_{cr,F}^{FEM}=914.4$ kN. The information from Table 3.14 and Table 3.15 allows determination of the unknown coefficients $c_1=0.790$ and $c_2=0.958$ defined in Eq. (3.22) and Eq. (3.23). Therefore, the analytical value of the critical buckling load $F_{cr,F}^{AN}=899.9$ kN is obtained throughout Eq. (3.21) and a good correlation between the two results is observed with only 1.5% standard deviation. The last step consists of finding both FEM and analytical results of the plate with interacting loads and to compare the two results. Through linear buckling analysis, to $\lambda_{cr,M+V+F}^F=1.602$, the effect produced on critical patch loading resistance is observed as the new critical patch load will be $F_{cr,M+V+F}^{F.FEM}=480.6$ kN. The resistance has been quite reduced approximately to half. Before the calculation of the c_4 coefficient necessary for the use of the analytical equation, A and B coefficients are provided.

Table 3.13. Reduction coefficients c_4 taking into consideration interaction between Patch loading, bending, and shear

ψ	Static scheme	c_4
-1.0		$\left(0.022\left(\frac{l_0}{a}\right)+0.023\right) \cdot A^2 + \left(0.431\left(\frac{l_0}{a}\right)+0.260\right) \cdot B^2 + \left(0.179\left(\frac{l_0}{a}\right)+0.163\right) \cdot A \cdot B$ $+ \left(0.196\left(\frac{l_0}{a}\right)+0.107\right) \cdot A + \left(-0.329\left(\frac{l_0}{a}\right)-0.453\right) \cdot B + \left(-0.391\left(\frac{l_0}{a}\right)+1.145\right)$
-0.5		$\left(0.033\left(\frac{l_0}{a}\right)+0.029\right) \cdot A^2 + \left(0.197\left(\frac{l_0}{a}\right)+0.332\right) \cdot B^2 + \left(0.160\left(\frac{l_0}{a}\right)+0.244\right) \cdot A \cdot B$ $+ \left(0.380\left(\frac{l_0}{a}\right)+0.112\right) \cdot A + \left(0.001\left(\frac{l_0}{a}\right)-0.673\right) \cdot B + \left(-0.593\left(\frac{l_0}{a}\right)+1.362\right)$
0.0		$\left(0.014\left(\frac{l_0}{a}\right)+0.043\right) \cdot A^2 + \left(0.266\left(\frac{l_0}{a}\right)+0.320\right) \cdot B^2 + \left(0.013\left(\frac{l_0}{a}\right)+0.289\right) \cdot A \cdot B$ $+ \left(0.703\left(\frac{l_0}{a}\right)+0.050\right) \cdot A + \left(0.158\left(\frac{l_0}{a}\right)-0.721\right) \cdot B + \left(0.013\left(\frac{l_0}{a}\right)+0.289\right)$

1.0



$$\left(0.049\left(\frac{l_0}{a}\right)+0.037\right) \cdot A^2+\left(0.304\left(\frac{l_0}{a}\right)+0.317\right) \cdot B^2+\left(0.022\left(\frac{l_0}{a}\right)+0.300\right) \cdot A \cdot B$$

$$+\left(0.438\left(\frac{l_0}{a}\right)+0.067\right) \cdot A+\left(0.035\left(\frac{l_0}{a}\right)-0.705\right) \cdot B+\left(-0.603\left(\frac{l_0}{a}\right)+1.405\right)$$

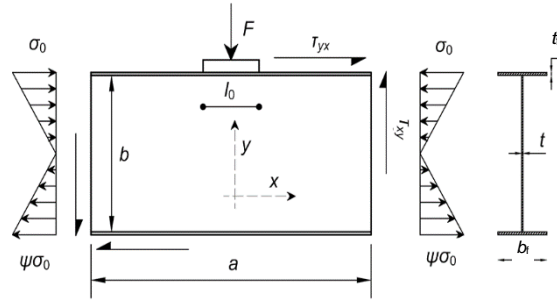


Fig. 3.14. Geometric and loading characteristic of the section studied
 t : thickness of the steel flange; b_f : width of the steel flange

Table 3.14. Parametric data involved in the design formula

F (kN)	F_x (kN)	V_y (kN)	V_x (kN)	ψ	A	B	l_0/a
300	900	360	720	-1	3	0.4	0.2

Table 3.15. Geometrical characteristic of the steel section

a (mm)	t (mm)	b (mm)	t_f (mm)	b_f (mm)	λ	α
2200	14	1500	18	500	107.1	1.466

They are obtained through Eq. (3.10) and Eq. (11) since they represent the relationship between patch loading, shear force, and bending moment. Therefore, from Eq. (3.24) with c_4 coefficient found in Table 3.13 considering the patch loading length corresponding to the design situation, the following result is obtained: $c_4=1.602$ and $F_{cr,M+V+F}^{F,AN} = 489.5$ kN. The difference between FEM and analytical results is less than 1.8%.

3.8 Conclusions

The stability of steel plates under combining patch loading, bending moment, and shear force is studied in this chapter by means of numerical FEM analyses with Strand 7 software. In particular, extensive parametric analysis has been done to evaluate the effect of geometries and the combination of loads parameters. From the FEM analysis, it was found that:

1. The slenderness is the most influential parameter of the plate stability;
2. The panel aspect ratio showed a slight influence with respect to the shear and bending actions;
3. The buckling deformation observed in the interaction of in-plane combined loadings depends on the amplitude of each load and is similar to either the buckling shape of steel plates under a single load or the combined deformation.

The influence of added bending and shear stress in a plate initially subjected to patch loading was investigated and an analytical formula was expressed to describe this influence.

The analytical formula provided a great accuracy since a comparison with the FEM analysis showed that for almost all cases, the deviation was inside the bounded region. Finally, a unique formula which includes all four parameters is proposed because many engineers could use favorably this methodology to evaluate the critical buckling load. A design example has been added in order to prove the validity and good correlation was found between the analytical and FEM results. The conclusion from this example shows that the analytical formula is accurate for whatever plate geometry is used and it also showed that bending moment and shear stress can be reached due to the girder self-weight and construction loads may considerably reduce the critical buckling load.

3.9 References

- [3.1] Kövesdi B, Alcaine J, Dunai L, et al., 2014. Interaction behaviour of steel I-girders part I: longitudinally unstiffened girders. *Journal of Constructional Steel Research*, 103: 327-343. <https://doi.org/10.1016/j.jcsr.2014.06.018>
- [3.2] Kövesdi B, Dunai L, 2016. Bending, shear and patch loading interaction behaviour of slender steel sections. *Procedia Engineering*, 156:199-206. <https://doi.org/10.1016/j.proeng.2016.08.287>
- [3.3] Graciano C, Zapata-Medina DG, 2015. Effect of longitudinal stiffening on bridge girder webs at incremental launching stage. *Ingeniería e Investigación*, 35(1):24-30. <https://doi.org/10.15446/ing.investig.v35n1.42220>
- [3.4] Tetougueni CD, Maiorana E, Zampieri P, et al., 2019. Plate girders behaviour under in-plane loading: a review. *Engineering Failure Analysis*, 95:332-358. <https://doi.org/10.1016/j.engfailanal.2018.09.021>
- [3.5] CEN (European Committee for Standardization), 2006. Eurocode 3- Design of Steel Structures-part 1-5: Plated Structural Elements, EN 1993-1-5:2006. BSI.
- [3.6] Braun B, 2010. Stability of Steel Plates under Combined Loading. PhD Thesis, Universität Stuttgart, Stuttgart, Germany.
- [3.7] Tong GS, Feng YX, Tao WD, et al., 2016. Elastic stability of plate simply supported on four sides subjected to combined bending shear and patch loading. *Thin-Walled Structures*, 107:377-396. <https://doi.org/10.1016/j.tws.2016.06.021>
- [3.8] Graciano C, Ayestarán A, 2013. Steel plate girder webs under combined patch loading, bending and shear. *Journal of Constructional Steel Research*, 80:202-212. <https://doi.org/10.1016/j.jcsr.2012.09.018>
- [3.9] Maiorana E, Pellegrino C, Modena C, 2008. Linear buckling analysis of unstiffened plates subjected to both patch load and bending moment. *Engineering Structures*, 30(12): 3731-3738.

<https://doi.org/10.1016/j.engstruct.2008.07.002>

- [3.10] Zetlin L, 1955. Elastic instability of flat plates subjected to partial edge loads. *Proceedings of the American Society of Civil Engineers*, 81(9):1-24.
- [3.11] Basler K, 1961. New Provisions for Plate Girder Design. American Institute of Steel Construction, p.65-74.
- [3.12] Rockey KC, Bagchi DK, 1970. Buckling of plate girder webs under partial edge loadings. *International Journal of Mechanical Sciences*, 12(1):61-76.
- [3.13] Khan MZ, Walker AC, 1972. Buckling of plates subjected to localized edge loadings. *The Structural Engineer*, 50(6): 225-232.
- [3.14] Graciano C, Lagerqvist O, 2003. Critical buckling of longitudinally stiffened webs subjected to compressive edge loads. *Journal of Constructional Steel Research*, 59(9): 1119-1146. [https://doi.org/10.1016/S0143-974X\(03\)00055-5](https://doi.org/10.1016/S0143-974X(03)00055-5)
- [3.15] Ren T, Tong GS, 2005. Elastic buckling of web plates in I-girders under patch and wheel loading. *Engineering Structures*, 27(10):1528-1536. <https://doi.org/10.1016/j.engstruct.2005.05.006>
- [3.16] Duchene Y, Maquoi R, 1994. Contribution, par voie numérique, à l'étude de la résistance des âmes aux charges transversales. *Construction Métallique*, 2:43-56 (in French).
- [3.17] Porter DM, Rockey KC, 1975. The collapse behaviors of plate girders loaded in shear. *Structural Engineering*, 53(8): 313-325.
- [3.18] Alinia MM, 2005. A study into optimization of stiffeners in plates subjected to shear loading. *Thin-Walled Structures*, 43(5):845-860. <https://doi.org/10.1016/j.tws.2004.10.008>
- [3.19] Maiorana E, Pellegrino C, Modena C, 2011. Influence of longitudinal stiffeners on elastic stability of girder webs. *Journal of Constructional Steel Research*, 67(1):51-64. <https://doi.org/10.1016/j.jcsr.2010.07.005>
- [3.20] Graciano C, Mendes J, 2014. Elastic buckling of longitudinally stiffened patch loaded plate girders using factorial design. *Journal of*

-
- Constructional Steel Research*, 100:229-236.
<https://doi.org/10.1016/j.jcsr.2014.04.030>
- [3.21] Alinia MM, Moosavi SH, 2009. Stability of longitudinally stiffened web plates under interactive shear and bending forces. *Thin-Walled Structures*, 47(1):53-60. <https://doi.org/10.1016/j.tws.2008.05.005>
- [3.22] Quang-Viet V, Papazafeiropoulos G, Graciano C, et al., 2019. Optimum linear buckling analysis of longitudinally multi-stiffened steel plates subjected to combined bending and shear. *Thin-Walled Structures*, 136:235-245.
<https://doi.org/10.1016/j.tws.2018.12.008>
- [3.23] Shahabian F, Roberts TM, 1999. Buckling of slender web plates subjected to combinations of in-plane loading. *Journal of Constructional Steel Research*, 51(2):99-121.
[https://doi.org/10.1016/S0143-974X\(99\)00020-6](https://doi.org/10.1016/S0143-974X(99)00020-6)
- [3.24] Jager B, Kövesdi B, Dunai L, 2017. I-girders with unstiffened slender webs subjected by bending and shear interaction. *Journal of Constructional Steel Research*, 131:176-188.
<https://doi.org/10.1016/j.jcsr.2017.01.009>
- [3.25] Graciano C, Edlund B, 2003. Failure mechanism of slender girder webs with a longitudinal stiffener under patch loading. *Journal of Constructional Steel Research*, 59(1): 27-45.
[https://doi.org/10.1016/S0143-974X\(02\)00022-6](https://doi.org/10.1016/S0143-974X(02)00022-6)
- [3.26] Strand 7, 2005. Strand 7 User's Manual. G+D Computing, Sydney, Australia.
- [3.27] Loaiza N, Graciano C, Chacón R, et al., 2017. Influence of bearing length on the patch loading resistance of multiple longitudinally stiffened webs. *Proceedings of Eurosteel*, 1(2-3):4199-4204.
<https://doi.org/10.1016/j.engstruct.2008.07.002>
- [3.28] Timoshenko S, Woinowsky-Krieger S, 1959. *Theory of Plates and Shells*. McGraw-Hill Book Company, New York, USA.
- [3.29] Matlab, 2017. *Matlab User's Manual*, MathWorks, Inc, R2017a. USA.
-

CHAPTER 4

Post-buckling behaviour of Steel Network Arch bridges

4.1 Abstract

In this chapter, the out-of-plane structural behaviour of Network arch bridges is investigated. Indeed, the arch's lateral deflection represents a serious issue in the bridge life. This issue might alter the aesthetical aspect of the bridge and in extreme cases lead to his out of service. On the other hand, the low lateral sensitivity of arch bridges under wind action or other lateral loads is often justified by the existence of a bracing system. In this work, the investigation of the out of plane structural behaviour of the network arch bridge as well as its structural capacity was done throughout intensive numerical analyses. The main objective was to highlight the structural response of the bridge subjected to vertical actions. Indeed, primarily, a study to describe the out of plane response of the steel arch bridge subjected to vertical loads located in the centre of the arch was presented and then the effect of a scenario of loss of one or more cables on the out-of-plane structural capacity of the bridge was investigated. Following the analyses, interesting findings were made. Indeed, the structural behaviour of the unbraced arch bridge displayed identical out-of-plane behaviour to that of an isolated arch. On the other hand, the dynamic sensitivity following a cable loss scenario mainly contributes to the reduction of the arch's capacity.

4.2 Introduction

The Network arch bridge concept and its structural performance have been introduced by Per Tveit [4.1] after the 1950s. Per Tveit defined Network arch bridges as tied-arch bridges where inclined hangers intersect each other at least twice [4.2]. They are still competitive nowadays for small to medium spans due to their architectural aspect and the good cost-performance ratio they provide. Fig. 4.1 shows the different hanger arrangement currently used in steel tied-arch bridge' projects. Several authors after Per Tveit studied the structural performance and the optimization process of the network arch. In 2009, Schanack and Brunn [4.3] studied different configurations of hanger

arrangement and presented a comparative study between network arch bridges with radial hanger arrangement and conventional tied arch bridges. Teich [4.4], [4.5] focused its research on the stress amplitude in the hanger's relaxation, the variation of hangers' force and fatigue on hanger's connectors. In addition, Zotti et al. [4.6] conducted researches on the stress analysis of network arch bridges while Pellegrino et al. [4.7] studied the fatigue on hanger arrangement considering four different hanger arrangements. Recently, an investigation of the structural performance of network timber bridges with various hangers patterns and considering stress distribution have been done and the results can be found in [4.8], [4.9]. The authors provided a rational basis for better use of the material in the network arch bridges.

Although network arch bridges present a good structural efficient, they are suffering likewise to tied-arch bridges large compression forces arisen into arch elements, which may create the instability in the structural element. The arch instability can be differentiated in three categories when talking about global buckling behavior as shown in Fig. 4.2. Several researchers have studied the instability behavior of a single arch element. Sakimoto et al. [4.10] conducted experimental tests on arches made of square hollow sections to study the out-of-plane buckling of the arch. They proposed the next column curves for the verification of the out-of-plane arch stability. Pi and Trahair [4.11], [4.12] developed and proposed design rules for arch buckling based on validated experimental tests. La poutré [4.13] investigated the elastoplastic out-of-plane buckling response of roller bent circular steel arches under a vertical force located at the crown. They performed several experimental tests and results showed the presence of plastic zones in the arch rib before the arch's failure. Spoorenberg et al. [4.14] performed sensitivity numerical analyses to evaluate the influence of initial imperfections on the out-of-plane buckling response of steel arches. The authors proposed a design rule to check the structural response of freestanding circular roller bent steel arches under symmetric loads. With regard to tied-arch bridges, most of the researchers directed their endeavor toward the in-plane buckling strength. Romeijn and Bouras [4.15] analyzed the influence of the arch and girder's stiffness on the stability strength through parametric studies. Palkowski [4.16] demonstrated the effectiveness to carry out proper modeling of girders/arches interaction to outcome safe results from a design point of view. The interest of out-of-plane buckling of tied-arch bridges initiated recently with Qiu et al. [4.17] who drove early works investigating the influence of vertical and lateral flexural stiffness on buckling mode. Liu et al. [4.18] developed analytical solutions to estimate the lateral buckling load for braced tied-arch bridges and the lateral stability mechanism has also been discussed. De backer et al. [4.19], [4.20] used advanced finite element analysis to derive practical calculation methods to assess the critical load in the arch. The results showed a difference with the one proposed by Eurocode 3 [4.21]. The necessity to include material non-linearity and imperfections for an accurate representation of out-of-plane buckling

behavior of arches was recognized in Japan by the end of the 1970s. In the past few years, many authors [4.14], [4.20], [4.22], [4.23] performed nonlinear analyses to assess the arch buckling. Lonetti et al. [4.24] performed various numerical analyses to assess the instability strength of tied-arch bridges under vertical loads. Nonlinear geometrical effects, as well as initial stress configuration, were considered in the analysis. The authors proposed new design methodologies that integrate the bracing system on the bridge behavior.

On the other hand, many studies conducted on arch bridges considered conventional actions related to the operational purpose of the bridge, which are included in the standards. However, the effects of abnormal or accidental actions have rarely been highlighted in previous researches on these types of bridges. These actions, whose origin could come from unpredictable natural or unnatural events and depending on their intensity, might be the cause of the progressive collapse of the structure. Indeed, many authors have recently addressed this issue in different structural systems. For example, in the case of cable-stayed bridges, studies on dynamic behavior and the possibility of progressive collapse following the loss of one or more cables were presented in [4.25]–[4.27]. The dynamic amplification effect on cable-stayed bridges following the loss of cables and due to moving load actions was studied in [4.28]–[4.30] while the study of the effect of damages on the reduction of the structural performance of mixed suspension-stayed bridges was investigated in [4.31]. Finally, the structural strength of steel structures in the case of extreme actions has been well presented in [4.32]–[4.34]. In the case of arch bridges, the loss of a cable is considered as an unusual or even accidental action that can lead to the progressive collapse of the bridge. The evaluation of the structural response and behavior of the arch bridge following the loss of one or more cables was presented [4.35] where the authors described the change in behavior in the structural elements in terms of bending moment, vertical displacement and stress.

From the literature, it is clear that the investigation of the stability of the arch in tied-arch and network arch bridge has caught the attention in the past of several researchers. Most of the past researches considered conventional loads for the study of the stability of the arch bridges. Indeed, many studies presented the lateral deformation of an arch bridge because of the effect of wind or other lateral loads. However, vertical accidental loads might occur on the arch element exhibiting behavior that could be different from that observed in the case of traffic or lateral loads. In addition, it could be added to the possibility of cables loss, which could lead to a reduction in the structural capacity of the arch. For this reason, this paper presents a study of both the out of plane structural behavior and capacity of a network arch bridge in the case of non-conventional actions. Initially, the out of plane structural behavior of the bridge following a load applied to the center of the arch was evaluated, then the influence of the loss of one or more cables on the lateral

capacity of the bridge under the action of traffic loads was investigated by the authors. Based on our analyses, interesting results on the behavior of the bridge under study were found. Indeed, it appears that the arch in network bridges behaves similar to an isolated arch under the action of a concentrated load, particularly in the case of an unbraced arch, which displays the first two modes of instability during stress evolution. On the other hand, in the case of a braced arch, the resistance increases considerably and will not display the second buckling mode. Finally, the loss scenario of one or more cables leads to the reduction of the out of plane structural capacity mainly due to the dynamic sensitivity of the arch after the event. The action can result in a reduction of the arch capacity up to 25% depending on the length of the braced arch.

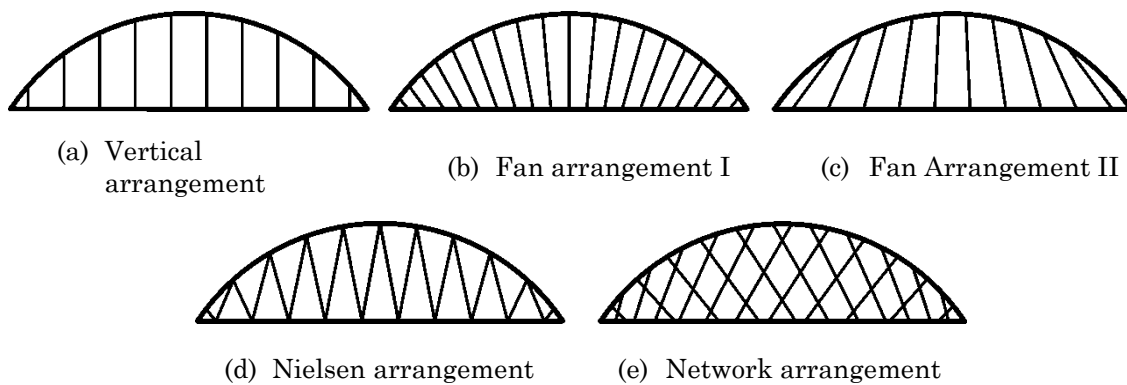


Fig. 4.1. Hanger arrangement for existing tied-arch bridges

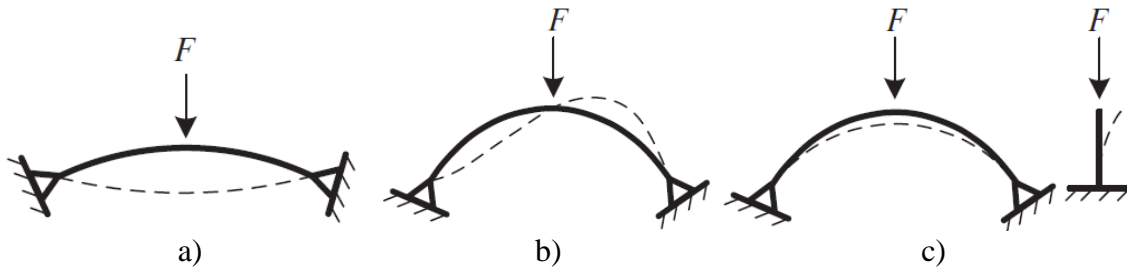


Fig. 4.2. Global instability behaviour of free standing arch; a) Snap-through; b) In-plane buckling; c) Out-of-Plane buckling extracted from Spoorenberg et al. [4.11].

4.3 Description of the bridge in study

The whole structure consists of steel bridges since the deck is not directly collaborating with steel girders. The geometry adopted in this study follows the current prescription and observation for which competitive spans are between 100 – 200 m for network arch bridges. Lonetti et al. [4.24] give information about the preliminary design data in use for design purposes. The bridge is assumed to be subjected primarily to permanent and traffic loads, thus neglecting any possibility of seismic action. The site or the bridge's location does not play a major role in the analyses that are to be carried out.

Table 4.1. Cross-section of structural elements. (1) Tie beam, (2) Arch, (3) Secondary beam, (4) Arch transversal beam, (5) Cable, (6) Lateral bracing

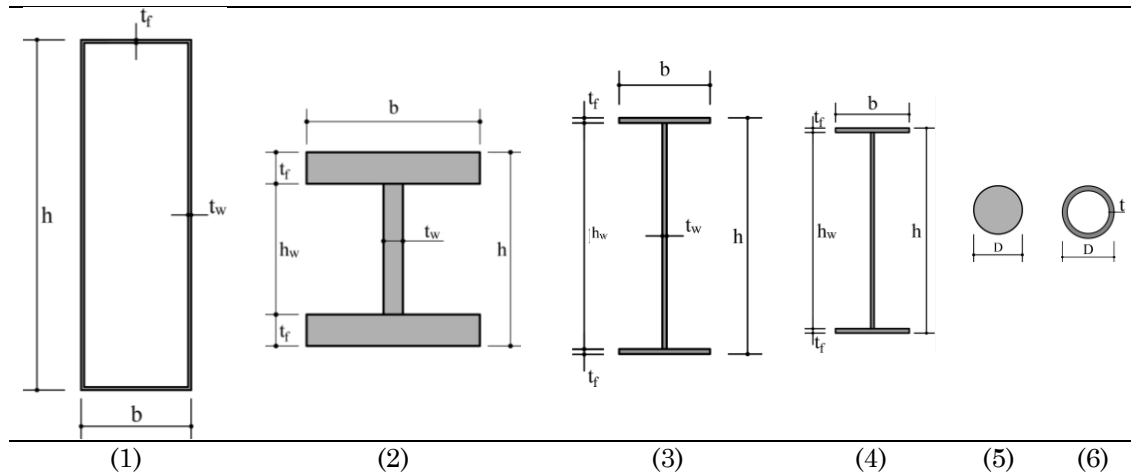


Table 4.2. Section dimensions of the structural elements considered in the analysis

	h [mm]	b [mm]	t_w [mm]	t_f [mm]	D [mm]	t [mm]
Tie Beam	1600	500	80	80		
Arch	474.6	424	47.6	77		
Secondary beam	650	250	12	14		
Arch transversal beam	398	141.8	6.4	8.6		
Cable					12	
Lateral bracing					250	5

4.3.1 Structural layout

A 100 m long and 10 m wide bridge was considered in our study. The height of the arch is fixed at 20 m. The structural pattern adopted in this study is a tied-arch bridge where the parabolic arches are made of high strength steel. Steel arch and tie beams are welded together before being transported to the construction site. In general, the connection between both structural elements are fully welded when all segments are in place and temporary supports removed. A generic representation of the network arch bridge is shown in Fig. 4.3a and the profile, as well as deck section, are found in Fig. 4.4. Finally, four different wind bracing systems are studied namely Syst.I (unbraced arch), Syst.II, Syst.III and Syst.IV (Fig. 4.3b). The system consists of n transversal beams interconnected or not with tubular beams which make a rigid frame. It is characterized by the length L_{br} or L_{Braced} and is particularly used to reduce the length of free end portal h_f displayed in Fig. 4.3. The information about the adopted geometry and structural cross-sections is given in Table 4.1 and Table 4.2.

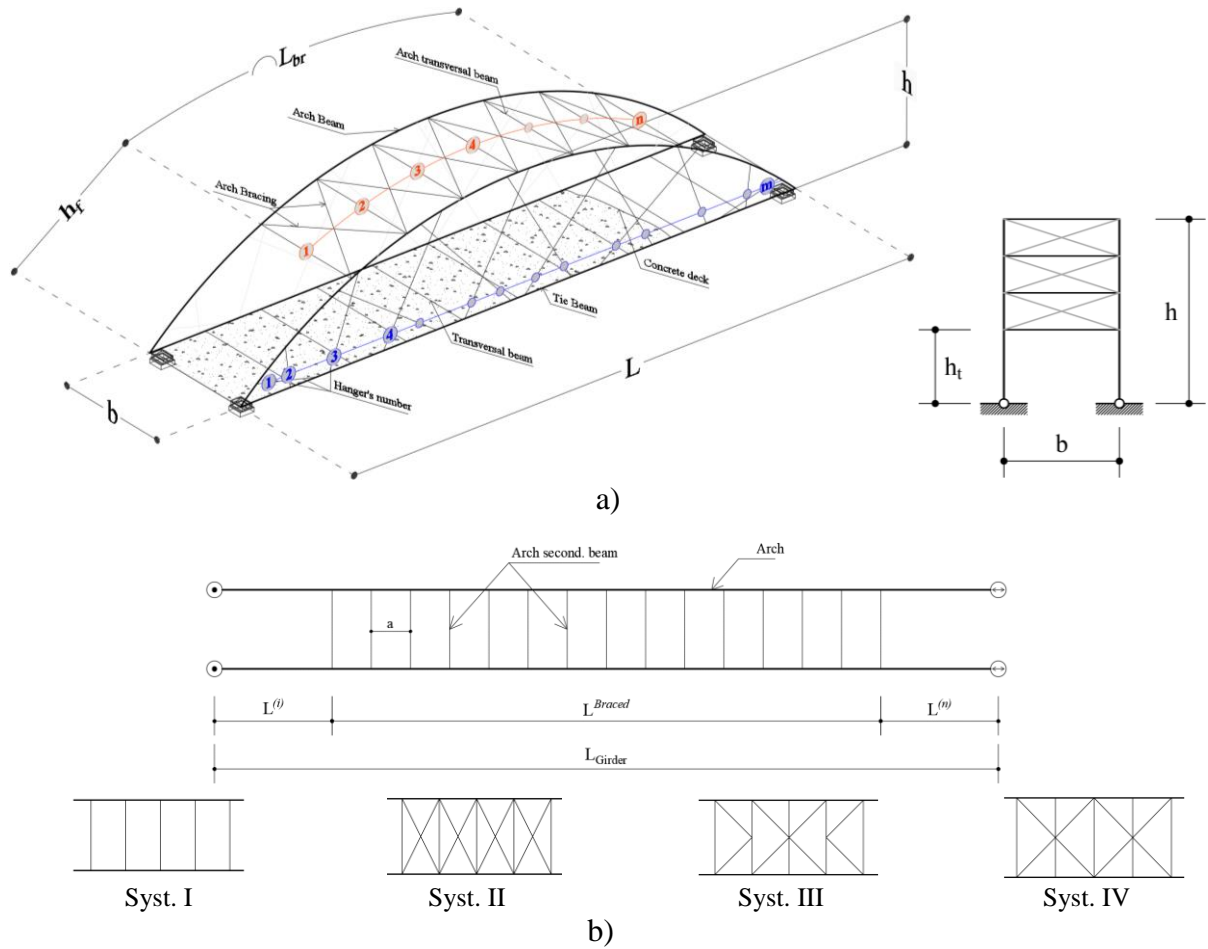


Fig. 4.3. Generic network arch bridge considered in the study

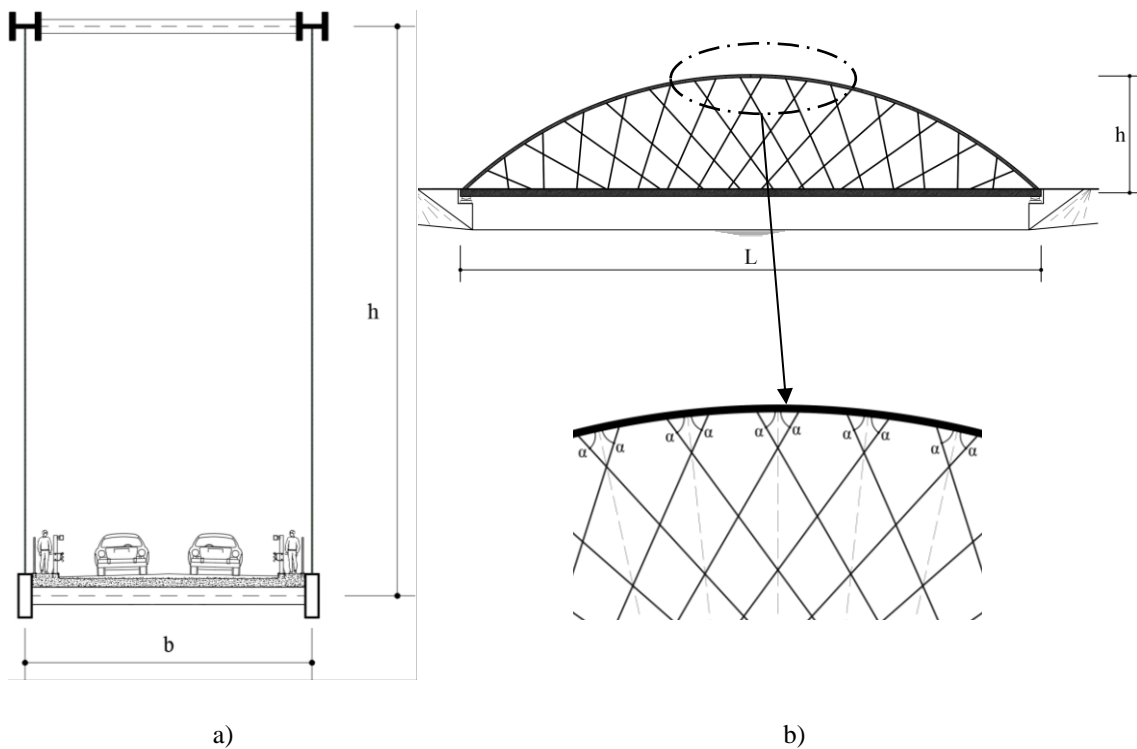


Fig. 4.4. a) transversal section of the bridge, b) longitudinal view of the arch

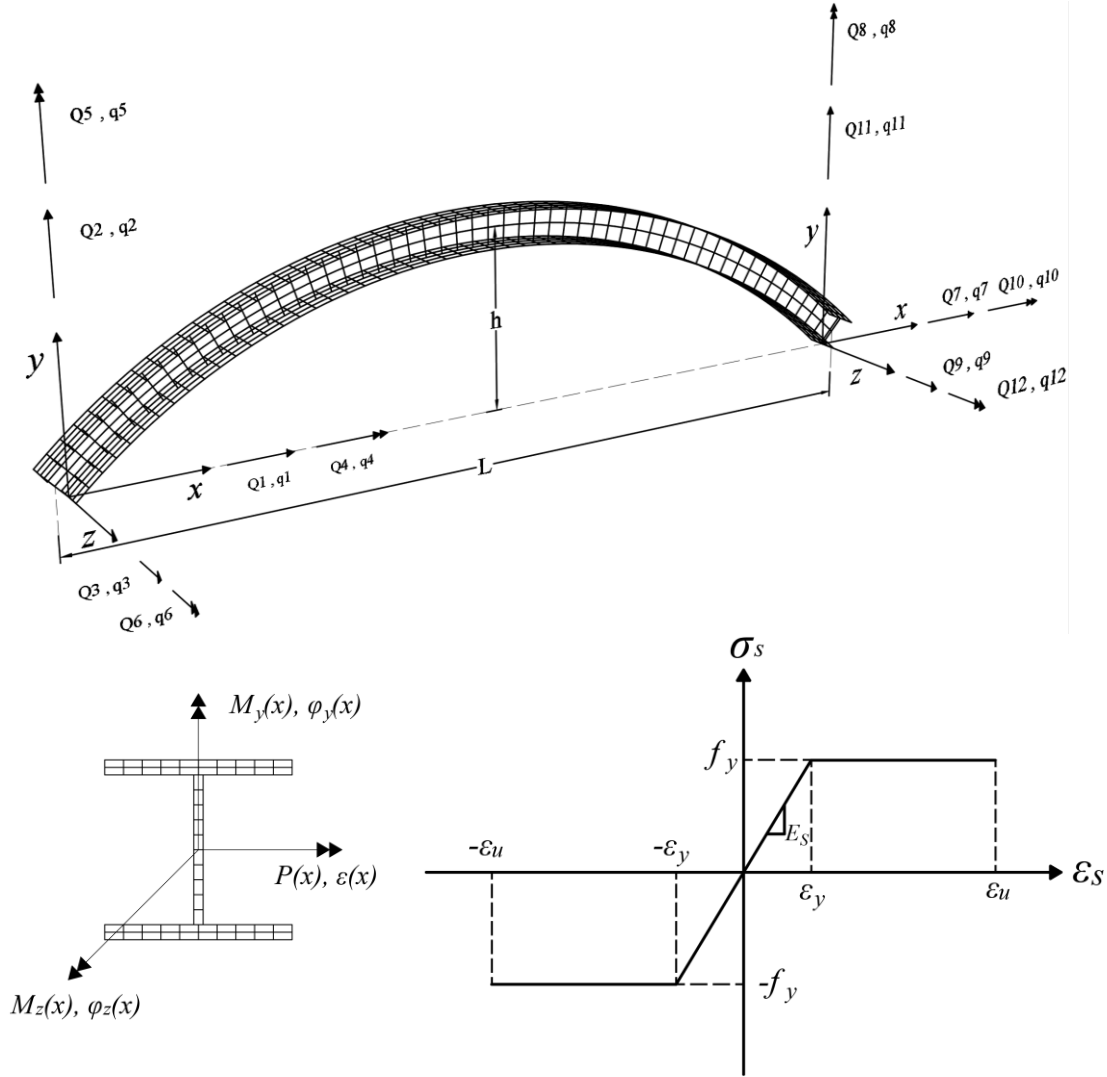
The structural form adopted is a tied arch bridge where the parabolic arches are made of high strength steel. Steel arch and tie beams are welded together. In general, the connection between both structural elements are fully welded when all segments are in place and temporary supports removed. A generic representation of the network arch bridge is showed in Fig. 4.3 and the section of the deck with its longitudinal profile are found in Fig.4.4.

Steel rectangular closed box section for the tie-beam whereas a 356×406×634 universal column for arches were used. Twenty-six inclined hangers are fastened to each arch and girder, which provide good in-plane support to these structural elements. They are made of circular strand cable from Freyssinet and are equidistantly distributed along the arch resulting in a lower bending moment in the arch due to local curvature. Guardrails and safety barriers are used to dissociate the carriageway to the sidewalks and are disposed before the arch. A 300 mm thick concrete slab below the sidewalks forms the deck. Since the deck is not collaborating directly with longitudinal beams, 10 m equidistant transversal beams are used to connect the two lateral tie beams. They are used in transferring lateral loads and provide lateral stability of the beams in the construction stage.

4.4 Finite Element Modeling

4.4.1 Theoretical background

The material and geometrical non-linearity have been considered through 1D elements. Moreover, one of the main aspects of the material nonlinear analysis is the use of fiber beam elements. Some authors proved the effectiveness of this method in the complex analyses of composites structures [4.36]–[4.38] and arch structures [4.39]. In fact, this method is able to collect nonlinear responses with great precision for structures. These elements can build the link between material properties (e.g. stresses and strains) and macroscopic structure-level based responses (e.g. deflection, overturning, twists, etc.).


Fig. 4.5. Fiber beam element

A three-dimensional fiber element within a local reference system is considered as shown in Fig. 4.5. The vector components of the nodal displacements and resisting force elements are illustrated by the displacement vector q and the resisting force vector Q , as follow:

$$q = \{q_1, q_2, q_3, q_4, q_5, q_6, q_7, q_8, q_9, q_{10}, q_{11}, q_{12}\}^T \quad (4.1)$$

$$Q = \{Q_1, Q_2, Q_3, Q_4, Q_5, Q_6, Q_7, Q_8, Q_9, Q_{10}, Q_{11}, Q_{12}\}^T \quad (4.2)$$

According to the nominated integration points, the element is generally subdivided into several segments. The behaviour at each numerical integration point is characterized by the deformation vector $d^s(x)$ and the resisting force vector $f^s(x)$.

$$d^s(x) = \{\varepsilon(x), \varphi_z(x), \varphi_y(x)\}^T \quad (4.3)$$

$$f_s(x) = \{P(x), M_z(x), M_y(z)\}^T \quad (4.4)$$

Where x represents the coordinate of a section under consideration within the local reference system. The meshing of the section consists of a bidirectional mesh formed by small blocks. The strain of each fiber is determined by section deformation vector $d^s(x)$ and its coordinates (y_{fiber}, z_{fiber}) along the section.

Taucer et al. [4.40] stated that there is no difference in the manner through which the state determination of a force-based fiber is realized. The section force vector is determined by Eq.(4.5) where $N(x)$ is the matrix derived from the interpolations functions and Q_0 is the thermal force vector of an element. The incremental element resisting force vector ΔQ is calculated following the Eq.(4.6) where Δq represents the incremental element displacement vector.

$$f_0^s(x) = N(x) \cdot Q_0 \quad (4.5)$$

$$\Delta Q = K^e \cdot \Delta q \quad (4.6)$$

The tangent element's stiffness matrix K^e of a force-based beam element is determined by Eq.(4.7) whereas the tangent section's stiffness $k^s(x)$ can be determined by Eq. (4.8). The unbalanced section between $f^s(x)$ in Eq.(4.9) and $f_0^s(x)$ derived from Eq.(4.5) will be reduced to a tolerable range throughout iterations.

$$K^e = \left\{ \int_0^L N^T(x) \cdot [k^T(x)]^{-1} \cdot N(x) \cdot dx \right\}^{-1} \quad (4.7)$$

$$K^s(x) = \sum_{=1}^{n_{fib}} I_{k,fiber}^T \cdot (E_{k,fiber} A_{k,fiber}) \cdot I_{k,fiber} \quad (4.8)$$

$$f^s(x) = \sum_{=1}^{n_{fib}} l_{k,fiber}^T \cdot (\sigma_{k,fiber} A_{k,fiber}) \quad (4.9)$$

Obviously, for either displacement or force-based fiber beam-column elements, the state determination of sections at integration points plays a major role in the state determination process of elements. In order to ensure computational accuracy, a number of fibers are generally required to mesh a cross-section. For this reason, the time spent by the computer in the state determination process of cross-sections takes the greatest part of the time spent in the state determination process of a fiber beam-column element. It is a reasonable way to improve significantly the computational efficiency through the reduction of the workload associated with the state determination process of cross-sections.

4.4.2 Numerical modeling

The results obtained in this study have been possible thank to an intensive FEM analysis. 1D beam elements have been used for all structural elements except the deck where 2D shell elements with eight nodes quad8 and

six degrees of freedom are used in the analysis. The deck is modeled as square panels between two transversal beams to consider the connection between the deck and transversal beams. Hanger's arrangement in this study follows an equal radial distribution on the arch rib as presented in Fig. 4.6a. Fig. 4.7 shows a full numerical model of the network arch where the bracing length L_{Braced} represents 70% of the total arch length. Self-weight of the bridge is directly provided by the software using 7850 kg/m^3 and 2500 kg/m^3 for the density of respectively concrete and steel materials. The deck is made of 300 mm reinforced concrete. Two footways of 1.0 meter each one and 8.0 meters of carriageway complete the entire deck. The 8.0 m width bituminous layer is applied above the carriageway while the waterproofing is used to protect the entire concrete deck. Both of them are carrying additional permanent loads equal to 2 kN/m^2 and 0.25 kN/m^2 respectively.

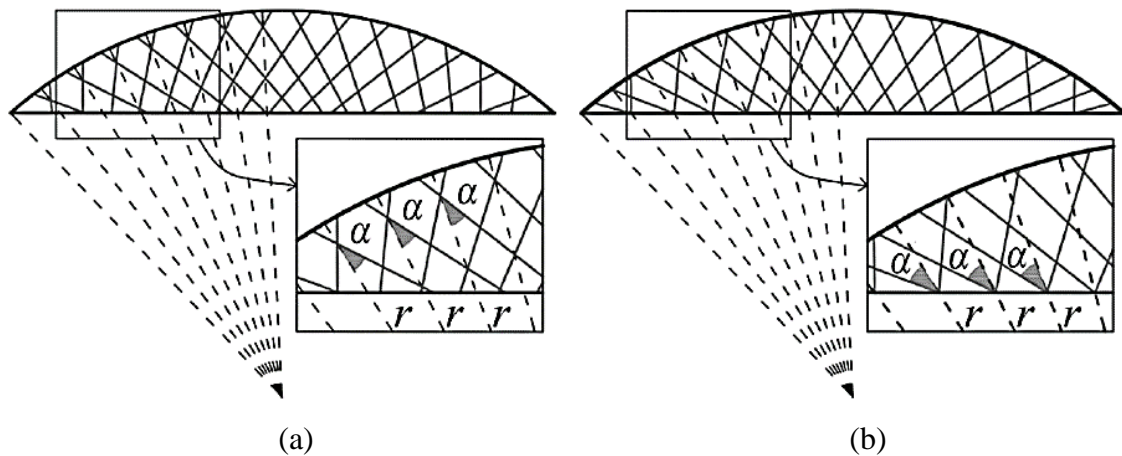


Fig. 4.6. Radial hanger arrangement: (a) equal distribution on the arch; (b) equal distribution on the tie beam

Fig. 4.8 represents the transversal distribution of traffic loads. The traffic loads are applied on the two notional lanes and remaining area according to EN 1991-1 [4.41]. Uniformly distributed loads are applied as vertical pressure while tandem loads are converted into stress representing pressure from each vehicle wheel.

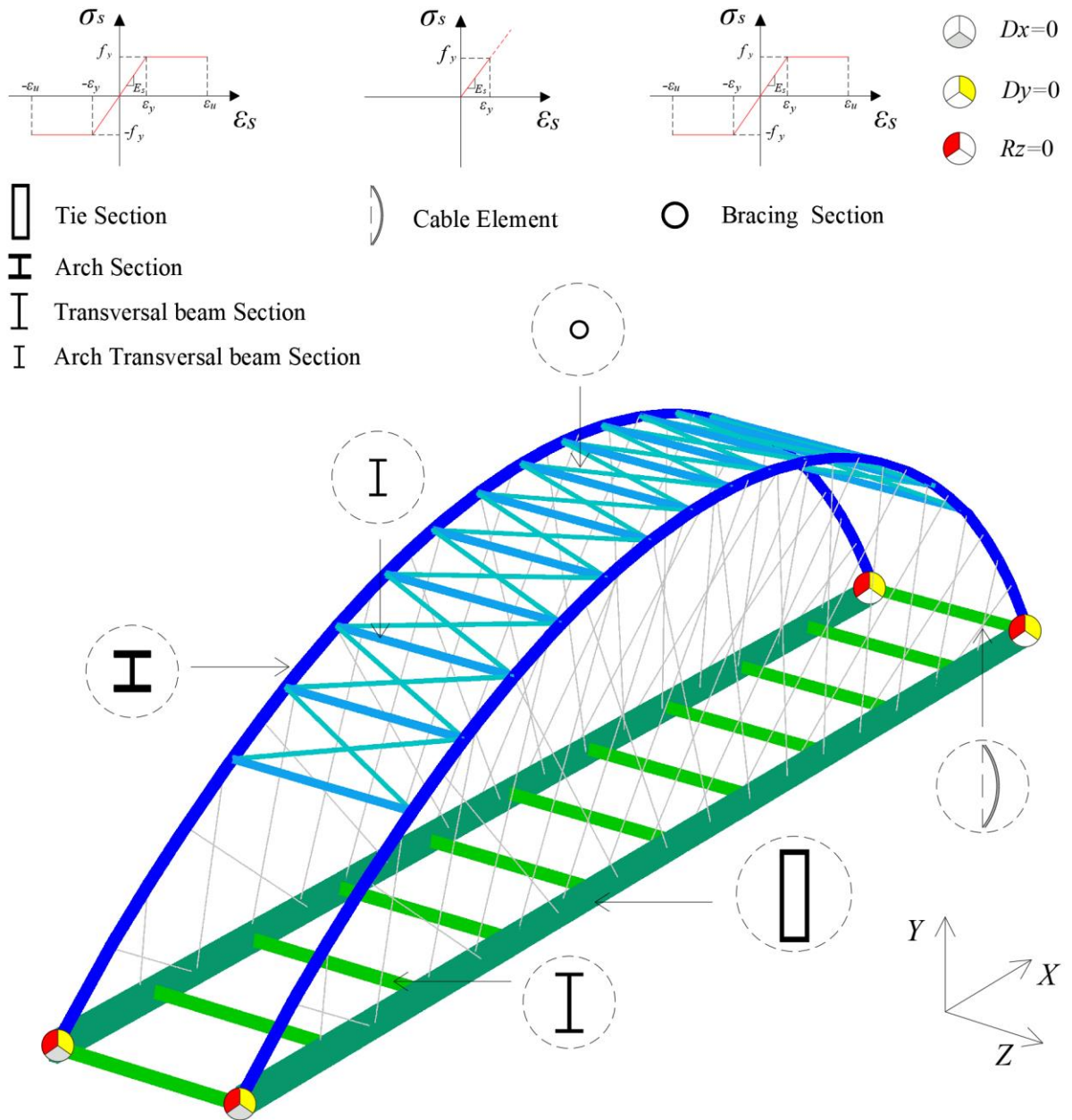


Fig. 4.7. 3D FEM model of a network arch bridge

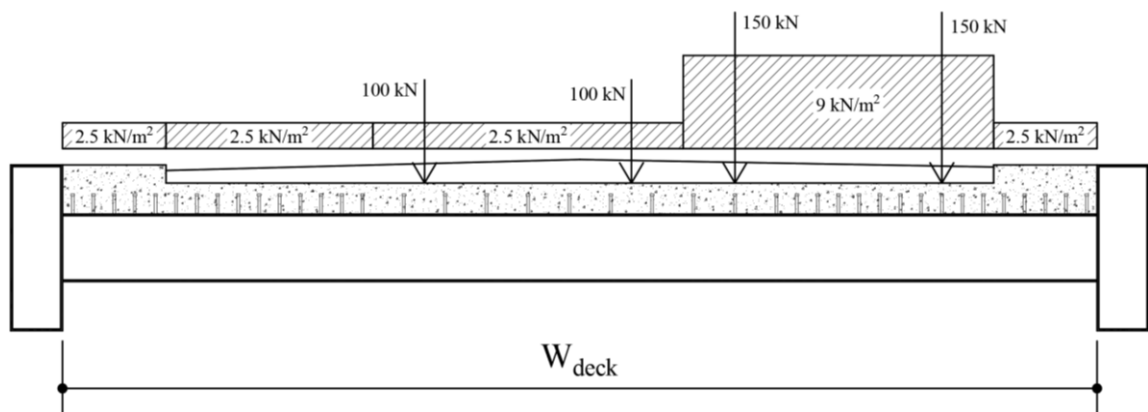


Fig. 4.8. Traffic load distribution on concrete deck

4.4.3 Types of analysis

The type of analysis is critical to understand the out-of-plane behavior of the arch. In fact, three types of analysis have been carried out for this purpose. Linear buckling analysis (L.B.A) is performed at an early stage to find the elastic critical traffic load. Then, geometric nonlinear analysis is performed to find the critical live load before the instability phenomenon in the arch section. Finally, pushover analysis will be performed to evaluate the global out-of-plane structural capacity of the arch for the network arch bridge. However, for the study of the behavior of the arch, it is necessary to take into account imperfections. For this reason, the P- δ effect and residual stress were considered through an equivalent geometric imperfection according to existing standards. Indeed, geometric imperfection is one of the critical details to take into consideration in the analysis since it describes the actual flaw deriving from the manufacturing process of the steel section. La poutré [4.13] studied carefully out-of-straightness of H-profile steel beam. The author proposed three polynomial equations that define the lateral, radial and twist imperfections. In the analysis, imperfections on the arch element corresponding to the first buckling mode and matching the recommendations from Annex D of EN 1993-2 [4.21] have been imposed for the L.B.A and G.N.A analysis.

To perform the GMNIA, a perfect elastoplastic material behavior has been used to characterize the structural elements of the bridge. Steel grade S420 for steel arch and tie-beam has been adopted while the other structural elements are made of S355 except for the cables that will be made of high strength parallel strand cable from Freyssinet. Finally, global imperfections of the arches have been imposed before nonlinear analysis. Three different out-of-plane imperfections have been applied at the level of the arch as shown in Fig. 4.9.

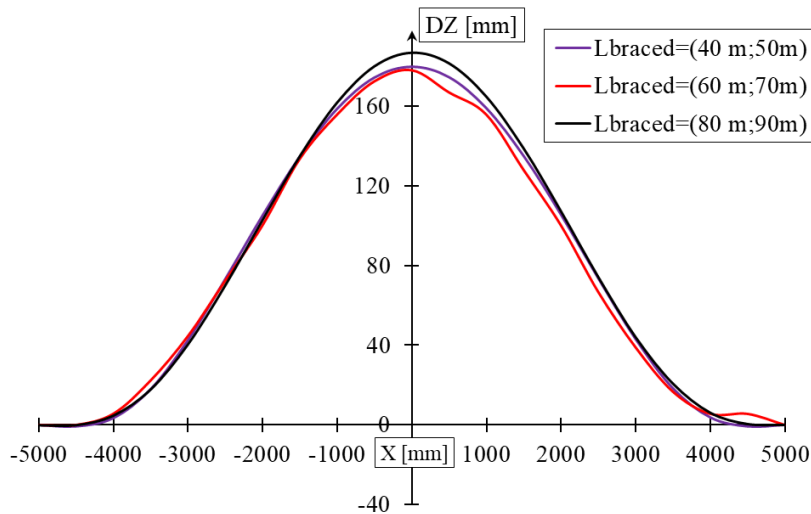


Fig. 4.9. Out of plane imposed imperfections for the investigated arches

4.4.4 Validation of the FEM result

One of the major issue when dealing with the FEM analysis is to validate the numerical model through a calibration process. Several authors to validate their numerical analysis used experimental results from previous works either on the same topic or on part of the topic in concern. In this study, since it is quite difficult to find experimental tests of the whole bridge, the authors used results from La poutré et al. [4.23]. The information regarding the experimental campaign has been summarized in section 2 taken in [4.13]. For this early analysis, the same geometric imperfections proposed by La poutré [4.13] has been used. GMNIA analysis has been done to take into consideration the modification of the actual stress due to the gradual change in the shape of the structure. During the analysis, vertical displacement is applied at the top of the arch increasing gradually the increment. The first hinge is observed at the point of imposed displacement as seen in Fig. 4.10. From the structural response, it is observed an increase of vertical force until the maximum after what the vertical reaction starts to decrease following a short softening curve before the release until zero. The failure mode is observed through the formation of three plastic hinges along with the arch element validating the classical theory of arch failure. Finally, the Force-displacement (lateral) diagram is plotted and compared to previous studies. A good correlation is observed between different curves as displayed by Fig. 4.11.

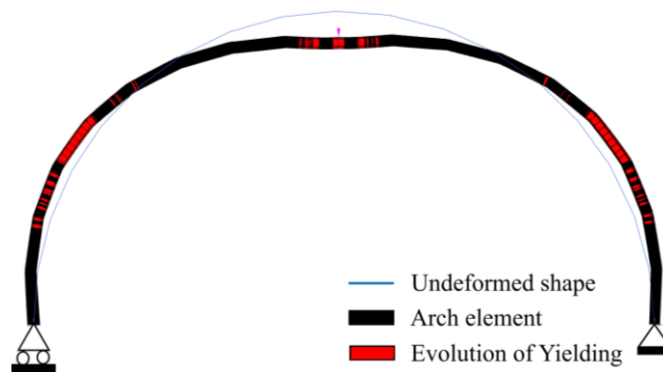


Fig. 4.10. Deformed shape and yielding state of the arch model. Geometry taken from La Poutré et al. [4.18]

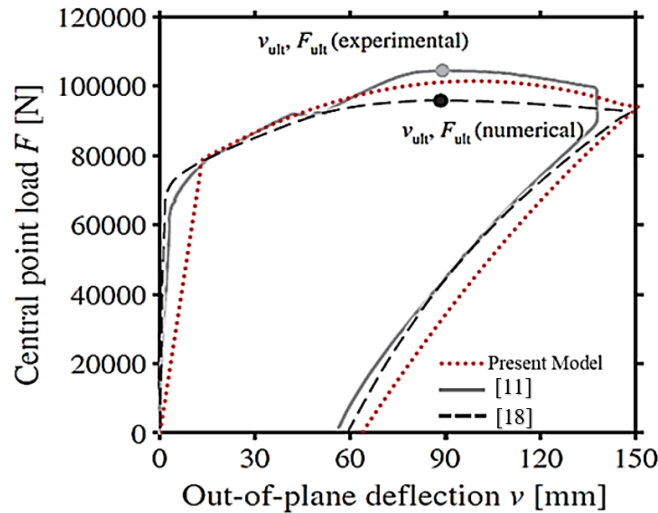


Fig. 4.11. Calibration of numerical models (Figure elaborated from La Poutré et al. [4.23])

4.5 Linear buckling and geometric non-linear analyses

Many researchers have paid their attention to the optimization of a generic network arch in order to reduce the total cost of the structure. Regarding hanger arrangement, a proposal of the optimal range for angle arrangement can be found in [4.6]. In this section, a comparison between geometric nonlinear and linear buckling analysis is presented.

In linear buckling analysis, hanger arrangement shows minor influence in respect to the bracing systems. Fig. 4.12a shows the variation of the live load factor in terms of the angle α for the first four instability modes. The live load factor slightly increases by increasing the angle α except for the case where $\alpha=60^\circ$. The difference is obvious for the fourth mode, which shows an increase of up to 9%. The buckling shapes of the unbraced arch are quite similar to the one of the straight simply supported beam. In fact, network arches can be represented as an I-profile where the flange in compression is the arch, the flange in tension being the tie beam and the web represented by hangers. The shapes are characterized by the formation of multiple half wavelengths in reference to the buckling mode as seen in Table 4.3.

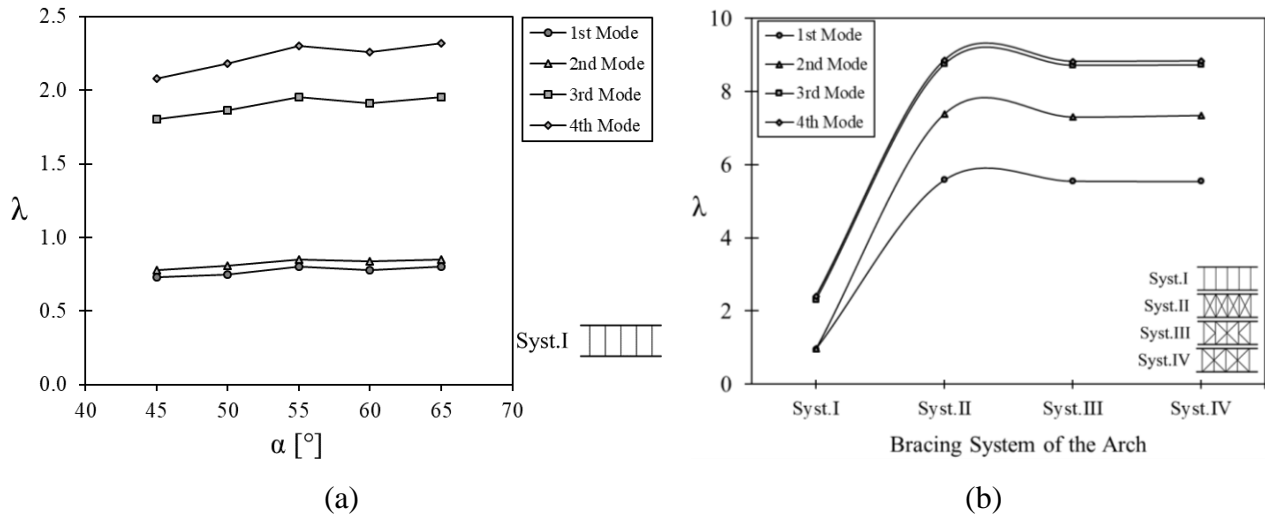


Fig. 4.12. Results from L.B.A; (a) Influence of angle hanger arrangement; (b) Influence of lateral bracing system

Table 4.3. Buckling shape of the first four mode for the Network arch bridge

Buckling	Angle α			
	60°	55°	50°	45°
1 st Buckling Mode (shape)				
2 nd Buckling Mode (shape)				
3 rd Buckling Mode (shape)				
4 th Buckling Mode (shape)				

Further analyses aiming to investigate the influence of lateral bracing show that the benefit of lateral bracing is obvious. Simple linear buckling shows that the live load factor is increased up to 6 times when providing the lateral bracing (Fig. 4.12b). It is worth noting that the critical live load will be reduced when performing the geometric nonlinear analysis since the deformed geometry is taken into account to establish the equilibrium equations, and both small and large finite strain may be considered. Results from geometric nonlinear analysis display a linear behavior in the first region until the maximum live load after what it keeps constant or slightly increases (Fig. 4.13). In addition, the nonlinear analysis allows drawing the effect of live loads to the arch out-of-plane displacement. The bracing system Syst. IV presents the most rigid solution since it allows a reduction of out of plane displacement with the same state of applied live loads as seen in Fig. 4.13. The influence of the stiffer bracing has also been investigated. From the nonlinear analysis, it

is observed that the arch is less sensitive to the out of plane buckling for Syst. IV when increasing the bracing stiffness (Fig. 4.14). The results are compared to those from the linear buckling where the critical live load considerably increases in function of the bracing' stiffness (Fig. 4.15).

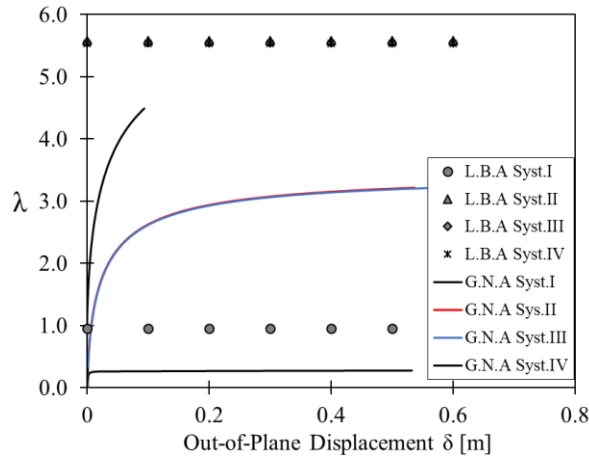
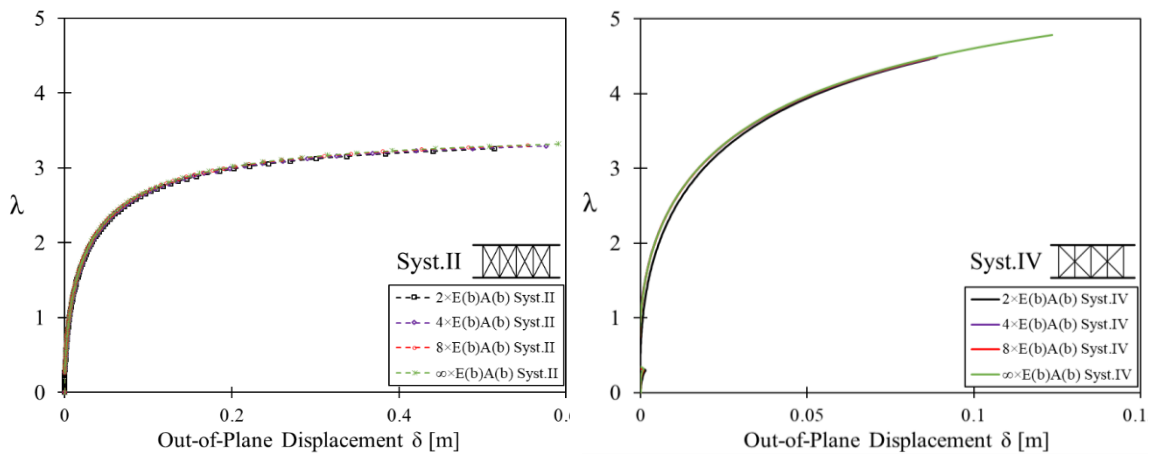


Fig. 4.13. Live load factor of the network arch from L.B.A and G.N.A analysis

EN 1993-2 [4.21] deals with the arch buckling by considering only the free end portal of the arch, which represents the non-braced part of the arch starting from the abutment. In this study, the influence of the braced length of the arch has also been evaluated. Indeed, by increasing the bracing part of the arch, the end portal of the arch decreases leading to less sensitivity to buckling.



a) Syst. II

b) Syst. IV

Fig. 4.14. Influence of the lateral bracing stiffness in the live load factor

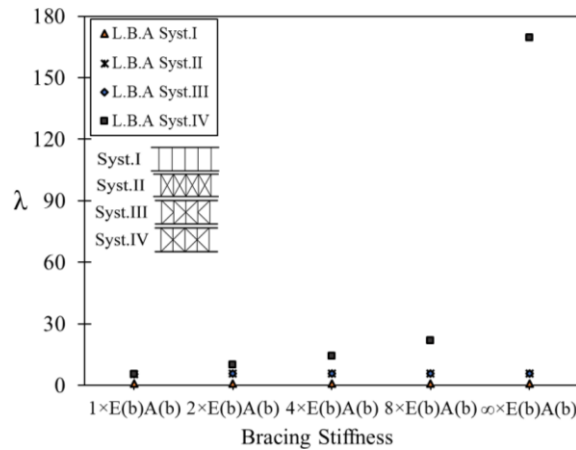


Fig. 4.15. Influence of the lateral bracing stiffness in the live load factor; a) L.B.A; b) G.N.A

The results from both Linear and geometric nonlinear analysis showed that the benefit of increasing the braced length of the arch is evident when Syst. I, Syst. II and Syst. III are used. In fact, the transversal beam of the arch is not sufficiently rigid to change the length involved in the lateral movement of the arch. In general, the critical live load may increase by increasing the braced zone of the arch. Fig. 4.16 and Fig. 4.17a shows the influence of braced zone of the arch through linear and nonlinear analyses. It is important to notice that the two analyses display close results when the length of the end portal is reduced. Finally, the lateral sensitivity of the arch in terms of the braced length is presented in Fig. 4.17b. The result shows for a specific live load a quasi-identical out of plane displacement of the arch at its center for the three bracing systems considered in the analysis.

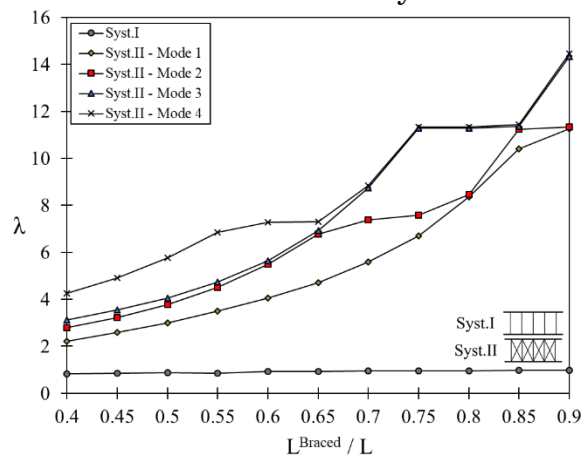


Fig. 4.16. Live load factor in function of the braced percentage of the arch in L.B.A

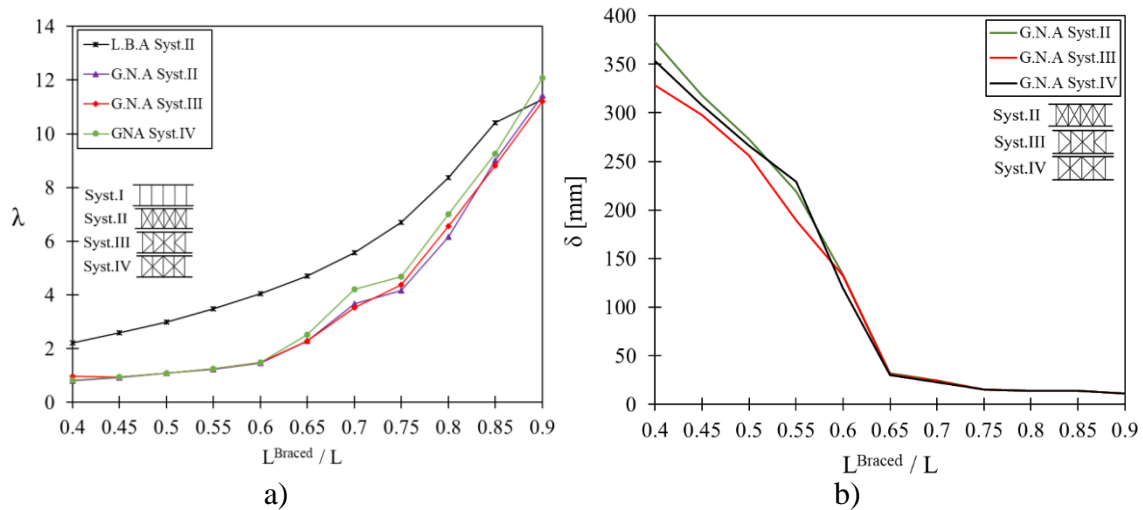


Fig. 4.17. Live load factor in function of the braced percentage of the arch in G.N.A; a) Variation in the live load factor; b) change in out-of-plane displacement of the arch

4.6 Structural behaviour of the arch under vertical loads at arch center

Based on careful geometric and material nonlinear analysis, the global lateral behavior of the arch under vertical loads can be drawn. In fact, through GMNIA, a good correlation has been observed between the lateral behavior of network arch bridge and both stress state and buckling of the arch. In order to reach the results, multi-steps analyses have been carried out. Initially, the FEM model is run only for the self-weight and permanent loads.

As the primary aim is to find the load response of the arches, a displacement scaling analysis has been chosen. Two vertical displacements are applied at the center of arches and are gradually increased. For arch-braced with syst. II, the displacement rate is increased until the arch member reaches the ultimate strain after what it is removed. Fig. 4.18 shows the flowchart with different steps of the analysis.

In general, the lateral sensitivity of both braced and unbraced arch bridges subjected to vertical loads is characterized by 3 states: one linear and two non-linear. From the stress point of view, the load increases linearly with the lateral displacement until the material reaches the yielding stress at point 2. Thus, the first hinge is formed with the partial plasticization of the section and will end the linear phase as shown in Fig. 4.19a and Fig. 4.20a. The location of the first hinge may vary depending on the length of the arch where lateral bracing has been applied. It is worth noting that the first hinge is prone to be formed near the support due to the reaction of abutment as seen in Fig. 4.21a. Indeed, a large bending moment is generally observed close to the support. This bending moment will vary slightly until the connection of the first hanger to the arch. The bending moment will decrease considerably due to the radial distribution of hangers. The first hinge will be formed at the point of maximum bending moment.

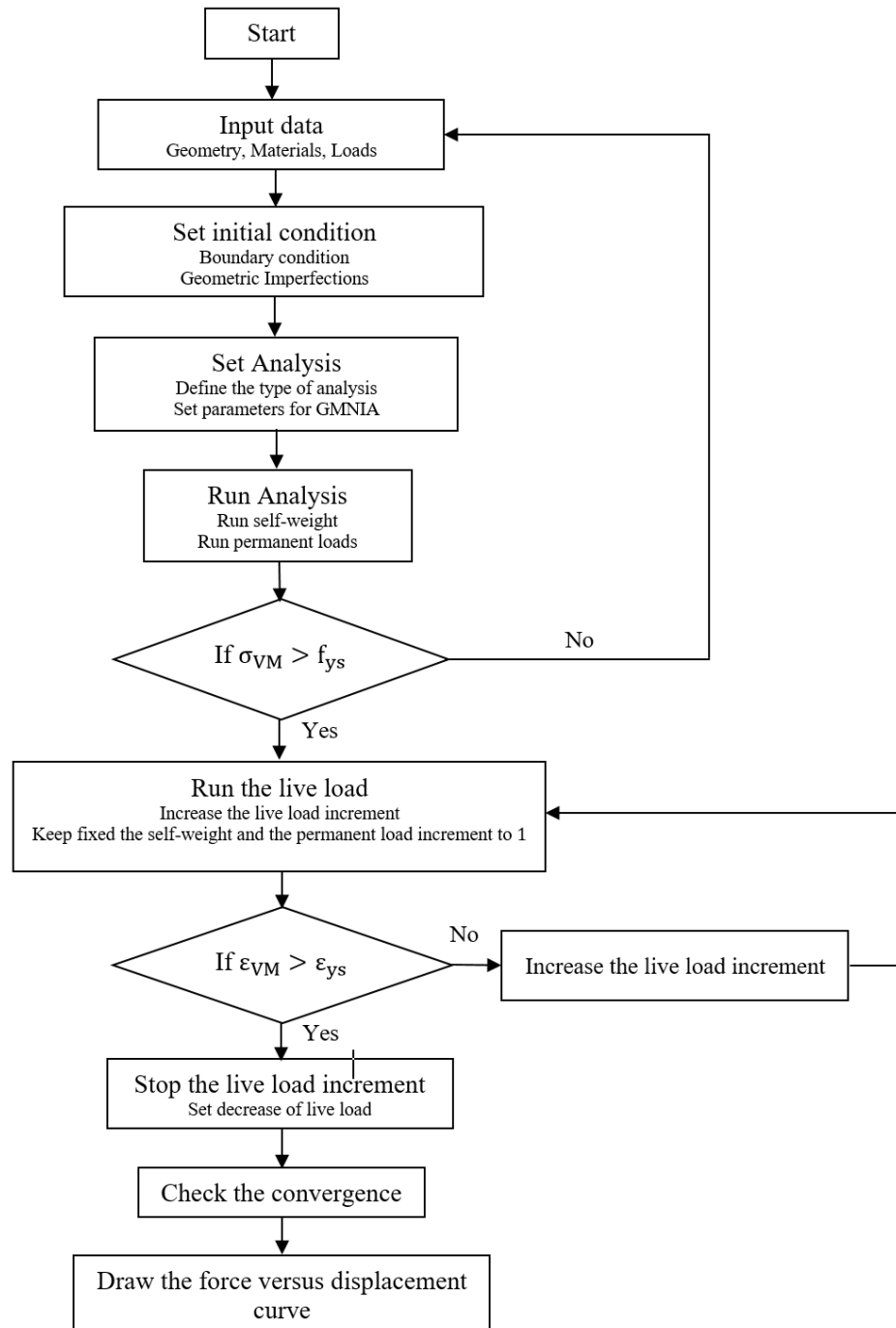


Fig. 4.18. Flowchart for the GMNIA procedure analysis in braced arches

Then, the bending moment will remain constant and the overload will be redistributed to nodes close to the occurrence of the first plastic hinge. In some cases, yielding is reached nearby to the arch center and spread toward the supports (Fig. 4.22 and Fig. 4.23). In this situation, cables fail to distribute the stress along the arch since the concentration of stress is observed close to the arch midspan. The first hinges are then formed at these points of high bending moment (Fig. 4.21b). Then, the out-of-plane displacement will continue to increase faster than the increase of vertical loads involving the full plasticization of the section. For the unbraced arch, the second buckling mode

happens in the second non-linear hardening of the section while for the braced arch, the section reached the critical strength and ultimate strain and will not undergo a second hardening (Fig. 4.19b and Fig. 4.20b).

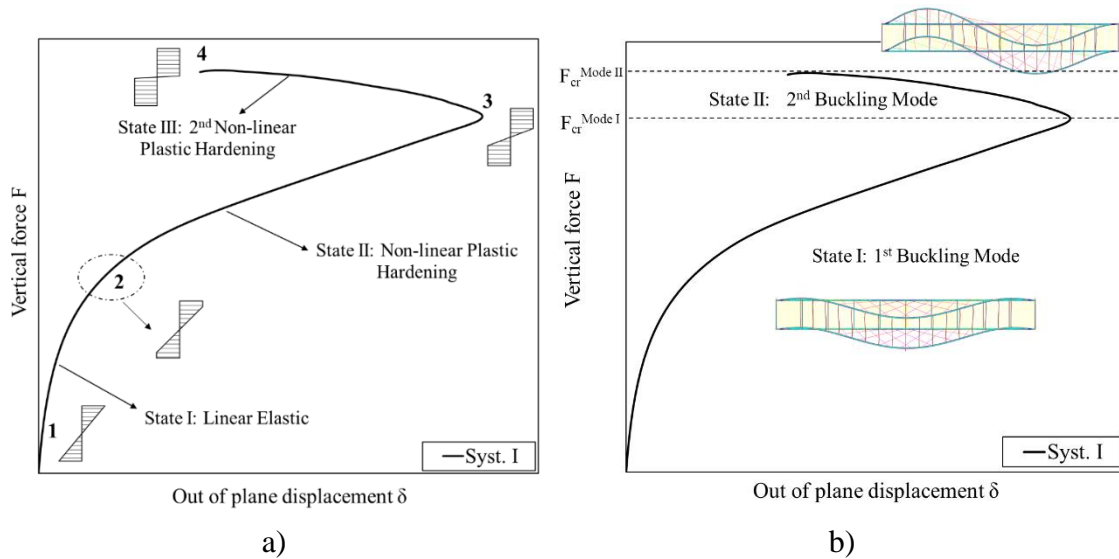


Fig. 4.19. Global lateral behaviour of the unbraced network arch bridge under vertical loads; a) Stress variation in the section; b) Buckling behaviour of the arches

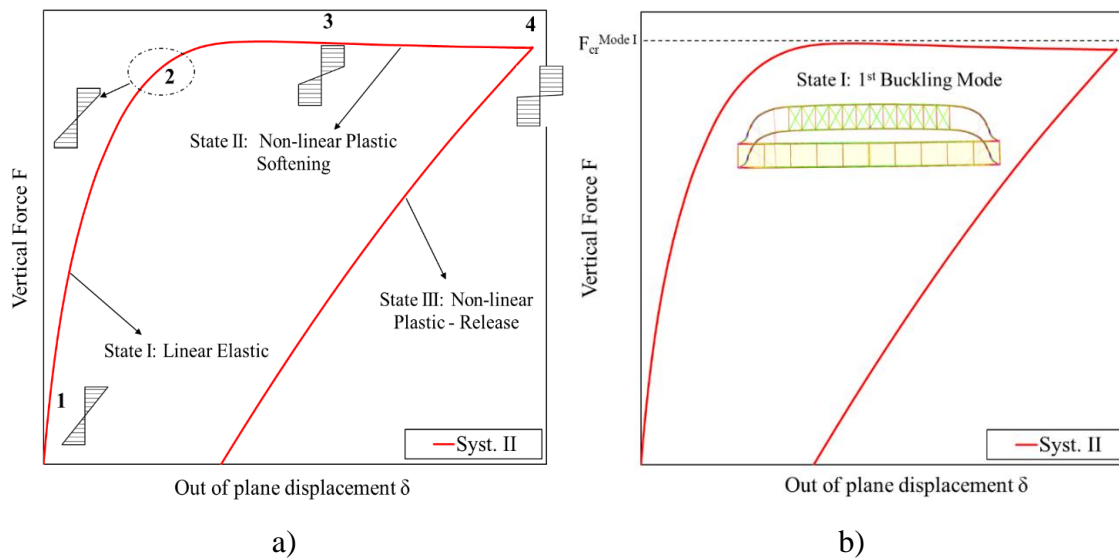


Fig. 4.20. Global lateral behaviour of the braced network arch bridge under vertical loads; a) Stress variation in the section; b) Buckling behaviour of the arches

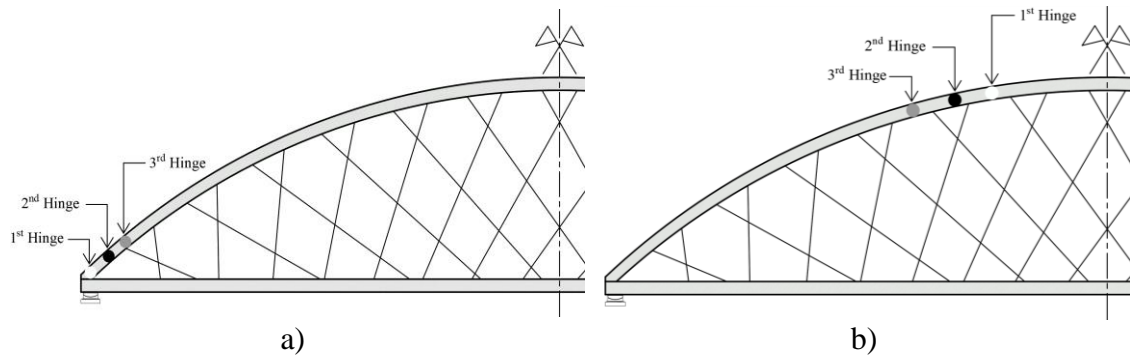
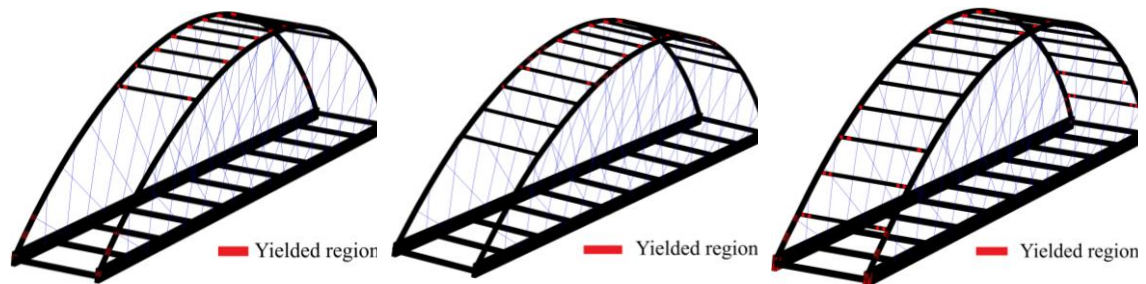
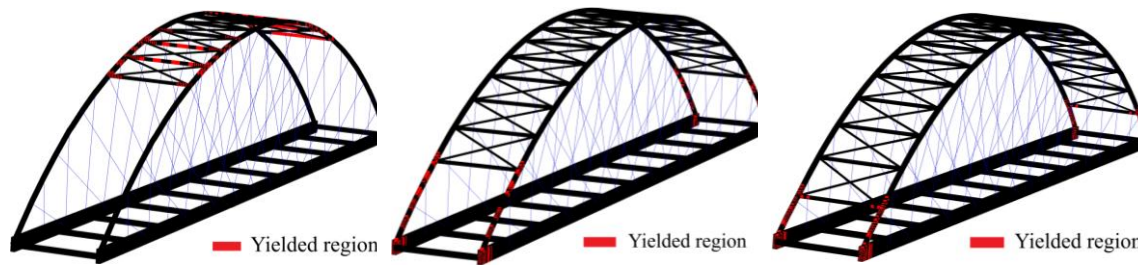


Fig. 4.21. Position of the three first hinges in the arch rib; a) First hinge close to the support; b) First hinges close to the arch midspan



a) $L_{braced} = 50\text{ m}$ b) $L_{braced} = 70\text{ m}$ c) $L_{braced} = 90\text{ m}$

Fig. 4.22. Stress state in the arches, formation of plastic hinges: Unbraced arches

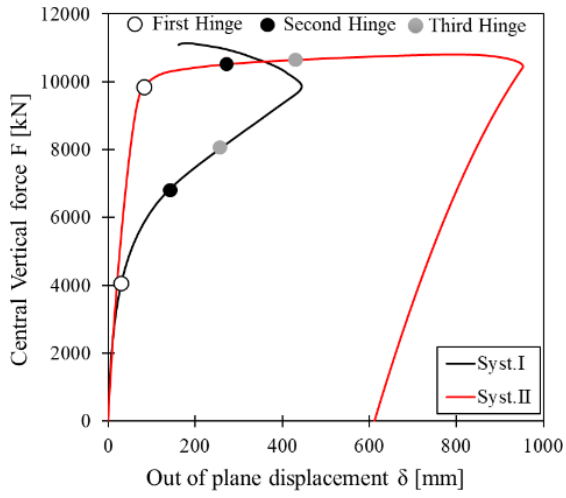


a) $L_{braced} = 50\text{ m}$ b) $L_{braced} = 80\text{ m}$ c) $L_{braced} = 90\text{ m}$

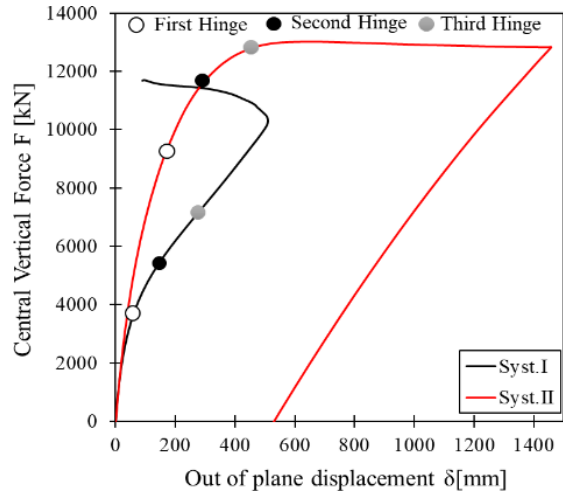
Fig. 4.23. Stress state in the arches, formation of plastic hinges: Braced arches

The results obtained from different braced length showed almost the same behavior. The first hinge is formed when the vertical force in the arch is more or less 4000 kN for unbraced arches following successively the formation of second and third hinges. It is worth noting that the successive hinges in the arches are formed shortly after the first hinge. Fig. 4.24 shows the stress level inducing the formation of the first three hinges. The benefit of wind bracing in the increase of lateral stiffness is evident as soon as both cases are drawn in the same graph. As soon as the length of the braced zone of the arch increases, the critical load increases faster than the lateral displacement. For the unbraced arch, the behavior observed is the same for different cases studied while the situation is quite different for the braced arch. In fact, for arches braced up to 80 and 90 %, softening behavior is observed after the

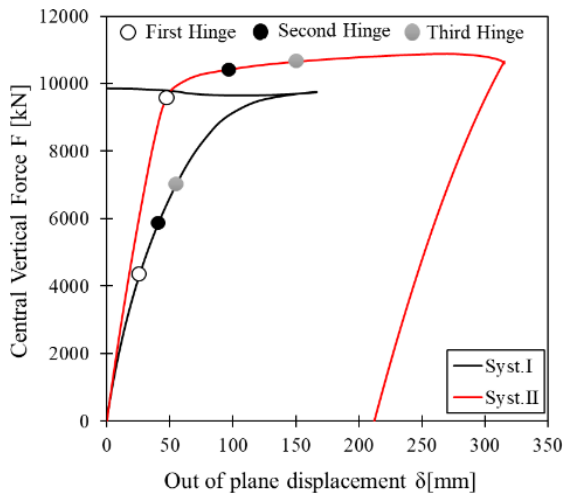
critical load is reached (Fig. 4.24d and Fig. 4.24e). When the free end portal increases for the arch with syst.1 (Fig. 4.24a – Fig. 4.24c), a slight softening is observed after the critical buckling load of the arch.



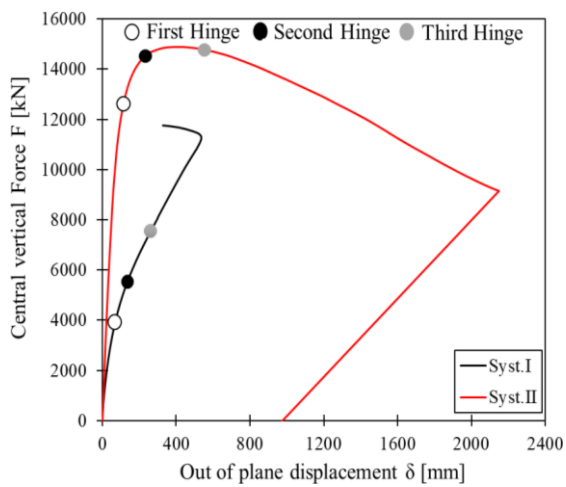
(a)



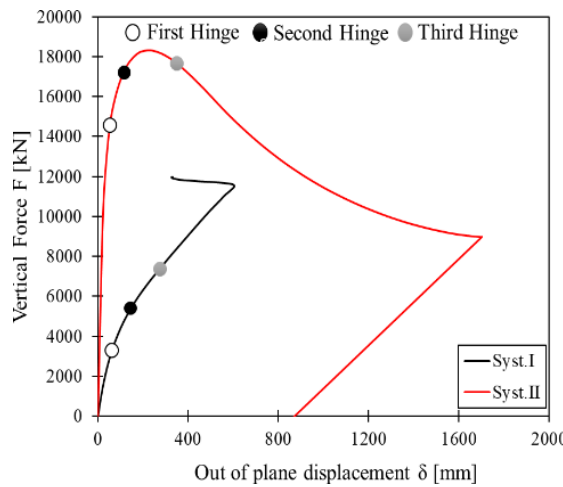
(b)



(c)



(d)



(e)

Fig. 4.24. Vertical live loads – lateral deflection curves for unbraced and braced arch bridge; (a) $L^{\text{Braced}}=50$ m; (b) $L^{\text{Braced}}=60$ m; (c) $L^{\text{Braced}}=70$ m; (d) $L^{\text{Braced}}=80$ m; (e) $L^{\text{Braced}}=90$ m

4.7 Structural behaviour of the arch under traffic loads

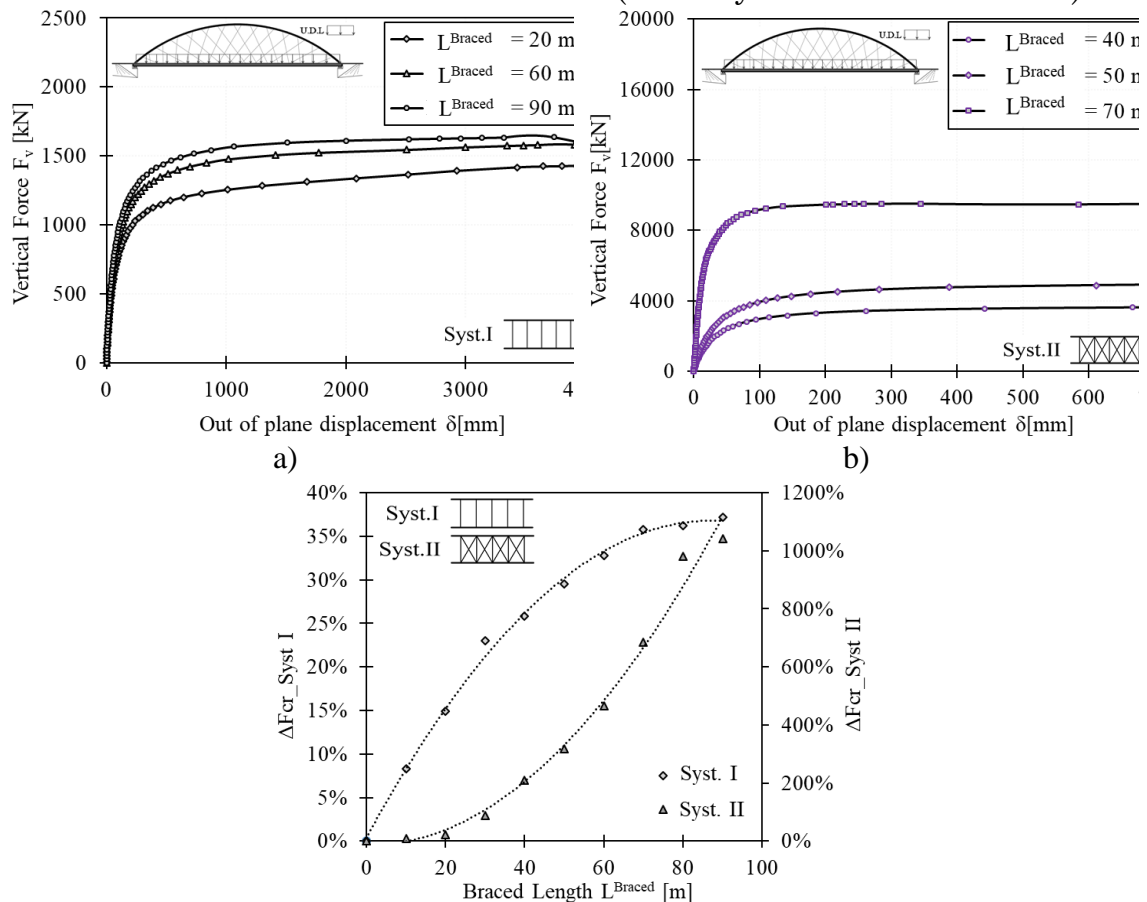
In this section, the structural behavior of the arch element will be studied. It will be presented first the stability of the arch under the traffic loads applied to the bridge deck through various linear and non-linear analyses. Then, the performance of the arch will be evaluated by taking into account two bridge conditions: undamaged bridge and damaged bridge.

4.7.1 Structural performance of the arch under traffic load

In this section, a study of the performance of network arch bridges will be conducted. In this subsection, two considerations have been made. The first was to study the structural capacity of undamaged bridges and the last to consider damaged network arch bridges. Damage, in this case, refers essentially to the accidental loss of one or more cables.

4.7.1.1 Undamaged bridge

In the case of a bridge without damage, the structural capacity is assessed in order to present the out of plane structural behavior of the arches under traffic loads. The results showed two different behaviors depending on the structural connection between arches (laterally braced or non-braced).



c)

Fig. 4.25. Out of plane behaviour of network arch bridges under traffic loads

In the case of network arch bridges without lateral bracing (Syst. I), the capacity follows an elastoplastic phase displaying a slight hardening followed by softening as shown in Fig. 4.25a. On the other hand, a perfectly elastoplastic behavior followed by strong hardening is observed when using lateral bracing (Fig. 4.25b). Finally, it is worth noting that the variation in the structural capacity of the bridge is strongly influenced by structural systems. Indeed, for braced bridges, the capacity could be 10 times greater than that of a bridge without bracing and lateral beams at the arch level. In addition, linear regression allows us to observe two different trends depending on the two systems (Syst. I and Syst. II). In the case of the consideration of the Syst. I, the structural capacity varies considerably for small braced lengths. After 60 m of braced length, the increase in capacity follows an almost constant rate of increase, in contrast to the behavior observed in the case of Syst. II as presented in Fig. 4.25c.

4.7.1.2 Damage Bridges

In relation to previous results and considerations made in the bridge industry, the case of Syst. II with a braced length of 70 m was considered in the following analyses.

4.7.1.2.1 Cable loss scenario

In order to consider the dynamic sensitivity of the network arch bridge following an accidental cable loss, the action was modeled as a dynamic action that occurs in a short period of time. Thus, first, a static analysis of the healthy bridge is made, then the internal forces in the cables are used to model the action of cable loss. In particular, in the first instance, all permanent loads were applied as a ramp function over a period of time T_1 followed by a steady-state until the final time T_2 of the analysis. A quasi-static analysis is carried out, which considers all permanent actions as static actions. On the other hand, the loss of cable is analyzed through a nonlinear times history that considers the dynamic aspect of the effect. However, the action was modeled as follows: The internal forces of the cables that represent initial forces are applied with as a ramp function until the period T_1 , then follow the steady phase over a period T_2 . The loss phase over a period T_3 is materialized by a progressive decrease with time of the initial forces and finally, a second steady phase within a period T_4 with null initial force is applied. Information about the parameters of the time history is shown in Fig. 4.26 with an estimated cable loss over a period of 2 seconds.

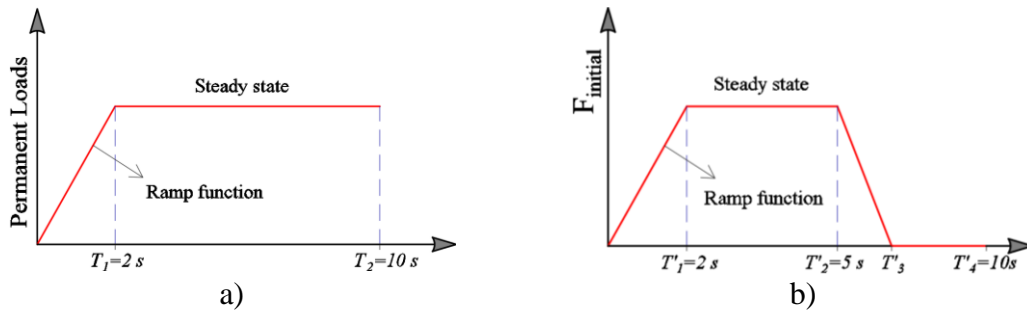


Fig. 4.26. Loading stages for analysis of global model: a) quasi-static analysis for permanent loads, b) time-history analysis for cable loss

The response of the network arch bridge was studied, focusing particularly on the out of the plane capacity of the arch. It should be pointed out that each arch of the bridge studied has 26 hangers. By isolating each arch, a nomenclature was made in order to simplify the analysis (Fig. 4.27a). With regard to the cable loss scenario, a cable was chosen arbitrarily. In the FEM model, this cable was removed and at the two ends, two forces of opposite direction to the internal forces and with same intensity are applied (Fig. 4.27b). Then, a non-linear dynamic analysis was performed on the model to study the dynamic sensitivity of the bridge just after a cable loss scenario.

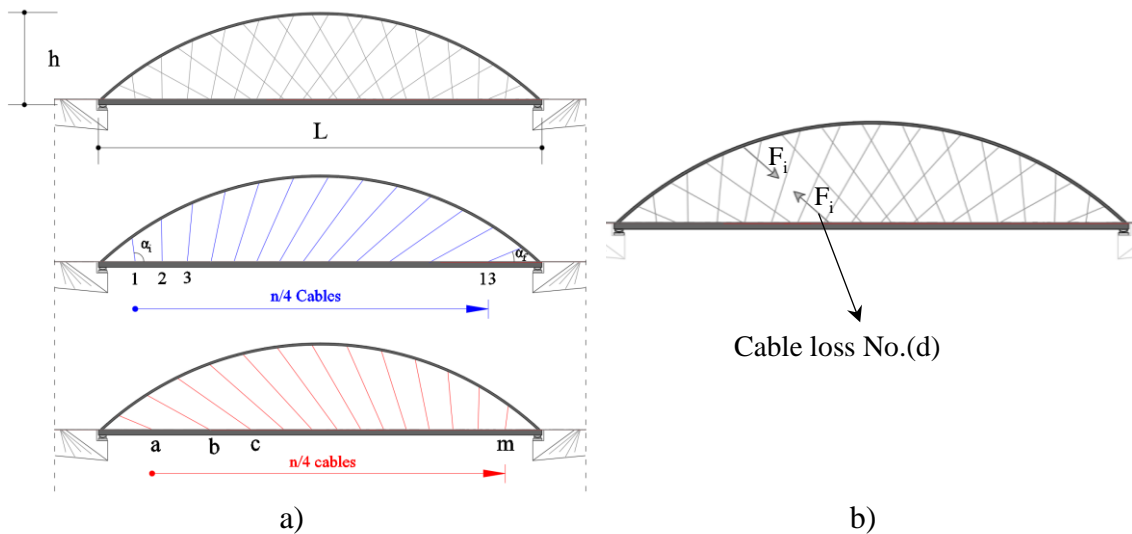


Fig. 4.27. Bridge configuration for cable loss scenario

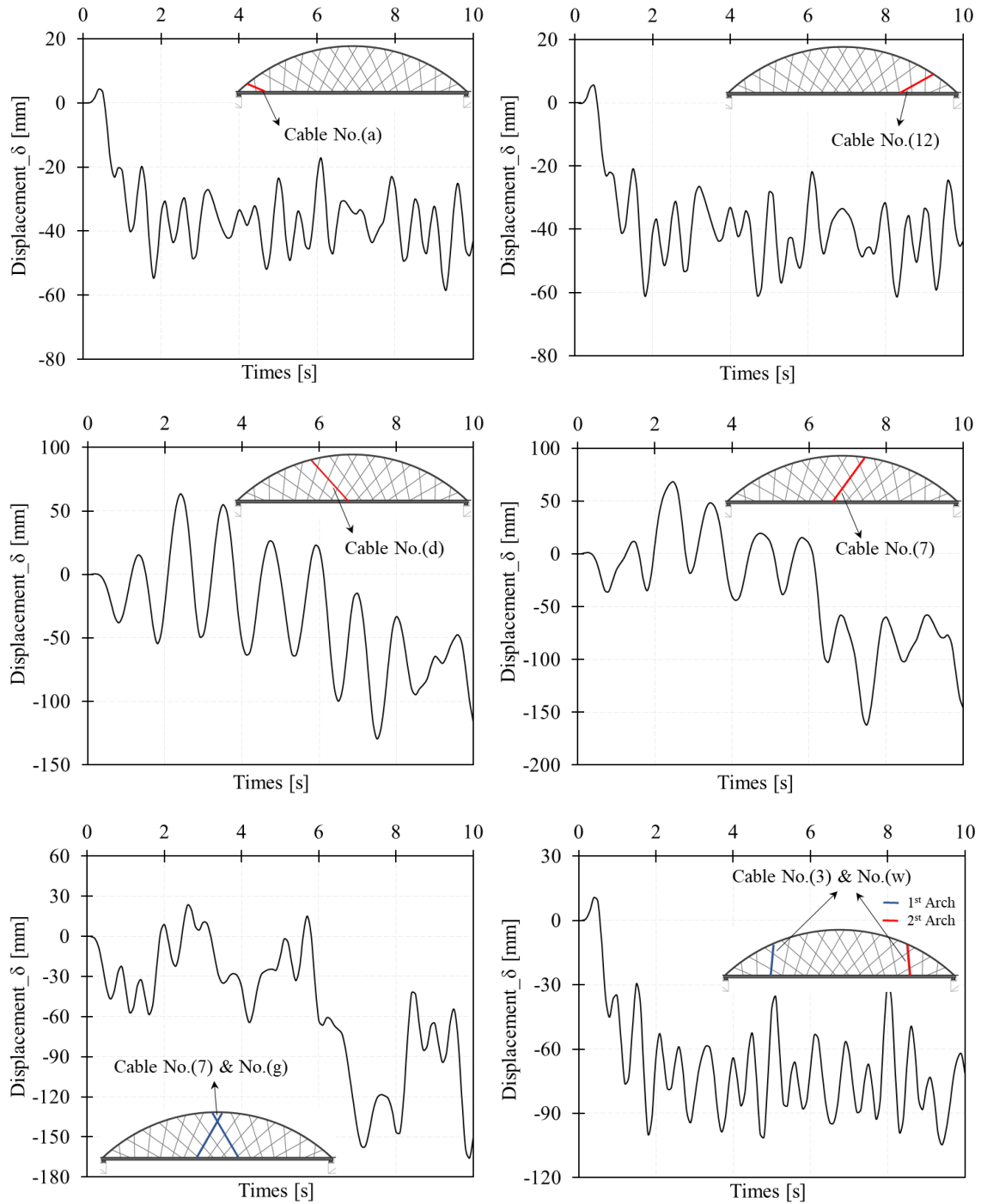


Fig. 4.28. Dynamic sensitivity of the bridge after cable loss scenarios

Fig. 4.28 shows the results of the dynamic sensitivity of the arch following a cable loss scenario. Studies considering various scenarios with the loss of one or two cables simultaneously were conducted. It should be highlighted that the dynamic response of the arch to cable loss depends mainly on the position of the cable. Indeed, the results show a high dynamic sensitivity of the arch after the loss of the cable near the bridge's abutments. This sensitivity decreases for cable loss close to the bridge's center. It could be

explained by the fact that the stiffness of the lateral bracing and adjacent cables on either side of the broken cable contributes significantly to the dynamic sensitivity of the arch. This hypothesis is confirmed since close to the abutment, lateral bracing doesn't exist or doesn't contribute efficiently to the stability. On the other hand, the observed out-of-plane displacements are significantly greater for cable loss at the bridge's center since at this position, internal forces in the cable are generally high. Finally, in the case of two cables loss scenario, the dynamic behavior of the arch element is almost identical to that observed after the loss of one cable. However, the only difference observed is the greater amplitude of out-of-plane displacement that the arch can achieve following a loss of two cables.

Afterward, a study of the effects that the dynamic response of the arch could have on its structural capacity. For this purpose, the final condition of the bridge after the dynamic analysis was kept. A pushover analysis considering only the effect of traffic load was done and the performance of the arch was determined. It is noteworthy that the performance curves differ according to the position of the cable loss. Indeed, for a lost cable located in the center of the bridge, the arch exhibits a less ductile behavior compared to the case where the lost cable is close to the abutments. On the other hand, the ultimate resistance of the arch for a cable loss scenario observed at the center of the bridge is lower than that observed when a cable is removed at the ends Fig. 4.29a.

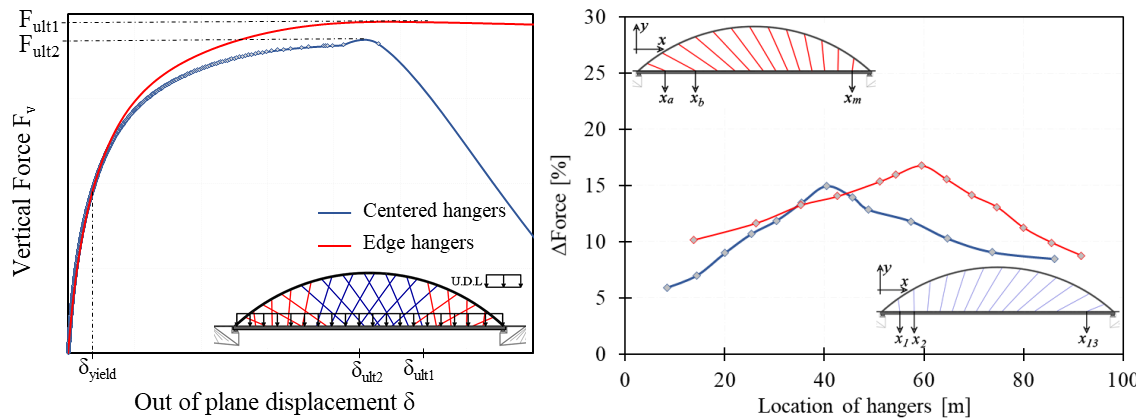


Fig. 4.29. Structural capacity of the arch subjected to one cable loss scenario

Finally, from the results, it appears that damage to a cable creates a reduction in the out-of-plane capacity of the arch and it depends on the position of the cable. Indeed, figure Fig. 4.29b shows the reduction of the ultimate force of the arch as a function of the position of the hangers, which is taken as the axis of the beam-Hanger connection. By varying the braced lengths, it is observed that as the braced length increases, the less the impact of the loss of a cable is experienced with a variation around 7% for $L_{braced} = 90$ m (Fig. 4.30a). On the other hand, for a braced length equal to 50 m, the variation between capacities can reach 25 % (Fig. 4.30b).

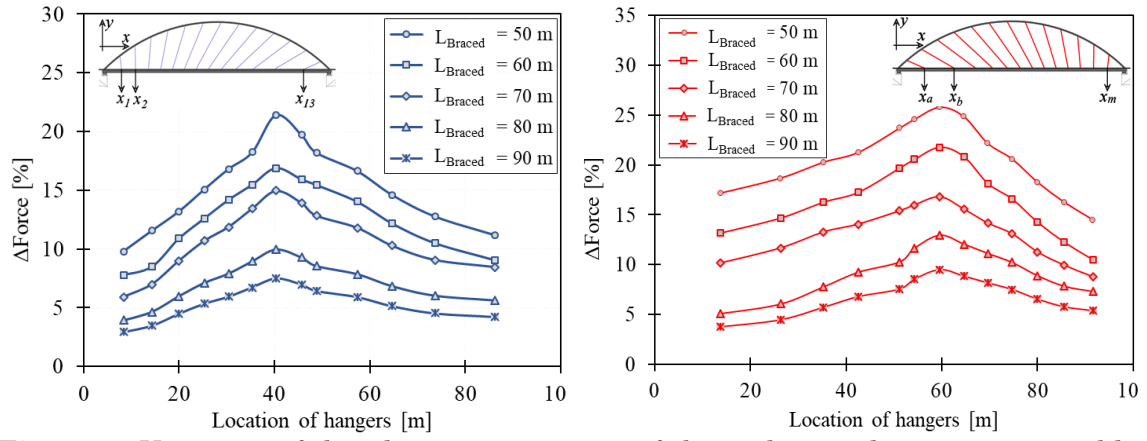


Fig. 4.30. Variation of the ultimate resistance of the arch considering various cable loss scenario for different braced length

4.8 Conclusion

The global out-of-plane behavior of network arch bridge has been studied in this chapter through intensive nonlinear analysis. Fiber beam elements have been used in the analysis in order to converge with great precision to the structural nonlinear responses. Initially linear and nonlinear analyses have been performed and compared together to show the influence of the actual deformation and stress in structural element to the arch lateral sensitivity. For all cases, geometric imperfections were considered to integrate the initial flaw of the section. Previous works on similar topics have been valuable because they allowed us to validate our numerical model. The main findings from the study are as follow:

Through geometric and material nonlinear analysis, the description of arch out-of-plane behavior can be made. It is characterized by linear behavior following by nonlinear behavior. In addition, the lateral bracing considerably increases the stability of the arch by creating additional support to the arches.

For arches without lateral bracing, multi-shape modes are observed. The arches move to the second buckling mode at the end of the first nonlinear phase. During this phase, an increase of vertical loads is still visible. On the other hand, another behavior is observed for braced arches, which display a slight softening at the end of the first nonlinear phase. The arches reached the critical live loads and the strain will continue to decrease with the formation of several hinges on each arch.

The results from finite element models show a gradual yielding of arch either from the support toward the arch midspan or from the arch midspan toward the support. The yielding process is fast for the early case and the hinges are formed rapidly until the braced region of the arch while in the latter case, the development of yielding is prevented by the bracing system.

The cable loss scenario generated dynamic actions on bridges element whose sensitivity mainly depend on the position of the cable. Indeed, the arch is less dynamic sensitive in the case of the loss of cable located to the center of the bridge. however, a large lateral displacement will also be observed in this case mainly due to the large reaction forces existing in the cable.

The reduction of lateral capacity of the arch after a cable loss scenario is related to the location of the hanger connection to the girder. The results showed the loss of a cable close to the center of the arch will display a great reduction of the lateral capacity and finally the reduction of the lateral capacity might reach 25 % in the case of the less stiff arch.

4.9 References

- [4.1] “The Network Arch .,” no. March, 2014.
- [4.2] *Anna Weronika Ostrycharczyk Network arch timber bridges with light timber deck on transverse crossbeams Anna Weronika Ostrycharczyk Network arch timber bridges with light timber deck on transverse crossbeams.* 2017.
- [4.3] F. Schanack, “Analysis of the structural performance of network arch bridges,” no. January 2009, 2016.
- [4.4] F. Schanack, “IN-PLANE ARCH BUCKLING OF NETWORK ARCH Paper for the 2009 World Steel Bridge Symposium by,” no. April, 2016.
- [4.5] S. Teich, “Entwicklung allgemeiner Entwurfsgrundsätze für Hängernetze von Netzwerkbogenbrücken,” vol. 80, 2011.
- [4.6] A. De Zotti, C. Pellegrino, and C. Modena, “A parametric study of the hanger arrangement in arch bridges.”
- [4.7] C. Pellegrino, G. Cupani, and C. Modena, “Author ’ s personal copy The effect of fatigue on the arrangement of hangers in tied arch bridges.”
- [4.8] A. W. Ostrycharczyk and K. A. Malo, “Parametric study on effects of load position on the stress distribution in network arch timber bridges with light timber decks on transverse crossbeams,” *Eng. Struct.*, vol. 163, no. February, pp. 112–121, 2018.
- [4.9] A. W. Ostrycharczyk and K. A. Malo, “Parametric study of radial hanger patterns for network arch timber bridges with a light deck on transverse crossbeams,” *Eng. Struct.*, vol. 153, no. October, pp. 491–502, 2017.
- [4.10] S. Akimoto and Y. Amao, “PROC. OF JSCE, No. 286, JUNE 1979,” no. 286, 1979.
- [4.11] N. S. Trahair, “BEAM-COLUMNS. Ih APPLICATIONS,” vol. 120, no. 7, pp. 2062–2085, 2006.
- [4.12] “beam element . Nour-Omid and Rankin (1991) used projectors for

- consistent linearization and presented a finite rotation analysis by co-rotation formulation. More recently, Simo and Vu-Quoc (1991) developed a geometrically exact beam model including,” vol. 120, no. 7, pp. 2041–2061, 2006.
- [4.13] C. C. Ontwerpen, F. Bouwkunde, and T. U. Eindhoven, “Stability experiments on circular steel arches,” 2004.
- [4.14] R. C. Spoorenberg, H. H. Snijder, J. C. D. Hoenderkamp, and D. Beg, “Design rules for out-of-plane stability of roller bent steel arches with FEM,” *JCSR*, vol. 79, pp. 9–21, 2012.
- [4.15] A. Romeijn and C. Bouras, “Investigation of the arch in-plane buckling behaviour in arch bridges,” vol. 64, pp. 1349–1356, 2008.
- [4.16] S. Palkowski, “Buckling of parabolic arches with hangers and tie,” *Eng. Struct.*, vol. 44, pp. 128–132, 2012.
- [4.17] W. Qiu, C. Kao, C. Kou, J. Tsai, and G. Yang, “Stability Analysis of Special-Shape Arch Bridge,” vol. 13, no. 4, pp. 365–373, 2010.
- [4.18] A. Liu, Y. Huang, Q. Yu, and R. Rao, “An Analytical Solution for Lateral Buckling Critical Load Calculation of Leaning-Type Arch Bridge,” vol. 2014, 2014.
- [4.19] A. Outtier, H. De Backer, and P. Van Bogaert, “Out-of-plane buckling curve for steel tied arch bridges OUT-OF-PLANE BUCKLING CURVE,” no. January, 2007.
- [4.20] H. De Backer, A. Outtier, and P. Van Bogaert, “Buckling design of steel tied-arch bridges,” *J. Constr. Steel Res.*, vol. 103, pp. 159–167, 2014.
- [4.21] CEN, “Eurocode 3 : Part 2: Steel bridges,” vol. 3, 2003.
- [4.22] M. A. Bradford, D. M. Asce, Y. Pi, and A. Liu, “Out-Plane Elastic-Plastic Buckling Strength of High-Strength Steel Arches,” vol. 144, no. 6, pp. 1–12, 2018.
- [4.23] D. B. La Poutré, R. C. Spoorenberg, H. H. Snijder, and J. C. D. Hoenderkamp, “Out-of-plane stability of roller bent steel arches — An experimental investigation,” *JCSR*, vol. 81, pp. 20–34, 2013.
- [4.24] P. Lonetti and A. Pascuzzo, “Instability design analysis in tied-arch

- bridges Instability design analysis in tied-arch bridges,” no. January, 2018.
- [4.25] M. Wolff and U. Starossek, “Cable-loss analyses and collapse behavior of cable-stayed bridges,” pp. 423–423, 2013.
- [4.26] U. Starossek and M. Wolff, “Progressive Collapse : Design Strategies Summary Collapse resistance,” *Symp. A Q. J. Mod. Foreign Lit.*, pp. 1–8, 2005.
- [4.27] C. M. Mozos and A. C. Aparicio, “Parametric study on the dynamic response of cable stayed bridges to the sudden failure of a stay, Part II: Bending moment acting on the pylons and stress on the stays,” *Eng. Struct.*, vol. 32, no. 10, pp. 3301–3312, 2010.
- [4.28] P. Lonetti, A. Pascuzzo, and A. Davanzo, “Dynamic Behavior of Tied-Arch Bridges under the Action of Moving Loads Dynamic Behavior of Tied-Arch Bridges under the Action of Moving Loads,” no. July, 2016.
- [4.29] F. Greco, P. Lonetti, and A. Pascuzzo, “Dynamic analysis of cable-stayed bridges affected by accidental failure mechanisms under moving loads,” *Math. Probl. Eng.*, vol. 2013, 2013.
- [4.30] Y. Aoki, “Analysis of the Performance of Cable-Stayed Bridges under Extreme Events,” no. April, 2014.
- [4.31] P. Lonetti and A. Pascuzzo, “Vulnerability and failure analysis of hybrid cable-stayed suspension bridges subjected to damage mechanisms,” *Eng. Fail. Anal.*, vol. 45, pp. 470–495, 2014.
- [4.32] M. Ferraioli, A. Lavino, A. Mandara, M. Donciglio, and A. Formisano, “Seismic and Robustness Design of Steel Frame Buildings,” *Key Eng. Mater.*, vol. 763, no. February, pp. 116–123, 2018.
- [4.33] A. Formisano, R. Landolfo, and F. M. Mazzolani, “Robustness assessment approaches for steel framed structures under catastrophic events,” *Comput. Struct.*, vol. 147, pp. 216–228, 2015.
- [4.34] A. Formisano, G. Di Lorenzo, and R. Landolfo, “Non-linear analyses and fragility curves of European existing single-story steel buildings,” no. October, p. 260020, 2019.

- [4.35] P. Lonetti and A. Pascuzzo, “A numerical study on network arch bridges subjected to cable loss A NUMERICAL STUDY ON NETWORK ARCH BRIDGES SUBJECTED TO CABLE LOSS,” no. May, 2018.
- [4.36] F. G. & P. L. Domenico Bruno, “Dynamic Mode I and Mode II Crack Propagation in Fiber Reinforced Composites,” *Mech. Adv. Mater. Struct.*, vol. 16, no. 6, pp. 442–455, 2009.
- [4.37] F. G. & P. L. Domenico Bruno, “Computation of Energy Release Rate and Mode Separation in Delaminated Composite Plates by Using Plate and Interface Variables,” *Mech. Adv. Mater. Struct.*, vol. 12, no. 4, pp. 285–304, 2005.
- [4.38] P. L. & A. P. Fabrizio Greco, “A moving mesh FE methodology for vehicle–bridge interaction modeling,” *Mech. Adv. Mater. Struct.*, 2018.
- [4.39] M. Laterza, M. D’Amato, and R. Gigliotti, “Modeling of gravity-designed RC sub-assemblages subjected to lateral loads,” *Eng. Struct.*, vol. 130, no. March 2018, pp. 242–260, 2017.
- [4.40] F. F. Taucer, E. Spacone, and F. C. Filippou, “A FIBER BEAM-COLUMN ELEMENT FOR SEISMIC RESPONSE ANALYSIS,” no. December 1991.
- [4.41] European Committee for Standardisation, “BS EN 1991-1-1:2002 Actions on structures,” vol. 3, no. 1, 1994

CHAPTER 5

Structural performance of steel cable-stayed bridges under blast loading considering different stay patterns

5.1 Abstract

Accidental or extreme events can induce abnormal loads on structures contributing to local damage of primary components or to the progressive collapse of the structure. Although hazards, which are usually difficult to be predicted, increase the complexity in the design, the need to determine the consequences on structures of these extreme events remains significant. The aim of this study is to evaluate the damage induced by an accidental load such as blast loading to a cable-stayed bridge. In the first part of the paper, through non-linear dynamic analyses, it was possible to evaluate the structural response of three configurations of cable-stayed bridges, then to figure out the possible immediate and forthcoming damages considering different loading parameters and position. Finally, a displacement-controlled static non-linear pushover analysis of the structure has been performed to evaluate the limit state of the structure for a random position of blast loading and to predict the possible damage state during an accidental event such as blast loading. The results indicate significant effects of the structural configuration of the bridge and stay patterns. The Fan cable-stayed bridge is found to be the most effective among the considered configuration in reducing the dynamic effect induced by the blast loading on the structure. In addition, the deck is found to be less critical in terms of blast load mitigation close to the abutment and the pylon.

5.2 Introduction

Structural robustness and collapse resistance are nowadays relevant research topics both in the design of new structures and for the safety assessment of existing ones. For most cases, a structure is considered safe if the design actions loading is less or equal to the design capacity of the structure. Other design approach consists of evaluating the structural performance of a structural system under the various conditions associated

with hazard events. This approach becomes adequate in the case of accidental loads derived from events such as crash, earthquake, collision, blast, etc... where the design actions are hard to be predicted in the design life of the structure. Moreover, the greater attention toward understanding the phenomena associated to blast loading and the assessment of the damage to structures or structural components under such threats observed in recent years is particularly justified by an increase of manmade and accidental explosions worldwide [5.1] – [5.3]. In these circumstances, different causes of the collapse of the structure are considered. Either the structure suddenly collapses due to the damage of a key structural component (piers, slab, deck, etc.) or the failure of the structural system is triggered by the local damage of a primary structural elements (cables, column, pylon, etc.) known as zipper-type collapse [5.4]–[5.6].

In the worldwide existing codes, the philosophy in the design is linked to the situation that structural damage of a structural primary component against abnormal loading condition may be allowed to occur but without triggering the collapse of the entire structure. Thus, not only the structural response for conventional loads (self-weight, live loads, wind loads, etc.) should be focused on but it is becoming urgent to study intensely the response after abnormal loads such as a hurricane, wind, flood, blast loading, etc. For this reason, several scientists have begun to study the ability of a structure to limit the redistribution of the forces of the structural elements adjacent to the element exposed to an accidental load or to mitigate the effect of damage [5.5], [5.7], [5.8]. These measures contribute to creating a robust structure able to resist against extreme events. However, the robustness and progressive collapse of a structure are two concepts closely linked. As a matter of fact, some researchers have studied the possible progressive collapse of structures during hazard events. Thus, the case involving a progressive collapse of a typical steel building has been studied in [5.6], [5.9]. Recent advances in research on the progressive failure of reinforced concrete structures have been presented in [5.10], [5.11] whereas the case of cable-stayed bridges has been studied in [5.4], [5.12]. Finally, tremendous research activities to investigate the damage criteria of suspended bridges subjected to aeroelastic wind effect are presented in [5.13], [5.14] whereas the influence of the cable damage on the dynamic response of suspended bridges has been investigated in [5.15]–[5.18].

In a very small number of previous studies, structural safety against blast loading that can lead to progressive collapse has been assessed in a probability-based approach. Even though the studies are mainly focused on earthquake engineering, it is observed nowadays a significant advance in the case of blast loading [5.19]–[5.23]. Many studies to define fragility curves have been conducted either on structural elements [5.24]–[5.26] or on buildings [5.27]–[5.30]. The study of fragility in the case of bridges subjected to blast loading is almost non-existent in the scientific literature. Indeed, many

authors have rather addressed their researches to study the structural response or performance of bridges [5.31], [5.32]. In particular, Hashimi et al. [5.33], Tang and Hao [5.23] presented satisfactory research on the structural performance of the bridge's components for a cable-stayed bridge subjected to blast loading throughout a dynamic analysis. The first authors focused on the variation of the blast loading location on the bridge deck and studied also the cable loss mechanism after a blast event while the second document is concentrated on the influence of the size of the blast loading source, the stand-off distance and presented also the effectiveness of FRP strengthening technics after blast loading.

The review reveals that abnormal loads can lead to the critical damage of structural components that could reach adjacent structural elements and ultimately cause a collapse of the structure. Based on this observation, the authors have found a clear motivation to focus their work on the study of the structural performance of cable-stayed bridges subjected to blast loads. However, the stay patterns might play an important role in the diffusion of the damage between the bridge's components and should be investigated in depth. Thus, the purpose of this research is to establish direct or indirect links between the collapse capacity of the structural elements of various cable-stayed bridges (Harp, Fan, and Semi-fan stay patterns) subjected to abnormal loads such as blast loading and the possible collapse of the bridge. To reach our objectives, the structural performance of three different cable-stayed patterns will be assessed thoroughly and only the dynamic effect deriving from a blast loading (neglecting the air blast released and its consequences on cars' glazing and people to simplify the study) will be considered. In particular, intensive static and dynamic analyses have been carried out on various cable-stayed bridges in order to determine a relationship between load intensity and structural response, then between structural response and the possibility of the collapse of the bridge. Finally, an investigation of the likelihood of exceedance of the structural capacity of the bridge's structural components subjected to blast loading will be presented. In the first part of the study, only the cases of blast loading taking place on the deck will be considered. In particular, the document will be subdivided into three sections besides the introduction and conclusion. A description of the bridge will be presented firstly, followed by the numerical modeling, numerical analysis, and discussion of the results and finally, a section on the blast fragility will be presented. In the companion study, the authors will focus on actions on the pylon and piers. Satisfactory results from the analyses show that Fan configuration presents a better resistance in the case of blast loading event even though it displays the most rigid structure. Among other things, the possibility of total structural failure would arise because the dynamic action of the load causes not only excessive damage to the deck but also to the stay cables adjacent to the impact area.

5.3 FEM analysis

5.3.1 Description of the bridges

The cable-stayed bridge is nowadays widely used around the world owing to the great advantages it displays for long-span bridges. A generic cable-stayed bridge consists on deck, pylons and inclined cables known as stays, which serve as internal support and provide additional vertical stiffness to the deck. In this study, three different typologies of cable-stayed bridge namely fan, semi-fan and harp cable-stayed bridges have been considered. They differ mainly in the pattern of the cable stays. A generic bridge under this study indeed consists of two lateral spans of 99.2 m long and one central span of 204.6 m long. The bridge deck is made of 1.15 m deep and 13.0 m wide steel orthotropic box girder, which includes three traffic lanes and two footways. It consists of a closed hexagonal steel box section with 20 mm thick flanges and webs. In addition, trapezoidal stiffeners are installed on all the section of the deck spaced 350 mm from center to center while vertical stiffeners each 2750 mm were provided in the deck section to limit excessive displacement and increase the buckling resistance. Rectangular closed box sections have also been considered for the pylon, the transverse beam, and the base pylon. The pylon is considered as the vertical element above the steel deck whereas the base pylon is taken as a vertical element below the steel deck. Two transverse beams are used to connect the vertical elements and form with the vertical element the “H” shaped pylon. The geometry and geometrical characteristics of the structural elements are given in Fig. 5.1 and Table 5.1.

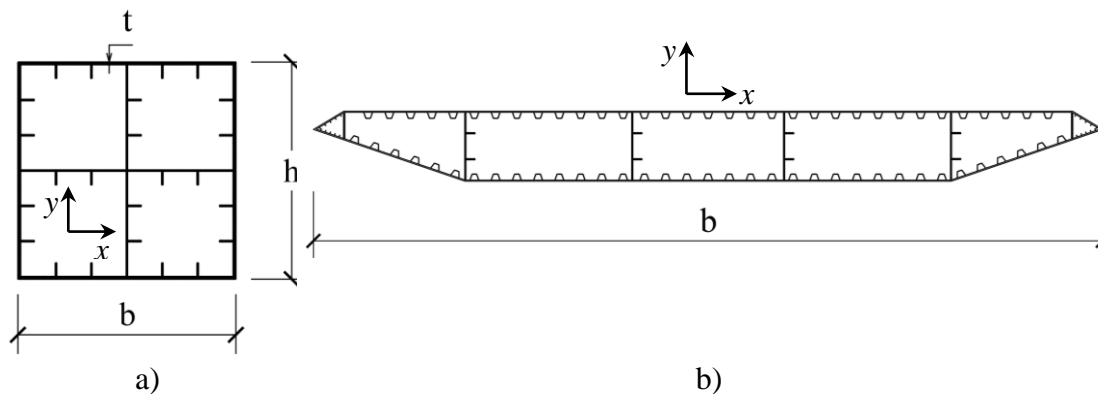


Fig. 5.1. Geometry and Section of structural elements of the cable-stayed bridge. a) Closed box section for pylon, transverse and base pylon b) Deck section

Table 5.1. Dimension of the structural element of the cable-stayed bridge

Transverse	Pylon	Base Pylon	Steel Deck	Unit
------------	-------	------------	------------	------

b	1800	2800	3200	13000	mm
h	2800	2800	3200	1150	mm
t	40	40	40		
A	441600	521600	585600	642331,3	mm ²
i_{xx}	4.88×10^{11}	6.41×10^{11}	9.47×10^{11}	1.59×10^{11}	mm ⁴
i_{yy}	2.37×10^{11}	6.41×10^{11}	9.47×10^{11}	9.37×10^{11}	mm ⁴

5.3.2 Blast loading modeling

From the structural design point of view, a blast loading carried by vehicles is considered as the relevant case since vehicles are able to carry a large number of explosives. Blast loading compared with other accidental events such as earthquake, impact, wind, releases a much higher dynamic pressure than other phenomena [5.34]. Although the pressure developed after the explosion attenuates quickly with the time, it greatly contributes to localized damage to the exposed structural members. Deng and Jin [5.35] stated that the maximum effect during blast loading is observed in the positive phase since the structural mass participating in dynamic response is engaged later due to the short duration of the blast. When assessing the structural blast resistance, one of the most important things is the correct modeling of the blast loading. Indeed, it is difficult and quite complex to study the structural response of the bridge's component subjected to an explosive because the ignition of the explosion and the interaction between bridge and shock wave are included. During an explosion, energy is rapidly released, which generates a blast wave. In the consideration of conventional explosive such as TNT, the process of energy released is a rearrangement of its atoms [5.3]. Many scientists [5.3], [5.23], [5.35] studied the modeling of the blast wave and they stated that the characteristics of blast waves are strongly dependent on the explosive material, the distance of the explosive source and how the generated blast wave is transferred to the structure. In the blast analysis, the scaled distance (Eq. (5.1)) is considered as the parameter that most affects the peak pressure acting on structures [5.36].

$$Z = \frac{R}{W_{TNT}^{1/3}} \quad (5.1)$$

Where Z is the scaled distance, R is the stand-off distance known as the distance between the center of the source and the point of impact on the structure in [m] and W the amount of the equivalent weight of TNT in [kg]. Many scientists used empirical approaches to develop simplified expressions of the peak overpressure released from a blast event [14]. Friedlander's

equation is widely used to express the relationship between the pressure intensity versus the time (Eq. (2)-(3)).

$$P_r(t) = P_{atm} + P_{max} \left(\frac{t-t_a}{t_d} \right) \cdot e^{-b((t-t_a)/t_d)} \quad (5.2)$$

$$P_{max} = \frac{1}{Z} \cdot \left[\frac{1772}{Z^2} - \frac{114}{Z} + 108 \right] \quad (5.3)$$

Where P_{atm} is the ambient pressure, t_a , t_d are respectively the arrival time and the duration time of the positive phase as shown in Fig. 5.2.

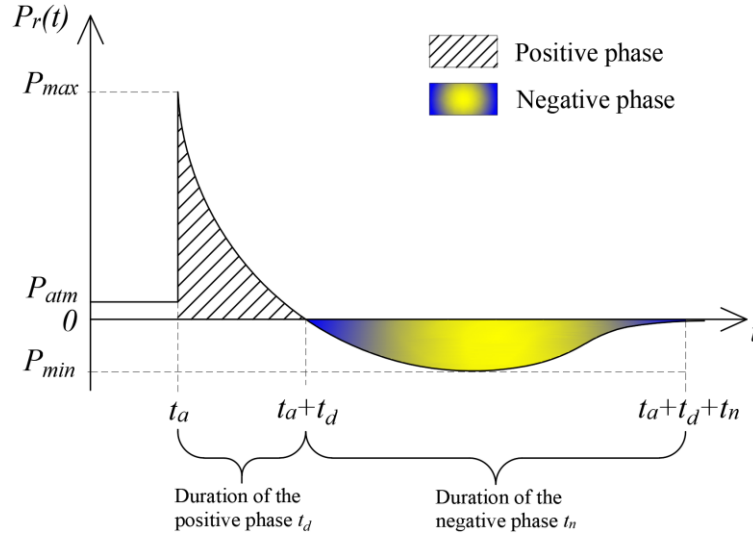


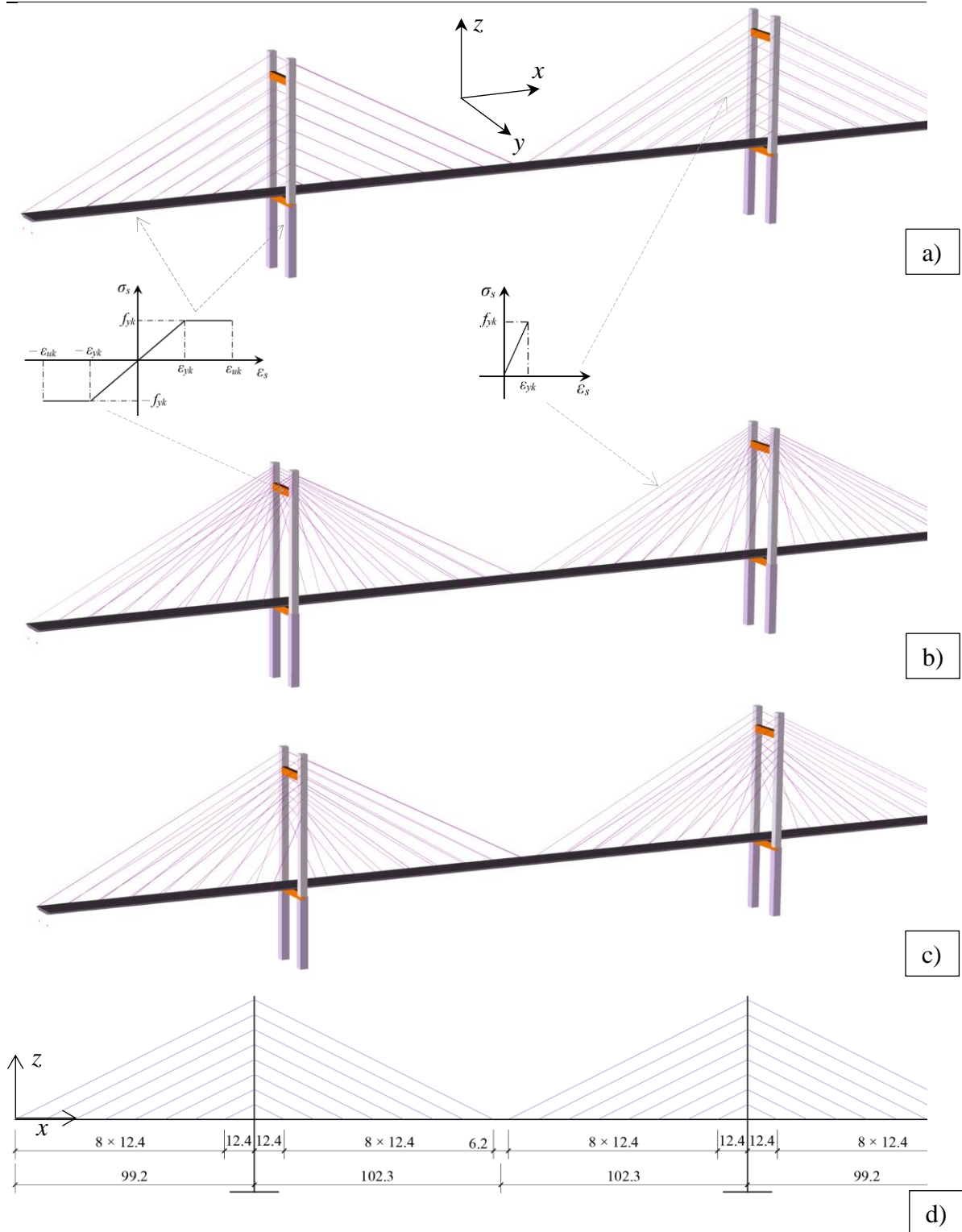
Fig. 5.2. Blast pressure distribution over time

5.3.3 FEM Modelling

The actual numerical model has been made throughout Strand7 [5.38]. In particular, the structural elements were modeled using 1D fiber beam element. In the analysis, the structural elements are connected to each other by a fixed joint with zero degrees of freedom as is done in the practice of such bridges.

Cable stays are directly connected to pylons while rigid links are used to create the appropriate connection between the deck and cables. For simplicity, abutments were not modeled and were replaced by fixed constraints. Then, elastic links with high vertical stiffness were used as bearing at both bridge end and above the transversal beam. High strength steel material was considered for deck, pylons, and piers whereas the stress distribution was considered elastic in the cables and was limited to $0.55 \times f_u$ to satisfy the fatigue criteria. On the other hand, to consider the cable's sag effect due to the change in the shape under varying stresses, Ernst's equation [5.39] has been used to derive the equivalent elastic modulus of the cable. Perfect elastoplastic stress-strain diagrams for different elements excepted cables

were used in the analysis. Fig. 5.3 shows the perspective view of the bridges under study, the longitudinal profile and the transverse view of the pylon.



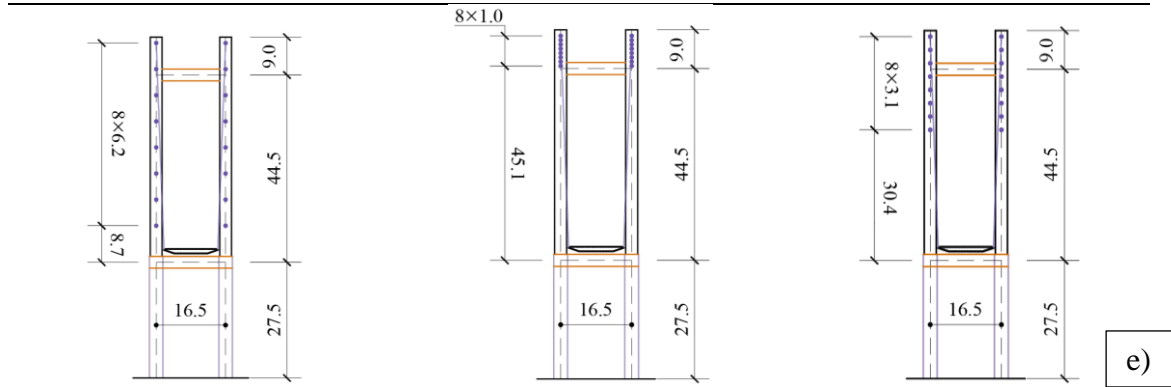


Fig. 5.3. Geometrical characteristic of the bridges. a) Harp bridge; b) Fan bridge; c) Semi-Fan bridge; d) Longitudinal profile of the bridge; e) Transverse section of the pylon from the left to the right Harp, Fan and Semi-fan system

5.3.4 Material characteristics

The material model used for deck, pylon, and transverse follows the perfect elastoplastic law whereas the stays follow an elastic law. It should be emphasized that the nonlinear geometric behavior of the cable has been taken into account through the change in the cables' elastic modulus. A summary of constitutive parameters is given in Table 5.2. However, it must be pointed out that blast loading is characterized as a high impact loading, which rapidly increases the strain rate of the structural member to which the load is applied. Many authors [5.6], [5.20], [5.24] stated that concrete and steel materials stresses are modified and their ultimate and yield stresses increase due to the high strain rate. The most common equation to consider the effect of the strain rate is known as the Cowper-Symonds equations defined in Eq. (5.4) where f_{yd}^d is the dynamic yield stress under high impact rate, f_{yd} is the static yield stress, $\dot{\epsilon}$ is the strain rate and C and q are constants. Moreover, C = 40.4 and q = 5 for low strength steel while C = 3500 and q = 5 for high strength steel will be considered as defined in [5.40].

$$\frac{f_{yd}^d}{f_{yd}} = 1.0 + \left(\frac{\dot{\epsilon}}{C} \right)^{1/q} \quad (5.4)$$

Table 5.2. Material characteristics of the structural members

Steel grade	Structural element	Constitutive model	Yield stress [Mpa]	Failure strain
S420	Deck	Elasto-plastic	420	5 %
S355	Pylon, Transverse	Elasto-plastic	355	4 %
SWRH72B	Cable	Elastic	1023	4.8 ‰

5.3.5 Load analysis

In this paper, blast loads are considered as the leading variable load whereas traffic loads are taken as accompanying actions. The self-weight is directly provided from the software and it is a function of the material density and the characteristics of the section. A uniformly distributed load $G_2=48.7$ kN/m is applied along the deck which represents asphalt layer, safety barrier, and waterproofing layer. The pre-tension force on the stays is calculated throughout an optimization process in order to compensate 95% of the permanent loads with the maximum displacement limited to 10 mm. Traffic loads are defined according to European norms [5.41]. To reach our goal, load combinations for accidental design situations as defined in [5.42] were used where the partial coefficients are given within the code.

5.4 Numerical analysis and discussion

Due to the lack of existing experimental models of such kind of bridges, it was not able to compare the preliminary static analysis to experimental results. The first stage of analysis consisted of determining the actual stress of the bridge in the traffic condition. Then, a series of dynamic non-linear analyses have been carried out on the three different typologies of cable-stayed bridges under study. The dynamic analysis of the blast action is performed on bridge models in the stressed and deformed shape from the permanent and traffic loads. Initially, a direct comparison is made between the results of displacements, strain and stresses obtained for the three types of configurations. Then, the most unfavorable configuration in terms of stress is studied individually, varying different locations of the impact with the deck.

5.4.1 Stress analysis

From the first analyses and considering the global reference system of the bridge defined in Fig. 5.3, the following observations are made. For the blast loading occurring at $x = 6.2$ m from the abutment, and the stand-off distance $R = 1$ (see Fig. 5.4), the maximum displacements reached by the deck in a short time history after the blast detonation is summarized in Table 5.3. The results show that the displacement reaches intolerable levels for an equivalent weight greater than 750 kg. In particular, the maximum displacement of the deck is observed for the Harp configuration regardless of the size of the blast loading source. It is also found that the difference in the structural response is obvious for the weight larger than 750 kg while the displacement is quite identical for equivalent weight lower than 500 kg as shown in Table 5.3. Referring to the strain analysis, the main difference is displayed for $W = 1000$ kg. Indeed, in this particular case, the maximum strain reached the plastic strain limit for Harp configuration while for other stays patterns, it remains below the plastic strain limit. Finally, the structural

component subjected to the blast loading reaches quickly the allowable stresses just after detonation. Indeed, in the case studied, all the equivalent weights of TNT considered succeed in creating stress reaching the stress limit at a very short time step (see Fig. (5.4)).

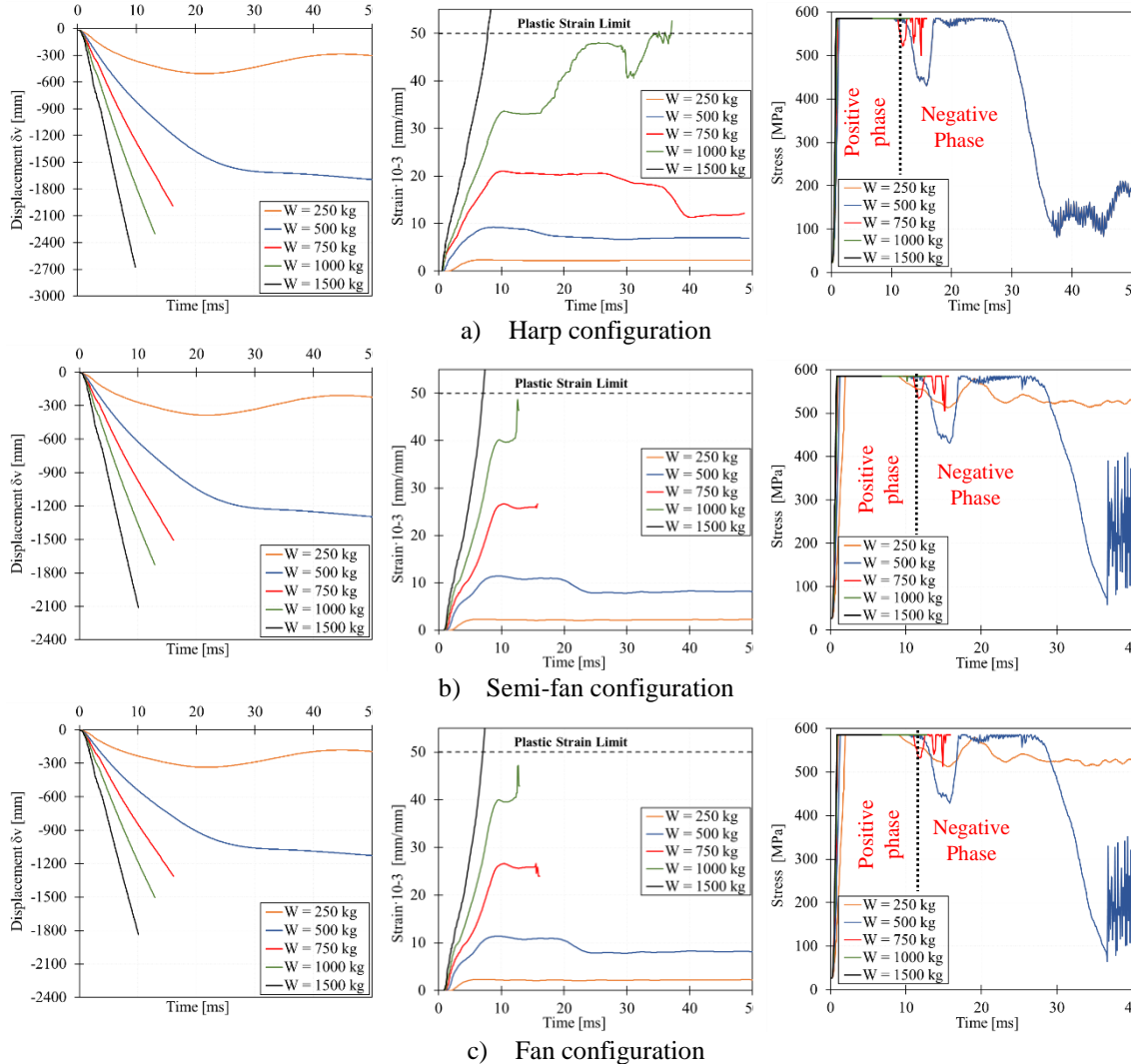


Fig. 5.4. Structural response of the three cable configuration in the case of blast at $x= 6.2$ m. From the left to the right displacement, Strain and Stress of the bridge’s deck

However, in this case, the Harp configuration seems to dissipate the dynamic action better than the other two because the stress fluctuates less. These fluctuations are visible only on the negative phase of the action as shown in Fig. 5.4 and may accelerate secondary damage such as fatigue that would result from a large variation in the internal stresses of the element.

Table 5.3. Maximum vertical displacement of the deck under a blast loading at stand-off $R = 1m$

Equivalent TNT weight	Cable-stayed bridge configurations		
	Harp	Fan	Semi-fan

W = 250 kg	- 2678 mm	- 1774 mm	- 2109 mm
W = 500 kg	- 2297 mm	- 1489 mm	- 1728 mm
W = 750 kg	- 1989 mm	- 1286 mm	- 1508 mm
W = 1000 kg	- 1421 mm	- 1126 mm	- 1298 mm
W = 1500 kg	- 406 mm	- 331 mm	- 385 mm

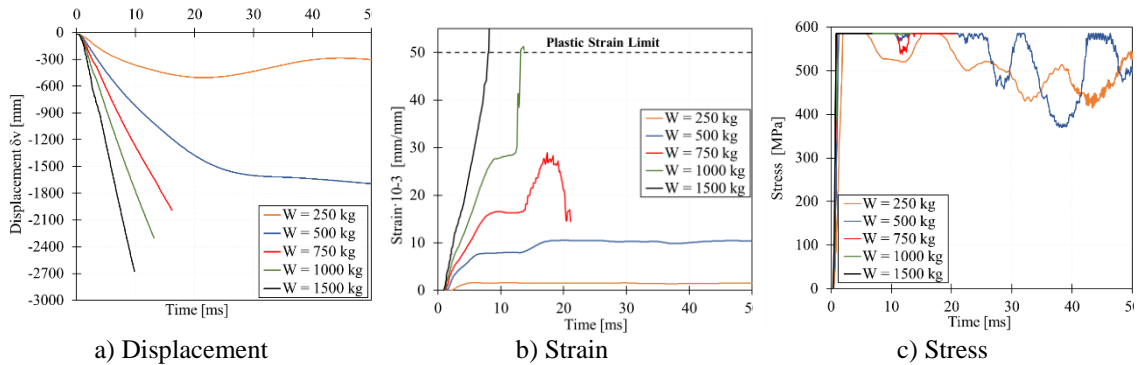


Fig. 5.5. Structural response of the Harp pattern with blast at $x = 62.8$ m and $R = 1$ m. a) Displacement b) Strain c) Stress

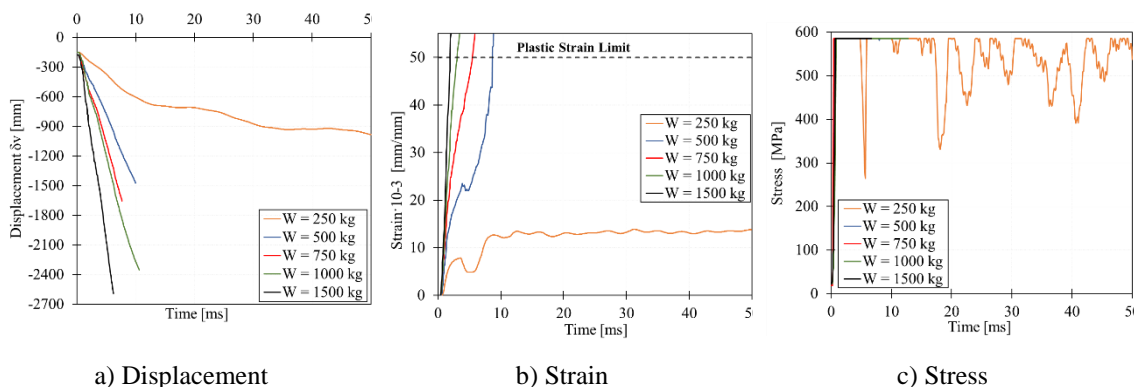


Fig. 5.6. Structural response of the Harp pattern with blast at $x = 201.5$ m and $R = 1$ m. a) Displacement b) Strain c) Stress

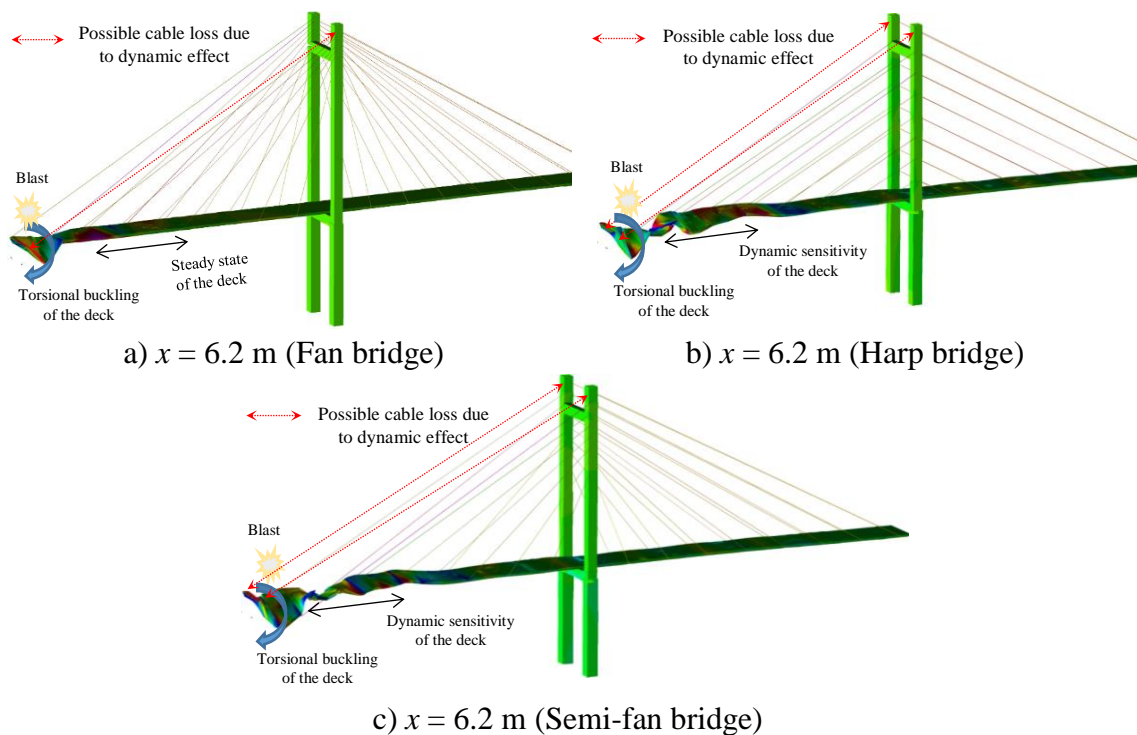
Finally, with a random stand-off distance, the displacement, stress and strain variation in the section close to a blast loading increase by increasing the dimension of the blast loading source. Indeed, the damaging effects in the bridge structural response induced after blast loading increase as the equivalent weight of TNT increases.

It is noteworthy that assessing the internal strain state of the section has a critical issue. Indeed, following the blast event, the admissible stress is quickly reached, but its consequence is critical if the state of internal strain is higher than the maximum plastic strain. Although the strain state seems high for the three configurations studied with most of them exceeding the yielding strain, the worst situation is reached for the equivalent mass of the TNT equal to or greater than 1500 kg. Therefore, the maximum plastic strain is exceeded with the possible breakage of the deck at this position.

Later, two other positions of occurrence of blast loading along the deck at $x = 68.2$ m and $x = 201.5$ m (Mid-span) were studied (Fig. 5.5 and Fig. 5.6). It is observed that the displacement at time history $t = 0$ ms is 192 mm at the mid-span (Fig. 5.6a) which are from traffic and permanent loads. In addition, the displacements following blast loading are more relevant for an event occurring in mid-span as the outcome of comparing the results of Fig. 5.5a and Fig. 5.6a for any equivalent TNT weight.

In terms of strain, it has been observed that for a blast loading occurring in the mid-span, the consequences are much more significant, because, before the stress generated by a blast load, the deck already has a significant level of stress and strain due to permanent and traffic loads. As a matter of fact, in this particular case, from equivalent loads greater than 500 kg, the plastic strain limit would be reached as shown in Fig. 5.6b. When the event takes place at $x = 68.2$ m, the internal strain of the deck section is higher (Fig. 5.5b) than if the action takes place at $x = 6.2$ m. However, it would require action with an equivalent weight greater than 1000 kg to cause serious damage.

Finally, the stress conditions are quite similar in that the blast event, which strongly contributes to the achievement of yielding stress in a short time. The only difference is observed in the considerable fluctuation of the stress, especially for the action taking place in the mid-span for low-intensity loads as shown in Fig. 5.6c.



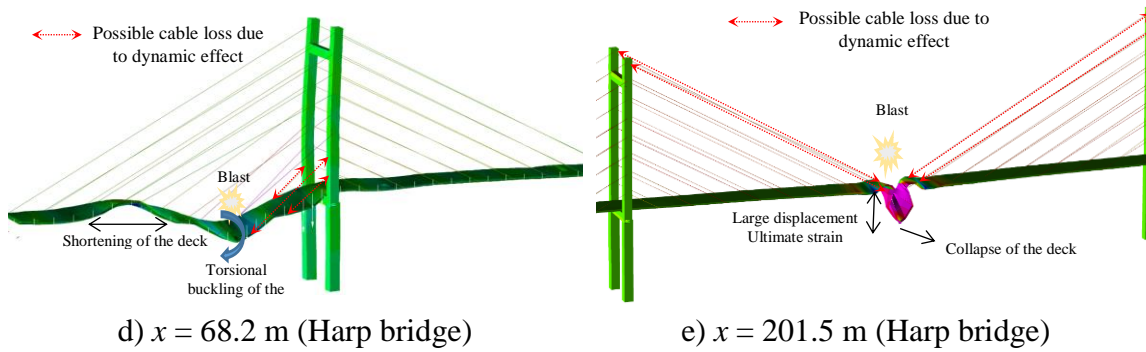


Fig. 5.7. Blast loading analysis in cable-stayed bridge. a) $W = 500$ kg, b) $W = 500$ kg, c) $W = 500$ kg, d) $W = 500$ kg, e) $W = 1500$ kg

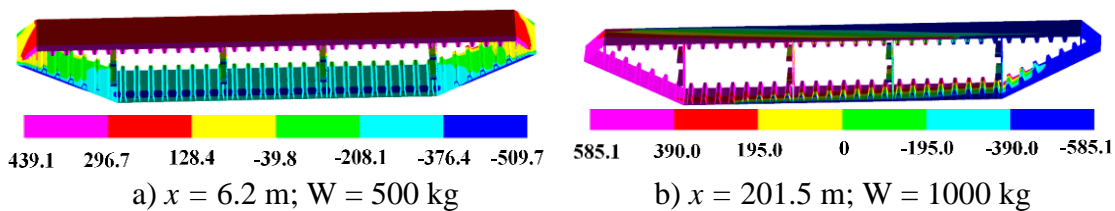


Fig. 5.8. Total fibre stress in MPa of the deck of Harp configuration for two different blast intensities at two different locations, a) $x = 6.2$ m and b) $x = 201.5$ m.

A detailed analysis of the deck revealed the possibility of a gradual collapse that could be caused by the dynamic action of a blast load. In the case of a cable-stayed bridge, progressive collapse can be caused by the loss of two or more cables [5.4]. For an extreme event such as blast loading, the loss of cables may be due either to the consequences of an air blast and reflected pressure near the stays. Other reasons could be the reaching of the excessive tension limit of the cable or finally to the collapse of the deck that would cause the cables near the failure zone to break. In this investigation, the last two cases were considered.

The first case studied considers the Fan configuration where the blast loading occurs close to the abutment. The results show a limited displacement of the deck at the impact area, a steady condition of the deck when moving far from the impact area, a torsional buckling similar to the case of Fig. 5.7a. Higher dynamic sensitivity in response to blast action is observed for Harp and Semi-fan bridges as displayed in Fig. 5.7b&c. However, in the Fan configuration, the blast action close to the abutment could result in the loss of a single cable, especially the one affected by the torsion of the deck (Fig. 5.7a).

The analysis also revealed that in the case of Harp bridges (Fig. 5.7b&d), the dynamic action creates a torsional buckling of the deck, which may result in a reduction of its structural capacity. In these cases, two cables are likely to be damaged for the impact at $x = 6.2$ m (Fig. 5.7b) whereas three cables are likely to be damaged for the impact at $x = 68.2$ m (Fig. 5.7d), particularly because they will have reached their ultimate stress. This is less relevant because the action lasts for a short period and the damage will only be confirmed by repeating such actions. In the case where the action is caused

by a large mass (Fig. 5.7e), the consequences are more severe because a total breakage of the deck element around the impact area is observed causing a loss of the four cables adjacent to the detonation zone. Finally, besides the global instability of the deck observed after a blast event, an evaluation of the internal distribution of stresses presents a possible local instability of the section of the deck around the impact zone. In particular, for a significant blast loading, a combination of positive and negative stress was observed throughout the section as shown in Fig. 5.8b. For less relevant blast loading, the upper part of the deck is likely to be in tension whereas the lower part being compressed Fig. 5.8a.

5.5 Fragility analysis

From the results of the analysis performed so far, it is clear that the consequence of blast loading can be extreme for the deck and therefore for the whole bridge through the progressive collapse mechanism. For this reason, it is also important to associate the structural response of the bridge deck to the likelihood of exceedance of capacity thresholds of the deck elements during a blast event.

5.5.1 Methodology

The common way to study the structural performance under a non-deterministic approach is through the fragility assessment. The method aims to determine the likelihood of exceedance of the structural capacity during accidental events conditioned by the intensity measure that represents the actions [5.28]. The performance-based design has been widely adopted by engineers to design structures. In particular, fragility analysis has been widely performed in the last two decades [5.43]–[5.45]. Recently, the method has been used also for structures subjected to various natural hazards such as flood [5.46], windborne debris in hurricane mitigated regions [5.47], and fire [5.22]. The system fragility can be obtained throughout the Monte Carlo simulation, which is the most challenging method and expensive computationally since it takes into account different structural components as well as the linked uncertainties. Another method less expensive is to use the direct integration method and to combine different component fragility curves to get the system fragility [5.43] and will be used in this research.

In the fragility analysis, the consideration of uncertainties is fundamental. Three different types of uncertainties that are regularly considered in many engineering fields have been defined and presented in [5.24]. In this study, the uncertainties in the accidental load and structure will be mainly considered whereas the interaction mechanism uncertainties will be considered as the consequence of the first two.

5.5.2 Material and geometry uncertainties of the bridges

Several steel cable-stayed bridges were analyzed in the scope of the fragility assessment. Same as the stays patterns considered and presented above, Harp, Fan, and Semi-fan bridges are reproduced. The bridges are considered not to be in the seismic zone in order not to consider a case of multi-hazards since the principal hazard in our study is a blast loading. In addition to the stays patterns, three different pylon profiles were also considered as presented in Fig. 5.9. Bridges modeling follows the same approach as discussed in the previous sections of the paper. The mean values of the bridge geometrical characteristics, as well as the bridge's structural components, are kept the same consideration in the first analyses. Two statistical parameters namely the mean value $\bar{\mu}$ and the coefficient of variation cv are adopted for the variability of the geometry of the structural components.

Since constructional steel is a material produced under tight quality control procedures, a cv of 0.10 is used for steel profile as proposed in [5.48]. The steel grade remains the same as defined in Table 5.2 whose parameters are considered as the mean value. The steel strength is taken higher as considered by the Cowper and Symonds model [5.49]. The main components in the analysis follow the Lognormal distribution. Table 5.4 summarizes the use of defined uncertainties for material and geometrical characteristics whereas in Table 5.5, are presented the uncertainties in the structural component section.

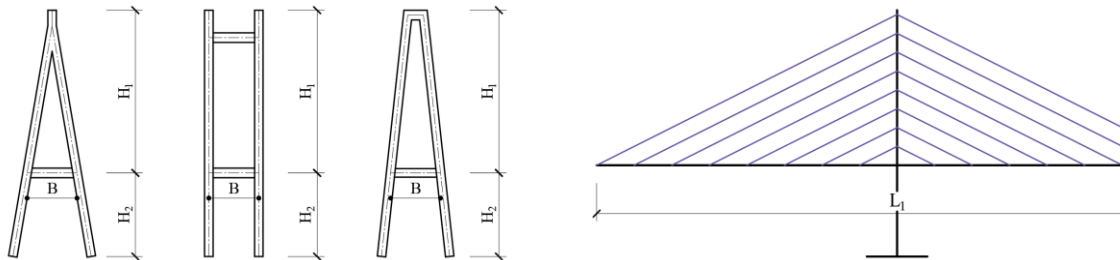


Fig. 5.9. Geometrical characteristics of the bridges. From the left to the right: Inverted Y-shaped profile; H-shaped profile, A-shaped profile

Table 5.4. Uncertainties in geometrical and material characteristics of the bridge

Symbol	Description	Mean	Unit	Cv	Distribution
f_{yk}	yielding strength deck	420	MPa	0.10	Lognormal
E	Young modulus	210000	MPa	0.03	Lognormal
L_1	Length of the midspan	203	m	0.09	Lognormal
H1	Height of the pylon	53.5	m	0.04	Lognormal
H2	Height of the base pylon	27.5	m	0.01	Lognormal
B	Bridge width	13	m	0.01	Lognormal

Table 5.5. Uncertainties in the section of structural component

Structural components	Description	Mean	Unit	Cv	Distribution
Deck		642331.3	mm ²	0.01	Lognormal
Base pylon	Section	585600	mm ²	0.04	Lognormal
Pylon		521600	mm ²	0.04	Lognormal
Transverse		441600	mm ²	0.02	Lognormal

5.5.3 Blast fragility analysis

The fragility of a structure resulting from blast loadings is its probability of failure made contingent on the occurrence of a blast event of a specific hazard intensity. If D is the structural demand owing to the random blast event of k th hazard intensity level, I_k and C_j is the structural capacity to resist the load effect corresponding to the j th limit state, then the blast fragility can be obtained throughout Eq. (5.5).

$$PF_{jk} = P(D \geq C_j | I_k) \tag{5.5}$$

The probability of failure is calculated by simulating a large number of samples including uncertainties in material, geometry, and hazard. If the vector ξ represents the weight of blast source, W and the location of the blast with respect to the structure known as the stand-off distance R and the planar location (x_k, y_k) . In this study, the structural demand is computed for each occurrence of the blast event with different intensity and then is investigated if it satisfies the defined failure criterion. The blast fragility function is then obtained throughout Eq. (5.6).

$$PF_{jk} = P(\delta_D \geq \delta_C | W) \tag{5.6}$$

Using the first-order reliability approach that takes into account the first and second moments of individual distributions, Eq. (6) is simplified into Eq. (7).

$$PF_j = \Phi \left[\frac{\ln(\bar{\mu}_D / \bar{\mu}_C)}{\sqrt{\sigma_{\ln D}^2 + \sigma_{\ln C}^2}} \right] \tag{5.7}$$

Where $\bar{\mu}_D$ = median estimate of the structural demand and $\bar{\mu}_C$ = median estimate of the structural capacity. $\sigma_{\ln D}^2$ = lognormal standard deviation of the structural demand and $\sigma_{\ln C}^2$ = lognormal standard deviation of the structural capacity. Cornell et al., [5.50] derived the relationship between the estimate of the median and the intensity of the actions as shown in Eq. (5.8).

$$\bar{\mu}_D = aI_j^b \text{ or } \ln(\bar{\mu}_D) = \ln a + b \ln(I_j) \tag{5.8}$$

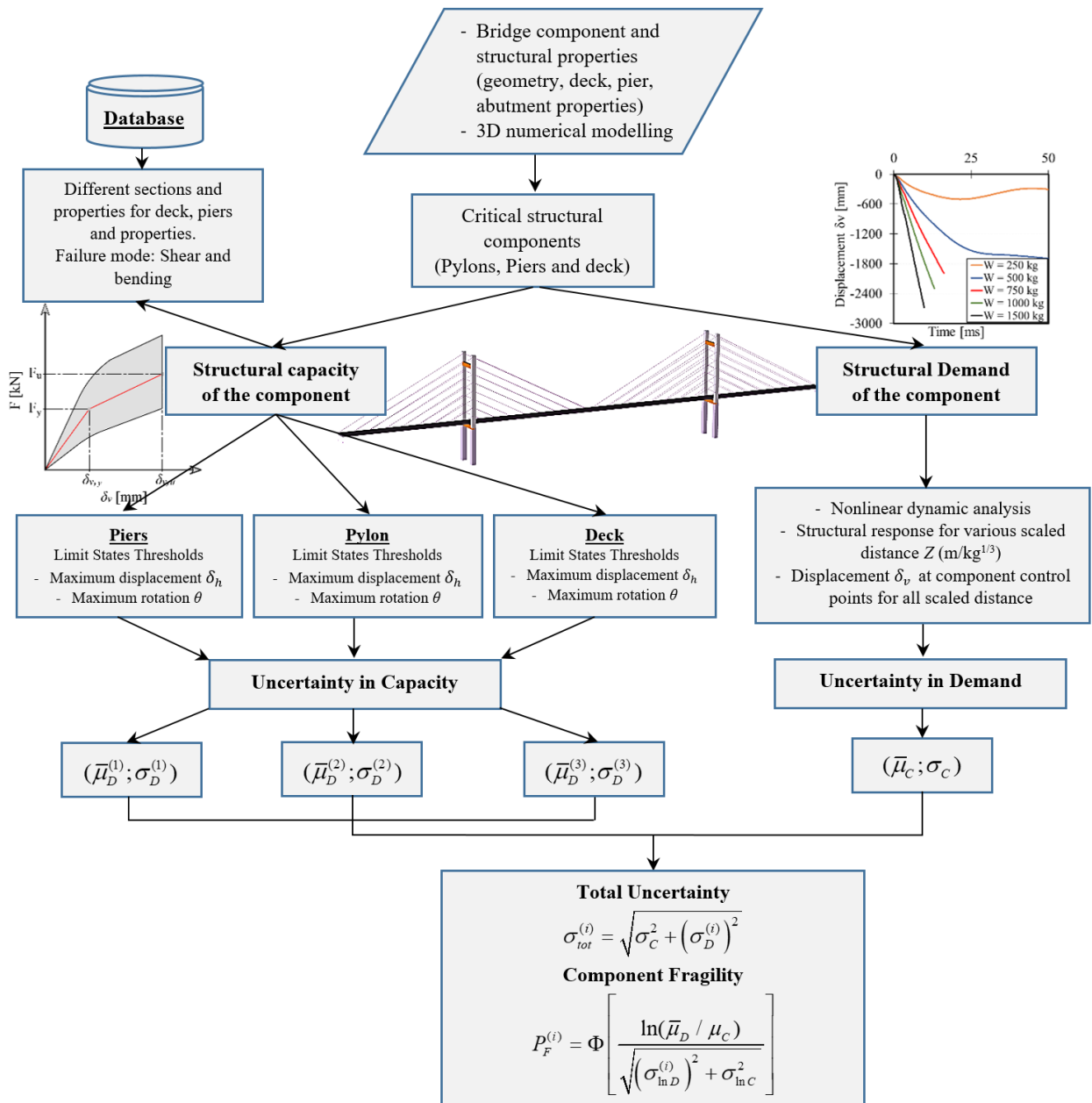


Fig. 5.10. Flowchart for the capacity and demand assessment of cable-stayed bridges

The methodology adopted by the authors for the derivation of the fragility curves is outlined in the flowchart (see Fig. 5.10). It uses the component-based approach in which the fragility curve of the system results from the unconditional combination of the fragility of each structural component of the bridge. In each case, structural capacity is assessed on a stock of bridges that vary in dimensions and the cross-section of the structural elements. The same is also true for structural demand, which is evaluated through nonlinear dynamic analysis for different values of scaled distance, taken in this case as intensity measure.

5.5.4 Structural capacity

In the capacity study, more than thirty models were studied, varying the geometry of the bridge, the characteristics of the material, the pylon profiles (see Fig. 5.9), and the cross-sectional area of the deck. Then, a series of nonlinear pushover analyses of the bridge in the vertical direction were performed, which corresponds indeed to the principal direction of the damage of the deck. From the analyses, idealized bilinear curves were derived and a set of the structural performance depending on the bridge's parameters is drawn as presented in Fig. 5.11. The set of performance displays a hardening behavior with a displacement ductility (Eq. (5.9)) varying from 2.6 to 4.2. Afterward, the same process was done for the other two stays patterns and the statistical parameters of mean performance were collected and presented in Table 5.6.

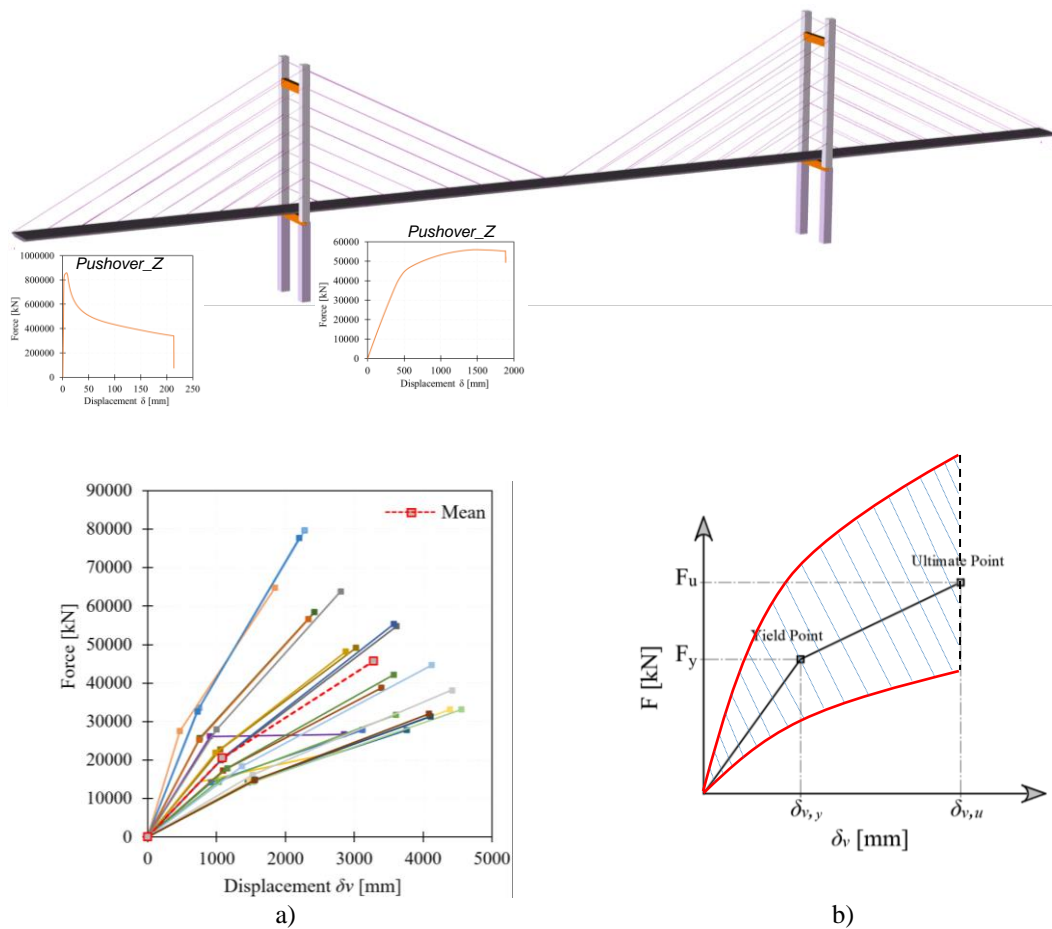


Fig. 5.11. Bilinear force-displacement relationship of cable-stayed bridges a) Set of bilinear capacity curves of deck in Fan cable-stayed bridge; b) Set of the structural performance

Table 5.6. statistic properties for structural parameters of cable-stayed bridges

Stay patterns	Parameter		Statistic values		Ductility μ_δ
			$\bar{\mu}_C$	σ_C	
Harp	$\delta_{v,y}$	mm	863.8	98.9	4.47
	F _y	kN	29586.2	3159.1	
	$\delta_{v,u}$	mm	3864.1	182.4	
	F _u	kN	65356.8	5896.7	
Fan	$\delta_{v,y}$	mm	1042.3	126.6	3.35
	F _y	kN	30894.6	3278.9	
	$\delta_{v,u}$	mm	3489.4	268.8	
	F _u	kN	68595.7	7212.3	
Semi-fan	$\delta_{v,y}$	mm	985.5	119.4	3.58
	F _y	kN	32489.1	3654.7	
	$\delta_{v,u}$	mm	3527.3	295.2	
	F _u	kN	70125.5	6478.4	

The Harp configuration presents the most flexible in all with the highest ductility. On the other hand, the Fan configuration, which had a good structural response in terms of vertical displacement, as presented in the previous section, is the most rigid and reduces the structure's ability to achieve disproportionate vertical displacements.

$$\mu_\delta = \frac{\delta_{v,u}}{\delta_{v,y}} \quad (5.9)$$

Where $\delta_{v,u}$ and $\delta_{v,y}$ are the mean value of ultimate and yielding vertical displacement after a nonlinear pushover in vertical direction.

5.5.4.1 Limit states and Damage Index

In the fragility analysis, structural damage after a hazard is a function of both intrinsic and extrinsic characteristics of the structure. In general, it is possible to study the undergone damage by classifying them according to the damage index [5.51]. This index includes the structural response observed and the definition of limit states. The limit states often derive from experimental campaigns or computational resources. Regardless of the method used, the damage indexes are often defined by means of curvature ductility, rotation ductility, displacement ductility, etc. Indeed, several authors [5.5], [5.24], [5.37] considered two parameters as failure criterion under accidental loads: the rotation angle (θ) of the element's end support and the displacement ductility (μ_δ) [5.24].

The pushover analysis performed allowed defining the limit state for the study as presented in Fig. 5.12. In particular, five regions were adopted as highlighted in [5.52]: A – B: Elastic Range, B – C: Immediate Occupancy, C – D: Life Safety, D – E: Collapse Prevention and finally from E – F: Collapse

where B, C, D, and E represent the thresholds. A brief summary of the limit state range is presented in Table 5.7.

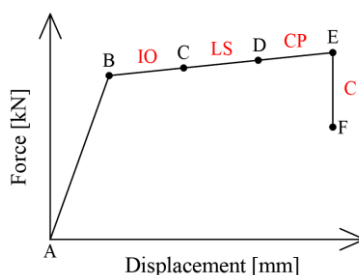


Fig. 5.12. Force-displacement relationship of a damage index

Table 5.7. Limit state for cable-stayed bridges under Blast loading [5.52]

Limit State (LS)	Threshold values of ductility			Structural performance registered
	Harp	Fan	Semi-Fan	
Immediate Occupancy	$\mu_{\delta} > 1$	$\mu_{\delta} > 1$	$\mu_{\delta} > 1$	Minor distortions observed
Life Safety	$\mu_{\delta} \geq 1.5$	$\mu_{\delta} \geq 1.1$	$\mu_{\delta} \geq 1.2$	Minor local buckling of the deck. Localized failure
Collapse Prevention	$\mu_{\delta} \geq 3.0$	$\mu_{\delta} \geq 2.3$	$\mu_{\delta} \geq 2.4$	Large Displacement. Flexural buckling in the localized region
Collapse	$\mu_{\delta} \geq 4.5$	$\mu_{\delta} \geq 3.3$	$\mu_{\delta} \geq 3.6$	Excessive displacement; Excessive strain

5.5.5 Structural demand

In the analysis of the demand, a set of various blast intensities were considered with the possibility of occurring at truly random positions along the longitudinal and transversal direction of the bridge deck (Fig. 5.13). The longitudinal position was limited to half of the bridge due to the symmetry and in the transverse direction, the random location of the blast event was considered. It has been considered a wide range of intensity measure by varying the equivalent TNT weight and stand-off distance.

The weight of an explosive is generally estimated by taking into account a relevant attack scenario, which would involve a vehicle or improvised explosive device carried by one or more individuals. The stand-off distance in the analysis of the robustness of the bridge deck is taken accordingly to the number of explosives considered. It is taken as the distance between the position of the center of the weapon and its vertical projection on the deck, which is the shortest path to reach the deck, thus causing the most intense impact on the deck. Therefore, the weight of the explosive is taken in the range 0 - 10000 kg and the stand-off distance will be taken in the range 0.2 - 4 m.

ct

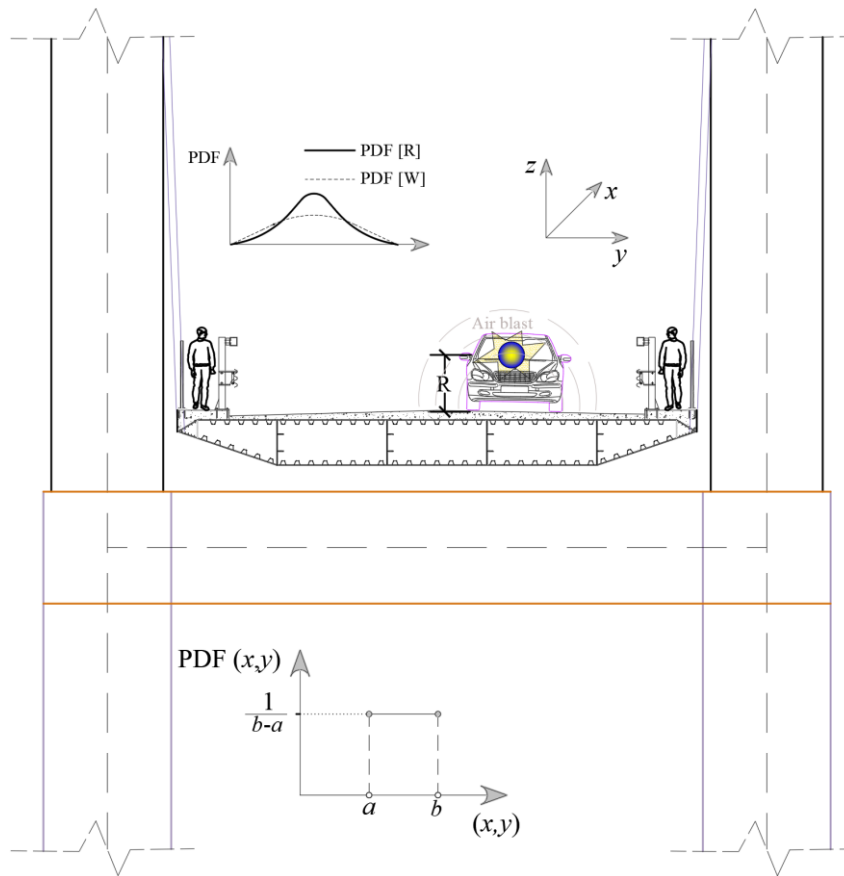


Fig. 5.13. Distribution of blast parameters for blast demand

The results from the analysis have been displayed in the lognormal scale as advised in [5.43] and the mean value of the vertical displacement has been expressed in terms of scaled distance Z and displayed in Fig. 5.14. The results show that the lognormal distribution of the vertical displacement follows the linear regression with a low dispersion rate. The regression line for each bridge model confirms the outcome that Harp bridge model displays larger vertical displacement than the two other bridge models with a higher dispersion of data. Finally, the negative slope is mainly due to the fact that the impact on the bridge deck is more severe by decreasing the scale distance, which is obtained either by decreasing the stand-off distance or by increasing the weight the TNT.

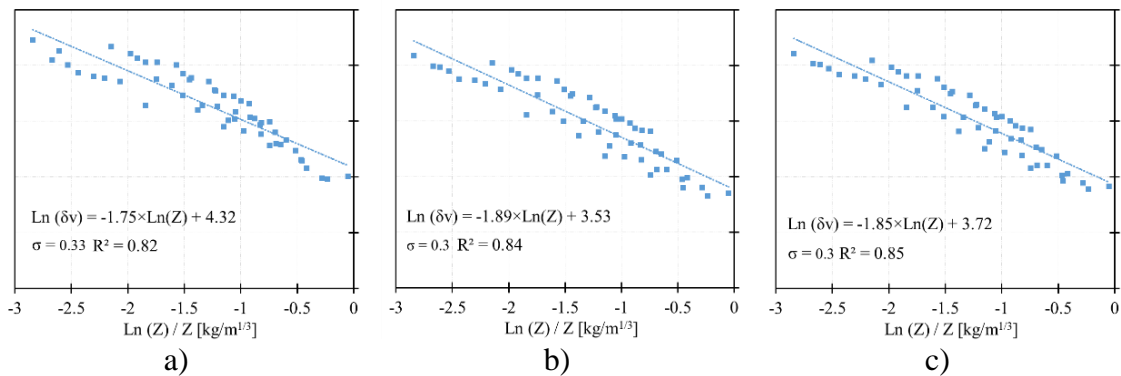


Fig. 5.14. Prediction of blast demand in cable-stayed bridges: a) Harp bridge model; b) Fan bridge model; c) Semi-fan bridge model

5.5.6 Structural demand

Following the results of structural capacity and demand where the statistical parameters defining the criteria of occurrence of different levels of damage have been identified, it is possible to draw the probability of reaching a limit state threshold of the bridge deck.

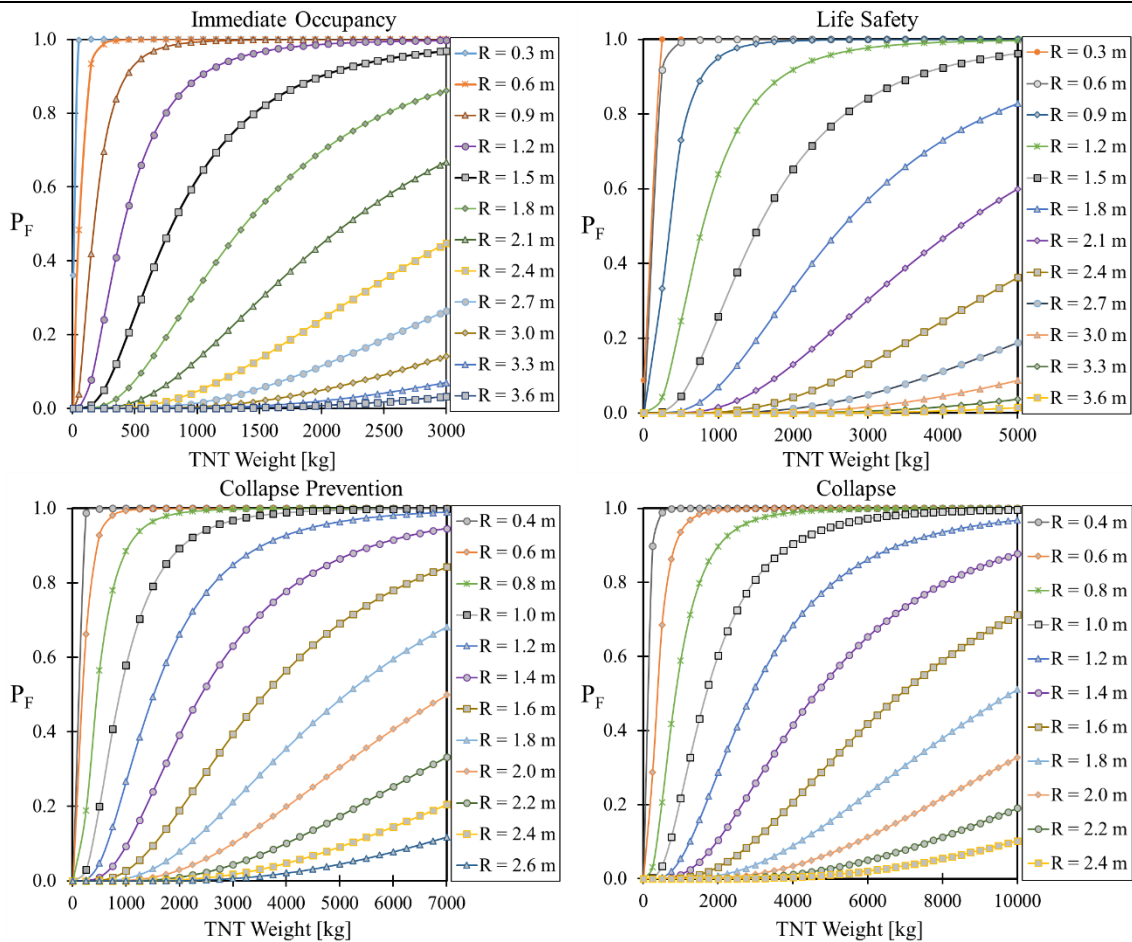


Fig. 5.15. Blast fragility for Fan cable-stayed bridge

In general, the observation is similar to that from the non-linear dynamic analysis performed in the previous sections. It is worth noting that the most influential parameter of the collapse of the deck is the stand-off distance. Indeed, a low probability of deck failure is observed as soon as one the detonation point moves away from the deck, i.e. for a relatively large stand-off distance. In addition, Fan patterns present several advantages. Although it is not favorable compared to the Harp configuration in terms of displacement ductility, the Fan configuration nevertheless displays a good structural response, which allows the bridge not to reach the limit states at the same trend as the other two configurations.

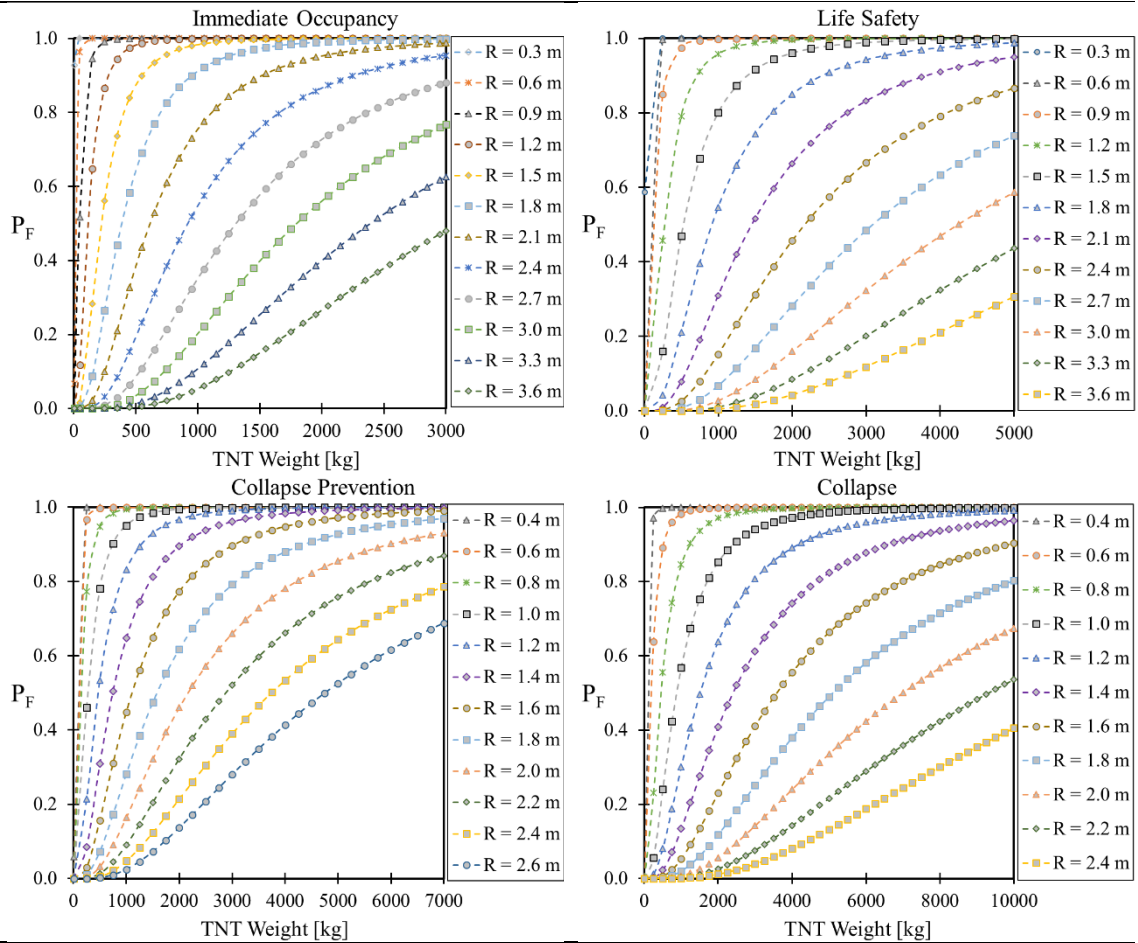


Fig. 5.16. Blast fragility for Harp cable-stayed bridge

5.5.6.1 Structural demand

The mass of the equivalent TNT considered in the analysis varies from 0 to 10000 kg (Fig. 5.15 - Fig. 5.17) even though it is very unlikely to have a terrorist attack with a mass of 10000 kg because it requires a heavy means of transport and the terrorist attack would then become very easily recognizable and prevented. The variation in terms of TNT weight makes it possible to highlight the robustness of structures such as cable-stayed bridges subjected to accidental and unpredictable events. Indeed, the situation prevailing in the various results shows the great capacity of the deck to avoid failure for a blast loading taking place on a random position. Obviously, the risk of collapse increases as soon as the equivalent weight increases.

To have a possible minor local buckling of the deck or a localized failure, the deck of a Fan configuration must be subjected to blast loading triggered by a mass of TNT around 300 kg. However, in order to have excessive displacements leading to the collapse of the deck and subsequently of the bridge, the TNT load must be around 1000 kg. It is important to note that a quantity of TNT lower than those mentioned above will produce similar or advanced damage for Harp and Semi-fan configurations.

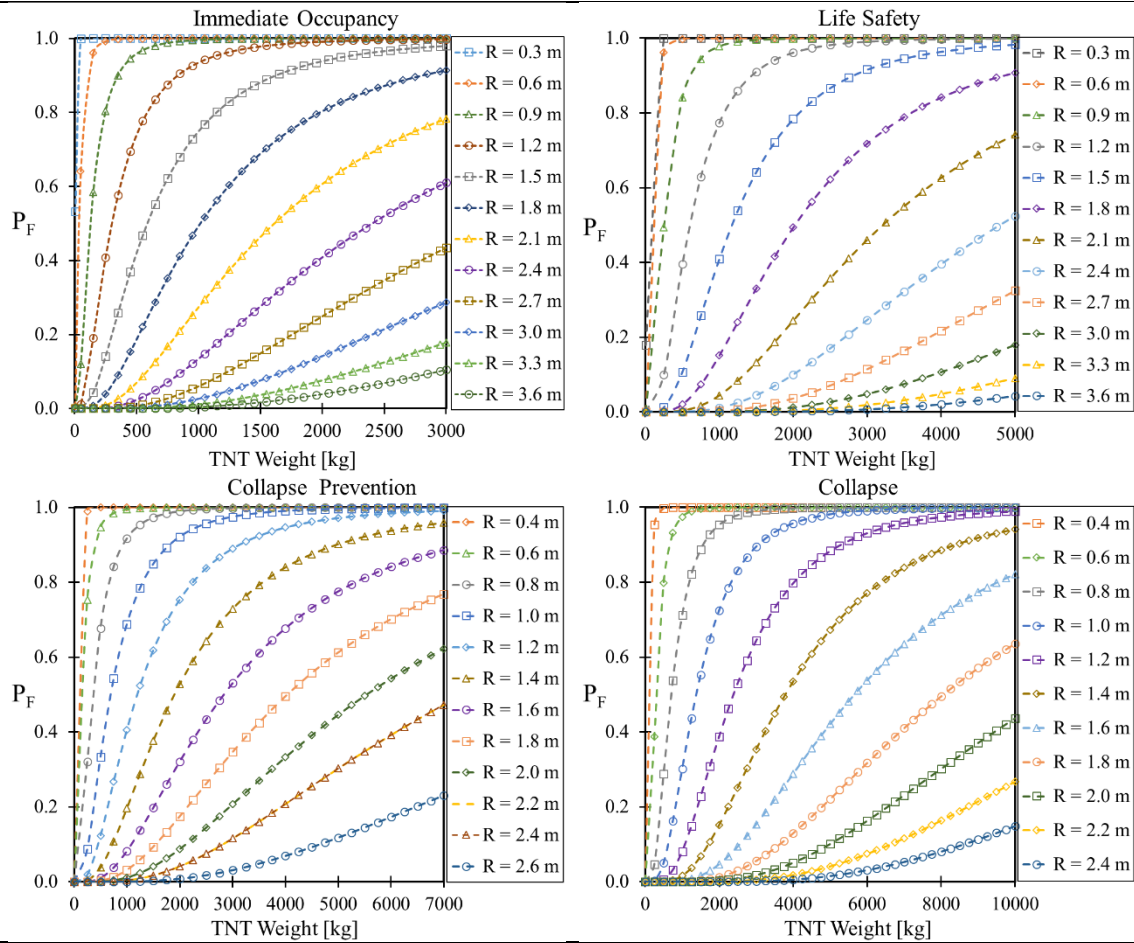


Fig. 5.17. Blast fragility for Semi-fan cable-stayed bridge

Contrary to the influence of the mass of TNT, which is less important from what emerges in the fragility curves, the stand-off distance has a more significant impact. It is important to highlight that the fragility results indicate that as the detonation occurs far from the deck, the probability of a possible failure of the bridge deck becomes lower. Indeed, by isolating two particular cases of stand-off distance $R = 0.4$ m and $R = 0.8$ m in a Fan configuration, we have the probability of collapse of the deck is reduced by 30% for a mass of 1000 kg TNT, by 45% for a mass of 500 kg (Fig. 5.15).

On the other hand, the variability is not as important for other cable-stayed bridge configurations. Indeed, considering the same stand-off distances as defined above, there is observed in a Harp configuration, a reduction in the probability of collapse of 20% for a mass of 1000 kg and 30% for a mass of 500 kg. This reduction will be in the order of 25% and 37% respectively for the 1000 kg and 500 kg masses of the Semi-fan configuration.

To calculate the limit state probability of exceedance as presented, a random distribution of blast loading scenario was considered. In addition, the quantity of TNT ranging from 0 - 10000 kg was considered but in reality, it is almost impossible to have an attack with a very large quantity of explosives because the transport would require significant logistical means that would reveal a suspicion on the part of the intelligence services. Thus, for masses

varying from 50 kg - 300 kg, which still represents quantities that would go unnoticed, it is very likely that there is no risk of collapse because the deck will succeed in withstand the loads caused by the explosion.

5.6 Conclusion

The structural efficiency of cable-stayed bridges considering three different typologies, namely (Harp, Fan, and Semi-fan bridges). Initially, a study of the structural response of bridges subjected to blast loadings of different intensities was carried out in this chapter. Then a study to highlight the consequences that a blast event could have on the possibility of progressive collapse. Finally, an analysis taking into account the probabilistic parameters was done on the structural components in order to find the likely failure. In the study, a series of non-linear dynamic analyses were used to find the structural demand of bridges considering different intensity measures while in the case of structural capacity, a pushover analysis was required to vary the geometry of the bridge and the cross-section of the structural components. From all these investigations, the following findings emerged:

- The Harp configuration presents a better configuration in terms of structural response under the action of blast loading. In addition, excessive displacement can be reached in the case of a large quantity of TNT used and the blast loading easily causes partial or total yielding of the bridge section closest to the point of detonation.
- Nonlinear dynamic analysis of a wide variety of bridges has established a relationship between structural demand following an extreme Hazard such as blast loading and scaled distance. This relationship in a lognormal distribution describes a negative correlation between the two parameters involved. Thus, the consequences following a blast loading action are more serious when the scaled distance is reduced.
- In this study, the authors also presented the need for an internal strain study of the sections. Indeed, in a case where stress analysis reveals the ease with which bridge sections reach their yielding and those even for small masses, it is important to know if the action at the limit will succeed in creating a collapse of the section.
- The study highlighted the feasibility and importance of the potential contribution of the derivation of the fragility curves of cable-stayed bridges. Through a probabilistic approach, the performance-based design for blast resistant structures are made and the likelihood of collapse for structural elements of the bridge is presented although this practice is commonly used on structures subjected to such hazards as (earthquake, flood, hurricane, wind, etc...).
- In the common case of a fragility analysis for an earthquake, generally the structural elements at high risk of exposure are piers, abutments and bearing. On the other hand, in the case of a blast event, the vulnerability of the deck must also be taken into account to the extent that this structural element remains highly exposed to action. Finally, the major difficulty that lies in the probabilistic analysis of this type of event consists in determining the hazard function since blast loadings are considered as a low occurrence probability event.

5.7 References

- [5.1] Jenkins BM, Gersten LN. Protecting Public Surface Transportation Against Terrorism and Serious Crime : Continuing Research on Best Security Practices. 2001;(September):124.
- [5.2] Kumar A, Matsagar V. Blast Fragility and Sensitivity Analyses of Steel Moment Frames with Plan Irregularities. *Int J Steel Struct.* 2018;18(5):1684-1698. doi:10.1007/s13296-018-0077-z
- [5.3] Son J, Lee HJ. Performance of cable-stayed bridge pylons subjected to blast loading. *Eng Struct.* 2011;33(4):1133-1148. doi:10.1016/j.engstruct.2010.12.031
- [5.4] Wolff M, Starossek U. Cable-loss analyses and collapse behavior of cable-stayed bridges. 2013:423-423. doi:10.1201/b10430-326
- [5.5] Formisano A, Landolfo R, Mazzolani FM. Robustness assessment approaches for steel framed structures under catastrophic events. *Comput Struct.* 2015;147:216-228. doi:10.1016/j.compstruc.2014.09.010
- [5.6] Elsanadedy HM, Almusallam TH, Alharbi YR, Al-Salloum YA, Abbas H. Progressive collapse potential of a typical steel building due to blast attacks. *J Constr Steel Res.* 2014;101:143-157. doi:10.1016/j.jcsr.2014.05.005
- [5.7] Olmati P, Brando F, Gkoumas K. Robustness Assessment of a Steel Truss Bridge. 2013;(April 2013):250-261. doi:10.1061/9780784412848.023
- [5.8] Abruzzo J, Matta A, Panariello G. Study of Mitigation Strategies for Progressive Collapse of a Reinforced Concrete Commercial Building. *J Perform Constr Facil.* 2006;20(4):384-390. doi:10.1061/(asce)0887-3828(2006)20:4(384)
- [5.9] Song BI, Sezen H. Experimental and analytical progressive collapse assessment of a steel frame building. *Eng Struct.* 2013;56:664-672. doi:10.1016/j.engstruct.2013.05.050

- [5.10] Abdelwahed B. A Review on Building Progressive Collapse, Survey and Discussion. *Case Stud Constr Mater.* 2019;11:e00264. doi:10.1016/j.cscm.2019.e00264
- [5.11] Adam JM, Parisi F, Sagaseta J, Lu X. Research and practice on progressive collapse and robustness of building structures in the 21st century. *Eng Struct.* 2018;173(March):122-149. doi:10.1016/j.engstruct.2018.06.082
- [5.12] Das R, Pandey AD, Soumya, Mahesh MJ, Saini P, Anvesh S. Progressive Collapse of a Cable Stayed Bridge. *Procedia Eng.* 2016;144:132-139. doi:10.1016/j.proeng.2016.05.016
- [5.13] Ubertini F. Effects of cables damage on vertical and torsional eigenproperties of suspension bridges. *J Sound Vib.* 2014;333(11):2404-2421. doi:10.1016/j.jsv.2014.01.027
- [5.14] Comanducci G, Ubertini F, Materazzi AL. Structural health monitoring of suspension bridges with features affected by changing wind speed. *J Wind Eng Ind Aerodyn.* 2015;141:12-26. doi:10.1016/j.jweia.2015.02.007
- [5.15] Materazzi AL, Ubertini F. Eigenproperties of suspension bridges with damage. *J Sound Vib.* 2011;330(26):6420-6434. doi:10.1016/j.jsv.2011.08.007
- [5.16] Lonetti P, Pascuzzo A. A numerical study on the structural integrity of self-anchored cable-stayed suspension bridges. *Frat ed Integrita Strutt.* 2016;10(38):359-376. doi:10.3221/IGF-ESIS.38.46
- [5.17] Ubertini F. Effects of cables damage on vertical and torsional eigenproperties of suspension bridges. *J Sound Vib.* 2014;333(11):2404-2421. doi:10.1016/j.jsv.2014.01.027
- [5.18] Lonetti P, Pascuzzo A. Vulnerability and failure analysis of hybrid cable-stayed suspension bridges subjected to damage mechanisms. *Eng Fail Anal.* 2014;45:470-495. doi:10.1016/j.engfailanal.2014.07.002

- [5.19] Sanaz R, Armen DK. A stochastic ground motion model with separable temporal and spectral nonstationarities. *Earthq Eng Struct Dyn.* 2012;41(11):1549-1568. doi:10.1002/eqe
- [5.20] Nassr AA, Razaqpur AG, Tait MJ, Campidelli M, Foo S. Strength and stability of steel beam columns under blast load. *Int J Impact Eng.* 2013;55:34-48. doi:10.1016/j.ijimpeng.2012.11.010
- [5.21] Mosoarca M, Anastasiadis A, Formisano A. New factors for the seismic vulnerability assessment of reinforced concrete buildings. *Int J Sustain Mater Struct Syst.* 2016;2(3/4):222. doi:10.1504/ijsmss.2016.078708
- [5.22] Lange D, Devaney S, Usmani A. An application of the PEER performance based earthquake engineering framework to structures in fire. *Eng Struct.* 2014;66:100-115. doi:10.1016/j.engstruct.2014.01.052
- [5.23] Tang EKC, Hao H. Numerical simulation of a cable-stayed bridge response to blast loads, Part I: Model development and response calculations. *Eng Struct.* 2010;32(10):3180-3192. doi:10.1016/j.engstruct.2010.06.007
- [5.24] Olmati P, Petrini F, Gkoumas K. Fragility analysis for the Performance-Based Design of cladding wall panels subjected to blast load. *Eng Struct.* 2014;78:112-120. doi:10.1016/j.engstruct.2014.06.004
- [5.25] Hao H, Stewart MG, Li Z-X, Shi Y. RC Column Failure Probabilities to Blast Loads. *Int J Prot Struct.* 2010;1(4):571-591. doi:10.1260/2041-4196.1.4.571
- [5.26] Momeni M, Hadianfard MA, Bedon C, Baghlani A. Numerical damage evaluation assessment of blast loaded steel columns with similar section properties. *Structures.* 2019;20(December 2018):189-203. doi:10.1016/j.istruc.2019.04.002
- [5.27] Olmati P, Petrini F, Bontempi F. Numerical analyses for the structural assessment of steel buildings under explosions. *Struct Eng Mech.* 2013;45(6):803-819. doi:10.12989/sem.2013.45.6.803

- [5.28] Khan S, Saha SK, Matsagar VA, Hoffmeister B. Fragility of Steel Frame Buildings under Blast Load. *J Perform Constr Facil.* 2017;31(4):04017019. doi:10.1061/(asce)cf.1943-5509.0001016
- [5.29] Kelliher D, Sutton-Swaby K. Stochastic representation of blast load damage in a reinforced concrete building. *Struct Saf.* 2012;34(1):407-417. doi:10.1016/j.strusafe.2011.08.001
- [5.30] Ding Y, Song X, Zhu HT. Probabilistic progressive collapse analysis of steel-concrete composite floor systems. *J Constr Steel Res.* 2017;129:129-140. doi:10.1016/j.jcsr.2016.11.009
- [5.31] Andreou M, Kotsoglou A, Pantazopoulou S. Modelling Blast Effects on a Reinforced Concrete Bridge. *Adv Civ Eng.* 2016;2016. doi:10.1155/2016/4167329
- [5.32] Hao H, Tang EKC. Numerical simulation of a cable-stayed bridge response to blast loads, Part II: Damage prediction and FRP strengthening. *Eng Struct.* 2010;32(10):3193-3205. doi:10.1016/j.engstruct.2010.06.006
- [5.33] Hashemi SK, Bradford MA, Valipour HR. Dynamic response of cable-stayed bridge under blast load. *Eng Struct.* 2016;127:719-736. doi:10.1016/j.engstruct.2016.08.038
- [5.34] FEMA. Primer for Design of Commercial Buildings to Mitigate Terrorist Attacks. *Risk Manag Ser.* 2003;(December).
- [5.35] Deng RB, Jin XL. Numerical simulation of bridge damage under blast loads. *WSEAS Trans Comput.* 2009;8(9):1564-1574.
- [5.36] Calculation of Blast Loads for Application to Structural Components. Administrative Arrangement No JRC 32253-2011 with DG-HOMEActivity A5 - Blast Simulation Technology Development.; 2013. doi:10.2788/61866
- [5.37] Verma SV. Blast Resistant Design of Structure. *Int J Res Eng Technol.* 2016;04(25):64-69. doi:10.15623/ijret.2015.0425010
- [5.38] Strand7 user's manuel. 2005.

- [5.39] Longitudinal Seismic Behavior of a Single-Tower Cable-Stayed Bridge Subjected to Near-Field Earthquakes. *Shock Vib.* 2017;2017. doi:10.1155/2017/1675982
- [5.40] Paik JK, Thayamballi AK. A concise introduction to the idealized structural unit method for nonlinear analysis of large plated structures and its application. *Thin-Walled Struct.* 2003;41(4):329-355. doi:10.1016/S0263-8231(02)00113-1
- [5.41] European Standard. Part 2: Traffic loads on bridges. Eurocode 1 Actions Struct. 2003;3(1991-2:2003).
- [5.42] CEN. EN 1990: 2002 - Basis of structural design. 2002:1-87.
- [5.43] Pang Y, Wu X, Shen G, Yuan W. Seismic Fragility Analysis of Cable-Stayed Bridges Considering Different Sources of Uncertainties. *J Bridg Eng.* 2013;19(4):04013015. doi:10.1061/(asce)be.1943-5592.0000565
- [5.44] Stefanidou SP, Kappos AJ. Bridge-Specific Fragility Analysis: When Is It Really Necessary? Vol 17. Springer Netherlands; 2019. doi:10.1007/s10518-018-00525-9
- [5.45] Xie Y, Zhang J, DesRoches R, Padgett JE. Seismic fragilities of single-column highway bridges with rocking column-footing. *Earthq Eng Struct Dyn.* 2019;48(7):843-864. doi:10.1002/eqe.3164
- [5.46] van de Lindt JW, Taggart M. Fragility Analysis Methodology for Performance-Based Analysis of Wood-Frame Buildings for Flood. *Nat Hazards Rev.* 2009;10(3):113-123. doi:10.1061/(asce)1527-6988(2009)10:3(113)
- [5.47] Herbin AH, Barbato M. Fragility curves for building envelope components subject to windborne debris impact. *J Wind Eng Ind Aerodyn.* 2012;107-108:285-298. doi:10.1016/j.jweia.2012.05.005
- [5.48] Simões da Silva L, Rebelo C, Nethercot D, Marques L, Simões R, Vila Real PMM. Statistical evaluation of the lateral-torsional buckling resistance of steel I-beams, Part 2: Variability of steel properties. *J Constr Steel Res.* 2009;65(4):832-849. doi:10.1016/j.jcsr.2008.07.017

- [5.49] Olmati P, Vamvatsikos D, Stewart MG. Safety factor for structural elements subjected to impulsive blast loads. *Int J Impact Eng.* 2017;106:249-258. doi:10.1016/j.ijimpeng.2017.04.009
- [5.50] Cornell CA, Jalayer F, Hamburger RO, Foutch DA. Management Agency Steel Moment Frame Guidelines. *J Struct Eng.* 2002;128(April 2002):526-533. doi:10.1061/(ASCE)0733-9445(2002)128:4(526)
- [5.51] Ding Y, Song X, Zhu HT. Probabilistic progressive collapse analysis of steel frame structures against blast loads. *Eng Struct.* 2017;147:679-691. doi:10.1016/j.engstruct.2017.05.063
- [5.52] FEMA. Prestandard and Commentary for the Seismic Rehabilitation of Buildings. *Rehabil Requir.* 2000;(1):1-518.

CHAPTER 6

General Conclusions and Futures Researches

6.1 General conclusions

Steel as a building material will continue to be used in the bridge industry owing to its favourable mechanical property and other advantages it presents. However, if an adequate measure is not taken during the construction process, inconvenient or unpleasant situations could occur leading to section disorders with the consequence of reducing its limit strength. It is one of the major issues observed in thin steel profiles used for bridge girders as it has been presented in the thesis. On the other hand, structures that once could easily reach their lifetime are increasingly confronted with probable malicious or extreme actions with a major consequence the partial or total collapse of the bridge. These two major issues represent the main interest of the investigations carried out, to which could be added the post-buckling study of an arch bridge where the study of the bridge's limit resistance was made. From the analyses performed, the following outcomes have been drawn.

The innovative analytical formula derived from intensive numerical analyses allowed concluding that the slenderness is the most influential parameter of the buckling of the plate subjected to combined in-plane loading.

The critical buckling is greatly influenced by the compressive stress state arising from the interaction of the in-plane loadings. Indeed, the critical buckling stress can be reduced up to half compared to the case of single loading case.

For arches without lateral bracing, multi-shape modes are observed. The arches move to the second buckling mode at the end of the first nonlinear phase. During this phase, an increase of vertical loads is still visible. On the other hand, another behavior is observed for braced arches, which display a slight softening at the end of the first nonlinear phase. The arches reached the critical live loads and the strain will continue to decrease with the formation of several hinges on each arch.

The cable loss scenario generated dynamic actions on bridges element whose sensitivity mainly depend on the position of the cable. Indeed, the arch is less dynamic sensitive in the case of the loss of cable located to the center of the bridge. however, a large lateral displacement will also be observed in this case mainly due to the large reaction forces existing in the cable.

Nonlinear dynamic analysis of a wide variety of bridges has established a relationship between structural demand following an extreme Hazard such

as blast loading and scaled distance. This relationship in a lognormal distribution describes a negative correlation between the two parameters involved. Thus, the consequences following a blast loading action are more serious when the scaled distance is reduced.

In the common case of a fragility analysis for an earthquake, generally, the structural elements at high risk of exposure are piers, abutments, and bearing. On the other hand, in the case of a blast event, the vulnerability of the deck must also be taken into account to the extent that this structural element remains highly exposed to action. Finally, the major difficulty that lies in the probabilistic analysis of this type of event consists in determining the hazard function since blast loadings are considered as a low occurrence probability event.

6.2 Future researches

The study of the steel plate and various bridges typologies allowed to understand that the structural responses depend on the type of loading, the characteristic material used and the structural systems. Due to the existence of a tremendous amount of steel bridges, most of which are approaching their service life, and considering other actions that contribute to promoting or accelerating damages observed, numerous studies have been conducted to evaluate the effectiveness of methods for strengthening steel structural elements. Recently, the effectiveness of the use of composite materials that were once used on concrete or masonry elements has been studied. Thus, as future development, the experimental and analytical study of strengthening of a steel plate using carbon fiber reinforced polymer will be made as part of our contribution to this innovative topic. Besides, it will interesting to dive into the study of the robustness of various structural system under extreme loading conditions.